Protein-Film-Mediated Strategies for the Electrochemical Immunosensing of Circulating Biomarkers



Felix Mateo Fleschhut
St. Edmund Hall, University of Oxford
Department of Inorganic Chemistry
A Thesis Submitted for the Degree of Doctor of Philosophy

“The first principle is that you must not fool yourself —

and you are the easiest person to fool.”

Richard Feynman

“Irrend lernt man.“

Johann Wolfgang von Goethe

This thesis is dedicated to my family

Declaration and Statement of Collaboration

I, Felix Fleschhut, declare that the work included in this thesis titled “Protein-Film-Mediated Strategies for the Electrochemical Immunosensing of Circulating Biomarkers” is entirely my own. All relevant published works are acknowledged by proper citation and referencing within the text. The following experiments were conducted in collaboration with other researchers:

All XPS data was collected by Dr. Wai-Man Chan (Oxford Materials Characterisation Service, University of Oxford). All measurements taken for the chapter on Faradaic Shotgun Tagging (Chapter 4) were acquired in collaboration with Dr. Mohamed Sharafeldin (Department of Chemistry, University of Oxford). The patient sample analysis was performed in collaboration with Dr Timothy James (Department of Clinical Biochemistry, John Radcliffe Hospital, Oxford University Hospitals, NHS Foundation Trust), who kindly provided the results obtained with an Abbott Architect, and Dr Mohamed Sharafeldin. The in-gel electrophoresis (SDS-PAGE) experiments were performed by Elisabeth Mira Rothweiler (Department of Medicine, University of Oxford).

Abstract: Protein-Film-Mediated Strategies for the Electrochemical Immunosensing of Circulating Biomarkers

Felix M. Fleschhut, St Edmund Hall, University of Oxford

Thesis Abstract submitted for the degree of DPhil Inorganic Chemistry

The electrochemical quantification of protein biomarkers from complex samples such as human serum promises vast potential for the solution of future healthcare challenges. **Chapter 1** will summarise the current state-of-the art and show that such assays can typically be categorized as either sandwich-type or label-free. Label-free methodologies directly transduce a single interfacial recognition event and therefore demand specially designed electrode modifications that come with challenges in stability. While sandwich methodologies offer high sensitivity, they are associated with considerably higher assay complexity as well as time and cost requirements. This work aims to expand the currently available range of methodologies by introducing three distinct approaches focusing on facile implementation as well as simple and stable sensing platforms. **Chapter 3** will introduce the first example of an amperometric dot blot assay for the detection of target protein from diluted serum. The proposed method dismisses any electrode functionalisation and aims to solve practical challenges regarding storage, transport and handling while catering clinical demands for the target proteins. **Chapter 4** aims to explore the use of ensemble redox labelling for the electrochemical quantification of target protein. Hereby, the non-specific redox tagging of all protein in serum in combination with antibody-mediated target recognition at an electrode surface is used to yield a voltametric assay offering facile and multiplexable sensing. **Chapter 5**, finally, elucidates the use of the electroactive protein Azurin as a transducing and anti-fouling building block for the formation of stable biosensory surfaces for target protein immunosensing based on redox-capacitance. A summary of results and an outlook for future work is provided in **Chapter 6**. All experimental details are summarised in **Chapter 2**. Supportive information is provided in the appendix (**Chapter 7**). All referenced work is listed in **Chapter 8**.

Acknowledgments

First and foremost, I would like to express the deepest gratitude to my supervisor, **Prof. Jason J. Davis**, for the opportunity to conduct research in his group, his feedback, the many chats and so many of the useful experiences I made during my time in Oxford. I would further like to express the deepest appreciation to my research collaborators; **Dr. Mohamed Sharafeldin, Dr. Timothy James, Dr. Wai-Man Chan, Elisabeth Mira Rothweiler** for their experimental assistance**.**

For their helpful advice, instructions, and discussions, I would like to thank **Tara Lurshay, Shaoyu Kang, Dr. Razieh Salimian, Dr. Xiaoxiong Li, Dr. Abdulghani Ismail, Dr. Robert Barber, Dr. Robert Hein**, and **Dr. Mohamed Sharafeldin**.

For their dedication in proofreading this thesis, I would like to thank **Mohamed, Shaoyu** and **Sophie Patrick**, and for their friendship, support and making any labwork much more interesting, for which I would like to thank the whole JJD group including **Robert Barber, Robert Hein, Daohe Yuan, Connor Ellis, Xuanxiao Chen, Morgan Millner, Lillian Leutloff, Anna Duncan and Sophia Abusamra**.

I am grateful to my family and friends for their unconditional support throughout all these years, providing a haven of tranquillity and source of motivation, without which I would never have reached any of the things I would consider my achievements. And **Mira** for our mutual support and deep friendship throughout so many years.

I have relied on so many people throughout these last years, I cannot possibly have mentioned them all. I would like to express my deep gratitude to all the people I shared some of this road with and who had an impact to my life in so many different ways.

Publications

Chapter 3:

Fleschhut, F., & Davis, J. J. (2024). An Amperometric Dot Blot Assay for the Quantification of Target Protein in Complex Media at Unmodified Electrode Surfaces. *In preparation*.

Chapter 4:

Sharafeldin, M.[§], **Fleschhut, F.**[§], James, T., & Davis, J. J. (2022). A Quantification of Target Protein Biomarkers in Complex Media by Faradaic Shotgun Tagging. **Analytical Chemistry**, 94(5), 2375-2382.

[§] M.S. and F.F. contributed equally to this work.

WIPO Patent: Davis, Jason; Sharafeldin, Mohamed; **Fleschhut, Felix**., WO2023037111A1 ELECTROCHEMICAL SHOTGUN TAGGING ASSAY (08.09.2022)

Abbreviations and Symbols

3-MPA	3-mercaptopropionic acid
4-MBPA	4-mercaptophenyl boronic acid
Ab	Antibody
AFM	Atomic force microscopy
Az	Azurin
BC	Before Christ
BSA	Bovine serum albumin
C', C''	real/imaginary capacitance
c.f.	Confer
ca.	*circa*
Cdl	Double layer capacitance
C_r	Redox Capacitance
CRP	C-reactive protein
CT	Charge transfer
cTnI	Cardiac Troponin I
CV	Cyclic voltammetry
CVD	Cardiovascular diseaese
CytC	Cytochrome C
Da	Dalton
DPV	Differential pulse voltammetry
E	Potential

E_{pa}/E_{pc}	Anodic/cathodic peak potential
e.g.	*exempli gratia*
$E_{1/2}$	Half-wave potential
ECS	Electrochemical capacitance spectroscopy
EDC	1-Ethyl-3-(3-dimethylaminopropyl)carbodiimide
EIS	Electrochemical impedance spectroscopy
ELISA	Enzyme linked immunosorbend assay
EPADs	Electrochemical paper-based analytical devices
et al.	*et alia*
etc.	*et cetera*
EtOH	Ethanol
f	Femto-
FBS	Fetal Bovine Serum
Fib	Fibrinogen
g	Gram
h	Hour
HRP	Horse-radish peroxidase
hs	High-sensitivity
HSA	Human Serum Albumin
HT	Hexanethiol
Hz	Hertz
i	Anodic/cathodic peak current
i.e.	*id est*

Im	Imaginary
J	Joule
K	Kelvin
k	Kilo
LOD	Level of detection
M	Molar
MB	Methylene Blue
MB-NHS	Methylene Blue-NHS ester
MHA	Mercaptohexanoic acid
MI	Myocardial infarction
min	Minute
mol%	Molar percentage
MS	Mass spectrometry
MSD	Meso scale discovery
Myo	Myoglobin
n	Nano-
NHS	N-hydroxysuccinimide
Ω	Ohm
ω	Frequency
OEG	Oligoethyleneglycol
p	Pico-
PBS	Phosphate buffered saline
PBS-T	Phosphate buffered saline with Tween

PDMS	Polydimethylsiloxane
PEG	Polyethyleneglycol
pH	-log10[H+]
POC	Point of Care
POCT	Point of Care Testing
QCM	Quartz crystal microbalance
r	Radius, distance
RAP	Resonant acoustic profiling
Rct	Charge transfer resistance
Re	Real part
RIA	Radioimmunoassay
Rs	Solution resistance
s	Second
SAM	Self-Assembled Monolayer
SARS-CoV-2	Severe acute respiratory syndrome coronavirus 2
Simoa	Single molecular arrays
SPCE	Screen-printed carbon electrode
SPR	Surface Plasmon Resonance
t	Time
T	Temperature
TAT	Turn-around time
TMB	Tetramethyl Benzidine
UV-VIs	Ultraviolett-Visbile

V	Volt
vol%	Volume percentage
wt%	Weight percentage
Z', Z''	Real/imaginary impedance
Zw	Warburg element
µ	Micro-
π	Pi

Table of Contents

Declaration and Statement of Collaboration iii

Abstract: Protein-Film-Mediated Strategies for the Electrochemical Immunosensing of Circulating Biomarkers iv

Acknowledgments v

Publications vi

Abbreviations and Symbols vii

Table of Contents xii

Chapter 1 Introduction 1

1.1 Relevance of Protein Detection and Quantification 1

1.2 Overview of Electrochemical Immunosensing 2

1.2.1 Relevance of Electrochemical Protein Immunosensing 5

1.2.2 Principles for the Transduction of Immunorecognition Events at Electrode Surfaces 8

1.2.3 General Concepts of Electrochemical Sensing Methodologies 10

1.2.4 Recent Advancement in Facilitation and Scalability of Electrochemical Immunosensing Technologies 17

1.2.5 Current Challenges in Electrochemical Immunosensing 18

1.3 Protein Fouling and Currently Employed Anti-Fouling Strategies 19

1.3.1 Native Protein Adsorption at Electrode Surfaces 19

1.3.2 Current Anti-fouling strategies in Electrochemical Immunosensing 20

1.4 Functional Protein Film Formation on Plain and Self-Assembled Monolayer Functionalised Electrode Surfaces 22

1.4.1 Strategies for protein film formation on plain electrodes and Protein modification via EDC/NHS carbodiimide chemistry 22

1.4.2 Self-Assembled-Monolayers (SAMs) of 1-Hexanethiol and 6-Mercaptohexanoic Acid and Azurin Protein Electrochemistry on Alkanethiol SAMs 24

1.5 Quantification of CRP and cTnI – Current Transduction Approaches and the Need for Innovative Assay Methodologies 27

1.5.1 CRP and cTnI – a Suitable Model System for the Development of Diagnostic Platforms 27

1.5.2 Currently Available Platforms for the Clinical Quantification of CRP and cTnI 29

1.5.3 Current Research Towards the Electrochemical Quantification of CRP and cTnI 31

1.5.4 Demand for Novel Sensing Platforms for Future Point-of-Care Application 34

1.6 Thesis Aims and Scope 35

Chapter 2 Materials and Methods 38

2.1 Materials and General Considerations 38

2.2 Electrochemical Procedures and Electrode Preparation 40

2.3 Preparation Protocols and Characterisation 41

2.3.1 Self-Assembled-Monolayer (SAM) Preparation 41

2.3.2 Protein Immobilisation on SAM 42

2.3.3 Antibody Physisorption for Electrode Modification in Shotgun Tagging Assay (Chapter 4) 43

2.3.4 Protein Physisorption on Clean Surfaces for Dot Blot Assays (Chapter 3) 43

2.3.5 Coupling of Proteins with MB-NHS or Fc-NHS..... 44

2.3.6 UV-Visible Spectroscopy..... 44

2.3.7 Water Contact Angle 45

2.3.8 In-Gel Fluorescence 45

2.3.9 Sample preparation for XPS 45

2.3.10 Surface Plasmon Resonance (SPR) Measurement Procedures 46

2.3.11 Atomic Force Microscopy..... 48

2.4 Assay measurement protocols 49

2.4.1 Assay Protocols for Chapter 3 (Amperometric Dot Blot Assay) 49

2.4.2 Assay Protocols for Chapter 4 (Faradaic Shotgun Tagging Assay) 53

2.5 Microfluidic Setups 56

2.6 Theoretical Considerations and Calculations 58

2.6.1 Electrode surface area..... 58

2.6.2 EIS and ECS analysis..... 58

2.6.3 Estimations of Surface coverage 58

2.6.4 Limit of Detection 59

Chapter 3 An Amperometric Dot Blot Assay for the Quantification of Target Protein in Complex Media at Unmodified Electrode Surfaces 60

3.1 Introduction 60

3.2 Results and Discussion 65

3.2.1 Protein Surface Formation and Characterisation 65

3.2.2 Static Assay on Glassy Carbon Electrodes 72

3.2.3 Static Assay on Screen-Printed Carbon Arrays 75

3.2.4 Microfluidic Integration of Assay 85

3.2.5 Transfer to Other Electrode Surfaces 93

3.2.6 Theoretical Considerations for an Amperometrically Amplified Dot Blot Assay 95

3.3 Conclusions and Future Work 101

Chapter 4 Faradaic Shotgun Tagging for the Voltammetric Quantification of Target Protein in Complex Media 104

4.1 Introduction 104

4.2 Results and Discussion 108

4.2.1 Establishment of Assay Concept and Working Conditions 108

4.2.2 Static Assay for Single Target Protein 112

4.2.3 Static Assay for Multiple Target Proteins (Multiplexing) 115

4.2.4 Microfluidic Integration of Assay 116

4.2.5 Spike Recovery and Patient Sample Analysis 118

4.3 Conclusions and Future Work 120

Chapter 5 Electroactive Proteins as Low-Fouling and Transducing Building Blocks for Redox Capacitive Immunosensing of Target Protein 123

5.1 Introduction 123

5.2 Results and Discussion 127

5.2.1 Self-Assembled-Monolayer Formation and Characterisation 127

5.2.2 Protein Assembly and Electrochemical Addressability of Azurin on Hexanthiol SAM 136

5.2.3 Assembly and Electrochemical Adressability of Azurin on Mixed SAM of 1:49 MHA:HT 145

5.3 Conclusions and Future Work 152

Chapter 6 Conclusions and Outlook 155

Chapter 7 Appendix 158

7.1 Appendix Chapter 3 158

7.2 Appendix Chapter 4 164

7.3 Appendix Chapter 5 174

References 178

Chapter 1

Introduction

1.1 Relevance of Protein Detection and Quantification

Proteins are essential to all living organisms and constitute a significant class of biomolecules. The oligomers composed of amino acids account for over 50% of cell dry weight, making them the largest group of biomolecules.[1] Protein networks govern enzymatic catalysis, regulate gene expression, transmit signals, provide structure, and mediate bioenergetics in cells.[2] Detecting and quantifying protein concentration proves valuable in various applications, from pathogen detection[3] and systems analysis,[4] to disease diagnostics and guided therapy.[5] The interest in developing platforms for protein detection has risen significantly in recent decades, impacting fields like cancer diagnosis,[6] food science,[7] and the early detection of inflammatory markers.[8] While centralized labs have long driven clinical testing progress, decentralized diagnostics, known as point-of-care (PoC) testing, are emerging as a promising tool for modern medicine.[9] These instruments, characterized by short turn-around time, low sample preparation demands, minimal end-user intervention, and portability, are growing in use. Examples include pregnancy tests,[10] home testing kits for SARS-CoV-2 (the virus causing Covid-19),[11] and clinical devices for cardiovascular testing.[12] The impact of such technologies is expected to grow, especially in resource-limited settings and personalized medicine.[13] Advances in connectivity, driven by wearable and clinical PoC

diagnostic kits, are shaping the future of healthcare.[14] Sensors, especially biosensors, play a pivotal role, enabling a new approach to global health, and affordable and widely applicable sensor technology could revolutionise early diagnostics for the global society.[15] In remote settings without access to centralized laboratories, such technologies are crucial. However, despite their potential, there are challenges that must be addressed for these sensors to reach their full potential.

This chapter summarizes key concepts related to sensor development, focusing on the role of electrochemical immunosensors within the broader category of chemical sensors. It explores the principles guiding electrochemical immunosensing of protein biomarkers, discussing its place in the realm of electrochemical biosensors and addressing current challenges in applying electrochemical protein biosensors in real-world scenarios. The background pertinent to electrode modifications in this thesis is presented, including a brief summary of native protein adsorption on electrode surfaces and currently available anti-fouling strategies. The chapter then delves into recent advancements in the development of electrochemical immunosensors for the biomarkers C-reactive protein (CRP) and cardiac Troponin I (cTnI), the two standard markers used in this work. Finally, the chapter concludes with an analysis of the thesis's aims and scope.

1.2 Overview of Electrochemical Immunosensing

Sensors in their broadest definition include any device capable of responding to an external stimulus or signal. For the purposes of this work, the definition of an electrical sensor is narrowed down to devices responding with electrical signals to received

stimuli, which may include any physical property. A sensor is thus considered a device that transforms information into electrical signals, which can be manipulated by other electronic devices. As the transmission of information always requires transmission of energy (transduction), this renders a sensor a special kind of transducer.[16] More intricate sensors may comprise multiple transducers, especially if transforming specific energies into electrical energies involves multiple processes. For a sensor to relay information about the stimulus, it is paramount to gain understanding of the transfer function, $s = F(x)$, that relates the measured electrical response x to a given input stimulus s. This understanding is acquired through sensor calibration.

Chemical sensors, broadly defined, quantify or analyse the presence or concentration of chemical substances, referred to as analytes. Biosensors, a subset of chemical sensors, convert a chemical reaction event between an analyte and a bioreceptor (such as the binding of antibody to antigen) into an electronically measurable signal.[17] A bioreceptor interacts specifically with the analyte, triggering a biorecognition event, which is then transformed into a measurable signal through a transducer and often electronically processed. Electrochemical biosensors in turn employ electroanalytical methods on an electrode surface to transfer a primary transducer signal into an electronic readout for the quantification of interaction between a bioreceptor and an analyte.

Important factors to evaluate the performance of such interfacial biosensors will be introduced in the following and include the specificity, sensitivity as well as the level of detection (LOD).

Specificity, defined as the ability of an analytical method to distinguish the analyte of interest from other interfering signals, is crucial for chemical sensors.[18] Achieving

specificity in a chemical sensor depends on the transduction method employed in a particular methodology. In general terms, specificity is attained by designing the sensing device or technique to activate the transducer when combined with the specific target analyte while remaining inactive with any other molecule. This design always involves a recognition process, where the target analyte interacts with a recognition element. The recognition element interacts specifically with the target analyte, often binding to the target molecule. Subsequently, such interaction translates into a change in physical properties accessible to the transducer. Recognition can involve a variety of different principles – examples are the specific enzymatic oxidation of glucose to gluconolactone by glucose dehydrogenase within glucose meters for enzymatic recognition,[19] antibodies binding to antigen,[20] or aptamers as an example of nucleic acid based binding moieties.[21] For immunosensors antibodies are used to capture the target antigen through biomolecular interaction of their binding regions.[22]

Another essential property of any sensor is its capacity to generate a significant change in readout upon the addition of the analyte. Sensor sensitivity is defined as the change in readout per unit change in the input stimulus.[15] If the transfer function $F(x)$ is a linear function in the input variable x (e.g. analyte concentration), as in Eq. 1, the sensitivity is given by the proportionality coefficient A.[16]

$$F(x) = Ax + B \qquad \text{Eq. 1}$$

In real-world scenarios, few transfer functions are linear across the entire range of possible stimulus strengths (e.g., concentration). Therefore, a linear range is often defined as the part of the transfer curve approximated by a linear function. The data can also be transformed mathematically, before a linear approximation is applied. The most

prominent example of this kind is a logarithmic transformation in x to yield a linear function as shown in Eq. 2.

$$F(x) = A \ln(x) + B \qquad \text{Eq. 2}$$

While more complex transformations exist in the literature, the mentioned functions suffice for this work due to their broad applicability. Furthermore, the limit of detection is defined as the lowest concentration still distinguishable from any background signal (see 2.6.4).[17]

Other factors to consider in the design of biosensors are their stability, repeatability and robustness, which are not as rigorously defined as the above. However, stability is generally understood as the capability of the sensor interface to resist degradation of signal generation over time, while repeatability can be assessed to some extent by the standard deviation between multiple measurements. The robustness is the interface's property to produce similar results for different measurement conditions and is not easily accessible, but can somewhat be inferred from the general sensor performance.

1.2.1 Relevance of Electrochemical Protein Immunosensing

In the realms of clinical diagnostics, drug discovery, and therapeutic intervention monitoring, quantifying proteins in biological samples has become a reliable and valued tool. [23] The assessment of various protein markers benefits the identification of abnormal metabolic states, physiological conditions, and diseases.[24-26] While comprehensive whole proteome analyses, particularly through mass spectrometry (MS)-based techniques,[27] are available, their cost and complexity limit broad applications for early diagnostics or prevention.[28] In recent decades, many alternative approaches have been proposed. Biosensors for the specific analysis of certain target

proteins using diverse interfacial recognition and transduction processes have emerged as a major area of development.[29] In the diverse landscape of biosensors, immunosensors, utilizing antibodies as recognition elements, have been pivotal. Ongoing research and advancements in antibody technology ensure their continued relevance.[30] The various technologies that have been proposed for the transduction of the antibody-antigen interaction range from chemo-optical methods like the enzyme-Linked-Immunosorbent assays (ELISA), surface plasmon resonance (SPR) based techniques, and mechanical approaches such as the quartz crystal microbalance (QCM), to electrochemical methodologies (e.g. impedimetric, or amperometric sensor platforms).[15] In clinical protein quantification from complex biological samples, the enzyme-linked immunosorbent assay (ELISA) has long been acknowledged for its established specificity and sensitivity.[31] Traditional ELISA, utilizing pairs of antibodies with an attached enzyme label, provides a quantifiable colorimetric output. Evolving into derivatives like single-molecular arrays (Simoa),[32] and electrochemiluminescence-based immunoassays (e.g., Meso Scale Discovery - MSD),[33] ELISA variants enable routine detection at sub-picogram per milliliter (sub-pg mL^{-1}) levels. Furthermore, it is available in a semiautomated format compatible with clinical analyzers.[34] However, it is important to note that all ELISA formats require centralized laboratories, expensive instrumentation, intricate procedures, and relatively lengthy assay durations (typically 6-8 hours). These factors limit their utility in resource-limited or point-of-care (POC) settings.[35]

In contrast, electrochemical biosensors, offering comparable sensitivity (typically down to pg mL^{-1} levels),[36] present the opportunity to develop cost-effective and highly scalable platforms.[37] These advantages position electrochemical methodologies as

particularly promising for POC applications in future healthcare settings.[38] Additionally, compared to their optical or mechanical counterparts, electrochemical setups are easily miniaturized, providing portability and applicability in resource-limited settings in combination with high scalability of their manufacturing process.[39] Recent advancements in the production of low-cost, disposable electrodes exemplify this trend.[40] Furthermore, due to their facile microfluidic integration, a diverse array of microfluidic electrochemical immunoassay strategies has been explored as cost-effective POC alternatives for automatable and straightforward handling.[41, 42] Consequently, electrochemical immunosensors are recognized for their significant value in future diagnostics.[43] This growing recognition is reflected in the increased research interest, as evidenced by the rising number of publications per year in the field (see Figure 1-1).

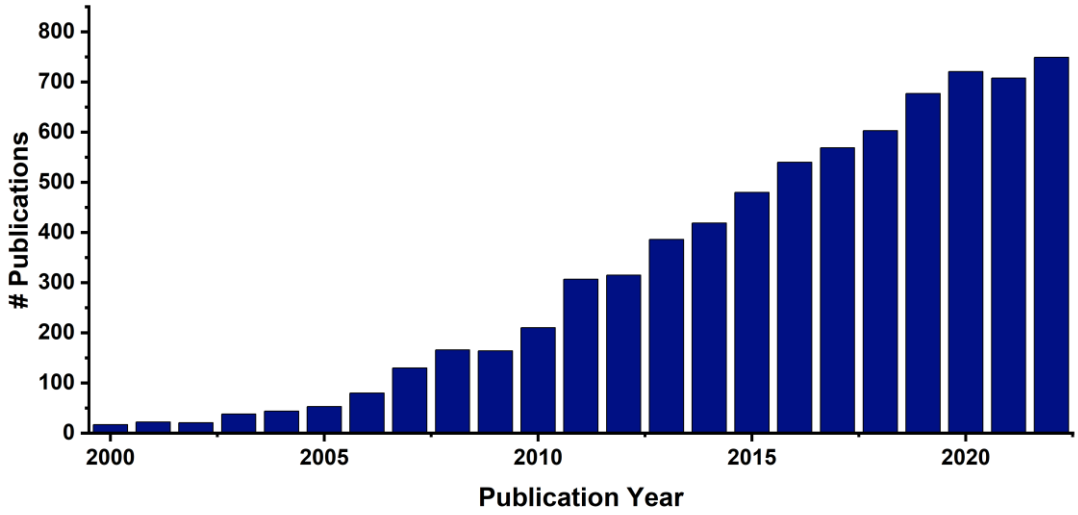


Figure 1-1 Number of published papers found with a search for the keywords "electrochemical immunosensors" versus the year of publication. Source: web of science.

1.2.2 Principles for the Transduction of Immunorecognition Events at Electrode Surfaces

The numerous electrochemical biosensor examples proposed in recent years underscore the range of transduction variants available in this research field. The methodologies at hand are often categorized based on the electrochemical technique applied for assay evaluation, primarily impedimetric, voltammetric, and amperometric techniques (discussed in 1.2.3). However, the majority of proposed assays can also be categorized into either electrochemical sandwich-based methods, or label-free methodologies.[44] The latter include mainly impedimetric, and redox-capacitive techniques. The electrochemical sandwich-based techniques are valued for their high sensitivity and specificity delivered by employing a labelled recognition element that binds to the target analyte in a second step after the target capture at a surface bound recognition element.[43] The utilised label can, for example, consist of a redox tag, an enzyme-label,[45] or nanoparticles featuring multiple such moieties,[46] for an amplification of signal. In contrast, label free methodologies omit a secondary label and are valued for their facile implementation. These approaches, relying on a single bio-recognition event at an electrode surface, aim to directly convert the binding event into a measurable signal by assessing changes in the accessibility of the electrode surface during the recognition event.[47] Among label-free setups, impedimetric techniques are one of the most common approaches. These methodologies utilize a pair of solution-phase redox probes (e.g., Ferrocyanide and Ferricyanide) to transfer charge with an electrode. The charge transfer resistance effectively transduces changes at the electrode surface when an analyte binds to a surface-tethered recognition element.[48] As a common alternative technique, redox capacitance-based methodologies use a surface-tethered

electroactive probe, such as a ferrocene derivative, addressable from the underlying electrode. The electrochemical accessibility of this so-formed surface changes when a recognition event happens close to the surface charge. This change in addressability can be evaluated through different electrochemical techniques.[49-51] The mechanism for this is still not entirely elucidated but has been attributed to changes in the electrostatic environment of the surface charge before.[50]

In summary, labelled techniques always depend on secondary labels, while the latter two methodologies allow for label-free protein quantification.[52] Additionally, redox-capacitance-based methodologies are sometimes referred to as reagent-less due to their omission of any solution probe (see Figure 1-2).[53] The label-based methodologies exhibit high sensitivities and turn-on signals (discussed in 1.2.3) akin to established techniques like ELISA, attributed to the use of redox, enzyme and/or nanoparticle labels.[54, 55] However, they inherently rely on label generation, multiple washing, and incubation steps, leading to increased complexity, user intervention, time, and cost.[56] In contrast, label-free electrochemical methodologies directly transform the capture of the target analyte at recognition elements tethered to an electrode surface into a measurable signal. However, such techniques commonly require specifically designed electrode interfaces to maximize specificity in complex media,[57-59] as discussed in 1.3.1.

Each of the mentioned transduction principles can be evaluated using different electrochemical sensing modes to interrogate the transducer, which will be discussed in the following section.

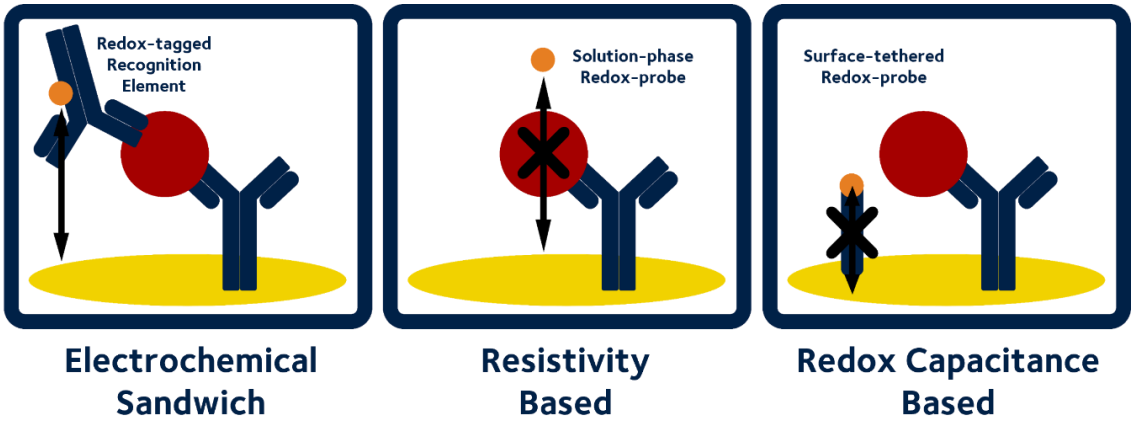


Figure 1-2 Schematic Illustration depicting the three main concepts employed for electrochemical immunosensing within the currently available techniques: electrochemical sandwich, resistivity-based and redox capacitive methodologies. The latter two are further classified as label-free in contrast to the first method employing a labelled secondary antibody.

1.2.3 General Concepts of Electrochemical Sensing Methodologies

In general, electrochemical techniques used to interrogate an electrode surface can be categorized as current-, potential-, and impedance-based measurement techniques.[60] These can be further classified into voltammetric, potentiometric, amperometric, coulometric, and impedance spectroscopic methods.[43] Voltammetry involves measuring current during a sweeping potential input, which can take various forms such as linear or cyclic sweeps, staircase, or pulsed potential time profiles (discussed in more detail in 1.2.3.1). Potentiometry, amperometry, and coulometry evaluate the corresponding electrical signal response (i.e., potential, current, and charge transferred) at a given time under a static current or potential being applied. Impedance spectroscopy, finally, describes the measurement of the current output signal as the reaction to a sinusoidal input voltage, hence the impedance. While impedance spectroscopy is most commonly employed when a solution phase redox probe is interrogated, voltammetric methods are the preferred choice to quantify electrochemical labels on an associated electrode

surface. Amperometric evaluation on the other hand are often used when amplification via catalytically active labels is chosen, e.g. enzyme-substrate amplification.[61] All the mentioned techniques in combination with certain transduction mechanisms can be categorized according to their mode of signal generation as turn-on or turn-off. This classification denotes how the signal is generated by the specific capturing event. Turn-off signals correspond to methodologies where the binding event triggers a blocking in signal (e.g., faradaic EIS with a solution probe), while turn-on signals denote techniques that correlate a recognition event directly to an increased signal generation (e.g., redox amplified sandwich assay). Turn-on signals are often preferred due to their lower susceptibility to non-specific interactions at the interface. In the following the techniques most relevant in this work will be discussed in more depth (i.e., voltammetry, amperometry, impedance spectroscopy).

1.2.3.1 Voltammetry: Cyclic Voltammetry and Differential Pulse Voltammetry

Voltammetric techniques, including cyclic voltammetry (CV) and differential pulse voltammetry (DPV), serve as powerful tools for studying redox processes at electrode surfaces and have found extensive applications in electrochemical immunosensors.[43] In CV, a linear potential sweep is periodically applied to an electrochemical cell, inducing potential redox reactions at the electrode surface. The resulting current response is measured as a function of the applied potential. For a reversible charge transfer reaction between the electrode and a redox species, the cyclic voltammogram exhibits a characteristic symmetric shape with distinct peaks for oxidation and reduction (c.f. Figure 1-3). CV offers advantages, including the quick elucidation of information about redox reactions, such as formal potential and electron transfer kinetics. This kinetic information can for example be used to evaluate the change induced by an interfacial

binding event, which is relevant in the context of sensing applications. Anodic and cathodic peak potentials (E_{pa}, E_{pc}) and their associated peak currents (i_{pa}, i_{pc}) are directly obtainable from the voltammogram, enabling quick and simple evaluation for sensing applications. In the context of electrochemical biosensors, CV is crucial for characterizing surface functionalization and the system's electrochemical properties. It has also been used for the direct quantification of on-surface binding processes together with labelled transduction approaches.

Differential pulse voltammetry (DPV), a derivative of linear sweep voltammetry, is renowned for enhanced sensitivity and resolution. In DPV, a series of discrete potential pulses is superimposed onto a linear potential sweep (see Figure 1-3), enabling sensitive detection of electroactive species in a solution while largely eliminating dielectric charging contributions. DPV is particularly relevant in electrochemical biosensors for detecting trace concentrations of electrochemically active species reporting on target analytes at the surface.[62] CV and DPV offer high sensitivity (down to nM ranges for redox species in solution, limited mainly by the capacitive currents),[63] rapid measurement times (in the range of seconds), and versatility in investigating redox processes and analysing electroactive species, making them essential in biosensor development.[64] Notably, sandwich-type immunoassays heavily rely on sweeping voltammetry methodologies like DPV to detect the electrochemical signal of the labelled secondary antibody. In this format, the signal increases with target concentration, representing a turn-on signal mode. However, there are examples where these techniques have been used in a label-free format, where the signal exhibits a turn-off character, typically associated with a decrease in peak current resulting from reduced electrode conductivity due to analyte binding to the surface.[65]

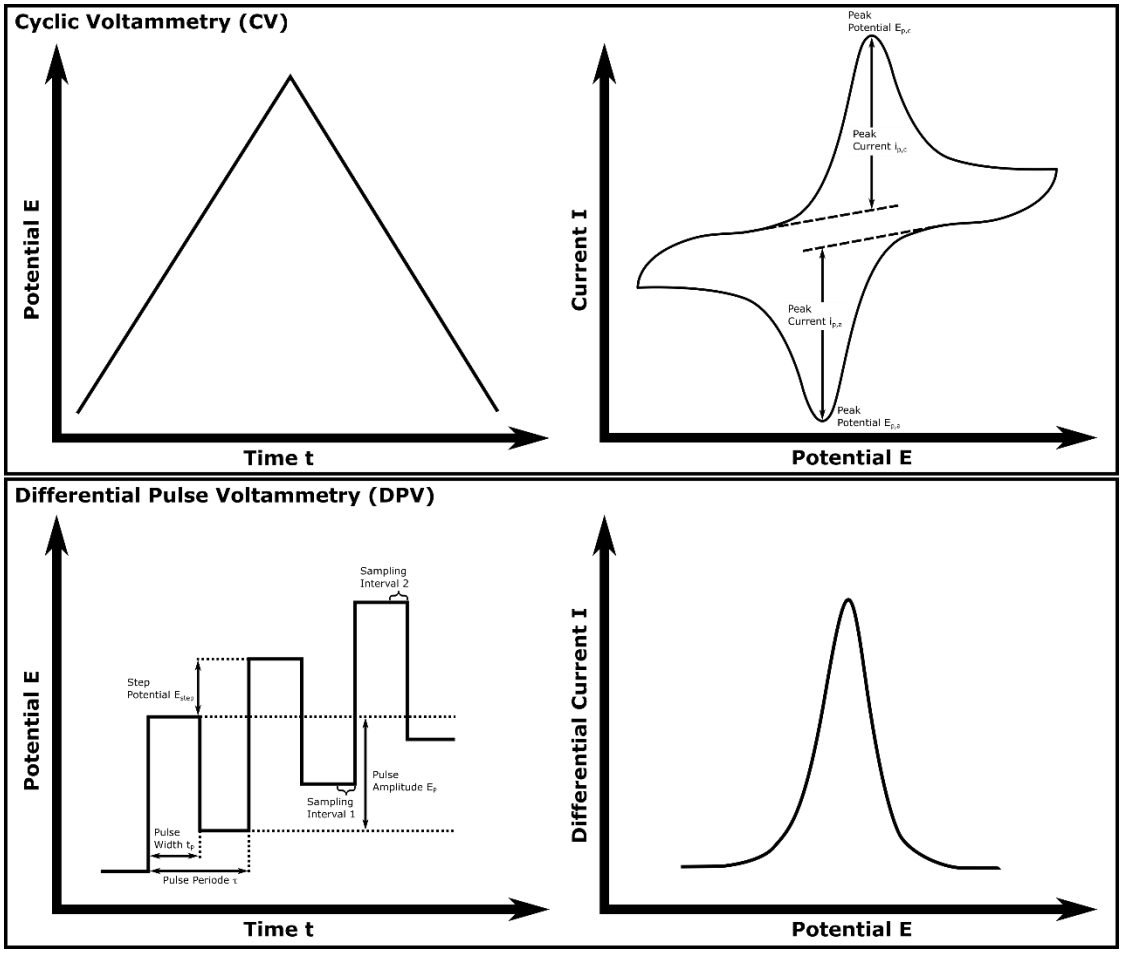


Figure 1-3 Schematic Representation of CV and DPV measurement techniques with electroactive species available for faradaic charge transfer with electrode. (Upper) Principle of cyclic voltammetry: Potential profile shown left is applied and corresponding current profile on the right is measured. (Lower) Principle of differential pulse voltammetry: Potential profile on the left is shown, the measured differential current (difference between measured current in sampling interval 2 and 1) is seen on the right.

1.2.3.2 Electrochemical Impedance Spectroscopy and Redox Capacitance Spectroscopy

Electrochemical Impedance Spectroscopy (EIS) involves applying an alternating current (AC) voltage to an electrochemical cell and measuring the resulting current response. The frequency of the AC signal is varied, allowing the interrogation of different timescales within the system. The impedance of the electrochemical system, comprising

resistance (real part, Z') and reactance (imaginary part, Z''), provides insights into properties such as charge transfer resistance, double-layer capacitance, and mass transport.[66] EIS, with its high sensitivity and ability to discriminate between electrochemical processes with different timescales (e.g., charge transfer, capacitive charging, diffusion limited processes),[67] is valuable in biosensors for investigating biorecognition element immobilization, monitoring binding events, and directly detecting target analytes. Considered an equilibrium method due to the minimal voltage variation applied (typically below 100 mV), it is suitable for sensitive biosensing applications, offering label-free detection without a secondary labelled antibody.[68] However, the interpretation of impedance data can be difficult, and the technique may be less suitable for real-time monitoring due to longer measurement times, depending on the specific setup and application. Typically, the Nyquist plot (c.f. Figure 1-4), showing the imaginary component plotted against the real component of the impedance for each observed frequency point, is evaluated. An equivalent circuit, representing the system as an electric circuit, aids interpretation.[69] The Randles equivalent circuit, commonly applied, features components for double-layer capacitance, charge-transfer resistance, and a Warburg element (resembling diffusive processes). The charge transfer resistance (R_{ct}) is evaluated as the diameter of a semicircle fitted to the charge-transfer-limited frequency range (see Figure 1-4). However, due to difficulties of choosing a suitable equivalent circuit and associated problems in fitting of the data, it is often preferred to just use the real part of the impedance at the inflection point directly as the charge transfer resistance.[70]

EIS enables the label-free protein quantification and has been used extensively for the development of electrochemical protein immunosensors.[68] In this label-free

configuration, an increase in charge transfer resistance reports on analyte binding to the surface, as the bound protein form a physical barrier hindering charge transfer. This mode provides a signal with turn-off character as the exchange of charge is diminished with increasing analyte concentration.

Recently another derivative of EIS has emerged using the spectroscopic technique to interrogate an on-surface redox probe (referred to as redox capacitive transduction in the above).[71] The impedance is hereby transformed to the complex capacitance according to Eq. 4 (see section 2.6.2). The inflection points of the semicircle in a capacitive Nyquist plot then determines the redox capacitance (C_r, c.f. Figure 1-4). If C_r is evaluated at two distinct potentials, one inside of the redox active window of the on-surface redox probe (ideally the half-wave potential) and one outside (c.f. Figure 1-4), the difference between the real capacitance at these two potentials (referred to as the differential redox capacitance ΔC_r) again changes upon interfacial binding on the electrode surface in close proximity to the redox probe. It has been demonstrated that this can be used as a turn-off signal for reagent-less sensing in multiple approaches.[72]

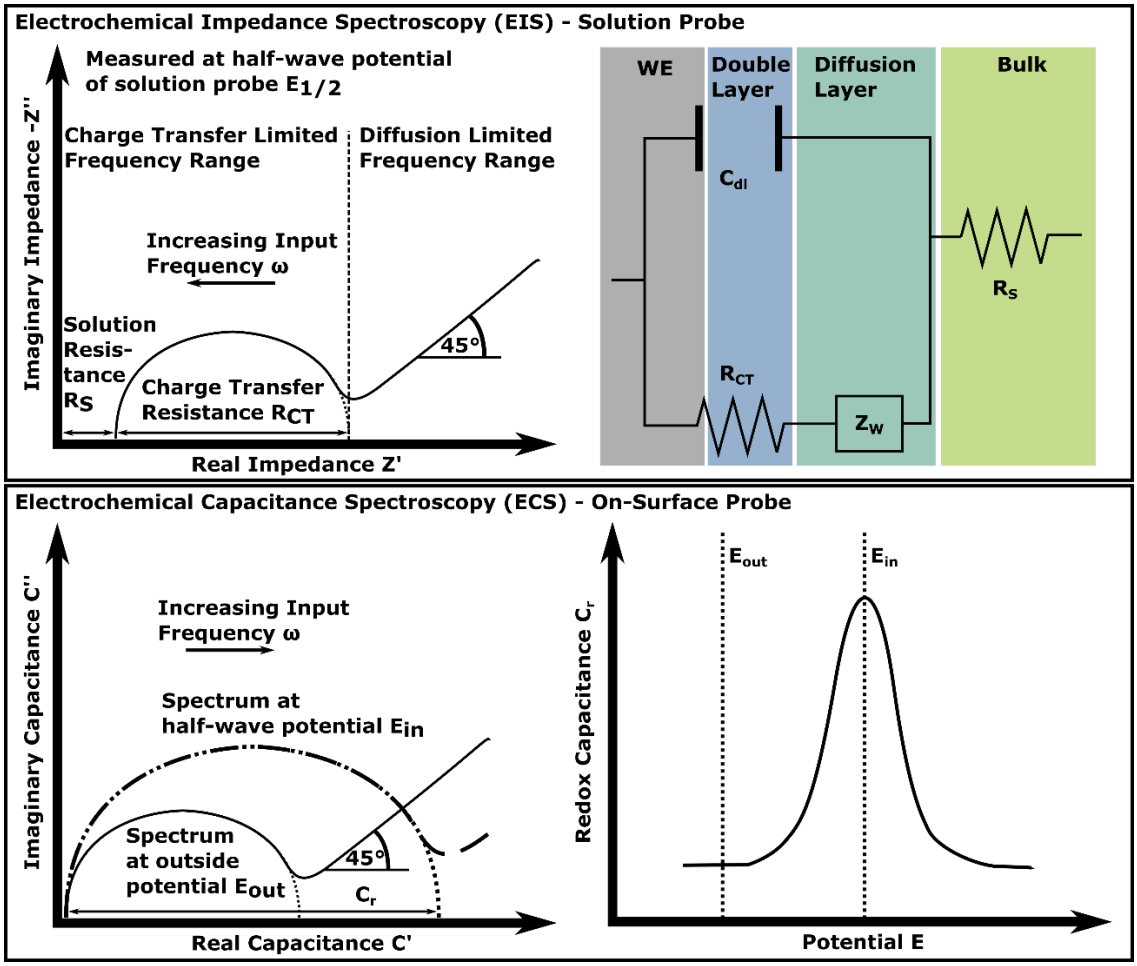


Figure 1-4 Schematic represantation of Electrochemical Spectroscopy Concepts. Upper frame: EIS spectrum as expected for solution probe in charge exchange with working electrode and the associated Randles equivalent circuit. Lower frame: Capacitive spectra as expected for a surface-tethered redox probe accessible for charge transfer from the working electrode recorded at potentials in and outside the charge transfer window and an associated capacitance-potential plot.

1.2.3.3 Amperometry and Enzymatic Amplification using the HRP-TMB couple

Amperometry is an electrochemical technique centred on measuring current at a constant applied potential. Current is recorded over time, offering insights into the kinetics of redox reactions at the electrode surface. The fundamental concept underlying amperometry is Faraday's law of electrolysis, which relates the quantity of charge transferred to the number of moles of a specific substance produced in a charge

transfer reaction at the electrode. Amperometry plays a pivotal role in the field of electrochemical biosensors in particular due to its relevance in amplified formats. Its benefits include high sensitivity, rapid response times, and the ability to operate under physiological conditions. Its ability to provide quantitative data in real-time makes it well-suited for continuous monitoring and point-of-care diagnostics. A commonly applied context is the evaluation of the enzymatically amplified assays. A relevant example for such application in the context of the presented work is the Horseradish-Peroxidase (HRP) catalysed oxidation of Tetramethyl Benzidine (TMB) in combination with the reduction of oxidised TMB at the electrode.[73] This reaction cycle leads to a current that theoretically depends on the number of HRP molecules available for catalysis, which has been used for the amplification of biorecognition events in sandwich type assays before.[74] This HRP-TMB amplification will be discussed in more detail in Chapter 3, where it is used extensively.

1.2.4 Recent Advancement in Facilitation and Scalability of Electrochemical Immunosensing Technologies

1.2.4.1 Microfluidic Integration of Electrochemical Immunosensors

Microfluidic integration of electrochemical sensing strategies has become a widespread approach to reduce manual sample handling, turnaround time, and required volumes, while increasing repeatability and standardisation.[75] Various techniques for designing microfluidic devices have been presented,[76] with one notable concept being the use of paper-based setups in combination with miniaturized electrodes, known as electrochemical paper-based analytical devices (ePADs). EPADs are cost-effective, self-pumping due to paper properties, and facilitate easy handling of small sample volumes,

offering disposable devices.[77] Another approach involves fabricating microfluidic setups from polydimethylsiloxane (PDMS), providing high-precision microchannels for reusable fluidic setups.[78] A recent technique gaining favour is the 3D printing of microfluidic devices, offering precision at favourable costs and time requirements.[79] In the context of this work the latter is used to build microfluidic appliances customised to the needs at hand (see 2.5).

1.2.4.2 Screen-Printed-Electrodes for Electrochemical Immunosensing

Simultaneously, disposable, inexpensive, and miniaturized electrodes have been developed to meet the demand for integrating electronics into miniaturized, disposable setups, including microfluidically integrated sensor concepts. A prominent and promising strategy is the fabrication of screen-printed electrodes, where carbon or gold inks are printed onto a flexible support.[80] These inks typically contain particles, a polymeric binder, and additional additives.[81] Current efforts are focused on applying electrochemical immunosensing principles to such screen-printed disposable electrodes. This amalgamation holds vast potential, promising to enhance the scalability and applicability of electrochemical immunosensing strategies further. In the context of chapter 3, the proposed assay is applied to screen-printed-carbon electrode arrays to showcase the applicability.

1.2.5 Current Challenges in Electrochemical Immunosensing

The research on electrochemical immunosensors has grown over the past decades, with current studies aiming to solve key challenges to advance sensing platforms for widespread global application.[48] The primary research focus is on enhancing electrochemical immunosensor technologies for decentralized point-of-care

applications.[82] The inherent properties of electrochemical methodologies, such as high sensitivity, low construction costs, simplicity, ease of use, and portability through miniaturization, make them suitable for such applications.[60] However, specific applications may require additional properties, driving efforts to develop techniques, methodologies, or modifications to meet current requirements. The most challenging questions to be addressed by current research include the suppression of signals arising from non-specific adsorption,[59] the stability of electrode functionalisation layers,[83] as well as the simultaneous quantification of multiple analytes, i.e. multiplexability.[84] Fundamental progress within these topics has the potential to revolutionise the current state of the art in biosensing and would come with major implications for its application in point-of-care settings. Other current research in the field spans the molecular resolution characterisation of sensing surfaces,[85] the ability to continuously quantify analyte concentrations in real-time,[83] and nanomaterial based signal amplification strategies,[86] among others.

1.3 Protein Fouling and Currently Employed Anti-Fouling Strategies

1.3.1 Native Protein Adsorption at Electrode Surfaces

The need for preventative methods to reduce the native adsorption of biomaterial onto surfaces has already been mentioned by Plutarch,[87] but has been known to cause problems for maritime transport within cultures of Phoenicians and Carthaginians as early as 1500 - 300BC.[88] While at late stages this includes the adsorption of major maritime organisms, causing significant costs for the maritime industry even today ($56M per year alone for the US Navy in 2010),[89] at an early stage so called biofouling is mainly driven by small molecules and proteins.[90] Any surfaces submerged in solutions

containing organic substances is subject to such biofouling and as such it poses a major challenge to electrochemical biosensors working in real-world samples due to the interference of non-target protein in signal generation.[91] The native adsorption of protein from complex samples such as serum or saliva onto surfaces has been studied thoroughly throughout the last decades.[92-94] Nevertheless, the mechanisms are still not fully elucidated and remain debated.[95] The main principles driving protein adsorption at solid surfaces are an entropic gain caused by conformational changes in protein upon adsorption as well as hydrophobic contributions from rearrangements of water molecules and salt ions at the solid-liquid interface, electrostatic interactions and to a lower degree also by hydrogen bonding and dipolar interactions.[96, 97] Therefore, the adsorption dynamic is influenced by factors such as temperature, pH, ionic strength, buffer composition and protein concentrations,[98] as well as the structure of the protein and the liquid-solid interface[97], but also other factors like the protein size.[99] The adsorption of proteins to electrode surfaces will constitute a major part of Chapter 3 and is used for Chapters 4 and 5.

1.3.2 Current Anti-fouling strategies in Electrochemical Immunosensing

Surface functionalization to suppress fouling at the liquid-solid interface is a significant focus of research in the electrochemical biosensing field.[100] Decreasing signal interference arising from non-specific protein adsorption is considered a crucial challenge for achieving higher applicability in real-world scenarios and point-of-care settings, particularly in label-free and reagent-less approaches.[101, 102] The main principle for any surface functionalisation aiming to reduce non-specific protein adsorption is based on employing highly hydrated surface structures minimising the entropic gain resulting from colloidal surface adsorption.[59] Various strategies towards reducing non-

specific adsorption at electrode surfaces have been proposed and studied including nanoengineered surfaces, membranes, hydrogel functionalisation or anti-fouling layers.[103] One of the most commonly employed strategies is the utilisation of polymeric or oligomeric structures tethered to the surface to provide hydrated layers resistant to fouling.[104] However, even the most efficient anti-fouling coatings are not able to prevent non-specific protein adsorption completely. This is even more the case as the surface of sensing platforms usually must not only include anti-fouling but also recognition elements to render the interface capable of sensing a specific analyte as discussed earlier.

Proteins themselves are known to possess non-fouling capabilities. This is due to their zwitterionic properties.[105] For this reason, a common and simple approach to prevent non-specific adsorption is to backfill the surfaces functionalised with recognition elements with proteins themselves to quench any remaining sites. Various proteins have been employed to form protective layers on sensor surfaces in a so-called backfilling approach leveraging the native tendency of proteins not to adhere to each other. Protein backfilling involves the formation of a protein layer on sensor surfaces to create a barrier that deters non-specific protein adsorption.[106] This approach capitalizes on the specific binding properties of proteins and their ability to occupy surface sites, thereby reducing the availability of binding sites for non-specific interactions later on. The success of protein backfilling relies on selecting proteins with desirable characteristics, such as stable adsorption and minimal interference with the target analyte. Numerous proteins have been explored for anti-fouling purposes, each offering unique advantages in specific applications. Bovine Serum Albumin (BSA), a commonly employed protein, is known to form a compact monolayer on surfaces, thereby creating a robust barrier

against non-specific protein adsorption.[107] BSA has commonly been used for its non-fouling capabilities in a multitude of proposed designs for electrochemical immunosensing platforms.[108-111] Park et al. reported on improved passivation of silica surfaces via denatured BSA over non-denatured BSA.[112] Ma et al. found soy bean protein to possess anti-fouling properties towards different proteins like BSA, fibrinogen or lysozyme depending on pH and salt concentration.[113] Also, other protein has been shown to exhibit some anti-fouling properties towards fibrinogen, Human Serum Albumin(HSA) and bacterial cells.[114, 115]

1.4 Functional Protein Film Formation on Plain and Self-Assembled Monolayer Functionalised Electrode Surfaces

Current electrochemical biosensor development relies mainly on functional interfaces capable of interacting specifically with the target protein biomarker. For immunosensors considered here, these functional interfaces always consist of an antibody tethered to the surface. In many cases additional functionalities, such as the anti-fouling agents mentioned in 1.3.2, are incorporated into the surfaces alongside the recognition elements. The strategies to anchor antibodies to glassy carbon and gold electrodes are introduced in this section.

1.4.1 Strategies for protein film formation on plain electrodes and Protein modification via EDC/NHS carbodiimide chemistry

As summarised in 1.3.1, proteins tend to adsorb at surfaces natively and this effect itself can be exploited to form functional films. Many examples of electrode modification through physisorption have been reported for the design of electrochemical

immunosensors. A common approach is the direct adsorption of antibodies to electrodes such as gold or carbon from a solution phase by prolonged exposure.[116] Similarly, protein interactions like the well-established Streptavidin-Biotin have been used to tether antibodies to films of physiosorbed proteins.[117] However, the tendency to physisorb at electrode surfaces is not restricted to proteins, but is observed for many classes of molecules. Therefore, another strategy for the formation of bio-functionalised electrode surfaces uses the adsorption of intermediate molecules which can then be chemically modified with antibodies. A third option is the use of chemical linkers that chemically bind to the surface and are then modified with antibodies in a subsequent step.[118] A prominent example of such chemical attachment of linker molecules is the sulfide bond-driven chemisorbtion of carboxy terminated alkanethiols to gold surfaces creating so called Self-Assembled Monolayers, which will be discussed in more detail in the next section due to their specific relevance in the context of this work. The most common moiety to be integrated for further functionalisation in this way are carboxylic acid residues. These end groups present an excellent target for further modification with proteins including antibodies via amide bond formation with amine residues on the proteins using carbodiimide chemistry.[119] The most commonly employed agent to mediate this carbodiimide coupling within biosensing is N-(3-dimethylaminopropyl)-N'-ethylcarbodiimide (EDC), which is commonly employed together with N-hydroxysuccinimide (NHS) to accelerate the reaction rate and increase the coupling efficiency. EDC activates carboxyl groups within one molecule, initiating their interaction with primary amine groups present in the other molecule, resulting in the formation of an amide bond. NHS participates in a chemical reaction with carboxyl groups, leading to the creation of a stable amine-reactive NHS ester intermediate. This intermediate can

then couple with primary amines under physiological pH conditions. The NHS-generated intermediate exhibits enhanced stability in comparison to the O-acylisourea produced when relying solely on EDC. Consequently, NHS is commonly used in combination with EDC for amide bond coupling. It's important to note that neither of these compounds leaves any residual elements within the final conjugate structure, effectively making these molecules zero-length cross-linkers.[120] Notably, preformed NHS conjugates can be utilised to functionalise proteins as has been done to introduce for example electroactive motives.

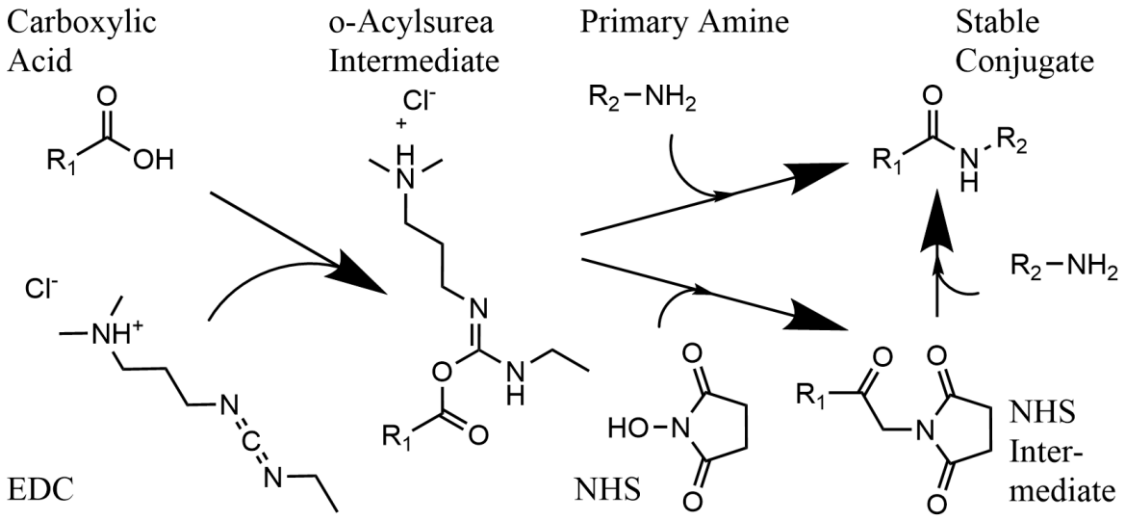


Figure 1-5 EDC/NHS mediated amide coupling between a carboxylic acid on one molecule and a primary amine on another molecule. Hydrolysis is not shown within the schematic.

1.4.2 Self-Assembled-Monolayers (SAMs) of 1-Hexanethiol and 6-Mercaptohexanoic Acid and Azurin Protein Electrochemistry on Alkanethiol SAMs

Self-assembled monolayers (SAMs) on gold surfaces have attracted significant attention in various fields, particularly electrochemistry and surface science, due to their remarkable properties and versatile applications. Among the diverse range of molecules

used to form SAMs, 1-hexanethiol (HT) and 6-mercaptohexanoic acid (MHA) have emerged as prominent candidates. These molecules play a pivotal role in modifying gold electrodes, affecting their surface properties and, subsequently, influencing electrochemical behaviour. This section provides a discussion of SAMs formed by hexanethiol and mercaptohexanoic acid on gold electrodes, exploring their preparation, structural characteristics, and electrochemical implications. SAMs on gold electrodes are generally formed by the spontaneous adsorption of organic molecules from a solution onto the gold surface.[121] Hexanethiol (C6H13SH) and mercaptohexanoic acid (C6H12O2S) are both alkanethiols and are known for their high affinity to gold surfaces.[122] The process of forming SAMs involves immersing a clean gold electrode into a dilute solution of the thiol molecules, allowing them to self-assemble onto the gold surface. The molecules form a densely packed, well-ordered monolayer on the gold surface. The gold-thiolate bond results from the S-Au interaction leading to chemisorption of thiols on gold surfaces.[123] This interaction leads to the formation of a highly organized and robust SAM with a well-defined packing density. Hexanethiol SAMs on gold surfaces have been extensively studied, and their structural characteristics are well-documented.[124] MHA is a prominent example of molecule used to introduce carboxylic acid functional groups to SAMs, making them relevant in sensing and molecular surface design.[125] The formation of SAMs on gold electrodes significantly influences their electrochemical properties. The densely packed and highly ordered structure of such functionalisation offers a barrier to electron transfer, resulting in slower electron transfer kinetics. This property has been exploited in applications such as molecular electronics. On the other hand, the carboxylic acid functionality of MHA SAMs can facilitate the immobilization of biomolecules and other ligands, making them

valuable in biosensing applications.[126] In summary, self-assembled monolayers on gold electrodes, particularly those formed by hexanethiol and mercaptohexanoic acid, offer a versatile tool for the modification and tuning of the physical properties of electrode interfaces.

An important example for the deployment of SAM surfaces in the context of this work is the use of such films for the study of protein electrochemistry. In particular, the irreversible physisorption of the electroactive protein Azurin on alkanethiol SAMs, which has been studied in depth throughout the last decades. As a presumed physiological electron transfer partner for cyt c_{551},[127] Azurin belongs to the group of small blue copper proteins.[128] The 14600 kDa protein contains a type I Cu site coordinated by two histidines, one cysteine and one methionine. The electron transfer in Azurin is mediated through a hydrophobic patch close to the Cu centre which sits inside the protein with a distance to the protein surface of around 0.7 nm.[129] It was shown by Gaigalas & Niaura, that Azurin that has been adsorbed on hexanethiol SAMs formed on polycrystalline gold electrodes, maintains its structure and that the copper centre in this way is accessible from the underlying electrode with a half wave potential of 94±8 mV vs Ag/AgCl.[127] Multiple reports confirm the adsorption of Azurin on alkanethiol SAMs, where the protein has been shown to orient its redox centre towards the surface (c.f. Figure 1-6) due to the hydrophobic patch close to the redox centre, which implies a favourable orientation for electron transfer.[130-133]

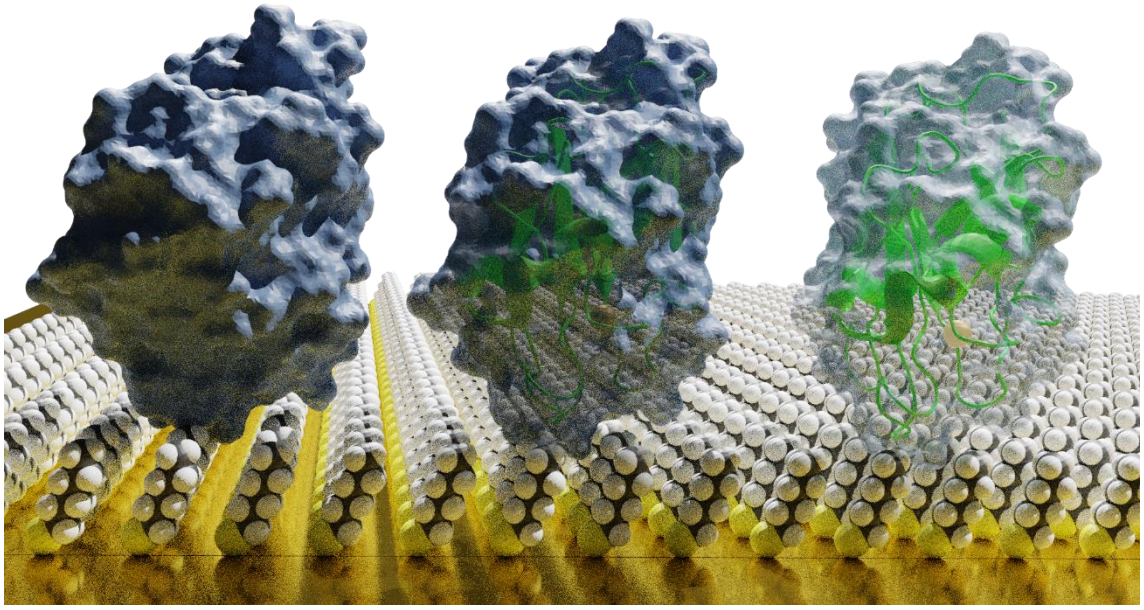


Figure 1-6 Schematic depiction of oriented assembly of the blue copper protein Azurin from *P. aeruginosa* onto a SAM of hexanethiol. The protein adsorbs favourably to the methyl residues via its hydrophobic patch on one of its sides rendering the copper centre accessible for electron transfer from the electrode surface.[134]

1.5 Quantification of CRP and cTnI – Current Transduction Approaches and the Need for Innovative Assay Methodologies

1.5.1 CRP and cTnI – a Suitable Model System for the Development of Diagnostic Platforms

Globally, cardiovascular diseases (CVDs) represent a leading cause of mortality and account for about 18 million deaths per year.[135] A large proportion of both fatal and non-fatal atherosclerotic CVD episodes occur in patients without any previously diagnosed CVD, whilst nearly half of patients with acute myocardial infarction (AMI), and one-third of those who die from sudden cardiac death, also have no previously diagnosed CVD.[135] The early identification of at-risk individuals represents, then, both a major healthcare

challenge and an opportunity. While an assessment of relevant biomarker concentrations in blood samples is often considered as part of CVD diagnosis, it may also present a much-needed predictive indicator for undiagnosed, at-risk, individuals. Among other markers, the combined quantification of C-Reactive Protein (CRP) and cardiac Troponin I (cTnI) has shown promising diagnostic value for CVD related diseases.[136-139]

Apart from their combined diagnostic value in CVD circumstances, CRP and cTnI are known for their high relevance in clinical application and have commonly been used as model proteins throughout sensor development. CRP is a pentameric, ring-shaped plasma protein primarily excreted by the liver.[140] The monomer contains 206 amino acids and a molecular mass of 23 kDa.[141] The measurement of CRP has a wide range of clinical application for its non-specific nature as a general biomarker for inflammation elevated levels of which imply, amongst other things, an increased risk of MI, sudden death, stroke and general vascular disease, but also autoimmune diseases or even viral infections.[142, 143] In healthy individuals, the serum concentration of CRP is reported to be around 2 µg mL^{-1},[144] which can increase 6-fold in cases of acute myocardial infarction,[145] while in severe cases it can rise to levels as high as 500 µg mL^{-1} with a half-life of about 19 h.[146] The concentration of blood CRP has been shown to correlate with different levels of cardiac risk as follows: CRP levels of <1 mg L^{-1} are associated with lowest risk, 1-3 mg L^{-1} intermediate risk, and levels >3 mg L^{-1} represent the highest risk.[147] CRP is, therefore, an effective marker for the early detection and implementation of therapeutic intervention for cardiovascular disease (CVD) and remains one of the most commonly applied molecular tests in clinical practice.[148] Especially in the context of CVD prevention, constant monitoring of CRP could prove to be crucial in future healthcare settings.[149]

Cardiac Troponin I (cTnI) is expressed solely in cardiac muscle rendering its serum levels a highly specific indicator of cardiac injury.[150] It belongs to the larger group of cardiac Troponins including cTnT, cTnI and cTnC,[151] and is a small protein of 209 amino acids with a mass of 24 kDa suspected to remain largely unordered (without a stable quaternary structure).[152] The median values for serum concentration of cTnI ranges around 0.003 ng mL^{-1} and a disease relevant cut-off is often considered the 99th percentile at 0.055 ng mL^{-1},[153] but levels can rise rapidly within the first 4 hours after myocardial injury up to roughly 196 ng mL^{-1} and persist at elevated levels for up to 10 days.[150] Research on the association of cTnT and cTnI with CVD shows that elevations in the latter are more strongly related to CVD outcome, with cTnT data more strongly linked to non-CVD mortality.[154, 155]

As mentioned in the above, assays for the quantification of CRP and cTnI in patient serum are standard clinical procedures and therefore provide well suited examples to analyse the current state and future needs for such application.[156, 157] Furthermore, the two markers are frequently used throughout sensor research providing a basis facilitating the comparison between different methodologies.

1.5.2 Currently Available Platforms for the Clinical Quantification of CRP and cTnI

A broad range of methods for the detection of CRP in the range of 0.01 to 10 mg L^{-1} including immunonephelometry, immunoturbidimetry, high-sensitivity enzyme-linked immunosorbent assay (ELISA) and resonant acoustic profiling (RAP) have been the first to be developed.[158] In the mid-1990s, the so called high-sensitivity CRP (hs-CRP) ELISA assay was developed for a better assessment of the lower serum concentrations of CRP

relevant to an assessment of heart disease and stroke risk.[142, 159, 160] Even today, ELISA assays remain the gold standard for clinical CRP quantification.[8]

Similarly, clinical cTnI detection has been under development for decades. The radioimmunoassay (RIA) was the first detection method developed for the measurement of serum cTnI with an associated turn-around-time (TAT) of 2 days and an LOD of 10 ng mL^{-1}.[161] At a similar time, a study on serum troponins led to the development of a first-generation immunoassay using a new one-step enzyme immunoassay (with a measuring range of 0.1–15 μg L^{-1}).[162] The subsequent fourth generation of this assay significantly improved the performance in serum media (LOD of 10 ng L^{-1}).[163]

When considering the performance of an analytical method for any point-of-care (POC) application, practicality and reliability are essential. In general, these depend on the required operator skill levels, turnaround time (TAT) (i.e., speed of analysis), sample type and volume, as well as assay precision, limit of detection, and dynamic range.[164] Current commercially available systems for clinical CVD assessment have been summarized in detail in a comprehensive review.[149] The Alpha Dx System, VIDAS® Emergency Pane, Cobas h232 System, Triage Cardiac Panel, FIA 8000/Getein 1100 Analysers are notable 'lab-on-chip' devices utilising immunochromatography, fluorescent-, radio-, chemiluminescent-, and optical immunoassay methodologies. Most of the aforementioned commercial devices, with diverse transduction, enable fast detection (≤30 min) using a relatively low volume of human samples (<300 μL). However, these systems whilst useful, are still limited in POC applicability by the cost and size of equipment, as well as the specialist skills and logistics required.[165] As the most relevant

POC devices the i-STAT, Minicare I-20, and Cobas h232 currently provide the few handheld tools available for the clinical diagnostics of CVDs.[149] These devices target only a limited set of single cardiac biomarkers not including CRP. The high cost of the disposable cartridge used (ranging around a few hundred US dollars each) remains a major obstacle for their widespread adoption.

It is well known that CVDs disproportionately affect economically disadvantaged populations often situated in more remote regions.[149] This can largely be attributed to factors including access to care, differential treatment, and referral patterns as well as patients' socioeconomic status.[166] Especially in light of these facts, methodologies that can further reduce the hurdles for sufficient access to healthcare and early diagnostics are considered potential game changers. Due to their distinct properties mentioned in 1.2.1, electrochemical methodologies are expected to be of major importance for future solutions to such healthcare challenges. Nevertheless, devices for the electrochemical quantification for the system of biomarkers of CRP and cTnI meeting the clinical guidelines are currently not commercially available, despite the significance of this marker system.[167]

1.5.3 Current Research Towards the Electrochemical Quantification of CRP and cTnI

Most current research towards the development of electrochemical platforms for the quantification of CRP and cTnI focuses on immunosensors with improved sensitivity and levels of detection readily applicable in point-of-care settings. Label-free assays have gained much attention within recent years due to the more facile handling and potential in reducing cost. The most commonly employed approach for label-free quantification relies on measurements of charge transfer resistance of a solution redox probe across

an electrode in an impedance-based setup as introduced in 1.2.2. Frequently, self-assembled monolayers (SAMs) are utilised to functionalise gold electrodes with antibodies to render them receptive for target capture. Johnson et al. demonstrated the superiority of antibodies for the detection of CRP on such a platform via EIS early on.[168] The same group addressed the problems arising from drift in such setups by using elaborated equilibration protocols yielding quantification of CRP down to 0.2 µg mL^{-1} in buffer.[169] Recent examples include the utilisation of a SAM of 4-mercaptophenyl boronic acid (4-MPBA) for antibody anchoring to quantify CRP in buffer down to concentration in the range of few µg mL^{-1}.[170] Utilising the formation of a SAM of L-Cys on gold-nanoparticles, Boonkaew et al. demonstrated the quantification of CRP in serum down to 5 µg mL^{-1} on graphene-modified screen-printed-carbon-electrodes functionalised with SAM coated gold nanoparticles for antibody immobilisation.[171]

Another common approach is the physisorption of receptive molecules onto the electrode surfaces often accompanied by blocking with common proteins like BSA (as introduced in 1.3.2). Oliveira et al. showcased such a platform using screen-printed gold electrodes to quantify CRP in serum down to concentrations of 0.78 µg mL^{-1} using EIS as well as DPV in a solution of ferrocyanide.[172] In another example of this, graphite electrodes with electrochemically reduced graphene oxide deposited onto them and a subsequent functionalisation via polymerisation of tyramine were utilised. Antibodies were physisorbed on the so formed electrode surfaces and DPV in a ferrocyanide solution employed to quantify CRP in human serum down to concentrations of 1.09 µg mL^{-1}.[173] Various nanomaterials have been utilised in a similar manner in combination with physisorbed antibodies to produce interfaces for the impedance-based quantification of CRP. Nanomaterials are also used in combination with chemical

coupling of antibodies to yield sensing electrodes. This approach has for example been demonstrated in a study employing a ZnO/porous carbon compound on carbon paste electrodes with subsequent EDC/NHS coupling of antibodies onto free carboxyl groups on this composite to quantify CRP impedimetrically (using DPV).[174] The use of polymer grafted from or onto electrode surfaces is another approach that recently gained attention for improving the performance of resistivity-based approaches. Notable examples for such platforms for the detection of CRP include the deployment of a pHEMA brush grafted from a polycrystalline gold electrode surface subsequently functionalised with antibodies to yield the detection of CRP in 5% FBS at a concentration as low as 0.9 µg mL^{-1} via EIS measurements in a ferrocyanide solution.[175]

In an effort to further facilitate the assays requirements by omitting the spiking of the sample with a solution redox probe, together with their colleagues Davis and Bueno introduced redox capacitive assaying as a so called reagentless technique.[176] A recent example of the application of this technique for the quantification of CRP has reported the use of an electroactive polymer layer modified with antibodies for a reagentless assay with an LOD of 0.5 µg mL^{-1}.[58] Similar efforts have been made for the quantification of cTnI in label-free strategies.[177] In contrast to label-free methods, the current research on label-based strategies for CRP and cTnI quantification mainly examines the use of secondary antibodies tagged with labels (e.g., redox species, nanomaterials, enzymes) to amplify the signal transduction.[177] Additionally much effort is focused on the development of elaborated electrode surface modifications to boost sensitivity and specificity in both label-free and labelled approaches to cTnI and CRP detection.[167]

1.5.4 Demand for Novel Sensing Platforms for Future Point-of-Care Application

The summary above shows that there is a need for sensing methodologies that can tackle future healthcare challenges mainly concerning the early and broadly applicable screening of patients in a decentralised and accessible format. As indicated earlier, electrochemical sensors are thought to possess many advantageous properties rendering them highly promising to provide solutions to such challenges. The current state of research of electrochemical immunosensors for CRP and cTnI is mainly focusing on improving the performance of already established sensing protocols that classify as either resistivity-based, sandwich-based or capacitance-based as summarized in 1.2.2. Although there are versatile concepts being introduced to improve the currently available methodologies, little effort is made towards the development of more innovative sensing methodologies that expand the current landscape of available concepts. Moreover, most current research focuses on the use of nanomaterials and specifically designed surfaces to improve the capabilities of established platforms. Although these efforts have produced valuable achievements with regards to sensitivity and specificity, the use of such sophisticated protocols in sensor development also increases the cost and complexity of the designed platforms. Simplicity, however, is a key factor in transferring bench-top methodologies to the world outside a lab, especially when things like home or remote point-of-care testing are considered. This creates a gap for the development of electrochemical sensor methodologies that shift complexity away from the surface design and provide a facile preparation as well as the potential for simple storage and transport of platforms. The early diagnosis of CVD provides a prime field of application for such methodologies as the potential impact for society is of significant measure, hereby as outlined earlier the biomarker couple of CRP and cTnI

provides a useful model system to test novel methodologies such as introduced in this work.

1.6 Thesis Aims and Scope

This thesis addresses the urgent need for innovative electrochemical methods to enhance the quantification of protein biomarkers. Current research mostly focuses on refining existing electrochemical assay methods, particularly through nanomaterial and molecular functionalization to increase sensitivity and specificity in immunosensor designs. While these contributions are valuable, the improvements remain constrained by the underlying assay methodologies. It is important to explore unconventional techniques, so that more disruptive solutions to future challenges can be found within the realm of biosensing methodologies. Furthermore, for the successful application of the full potential yielded by electrochemical immunosensors in future healthcare settings, scalability will be of uttermost importance. In today's market driven society, a solution will only be adoptable and beneficial for a wider society, if its production, distribution and application can be rendered facile and accessible. For these reasons the work proposed within this thesis focuses on the explorative development of novel immunosensor technologies. Rather than the optimisation and maximisation of distinct parameters like the sensitivity within certain settings, it is the aim of this thesis to expand the realm of available immunosensor techniques with facile application and scalability in mind. In section 1.2.2 it was concluded that there are three distinct approaches that the great majority of current methodologies can be categorized into, namely sandwich-type, resistivity-based and redox-capacitive assays. This work aims to introduce three distinct approaches each with the goal to pose a simple and scalable

solution for electrochemical immunosensing of protein biomarkers. The overarching aim is to extend the realm of biosensor techniques, bridging gaps left by current methodologies to offer new perspectives that allow to tackle some of the challenges in the field of point-of-care testing (POCT). This is done with a focus on cardiovascular markers for the particular examples introduced, but it is the set goal to explore the techniques as generally applicable solutions to current challenges in sensing rather than focussing solely on the two disease markers investigated. The current landscape of biosensors, and in particular for CVD biomarkers, faces several challenges, including sensitivity, specificity, complexity in design, robustness, stability, ease of handling, time requirements, and multiplexing capabilities. Where scalability of a sensor is mainly defined by the simplicity and stability of design, minimised handling requirements and multiplexability. Beyond laboratory settings, the real-world applicability of biosensors is crucial for their successful implementation in clinical settings. The thesis will prioritize the development of methodologies that consider practical constraints and facilitate seamless integration into routine clinical practice. It is important to acknowledge the boundaries of this research: While this thesis focuses on the practicability of the introduced methodologies, the development of fully mature, market-ready biosensors certainly extends beyond its scope. Similarly, as it is the declared aim of this work to explore novel concepts, it is not within the limits to arrive at fully optimised versions of any of the proposed technologies. Rather than claiming completeness, this work presents concepts that are meant to stimulate further exploration and adaption as well as optimisation and combination with established technology.

For this purpose, three separate concepts will be explored, each of which is based on the formation of a protein film on the sensing electrode. First, the electrochemical

implementation of a dot blot assay will be explored. This approach relies on the direct absorption of proteins from a complex sample and the subsequent specific capture of labelled antibodies by the target proteins within this film. The idea behind this concept is to omit any electrode modification while shifting any reagents including recognition elements entirely to the fluid phase to simplify electrode preparation, storage and handling. Secondly, the electrochemical implementation of a shotgun-tagging based assay will be investigated. This concept is based on the random, non-specific tagging of proteins in a complex sample, followed by the specific capture of target protein on an electrode carrying a film of target antibodies. The driving principle for this idea is to omit the use of a labelled recognition elements while retaining the advantages of a signal turn-on assay. Simultaneously, the proposed concept aims to achieve a multiplexable assay while omitting specific label generation and cost. The third concept being explored evolves around the use of the electroactive protein Azurin as a transducing and anti-fouling building block for a protein film-based redox capacitive immunosensing platform. The idea guiding this investigation is the combination of non-fouling and transducing elements in a readily available unit, which as a protein possess inherent stability in complex physiological samples, for the implementation of a reagent-less immunosensory platform.

Chapter 2

Materials and Methods

2.1 Materials and General Considerations

Unless stated otherwise, all chemicals mentioned were purchased from commercial suppliers and used as received. Bovine serum albumin (BSA), human serum albumin (HSA), fetal bovine serum (FBS), Myoglobin, Fibrinogen and human serum were purchased from Sigma-Aldrich and used as obtained. Biotinylated mouse anti-human CRP monoclonal antibodies (MCA6187B) (referred to as Biotin-Ab) and native human CRP (1707-2029) were purchased from BioRad. Methylene blue-NHS ester was purchased from Glen Research and used as provided. Nafion 117 4% solution in a mixture of lower aliphatic alcohols and water was purchased from Sigma-Aldrich and used as obtained. Goat anti-human CRP polyclonal antibodies (1707-0189G) and native human CRP (1707-2029) were purchased from BioRad. Anti-cardiac troponin I antibody (M155) (ab10237) and recombinant human cardiac troponin I (cTnI) protein (ab207624) were purchased from Abcam. Poly-HRP(80)-Streptavidin conjugates (65R-S105PHRP-FIT) (herein p-HRP) were purchased from Stratech Scientific Ltd and Biotin-Abs as well as p-HRP were used at a concentration of 250 ng mL^{-1} in 10 mg mL^{-1} BSA in PBS throughout. TMB high sensitivity substrate solution (herein TMB solution) containing H_2O_2 was purchased from BioLegend and used as obtained. Wild type Azurin from *P. Aeruginosa* was ordered from Sigma-Aldrich and diluted to 1 mg mL^{-1} in 20mM MES

buffer at pH 7.0, frozen in liquid nitrogen and stored at a temperature of -80°C until use according to a common protocol.[178] All other chemicals were purchased from Sigma-Aldrich/Aldrich/Merck and used as received.

Ultrapure water used throughout any experiments was purified to a resistivity of 18.2 MΩ cm via a Milli-Q System (Milli-Q Direct/Merck Millipore). Ratios are reported by volume (v/v) for all solvent mixtures. Phosphate buffered saline (PBS) was prepared by dissolving 16g of NaCl, 0.4g of KCl, 2.88g of Na_2HPO_4, 0.48g of KH_2PO_4 in 2L of water and the pH adjusted to 7.4 by adding small amounts of 1M KOH or 1M HCl when necessary. PBS with Tween-20 (PBS-T) was prepared by mixing 200 mL of PBS with 100 µL of Tween-20. MES buffer was prepared by dissolving 1.952 g of MES monohydrate in 100 mL of water. Buffer pH were adjusted using a pH210 Microprocessor pH Meter (Hanna Instruments Ltd, UK). Unless otherwise stated, all experiments were conducted at room temperature (denoted r.t.).

Wolfram Mathematica was used to solve differential equations and simulate the dose response curve according to the theoretical considerations summarised in 3.2.6. SPR affinity data was fitted using Biacore X100 Evaluation software assuming a 1:1 Binding model. Any other fitting was performed using the software OriginPro® (OriginLab Corp.).

Schematics were designed using the open source software inkscape[179], Blender[180] and Qutemol[181] as well as the commercial software Microsoft Powerpoint and Autodesk Fusion360.

2.2 Electrochemical Procedures and Electrode Preparation

All electrochemical measurements were recorded using a three-electrode setup. Measurements were recorded on a PalmSens 4 potentiostat powered by PSTrace 5.8 (PalmSens BV, Netherlands), or a PGSTAT302N (Autolab, USA). Glassy carbon disk electrodes (GCE) with diameters of 3.0 mm and gold disk electrodes with diameters of 2.0 mm were both from CHI. The outer diameter for both electrodes was 6.4 mm. Potentials were recorded against either a self-prepared saturated Ag|AgCl or a commercial leak-free Ag|AgCl reference (LF-2-100) electrode (Alvatek, UK), which was purchased from Alvatek. In all cases platinum wire counter electrodes were used. All solutions used were deaerated by bubbling nitrogen through the solution for at least 20 min before use and were kept under a blanket of nitrogen throughout the experiments where this was possible. In all electrochemical experiments the electrochemical cell was placed inside a Faraday cage to eliminate any electrical noise.

Electrode cleaning

Caution: Piranha solution is extremely dangerous, reacts violently with organic materials and must be handled with extreme care while always under a chemical fume hood. Full protective gear (goggles, heavy gloves and labcoat) has to be worn. It has to be taken care to always add the hydrogen peroxide to the sulphuric acid in this order when preparing the solution. It has to be made sure that no trace of organic solvent is left on the glassware used to prepare the solution as this can result in explosive reactions. Dispose of by diluting in abundant water in the sink.

Platinum electrodes were heated using a gas torch until glowing red and kept under a flame until no residual burning occurred and then rinsed with water. Glassy carbon electrodes were cleaned by sequential polishing with 0.3 and 0.05 µm aluminium oxide slurry and subsequent sonication in 1:1 EtOH:H_2O for 10s. Polycrystalline gold disk electrodes were cleaned by a commonly reported procedure.[182] First, the disk electrodes were polished sequentially with 1.0, 0.3 and 0.05 µm aluminia slurry and sonicated in 1:1 EtOH:H_2O for several minutes after each polishing step. Gold electrodes were immersed in freshly prepared Piranha solution (3:1 H_2SO_4:H_2O_2) for 10 min. Electrodes were then cycled in 0.5M KOH between -0.7 and -1.7 V vs Ag|AgCl for at least 20 cycles. Finally, electrodes were cycled in 0.5M H_2SO_4 between -0.2 and 1.3 V vs Ag|AgCl until CV currents stabilised. After each of the cleaning steps, the electrodes were rinsed with copious amounts of water and blown dry with nitrogen.

Screen-Printed-Carbon-Electrode Arrays were cleaned using 10 min treatment with oxygen plasma at an oxygen flow rate of 0.5 NL h^{-1} (norm litre per hour at 1013 mbar and 20°C). The arrays were then assembled with the 96-well plates using custom cut double adhesive tape (BENECREAT AJEW-WH0096-88, China). A Cameo 4 cutter (Silhouette, UK) was used to cut the tape into the shape for the 96-well plate.

2.3 Preparation Protocols and Characterisation

2.3.1 Self-Assembled-Monolayer (SAM) Preparation

Solutions for the formation of SAMs were freshly prepared prior to each experiment using HPLC-grade ethanol in glass vials, which were cleaned with Piranha solution, rinsed with water and blown dry with nitrogen. All SAM preparations were performed by

immersion of the surface in 1mM solutions of the specified molecule or mixtures thereof for 16 h. Mixtures were prepared so that the total concentration of the thiols reached 1 mM. Reductive desorption measurements were performed in 0.1M KOH solution using a linear voltage sweep from -0.5 V to -1.6 V vs Ag|AgCl (KCl) with a scanrate of 10 mV s^{-1}.

2.3.2 Protein Immobilisation on SAM

The surfaces carrying a SAM were washed with ethanol and water and dried under nitrogen flow. The quality of the SAM was checked by contact angle before any further treatment. Az physisorbs on the surface of linear alkanethiol CH_3-terminated SAMs through interaction with its hydrophobic patch. To form this surface, Az was diluted to a final concentration of 8 µM in 10 mM potassium phosphate buffer and the alkanethiol SAM covered surfaces were then incubated in the protein solution for 30 min.

For the covalent immobilisation of antibodies onto the carboxyl terminated SAM surfaces, an established protocol was used to create amidic bonds between the terminal carboxyl on the surface and surface amine of the proteins. The electrode was incubated in a solution of 200 mM EDC and 50 mM NHS for 15 min, rinsed with water and subsequently incubated in a 50 µg mL^{-1} solution of the respective antibodies in PBS for 1 h at room temperature. Thereafter, the surfaces were rinsed with buffer to remove any non-covalently attached molecules before any other experiments were carried out. A subsequent functionalisation with Azurin was carried out following the same procedure used for the pure HT SAMs as detailed above.

For the electrochemical characterisation of the surfaces formed, CV and ECS measurements were carried out in PBS using the setup explained in 2.2. CVs were recorded as stated in the associated data analysis or figures. ECS measurements were

carried out by first recording a spectrum at the half-wave potential of the Azurin extrapolated from the CV measurements. The frequency of the inflection point was then chosen to carry out a potential vs capacitance scan. All following scans were recorded at a potential or frequency kept at the initial values.

2.3.3 Antibody Physisorption for Electrode Modification in Shotgun Tagging Assay (Chapter 4)

For the functionalisation of glassy carbon electrodes (GCEs) with antibodies, the electrodes were first prepared as explained above (see 2.2). The electrodes were then incubated with 100 µg mL^{-1} of Ab at 4 °C for 16 h. EIS and DPV of antibody-decorated electrodes were measured in 5 mM $[Fe(CN)_6]^{4-/3-}$ to confirm successful surface functionalisation (Figure 7-9). Electrodes decorated with antibodies were washed with PBS buffer and incubated in 1 M ethanolamine in PBS for 1 h and subsequently with 1% FBS in PBS for 15 min to reduce nonspecific protein binding before measurements.

2.3.4 Protein Physisorption on Clean Surfaces for Dot Blot Assays (Chapter 3)

For any protein physisorption used throughout the dot blot assay proposed in this work (c.f. 2.4.1), clean electrodes (prepared by following the standard cleaning procedures, c.f. 2.2) were exposed to the protein solutions specified for the denoted time (2 min if not otherwise stated) and then washed as described in the associated assay protocol. For the experiments investigating the change in CV shape or charge transfer resistance over time, the same procedure was followed for each of subsequent incubations and cumulative incubation times were used. The SPR data observing the adsorption kinetics were recorded in a similar manner, where subsequent injections were used to record

the cumulative adsorption after the total exposure time after each of the injections (see 2.3.10.1).

2.3.5 Coupling of Proteins with MB-NHS or Fc-NHS

Polyclonal CRP-antibodies were labelled with MB-NHS or Fc-NHS according to a manufacturer's protocol. 90 µL of antibodies were prepared in HEPES buffer at pH 8.5 containing 120 mM NaCl and mixed with 5 µL of a solution of the dye molecule in DMSO so that the final concentrations of the protein reached 1 mg mL^{-1} (8 µM) and 80 µM for the dye. Solutions were mixed on a vortex mixer at 4°C for 24-48 h. The products were desalted using a ZebaSpin desalting centrifuge column. The final product was then mixed 1:1 with PBS buffer to yield 200 µL of protein-dye conjugates with a concentration of around 0.5 mg mL^{-1}. The concentration of antibodies in the final solution was measured using UV-Vis assuming an absorption coefficient of 210000 M^{-1} cm^{-1} at a wavelength of 280 nm.[183] This results in a concentration of 0.4 mg mL^{-1}. The UV-Vis spectrum of antibody-MB conjugates also shows a dominant absorption peak at 668 nm with another peak at 614 nm, which are typical for methylene blue.[184] Using the peak at 668 nm and a calibration with a serial dilution of methylene blue NHS in the same buffer solution the dye molecules per antibody can be estimated.

2.3.6 UV-Visible Spectroscopy

A Shimadzu UV-2401 spectrophotometer was used to obtain spectra of solutions in the ultra violet and visible range of wavelengths. All measurements were performed using a 100 µL quartz cuvette (Sub-Micro Cells, type 26, Starna, US). A baseline measurement was performed in the buffer solution used for the specific experiment as stated for each experiment.

2.3.7 Water Contact Angle

Contact angles were measured using a FTA1000B goniometer (First Ten Angstrom Inc.) in combination with the stationary sessile drop technique. The experiments were performed at room temperature and under ambient humidity. The measurements were conducted by forming a 20 µL droplet at the tip of a blunt microneedle (46620-330, VWR, USA), then lowering the needle to the surface until the droplet adheres to the surface and subsequently removing the needle. The average contact angle over a 20 second time series record was then measured and the average of three such recordings were taken as the resulting data.

2.3.8 In-Gel Fluorescence

For the in-gel fluorescence experiments, the samples were mixed with 4x Laemmli Buffer, boiled for 5min at 95 °C and 15µg protein loaded onto 4-12% Criterion® XT Bis-Tris protein gel, 26 well (Biorad©, #3450125) in 1x MES buffer (170 V, 55 min). Samples were prepared by labelling 1mg mL^{-1} BSA in MES buffer according to the standard preparation as for the assay. Methylene blue shows fluorescence upon absorption of light around a wavelength of 665 nm and emits light with a peak at around 686 nm. Therefore, the labelled BSA shows fluorescence (imaged on a Li-Cor Oddysey© DLx) when illuminated in the gel, while the fluorescence is absent for the native BSA. On the contrary Coomassie staining labels both proteins native and labelled at the expected mass of around 66kDa.

2.3.9 Sample preparation for XPS

Samples for XPS analysis were prepared on pieces of gold coated silicon wafers cut into 5x5mm squares. The samples were prepared by following the standard procedures for

SAM and Azurin surface formation (see 2.3.1 and 2.3.2). Samples were then dried under a gentle stream of nitrogen and submitted for further analysis. The analysis was performed on a K-Alpha XPS (Thermo Scientific, USA).

2.3.10 Surface Plasmon Resonance (SPR) Measurement Procedures

The SPR experiments for the affinity investigation of CRP antibodies towards native and MB-labelled CRP were performed on a Biacore X100 system (Cytiva Life Sciences, GE) using the associated SIA Kit Au (BR100405) chips. Any other SPR measurements were performed on an SPR spectrometer (SR7500DC) system in combination with an automatic sampler (SR8100), a semiautomatic valve (SR8300) and a pump (SR8600) all manufactured by Reichert (Reichert Inc., Ametek, USA). This system was used together with quartz chips coated with gold (13206060-30, Reichert). Gold chips are prepared by cleaning with Piranha solution for at least 20 min. Subsequently chips were either functionalised with a SAM according to the specific protocol or directly inserted into the aperture. For assembly, the lens was first cleaned using ethanol and lens cleaning tissue (11517362, Fisher Scientific, USA). Then 0.75 µL of immersion oil (nd=1.515, 000580, Nikon) were spotted onto the lens. The chip was dropped onto the oil and it was made sure the oil spread across the whole surface touching the lens. The aperture was then closed. If not otherwise stated the flow used throughout any experiments was 10 µL min^{-1}. Any masses denoted as SPR results were calculated from original units (RU/RIU) by a division with factor 10 as stated in the manufacturer's protocol.

2.3.10.1 SPR Measurements Procedures for Dot Blot Assay (Chapter 3)

The specificity of interaction of the CRP antibody with a target protein surface was measured. For this purpose, a clean gold chip prepared as explained above was used in

the SPR setup. A solution of target protein (CRP, 20 µg mL^{-1}) was then injected into one of the two channels for 60 min for the protein to form a physisorbed film on the surface. The channels were subsequently both exposed to an injection of 1 mg mL^{-1} BSA for 60 min to block any remaining surface sites. A subsequent injection of CRP-antibody for 20 min (as used in the assays) was performed to find the level of specific interaction to be expected in the assay.

The cumulative adsorption of protein from a solution of 1% FBS in PBS was measured using a clean gold chip in the standard SPR setup. Subsequent injection of protein solution for the specified durations were then carried out and the cumulative mass adsorbed was recorded versus the total time of exposure.

2.3.10.2 SPR Measurement Procedures for the Shotgun Tagging Assay (Chapter 4)

The antibody antigen affinity studies presented in Chapter 4 were recorded on the Biacore X100 instrument using the standard manufacturer's protocol for the affinity assay. First, the antibody surface was formed by the standard physisorption protocol from a 100 µg mL^{-1} solution of Ab at 4 °C for 16 h (see 2.3.3). The so modified gold chip was then mounted into the instrument and the assay was performed using the manufacturer's guidelines.

The SPR specificity measurements for the Shotgun assay were acquired using the standard SPR setup (Reichert) mentioned earlier. For this purpose, a gold chip was modified with antibodies by the standard physisorption protocol from a 100 µg mL^{-1} solution of Ab at 4 °C for 16 h (see 2.3.3) and then mounted into the instrument. Interfering proteins and antigen were then injected for 15 min each and the response recorded.

2.3.10.3 SPR Measurement Procedures for the Azurin Film Surfaces (Chapter 5)

The SPR data for the coupling of antibodies to the mixed SAM surfaces was measured using the standard SPR setup (Reichert, as mentioned above). For this purpose, SAMs were prepared on gold coated quartz chips according to the standard protocol (see 2.3.1) and then mounted into the SPR system. Subsequently, a solution of 200 mM EDC and 50 mM NHS in PBS was injected for 15 min, the channels were rinsed with buffer by running PBS at a flow rate of 100 µL min^{-1} for 1 min. This is immediately followed by an injection of a 50 µg mL^{-1} solution of the respective antibodies in PBS for 1 h at room temperature. Thereafter, the surfaces were again rinsed with buffer to remove any non-covalently attached molecules before any other experiments were carried out. Any functionalisation of the surface with Azurin was carried out by an injection of an 8 µM solution of the protein in 10mM potassium phosphate buffer for 30 min. Antibody coupling onto Azurin surfaces (physisorbed on HT-SAM) were carried out following the same procedure as for the coupling onto the mixed SAMs.

Any specific or non-specific response of the so formed surfaces to antigen or interfering protein solutions (as specified in the associated figures) were carried out by injecting the interrogated protein solutions to the flow system for 15 min and recording the change in response upon the injection.

2.3.11 Atomic Force Microscopy

Tapping Mode Atomic Force Microscopy (TM-AFM) was carried out with a DI ADM from Digital Instruments (Veeco, US) in combination with an IV controller and a vertical engage scanner (J(AS-130)) or a JPK Nanowizard (Germany). The experiments were undertaken in air and the tips used in intermittent contact mode from MikroMasch

(series 15) were typically employed at a frequency of 325 kHz. The software Gwyddion (available at http://gwyddion.net/) was used for the data analysis and post-processing of images.

2.4 Assay measurement protocols

2.4.1 Assay Protocols for Chapter 3 (Amperometric Dot Blot Assay)

2.4.1.1 Static Assay Protocol

Solutions of CRP spiked in 1%FBS, a 250 ng mL^{-1} solution of poly-HRP-Streptavidin (pHRP) and a 250 ng mL^{-1} solution of Biotin-Ab in 1%BSA (10mg mL^{-1}) are all prepared in PBS. GCEs are cleaned according to the standard protocol. The electrodes are then exposed to 20 µL of the CRP samples for 2 min then washed two times with 500 µL PBS-T each. Subsequently, the electrodes are exposed to 20 µL Ab solution for 20 min, then again washed with PBS-T. And then the electrodes are exposed to 20 µL pHRP-solution for 20 min, then washed again with PBS-T. The GCEs are then inserted into an electrochemical cell with an Ag|AgCl reference and a Pt counter electrode filled with 1 mL of PBS. A Chronoamperometric measurement is started with a bias voltage of 0.1 V vs Ag|AgCl and left for equilibration for 500s. 100uL of TMB substrate solution is added to the well and the measurement is left for equilibration to a steady state current for 5000s. The average current of the last 60 seconds of the measurement is taken as one datapoint. For the final result three of such datapoints from different electrode arrays were averaged.

2.4.1.2 Microfluidic Assay Protocol

Solutions of CRP spiked in 1%FBS, a 250ng mL^{-1} solution of poly-HRP-Streptavidin (pHRP) and a 250 ng mL^{-1} solution of Biotin-Ab in 1%BSA (10mg/mL) are all freshly prepared in PBS. GCEs are cleaned according to the standard protocol. The electrodes are then exposed to 20 µL of the CRP samples for 2 min then washed two times with 500 µL PBS-T each. Subsequently, the electrodes are exposed to 20 µL Ab solution for 20 min, then again washed with PBS-T. And then the electrodes are exposed to 20 µL pHRP-solution for 20 min, then washed again with PBS-T. The GCEs are then inserted into the microfluidic cell and PBS is pumped through the channel across the electrode with a flowrate of 200 µL min^{-1}. A Chronoamperometric measurement is started with a bias voltage of 0.1 V vs AgAgCl and left for equilibration for 10s. 100uL of TMB substrate solution are injected to the flow system and the measurement is left running until the current has reduced to the background level. Then another injection is performed. This is repeated at least three times and the integrated area of three peaks is averaged. This whole procedure is done at least three times independently for each concentration investigated and the average of these three measurements is used as the final result. For the results obtained on different electrode surfaces the specified cleaning procedure (c.f. 2.2) was used, while all other details mentioned above were kept the same. For the results obtained on the 3-MPA SAM, the SAM was prepared according to the standard protocol (see 2.3.1), and then EDC/NHS coupling as described earlier for other proteins (c.f. 2.3.2), was used to couple all proteins from a complex sample to the SAM surface. The assay was then carried out as detailed above. For the different adsorption times reported for the cTnI quantification, the time of adsorption of proteins from the complex

sample to the electrode surface was varied, all other details of the assay were performed according to the above protocol.

2.4.1.3 Screen-Printed Carbon Electrode Assay Protocol

Solutions of CRP spiked in 1%FBS, a 250 ng mL^{-1} solution of poly-HRP-Streptavidin (pHRP) and a 250 ng mL^{-1} solution of Biotin-Ab in 1% BSA (10mg/mL) are all prepared in PBS. SPCE arrays are cleaned and assembled with the 96-well plates according to the standard protocol (c.f. 2.2). SPCEs are then exposed to 20µL of the CRP samples for 2 min (unless otherwise stated) and then washed two times with 100 µL PBS-T each. Subsequently, the wells are exposed to Ab solution for 20 min, and again washed with PBS-T. Then, the SPCEs are exposed to pHRP-solution for 20 min, then washed again with PBS-T. The SPCEs are then inserted into an electrode array holder and 100uL of PBS is spotted into each well. A Chronoamperometric measurement is started at 0.1V vs Ag|AgCl and left for equilibration for 200 s. 100 µL of TMB substrate solution is added to the well and the measurement is left for equilibration to a steady state current for 1200s. The average current of the last 6 seconds of the measurement is taken as one datapoint. Per Array, usually 3 electrodes are exposed to the same concentration of CRP. The average of these three electrodes is then taken as the result for one array. For the final result three of such datapoints from different electrode arrays were averaged.

2.4.1.4 Specificity and Spike Recovery Measurements

For all platforms, specificity measurements were performed by running the associated standard assay procedure (c.f. 2.4.1.1, 2.4.1.2, 2.4.1.3) with interfering proteins (BSA, HSA, Fibrinogen, Myoglobin) and target or interfering analyte (CRP, cTnI) at indicated concentrations. Spike recovery experiments were performed running the associated

assay with the spiked solutions of complex sample (1%FBS containing CRP or cTnI) and using the response function obtained from the dose response curve to back-calculate the target concentration.

2.4.1.5 Other Assay Control Experiments

2.4.1.5.1 Signal of Clean versus HRP Coated GCE upon Substrate Injection

A control experiment was performed to rule out any residual signal and to test the specific current produced upon the presence of HRP on the working electrode for an injection of the TMB substrate solution in the microfluidic setup. For this purpose, a GCE cleaned according to the standard protocol (c.f. 2.2) is either first coated with pHRP by incubation in 250 ng mL^{-1} for 30 min and subsequently mounted, or directly mounted into the flow cell and subjected to a injection of 100 µL of a mixture of 1:1 TMB:PBS or pure TMB substrate solution. The current is measured in a chronoamperometric measurement as stated above in the assay protocol (see 2.4.1.2).

2.4.1.5.2 Signal from MB-Ab and Fc-Ab Conjugates on BSA or CRP Coated Electrodes

For the analysis of specific signal generated by the binding of MB-Ab and Fc-Ab conjugates produced according to the protocol in 2.3.5 to antigen surfaces, first, clean electrodes were exposed to protein solution for film formation (either 20 µg mL^{-1} CRP or 100 µg mL^{-1} BSA). The so formed surfaces were then subjected to electrochemical analysis as detailed in the results section and subsequently exposed to the antibody-conjugates before another electrochemical measurement was taken.

2.4.2 Assay Protocols for Chapter 4 (Faradaic Shotgun Tagging Assay)

2.4.2.1 Solution Phase Redox Tagging of Protein Samples with MB-NHS

Fifty microliters of freshly prepared methylene blue–NHS ester solution (final concentration of 10 μg mL^{-1} upon mixture with the sample) in DMSO was immediately mixed with 50 μL of the protein sample aliquoted in 100 mM MES buffer at pH 6.0, 1% FBS in 100 mM MES, or 1% human serum (HS) in 100 mM MES, depending on the experiment at hand. The mixture was vortexed and incubated for 30 min without stirring. Twenty microliters of a mixed solution of 1 M ethanolamine and 1 M hydroxylamine were then added to the reaction mixture and incubated for 5 min to quench any unreacted MB-NHS ester. The concentration of MB-NHS (10 μg mL^{-1} equivalent to 19 μM in the test solution) was chosen in accordance with the manufacturer's protocol suggesting a 5-fold excess of NHS ester over total protein. Total protein concentration in 1% serum was estimated at 50 mg mL^{-1} (4 μM in test solution).

2.4.2.2 Static Assay Protocol

Prepared electrodes were incubated with 15 μL of the labelled protein samples for 15 min, washed with PBS, and immersed in degassed 0.1 M KCl, and then DPV curves were recorded between −0.60 and 0.00 V vs a saturated Ag/AgCl reference electrode with platinum (Pt) counter electrodes (100 mV/s scan rate with 50 mV pulses in 0.01 s). Peak heights were calculated after subtracting the background current at ≈−0.40 V (vs Ag/AgCl), a potential consistent with previous literature on methylene blue–NHS conjugates.[185-187] Current densities were calculated relative to the geometric electrode surface area (3.0 mm diameter).

2.4.2.3 Microfluidic Assay Protocol

An antibody-coated electrode was introduced into the microfluidic chip and fitted tightly. Inlets of the microfluidic cell were connected to a Harvard Apparatus Standard Infuse/Withdraw PHD 2200 syringe pump. Before each measurement, the microfluidic cell was washed with DI water and dried with nitrogen, and then the two loading chambers (Figure 4-6) separately filled with 25 µL of 20 µg mL^{-1} MB-NHS in DMSO and 25 µL of protein solution. The loading apertures were then closed using Kapton tape and 0.1 M KCl pumped through both inlets of the cell with a flow rate of 10 µL min^{-1} for 5 min, allowing the two solutions to actively mix inside the flow channel. When the electrode chamber was filled, the flow was stopped for 10 min to incubate the electrode with the tagged protein. Subsequently, the cell was washed with 0.1 M KCl at a flow rate of 100 µL min^{-1} through each inlet for 2 min. During this, the flow cell was held with a slight positive angle toward the outlet end to prevent the formation of air bubbles. DPV curves were then recorded in 0.1 M KCl between −0.6 and 0.0 V vs the Ag/AgCl/Nafion reference electrode with a Pt counter electrode at a 100 mV/s scan rate and 50 mV pulses with a duration of 0.01 s.

2.4.2.4 Microfluidic Spike Recovery

For the spike recovery experiments in the microfluidic setup, selected known concentrations of both proteins were first analyzed to correct for interelectrode variation. Electrodes were then exposed to spiked human serum samples, and the measured DPV response used to estimate target protein concentration. Recovery was calculated as the ratio of resolved concentrations to the spiked concentration using linear semi-log fitting (see insets in Figure 4-7).

2.4.2.5 Assay Specificity Studies

High concentrations of common interfering proteins (1 mg/mL BSA, 1 mg/mL HSA, and 1 mg/mL fibrinogen) were labelled with MB-NHS as described above, and the tagged solutions were then incubated with antibody-modified electrodes for signal evaluation as described above. DPV signals were recorded and used to compare specific target protein responses (CRP or cTnI). The cross-reactivities of both target proteins toward the respective antibodies were also studied by incubating anti-CRP-modified electrodes with a high concentration of cTnI (100 ng/mL) and incubating anti-cTnI electrodes with a high concentration of CRP (200 ng/mL) and comparing responses to those generated by respective specific targets.

2.4.2.6 Patient Samples Analysis

12 patient samples provided by the Oxford University Hospital were analysed using the proposed shotgun protein labelling assay and estimated concentrations of CRP and cTnI were compared to results reported estimated using a commercial immunoassay platform (Abbott Architect).

2.4.2.7 Other Assay Control Experiments

2.4.2.7.1 Optimisation of Buffer Conditions

Optimization of the assay performance regarding labelling with MB-NHS was performed under different buffer conditions. For this purpose, the assay was performed as stated in the original protocol (see 2.4.2.2), but the buffer for the preparation of the protein solution was adjusted accordingly. Buffers used were 100 mM Acetate buffer at pH 5.0, 100mM MES buffer at pH 6.0 and 100mM potassium phosphate buffer at pH 8.0 and pH 9.0.

2.4.2.7.2 Electrochemical Signal from MB-tagged versus Native Protein Samples

The interrogated proteins (BSA, HSA, Fibrinogen, all 100 µg mL^{-1} as well as CRP, cTnI, both 50 ng mL^{-1}) were tagged with MB-NHS according to the standard protocol (c.f. 2.4.2.1). The proteins were then adsorbed to clean GCEs by incubation for 15 min, and remaining protein solution washed off by rinsing with 1 mL PBS buffer. Electrochemical interrogation of GCEs modified in this way was performed by running DPV as specified in the assay protocol (2.4.2.2). The concentrations of target protein CRP used include 1, 10, 100, 1000 and 6000 ng mL^{-1}.

2.4.2.7.3 Electrochemical Signal from BSA versus Ab Coated Electrodes

For the comparison of specific and non-specific response MB-labelled proteins were exposed to BSA modified electrodes and anti-body modified electrodes. GCEs were prepared according to the protocol for electrode preparation (c.f. 2.3.3) using either antibodies as in the original protocol or BSA (100 µg mL^{-1}). The electrodes were then exposed to the protein samples (BSA, HSA, both at 100 µg mL^{-1}, as well as CRP and cTnI at concentrations of both 10 and 100 ng mL^{-1}.

2.5 Microfluidic Setups

For the microfluidic experiments a Harvard Apparatus Standard Infuse/Withdraw PHD 2200 syringe pump was used together with 50 mL syringes (BD) and a Rheodyne® Model 9725 Injector, which were connected to the microfluidic chips via transfer tubing (Masterflex® Transfer Tubing, Platinum-Cured Silicone, 1/32"ID x 3/32"OD, Avantor®).

The microfluidic chips for the Shotgun assay (Figure 4-6 and Figure 7-16) as well as the Dot Blot assay (Figure 2-1) were designed using Fusion360 software and subsequently

printed using an ELEGOO UV-curing 3D printer with an ELEGOO translucent resin. The chips were designed to have smooth edges in the channels so that any turbulent flow would be minimized. A reference electrode was prepared by electrolysis in 0.1 M HCl at a plain silver wire (0.25 mm diameter). Subsequently, the so-formed reference electrode was coated with Nafion 117 by eight repeated cycles of incubation in 4% Nafion solution and air-drying. This and a platinum wire (0.20 mm diameter) counter electrode were then inserted into the microfluidic cell and fixed via a commercial adhesive epoxy resin (Araldite). The surface area of reference and counter electrodes can be estimated by the length inside the channel (1.5 cm) and their diameters. This results in a surface area of 0.12 cm^2 for the reference electrode and 0.1 cm^2 for the counter electrode.

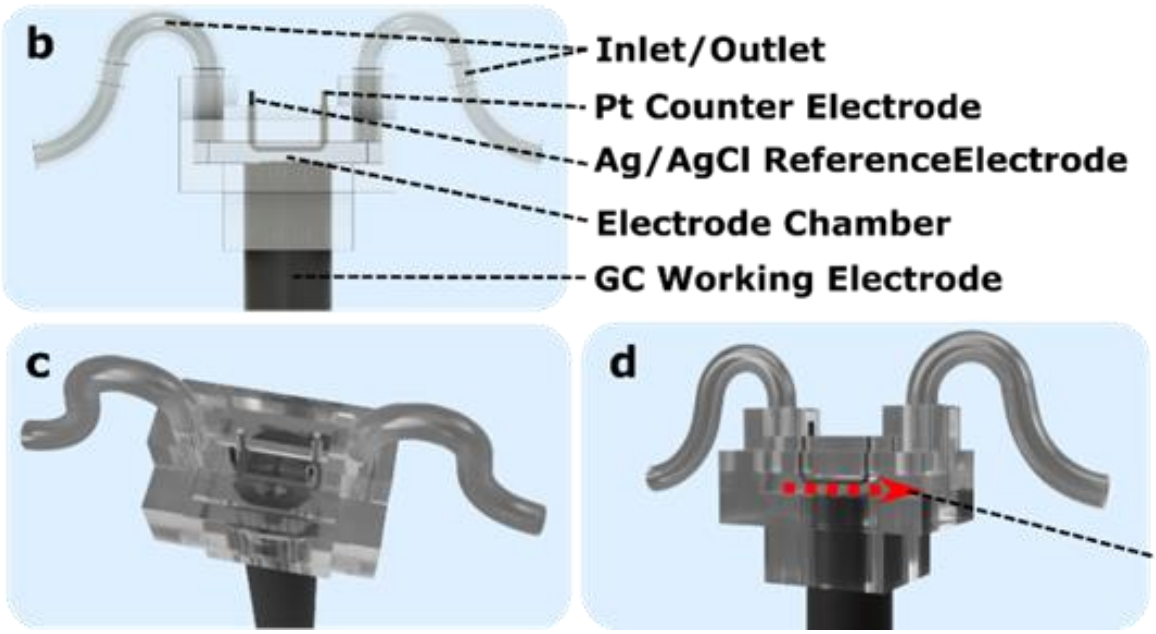


Figure 2-1 Schematic Illustration of the microfluidic cell used for the Amperometric Dot Blot Assay. The 3D-printed cells consist of an inlet and outlet connected by a channel functioning as the electrode chamber. The electrode chamber houses a platinum wire counter electrode and a Nafion coated Ag/AgCl reference electrode, which are both fixed on the upper side of the channel. The working electrode is inserted from the opposite side.

2.6 Theoretical Considerations and Calculations

2.6.1 Electrode surface area

For the calculation of the gold electrode surface area, the last anodic peak of electrode cleaning in H_2SO_4 was used. From transferred charge obtained by dividing the peak area A_{peak} by the scanrate ν, the surface area was calculated using the following formula according to Oesch and commonly accepted in literature[188]:

$$A_{el} = \frac{A_{peak}}{\nu \cdot 482 \frac{\mu C}{cm^2}} \qquad \text{Eq. 3}$$

2.6.2 EIS and ECS analysis

The complex impedance Z^* was converted to a complex capacitance C^* through the following physical definition, where $\omega = 2\pi f$ denotes the angular frequency of the input stimulus and i the imaginary unit:

$$Z^*(\omega) = \frac{1}{i\ \omega C^*} \qquad \text{Eq. 4}$$

This leads to the following relations between the real and imaginary parts of the impedance (Z' and Z'') and their capacitance counterparts (C' and C''):

$$C'(\omega) = -\frac{Z''}{\omega(Z'^2 + Z''^2)}\ ;\ \ C''(\omega) = \frac{Z'}{\omega(Z'^2 + Z''^2)} \qquad \text{Eq. 5}$$

2.6.3 Estimations of Surface coverage

Any estimates for surface coverages were calculated based on the assumption of close packing of circles which has a well-known closest packing density P according to the

following relation, where A_{ref} is a rectangular reference surface area, A_{circle} is the surface area of a circle with radius r and N represents the number of circles:

$$P = \frac{A_{circle}}{A_{ref}} = \frac{N \cdot \pi \cdot r^2}{A_{ref}} = \frac{\pi}{2\sqrt{3}} \quad \text{Eq. 6}$$

Assuming a circular exclusion radius of proteins, this formula can be used to relate a mass surface coverage C_{surf}, given in mass per unit surface area, with this exclusion radius in the following fashion with m denoting the mass of a single protein:

$$C_{surf} = \frac{N \cdot m}{A_{ref}} = \frac{m}{2\sqrt{3} \cdot r^2} \quad \text{Eq. 7}$$

This can be rearranged to yield a theoretical exclusion radius for a given mass surface coverage C_{surf} or used to calculate a theoretical coverage based on an assumption on the molecular exclusion radius r.

2.6.4 Limit of Detection

To estimate the limit of detection the background signal s_0 and its standard deviation σ is used to obtain the minimum distinguishable signal according to common procedures as $S = s_0 + 3\sigma$. This signal S is then used together with the transfer obtained for a specific assay to calculate the corresponding minimum distinguishable concentration as the LOD.

Chapter 3

An Amperometric Dot Blot Assay for the Quantification of Target Protein in Complex Media at Unmodified Electrode Surfaces

3.1 Introduction

As discussed in 1.1, timely diagnosis of early-stage diseases remains pivotal for facilitating prompt intervention and alleviating pressure on global healthcare systems.[189-193] Assessing circulatory biomarkers, including proteins and nucleic acids, offers an advance indication of patient well-being before clinical symptoms manifest.[23, 44, 194, 195] In contrast to existing clinical assays, which lack cost-effectiveness, scalability, and decentralized utilization, electrochemical sensors exhibit sensitivities comparable to prevailing standards,[196] with per-sensor costs ranging below $1.[40] Electrochemical sensors are particularly suitable for decentralized implementation due to their potential for miniaturisation, facile implementation and cost-effectivness.[197, 198] The realm of electrochemical sensing methodologies encompasses voltammetric, amperometric, or impedimetric detection methods and are generally classifiable as label-based or label-

free techniques.[44] As discussed in 1.2.2, the former involve two recognition events targeting distinct analyte sites,[199] while the latter hinge on a singular recognition process at the electrode surface typically in combination with a solution or surface-bound redox probe for transduction.[200] While label-based approaches based on two paired recognition events have demonstrated high sensitivity (achieving levels of detection down to fg mL^{-1} of protein)[201] along with specificity,[55] label-free sensors avoid the expense of label production and the need for dual recognition.[199] Additionally, a reagent-free and label-free configuration permits quantification without introducing reagents to the sampling solution.[202]

Due to the interfacial nature of transduction, both these methodologies and conventional clinical assays like ELISA encounter the issue of nonspecific protein adsorption at interfaces exposed to biological samples like serum or plasma.[203, 204] Such protein fouling poses a significant challenge, particularly for label-free assay formats, where nonspecific adsorption can lead to a notable false signal generation.[95] Native protein adsorption is a phenomenon observed across a wide spectrum of surfaces,[92, 93] and stems from intricate physicochemical interactions, primarily governed by electrostatic and hydrophobic forces.[94] The imperative to mitigate biofouling has prompted extensive endeavours in surface functionalization.[59] As a result, the majority of the aforementioned sensors rely on intricately designed interfacial architectures to reduce non-specific protein adsorption while selectively capturing target proteins from complex sample matrices. [59, 205]

As outlined in 1.3.2, a broad range of highly non-fouling interfacial designs have been applied for the functionalization of electrodes for this purpose. However, such

modification increases assay-costs, as well as manufacturing, storage and transport complexity and thereby impacts commercial scalability.

Moreover, the functionalization of sensor surfaces with recognition elements (e.g. antibodies) is complex and often yields a limited and non-uniform bio-receptor surface coverage, affecting assay performance.[206] So called Dot blot assays provide an alternative pathway omitting complex surface functionalisation. These types of assays are frequently employed in biomolecular analyses to assess protein-protein interactions, utilizing optical signal generation.[207] Unlike sandwich assays, dot blot assays necessitate just a solitary direct target recognition event. In the original form of the technique, a membrane (often nitrocellulose) is exposed to a protein solution, followed by a blocking phase, and a subsequent incubation with antibodies specific to the target protein. These antibodies are usually enzymatically labelled, triggering the production of an optically detectable substrate. Despite their utility, dot blot assays typically entail a turnaround time of several hours, a duration influenced by the kinetics of antibody binding, washing steps, and enzymatic reactions.[208] The limit of detection (LOD) for dot blot assays typically resides in the range of a few ng mL^{-1}. However, these assays encounter limitations when applied to biological samples containing interfering proteins, with few documented instances being available.[209] Moreover, only a scant number of publications elucidate the concept of electrochemical quantification methodologies applied to the established dot blot assay format. One of the two most notable examples encompasses a DNA hybridization assay,[210] which utilises the adsorption of single stranded DNA on a nitrocellulose membrane and subsequent recognition via a probe DNA binding an HRP-conjugate. The quantification is then performed amperometrically by transferring the substrate into an electrochemical cell

with a sensing electrode pre-modified by a blocking procedure. The quantification of DNA was performed in presence of a 3 base mismatched interfering DNA strand, but notably not in a complex sample including any protein or other interfering species. The second significant example comprises a paper-based quantification platform for the quantification of IgE,[211] which is based on the adsorption of IgE in a nitrocellulose membrane and a subsequent target recognition using goldnanoparticle coated with aptamers. The gold nanoparticles then catalyse the production of silver ions which are detected potentiometrically using a silver ion selective electrode in contact with the membrane. This assay showed a limit of detection in the μg mL^{-1} range and was tested to be specific at concentration of 100 μg mL^{-1}, but its performance was not tested in complex samples. Notably, there exist no examples utilising the direct native adsorption of protein on electrode surfaces for the quantification of target protein in complex samples. Thus, there remains significant potential for the investigation of concepts of electrochemical dot blot protein assays and their performance in the context of clinical POC sensing. While the mentioned instances illustrate the potential of dot blot assays in diagnostic contexts, they have not fully harnessed the advantages offered by electrochemical assays in conjunction with the simplicity and utility of direct dot blot assays. This fusion presents an opportunity to develop practical sensors suitable for point-of-care (POC) environments. Although amperometric sandwich assays employing enzyme-substrate pairs and recognition elements (like aptamers or antibodies) have been extensively employed for amplified target protein quantification on electrodes,[212-214] the potential of electrochemically amplified variations of dot blot assays for target protein detection within complex matrices still has to be elucidated. While the direct utilization of native protein adsorption at electrodes for amperometric target protein

detection could potentially pose a significant step towards robust electrochemical protein assays omitting the need for any fragile surface modification, it so far remains unreported. This study introduces the first instance of an amperometric dot blot assay for detecting C-reactive Protein (CRP) and cardiac Troponin I (cTnI) in diluted serum. The novelty here is the use of native protein adsorption directly on electrode surfaces. This omits any surface functionalisation and provides facile implementation of the assay. The technique demonstrates highly specific assay capabilities, with a responsive sensitivity encompassing clinically relevant concentration ranges for the target protein. Notably, this approach addresses practical challenges linked to the transition of sensing to clinical applications, including surface storage, transport, and handling of surfaces functionalized with sensitive molecules or geometries.

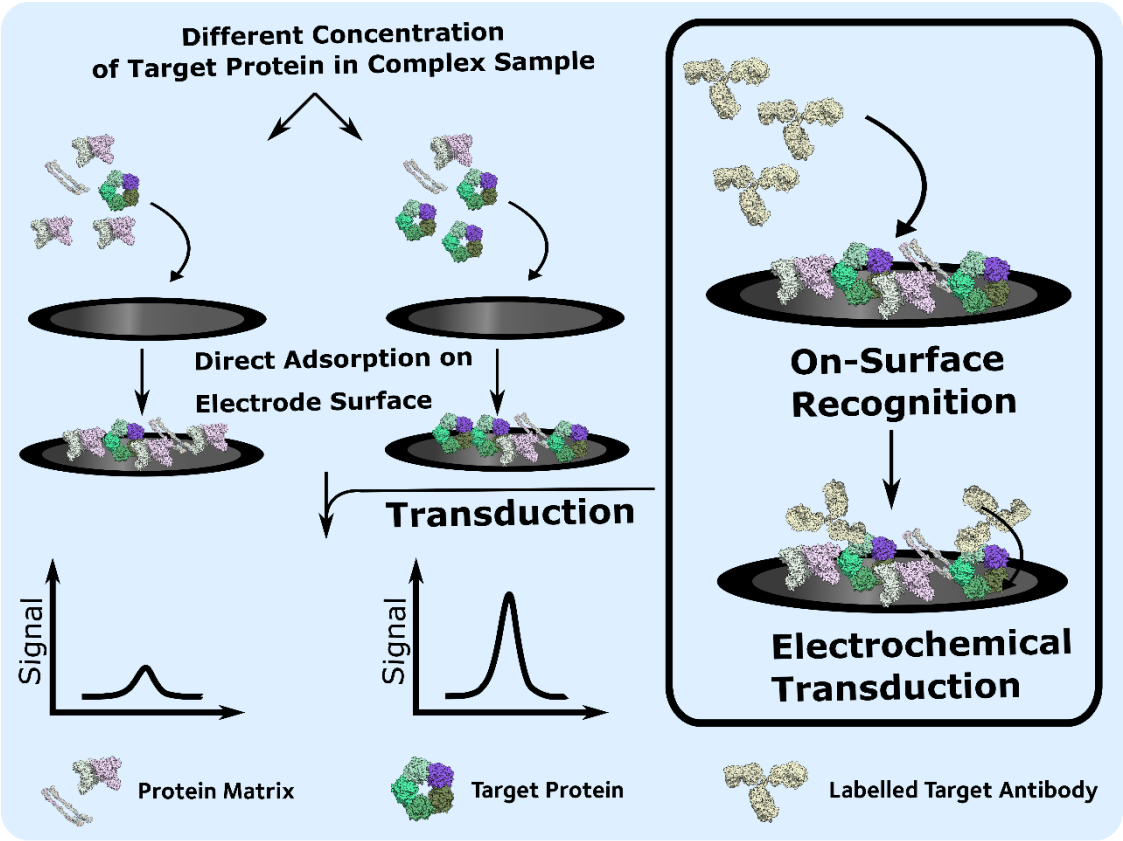


Figure 3-1 Schematic Illustration of the electrochemical dot blot assay concept utilising direct native adsorption of protein from a complex sample on an unmodified electrode surface in combination with an on-surface specific recognition event using labelled antibodies and electrochemical transduction for the quantification of target protein.

3.2 Results and Discussion

3.2.1 Protein Surface Formation and Characterisation

As stated, the efficacy of the electrochemical dot blot assay hinges on the electrode surfaces' capability to firmly adsorb a protein layer, encompassing the target protein accessible for recognition, while simultaneously retaining electrochemical activity for a solution-based redox probe. To gain an understanding of the film formation process, glassy carbon electrodes were subjected to a 1% diluted FBS solution in PBS for varying incubation durations. Subsequently, their electrochemical properties were assessed by

performing measurements in a ferrocyanide PBS solution. Figure 3-2 depicts the comparison between two CV measurements under such conditions, one taken with a cleaned GC electrode, the other one recorded at the same electrode but after 2 minutes of incubation in 1% FBS with subsequent washing using PBS-T. The example curves show the typical behaviour of a GC electrode in ferrocyanide solution with a reduction peak at 290 ± 5 mV and an oxidation peak at 180 ± 5 mV, both measured against Ag|AgCl (sat. KCl). The peak to peak separation of 110 ± 10 mV is higher than the theoretical value of 57 mV,[215] but this has been reported for mechanically cleaned glassy carbon electrodes elsewhere.[216] For the curve recorded on the electrode after 2 min of protein film formation the peaks are shifted towards more extreme potentials with the reduction peak at 500 ± 5 mV and the oxidation peak at 30 ± 5 mV. This results in a peak-to-peak separation of 470 ± 10 mV, which is significantly higher than that on the clean electrode. Further, the peak current can be seen to be significantly diminished on the electrodes carrying the protein film. Both of these observations indicate the formation of a blocking protein film on the electrode surface. To investigate the charge transfer resistance in more detail, EIS based impedance measurements were conducted for different exposure times of the electrode surface to the diluted protein solution (1%FBS). The resulting charge transfer resistance versus the exposure time are shown in Figure 3-3. This analysis shows protein adsorbed at the GC electrode is reaching a plateau-like state within 5 minutes of exposure indicating the quick film formation. The kinetics of a fast phase of adsorption followed by a slow phase of adsorption are matching previous reports from literature for protein adsorption.[94] Within 2 minutes the charge transfer resistance reaches a level about half the maximum reachable within 60 minutes of exposure.

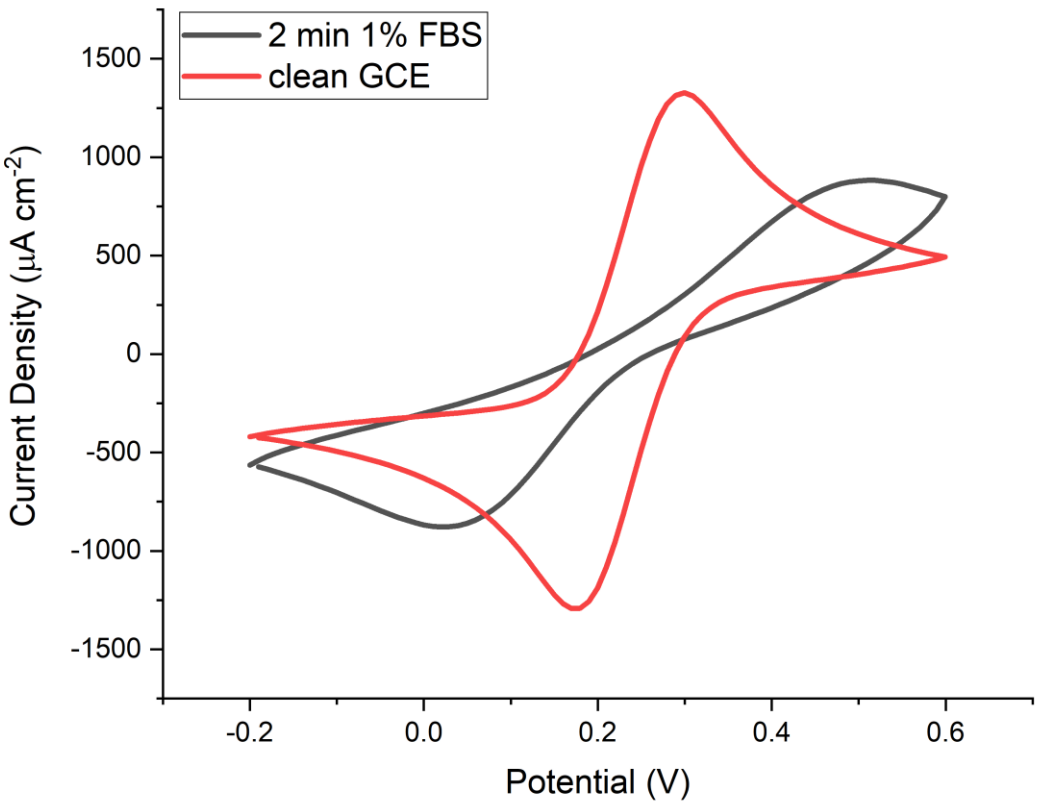


Figure 3-2 Cyclic voltammograms of clean GCE before and after 2 minute exposure to 1% FBS solution for protein film formation, performed in 5mM Ferrocyanide in PBS at a scanrate of 100 mV/s.

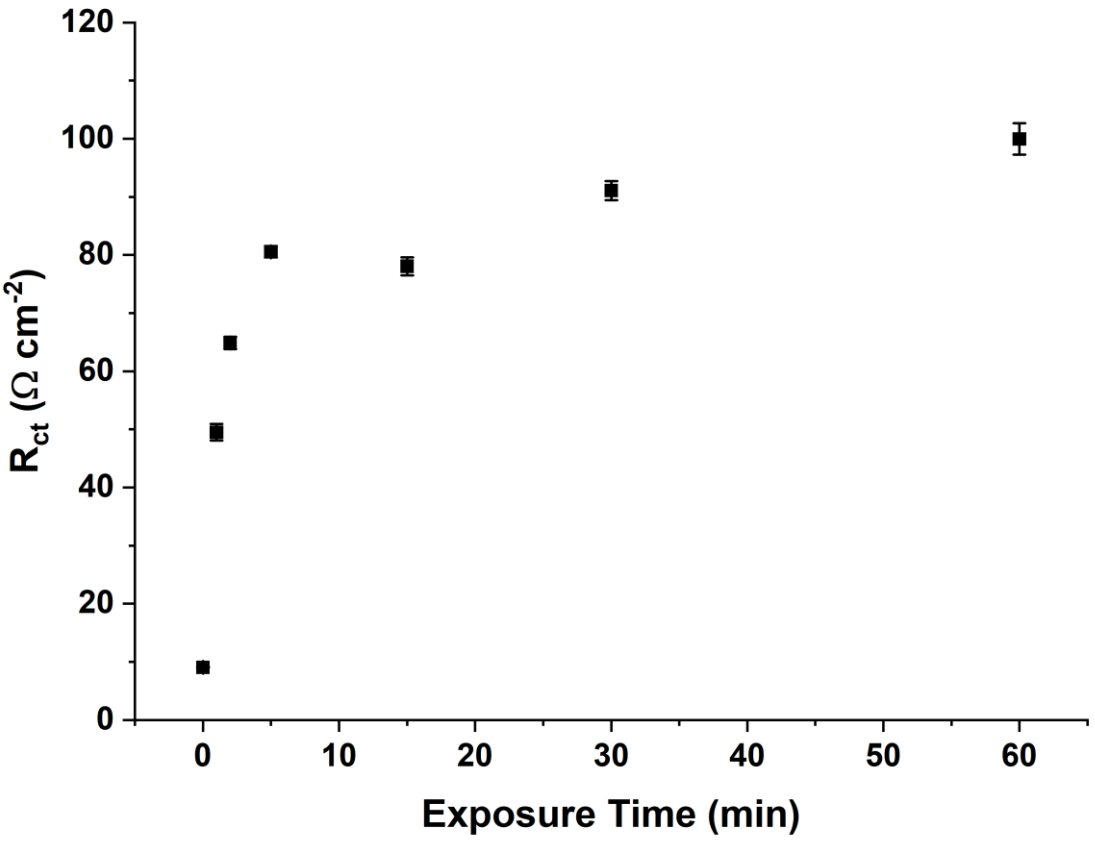


Figure 3-3 Charge transfer resistance across GCE plotted versus the exposure time of electrode to 1% FBS solution, recorded via EIS measurements performed in 5mM Ferrocyanide in PBS. Error bars represent standard deviation between three independent measurements.

As explained above, because the envisioned assay relies on the electrode remaining accessible to an electron transfer from a redox probe and a high abundance of target protein on the surface at the same time, there should be an optimal film structure, i.e. exposure time, that maximises both. The optimal time is not obvious and readily accessible to experiment, but 2 min exposure time was chosen for further experiments for its half maximum value of resistivity considered as a balanced compromise between high protein capture and high electron transfer accessibility.

The formation of a protein layer was further observed using SPR measurements. Although SPR can only be performed on gold surfaces, these measurements provide another perspective on the dynamics of the protein film formation. A 1-minute exposure of the gold surfaces to 1%, 10% and pure FBS results in surface concentration of adsorbed protein of 101 ± 2 ng cm^{-2}, 155 ± 4 ng cm^{-2}, 180 ± 17 ng cm^{-2}, respectively (c.f. Figure 7-1). Likewise, a 10-minute exposure results in adsorbed surface concentrations of 165 ± 4 ng cm^{-2}, 213 ± 5 ng cm^{-2}, 304 ± 16 ng cm^{-2} for the 1%, 10% and 100% FBS, respectively. The adsorbed mass for a monolayer of protein can be estimated based on BSA as the main constituent in the film assuming surface concentrations of different proteins are directly correlated with their respective concentration in the solution. Supposing a spherical shape of BSA with an exclusion radius of 5 nm (based on an average between its two ellipsoidal axes),[217] together with a mass of 66 kDa and using the theoretical surface coverage for a tight packing of circles, the theoretical surface concentration corresponds to an adsorbed mass of 127 ng cm^{-2} (c.f. 2.6.3). This value lies just above the value found for a 1-minute exposure in the SPR experiments further justifying the exposure time of 2 minutes chosen for later experiments.

For initial tests of the concept, the specificity of the interaction of antibodies with a protein surface formed through adsorption was measured in an SPR experiment. For these experiments a gold chip was coated with CRP by exposure to a protein solution and subsequent blocking with BSA. In a simultaneous control experiment performed in a second channel of the SPR instrument only BSA was used to coat the surface. The change in adsorbed mass upon exposure of the so formed protein films to target antibody is compared in Figure 3-4 and shows a change of 67 ± 3 ng cm^{-2} and 1 ± 1 ng cm^{-2} for the surface with and without CRP, respectively. The low increase in surface

adsorbed mass (4 ± 2 ng cm^{-2} and 5 ± 3 ng cm^{-2}, for the CRP and BSA surface respectively) upon exposure to a 1 mg mL^{-1} solution of BSA in both surfaces indicates the highly specific binding of antibodies to the target protein adsorbed to the surface suggesting the applicability of this principle in the hypothesised dot blot assay.

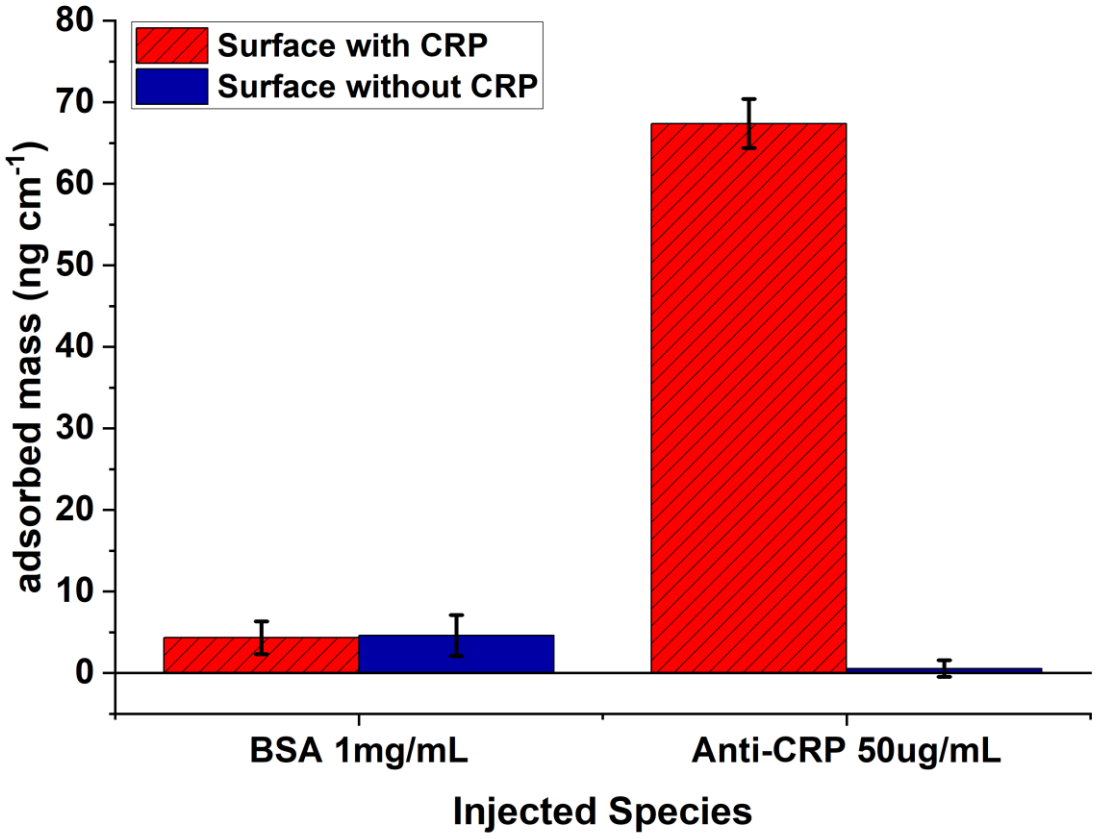


Figure 3-4 Mass adsorbed at clean gold surface coated with CRP (left) or BSA (right) (both subsequently blocked with BSA) after exposure to BSA (1 mg mL^{-1}) or CRP antibody (50 µg mL^{-1}). Measured via SPR, error bars denote standard deviation of three independent measurements.

To test the electrochemical transduction, CRP antibodies were labelled with a methylene blue NHS-ester (MB-NHS) derivative to establish a mode of electrochemical transduction of the specific binding event on the surface. Carbodiimide coupling of the MB-NHS targeting amine residues on the antibodies was employed for this purpose (c.f.

1.4.1). UV-Vis absorbance curves for the protein conjugate after desalting confirmed the successful formation of an antibody dye conjugate with one tag per protein (c.f. Figure 7-3).

However, after initial trial experiments using MB-antibody conjugates as the means to transduce the presence of target protein (c.f. Figure 7-4), it was chosen to move towards an enzymatically amplified approach for the electrochemical detection to cover the concentration range applicable in any clinical circumstances. This conclusion is also in line with theoretical estimates for the surface concentration of target protein based on the assumption that relative concentrations of proteins in solution and on surface are constant and supposing that a monolayer based on the dimensions of BSA as the main constituent (see above) is formed. For a serum protein concentration of 80 mg mL^{-1},[218] and a target protein concentration of 10 µg mL^{-1}, an estimation suggests a surface concentrations of target protein in the range lower than fmol cm^{-2}, which is low even for electrochemical modes of detection, in particular as typical clinical concentrations range far below 10 µg mL^{-1} (c.f. 1.5). Therefore, for all following experiments, the labelling of antibodies with enzyme for amperometric amplification based on the interaction between horse-radish-peroxidase (HRP) and tetramethyl benzidine (TMB) as a substrate for oxidation in the presence of hydrogen peroxide (H_2O_2) was employed.

3.2.2 Static Assay on Glassy Carbon Electrodes

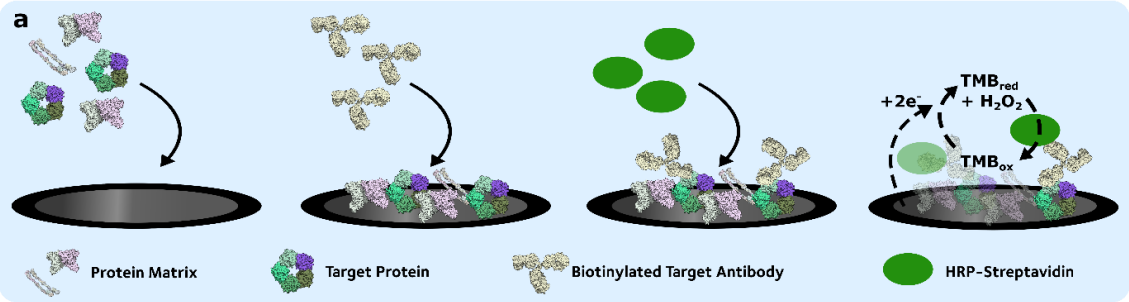


Figure 3-5 Schematic illustration of working principle for amperometrically amplified dot blot assay based on the native adsorption of a protein mixture to the electrode surface followed by target recognition using biotinylated antibodies and the binding of HRP-Streptavidin-conjugates to these. In the final step enzymatic oxidation of TMB and its subsequent reduction at the electrode report on target protein concentration.

For the amperometrically amplified Dot blot assay, biotinylated antibodies in combination with Streptavidin-poly-HRP conjugates were used instead of directly redox tagged antibodies. As shown in Figure 3-5, the amplified format of the assay still relies on the formation of a protein film from a complex sample solution directly on the electrode surface and the subsequent recognition of the adsorbed target protein within the film by biotinylated antibodies. In a next step the surface is exposed to a solution of a poly-HRP-Streptavidin conjugate to bind to the antibodies via the well-established Biotin-Streptavidin interaction.[219] In a last step the surface featuring the poly-HRP molecules is exposed to substrate solution containing H_2O_2 and TMB for an amplification process,[220] as explained in 1.2.3.3. Between each of these steps the surface is washed with buffer (PBS-T) to remove any residual reagents. In presence of H_2O_2, the oxidation of the TMB molecules will be catalysed by HRP, which in turn is then reduced at the underlying electrode. This creates a dynamic where oxidised TMB diffuses to the electrode to be reduced from where it diffuses back to eventually undergo another

oxidation creating a dynamically changing reduction current when the electrode is poised at a suitable potential. This current will reach a steady state after some stabilisation time where the TMB that is reduced at the electrode balances the oxidised TMB that travels to the vicinity of the electrode over time. The resulting steady state current is correlated to the number of HRP molecules on the surface and therefore also the surface concentration of target protein (cf. Figure 3-6).

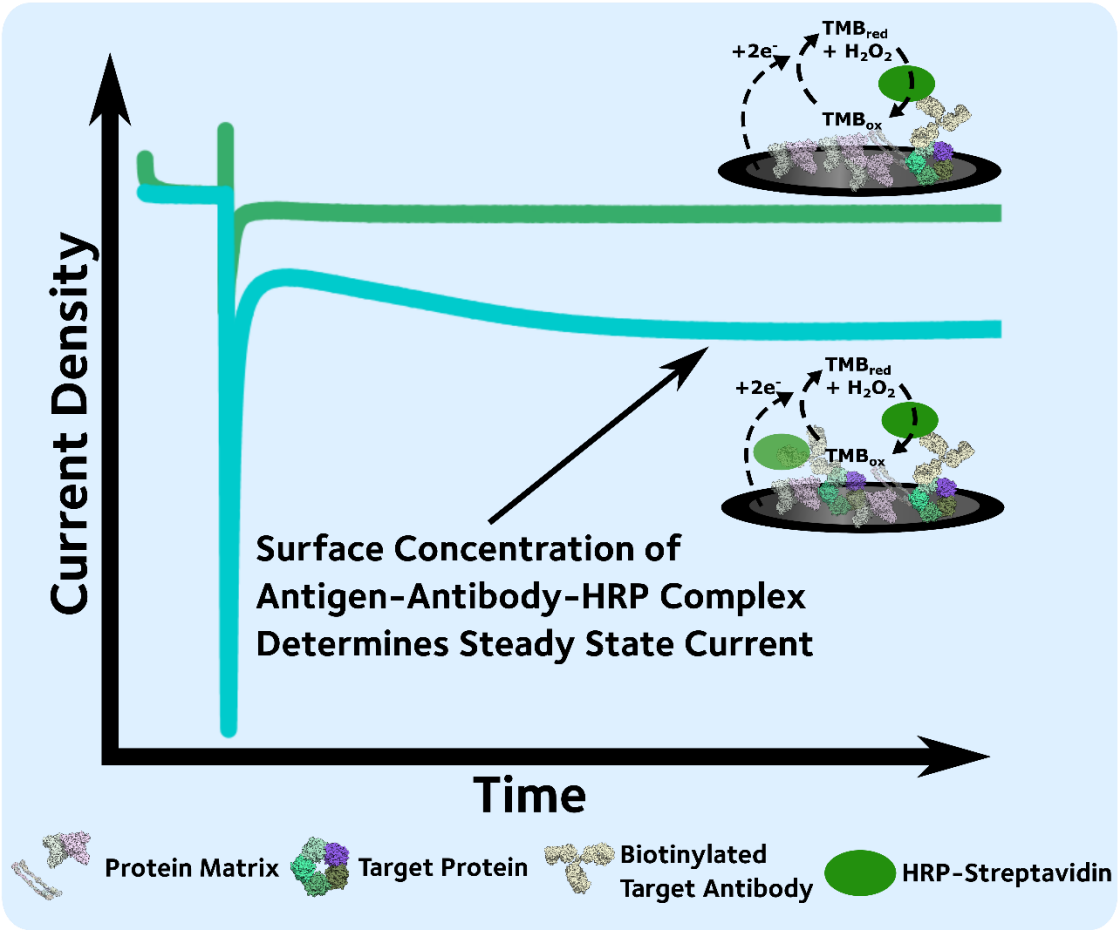


Figure 3-6 Schematic depiction of the establishment of the measured steady state current in the static amperometric dot blot format introduced in this work. TMB substrate solution is injected to the electrochemical cell after an initial equilibration phase. Rearrangement at the surface and the initial onset of TMB oxidation by HRP produces an initial current spike originating from the reduction of oxidised TMB at the electrode. After an initial equilibration phase a steady state current is reached were the

rate of reduction of oxidised TMB at the electrode becomes constant. This steady state current is correlated to the number of antigen-antibody-HRP complexes on the electrode surface and therefore reports on the initial target protein concentration.

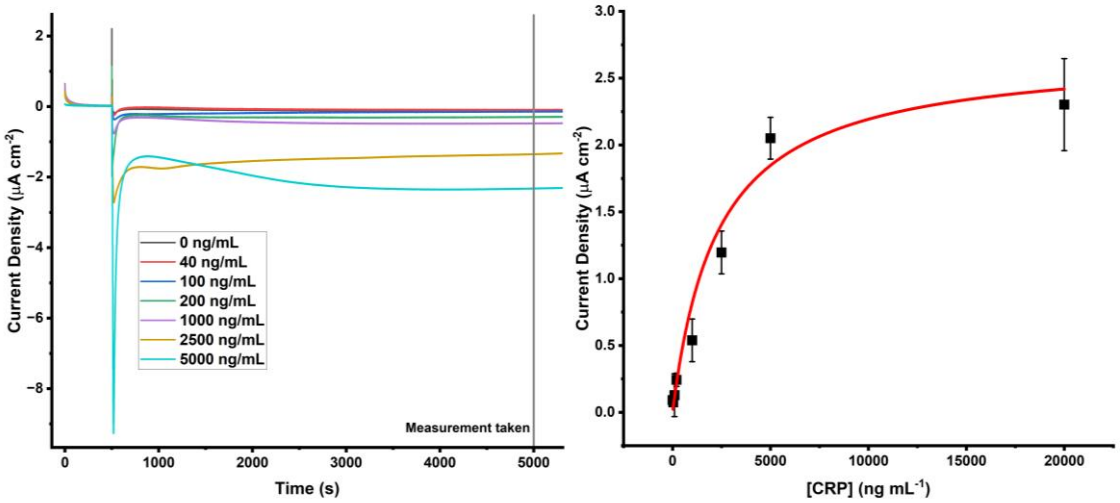


Figure 3-7 Left: Example curves for the static amperometric dot blot assay performed on GCEs. Right: Calibration curve showing the steady state current measured at 5000 s for different target protein concentrations obtained from such curves. Error bars denote standard deviation between three independent measurements.

Representative curves for the static assay and the resulting calibration curve recorded for electrodes formed by exposure to 1%FBS spiked with various concentrations of CRP target protein as explained above can be seen in Figure 3-7. The spikes visible at 500 s mark the injection of 100 µL substrate solution to 1mL of PBS buffer in the electrochemical cell. The current is then left to reach a steady state and the steady state current measured at 5000 s is plotted against the CRP concentration in the original sample to obtain the calibration curve. The data follows a Langmuir-type behaviour (curve in red), although it cannot be seen to completely plateau within the range of concentrations investigated. However, this behaviour will be discussed in more detail together with some theoretical expectations in section 3.2.6 later.

3.2.3 Static Assay on Screen-Printed Carbon Arrays

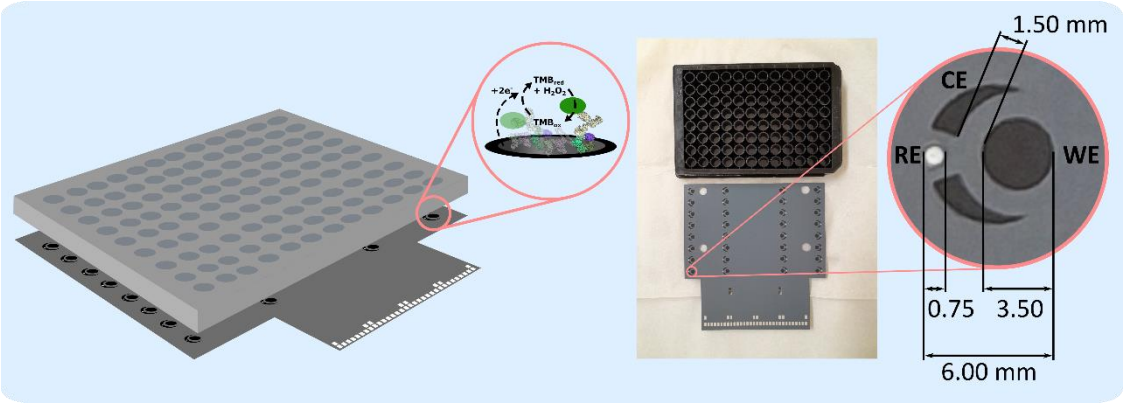


Figure 3-8 Illustrative depiction of amperometric dot blot assay performed on electrode arrays using the assembly of SPCE arrays and a 96-well plate. The assembly is performed using double adhesive and the electrodes are oxygen plasma cleaned before use. The dimensions of the electrodes (Ag|AgCl reference (RE) , carbon counter (CE) and working electrode (WE)) are indicated in mm.

As discussed in 1.2.4, the transfer of any electrochemical sensing methodology to disposable electrodes is a major requirement for its actual applicability in future POC settings. Moreover, such a transfer can also increase the frequency of data generation benefitting the development process. For these reasons, the procedure was transferred to a 4x8 screen printed carbon electrode array. For this the electrode array was cleaned by 10 minutes exposure to oxygen plasma and assembled with a 96-well plate via double adhesive tape to perform the assay inside the wells housing an electrode (see Figure 3-8 and section 2.1 for detailed protocol). The assay was then performed as detailed above. Due the smaller volume of the wells (added total volume of 200 µL) compared to the electrochemical cell used in the static assay, a steady state current is reached faster and the measurement time is reduced to 2000 s.

The data recorded on the arrays for CRP quantification in this way is shown in Figure 3-9, where the steady state current obtained after an equilibration time of 2000 s is plotted

against the concentration of CRP spiked into a 1%FBS sample. The curve can be seen to rise rapidly between 100 and 1000 ng mL^{-1} from which onward it drops back down to a level of roughly half the maximum attainable steady state current density. The rising part of the curve detailed in the right-hand side of Figure 3-9 shows sigmoidal behaviour as expected for assays of similar format and shows a linear range between 5 and 500 ng mL^{-1}. The data again deviates from an exact Langmuir-type behaviour, especially the region of the falling tail observed for concentration larger than 1000 ng mL^{-1}. These deviations and in particular the falling tail will be discussed in more detail in section 3.2.6, where some theoretical considerations of the investigated system are summarised. To investigate assay statistics, a linear curve was fitted to the data (see inset Figure 3-9), this yields a sensitivity of 0.0090 ± 0.0005 µA cm^{-2} (ng mL^{-1})$^{-1}$ and a LOD of 16 ± 6 ng mL^{-1}.

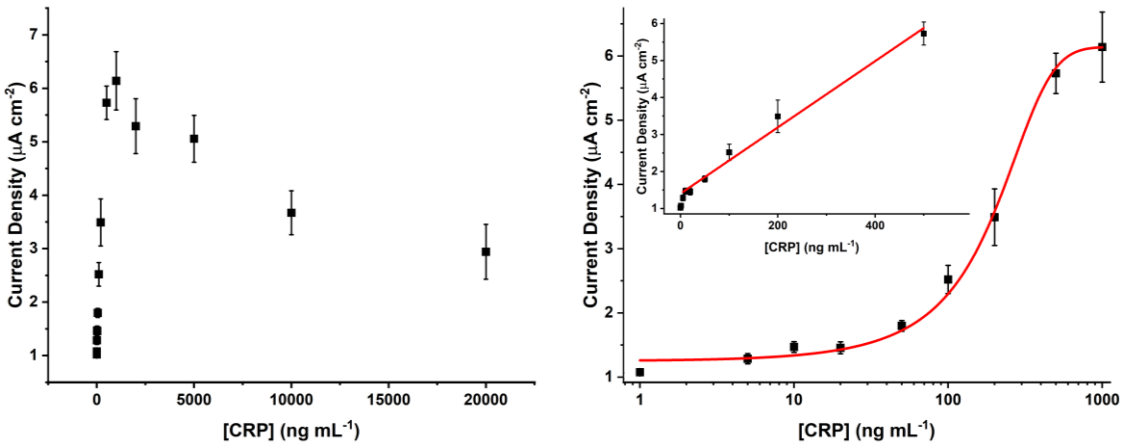


Figure 3-9 Left: Full dose response curve of static amperometric dot blot assay performed on SPCE arrays. Right: Increasing part of calibration curve. Inset: Linear range of calibration curve. All recorded for CRP spiked into 1% FBS. Datapoints are averages over three independent measurements on different arrays, each of which consist of three repeats on different electrodes in the same array. The red line resembles a logistic curve as a guide to the eye. The fit in the inset is a linear fit (R^2 = 0.98) to the linear range of the data with a slope of 0.0090 ± 0.0005 µA cm^{-2} (ng mL^{-2})$^{-1}$ and an intercept at

1.4 ± 0.1 µA cm^{-2}. Error bars denote standard deviation between three independent measurements.

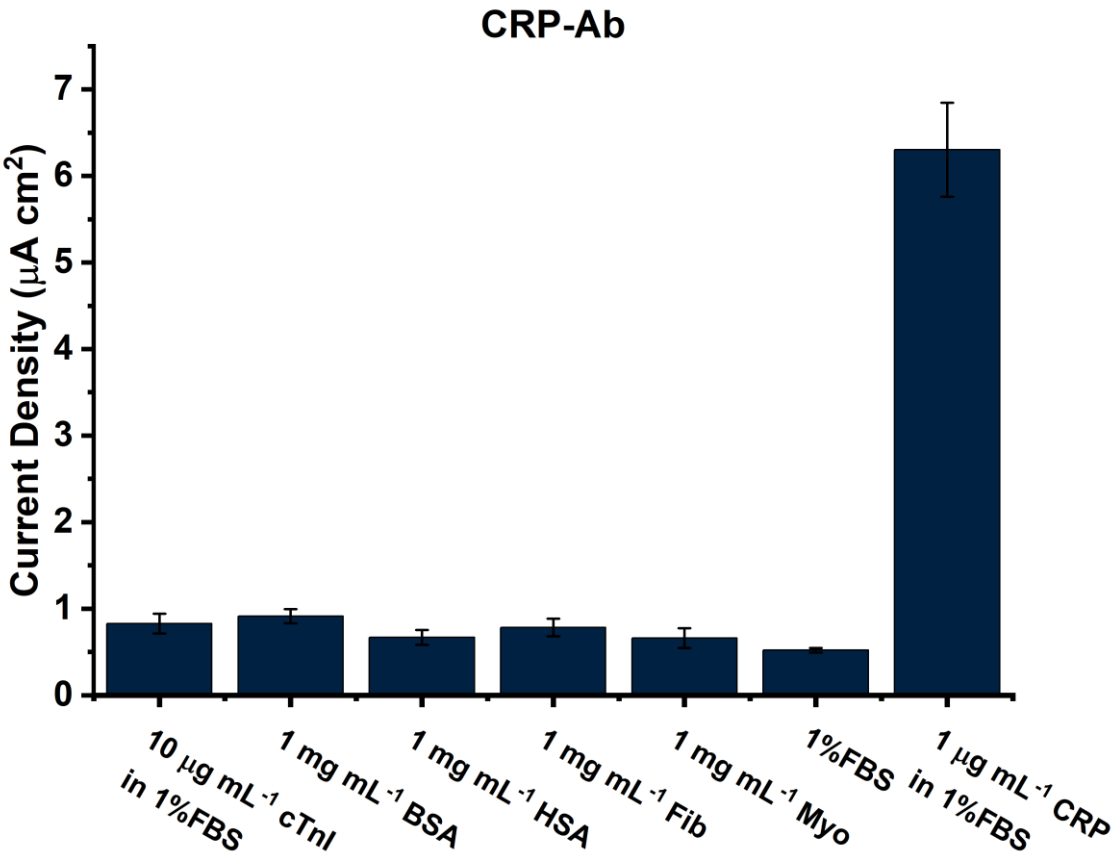


Figure 3-10 Specificity analysis for amperometric dot blot assay on SPCE arrays performed for CRP antibodies with different interfering proteins and specific protein spiked into 1% FBS. The proteins tested are BSA, HSA, Fibrinogen, Myoglobin (all at a concentration of 1 mg mL^{-1}) and cTnI at a concentration of 10 µg mL^{-1}, all spiked into 1% FBS.

For an investigation of the specificity of the measured response towards the signal obtained from the assay performed on different interfering proteins (BSA, HSA, Fibrinogen, Myoglobin, all at a concentration of 1 mg mL^{-1} and 1%FBS) were recorded and compared to a mid-range concentration of CRP (1 µg mL^{-1}) spiked into 1%FBS (c.f. Figure 3-10). Furthermore, the cross-reactivity to cTnI was tested by performing the assay with a solution of 10 µg mL^{-1} cTnI spiked into 1%FBS. It is evident from this data

that the generated signal is indeed specific to the relevant target protein and the signals from interfering proteins remain consistently below 20% of the specific signal for a mid-range concentration of target protein spiked in 1% FBS.

It was hypothesised that apart from the volumetric concentration of target, the relative concentration of target protein, i.e. the concentration relative to other proteins in the sample, could be a determining factor shaping the properties of the assay. To test the influence of the relative concentration of target protein in the original sample, similar experiments were performed with CRP spiked into plain PBS medium and 100% FBS. The resulting data for CRP in PBS can be seen in Figure 3-11 and is showing very similar behaviour to the data recorded in 1% FBS (sensitivity of 0.006 ± 0.0004 µA cm^{-2} $(ng\ mL^{-1})^{-1}$, LOD of 10 ± 6 ng mL^{-1}). The fact that the curve is not shifting significantly, indicates that the amount of CRP adsorbed within the protein layer does not change significantly upon addition of the interfering proteins from 1%FBS. Under the assumption that a fully occupied monolayer of protein is formed on the electrode, the absence of this change is surprising as a change of relative concentration of target versus non-target protein in solution would be expected to lead to a relative change within the protein monolayer. The absence of this change therefore indicates that a full monolayer is not formed under the conditions used and that the CRP adsorbed onto the surface therefore only depends on the concentration of CRP in the sample governed by the intrinsic adsorption properties of the protein. This argumentation obviously only remains true under the conditions used to perform the assay as presented, a change of parameters could very well cause a change in this behaviour, which is investigated later for cTnI. Furthermore, higher interfering protein concentration (>1% FBS) could still lead to the formation of a dense monolayer, where

the signal attained is shifted to higher concentrations due to the fact that the relative concentration of target to interfering proteins became a determining parameter.

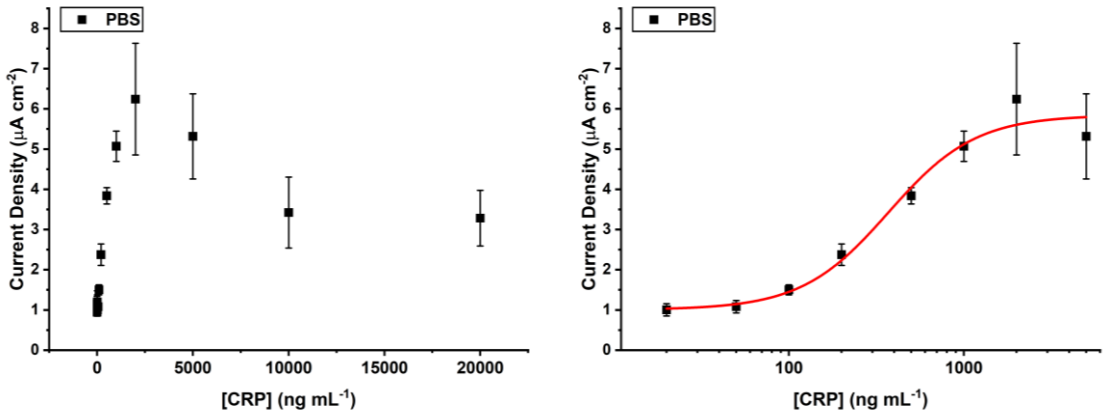


Figure 3-11 Calibration curve for static amperometric dot blot assay performed on SPCE arrays for CRP spiked into PBS-buffer. The curve is similar to the one obtained from CRP spiked into 1% FBS suggesting that the relative concentration of target to interfering protein is not determining the strength of signal or concentration of signal onset (under the assay conditions used). This indicates the amount of CRP adsorbed to the electrode under such conditions depends on intrinsic factors of the protein electrode interaction. The red fit resembles a logistic curve as guide to the eye. Data represent averages of three independent measurements and error bars the associated standard deviation.

According to these considerations, exposure to CRP spiked into 100% FBS instead of diluted serum, should lead to the formation of a fully occupied monolayer of protein and would therefore lead to a state where the target protein concentration depends on its concentration relative to the interfering protein within the sample. This would be expected to cause a shift of the curve towards higher concentrations of target protein. In fact, when such an experiment is performed the data for the steady-state current density are shifted as expected so that significant signals are only reached at 50 times higher concentrations compared to the 1% FBS calibration. The calibration curve for this experiment is shown in Figure 3-12. It also shows that the maximum attainable current

density is reduced (by more than three folds to 1.5 ± 0.2 µA cm^{-2}) while the errors obtained for each concentration are larger as expected for a protein layer of higher coverage and thickness.

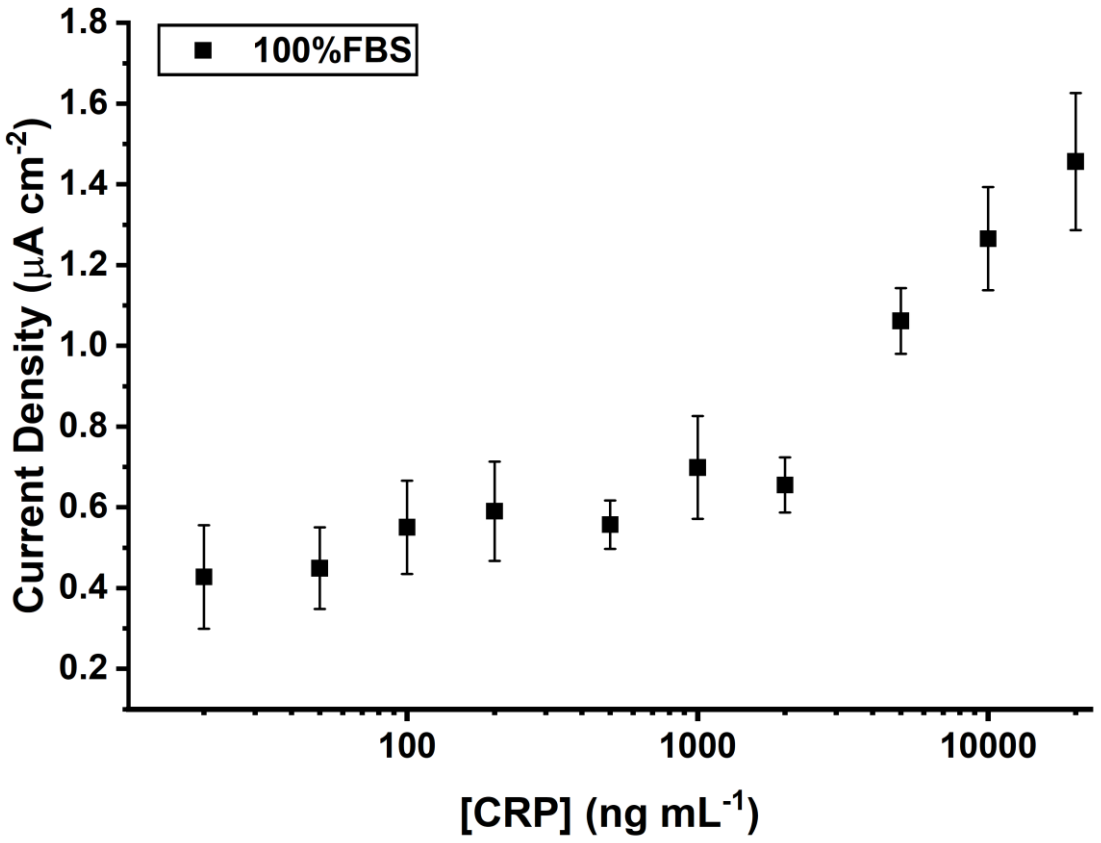


Figure 3-12 Dose response curve for amperometric dot blot assay on SPCE performed on CRP spiked in 100% FBS. As expected, the relatively higher concentration of interfering proteins competing for adsorption on the electrode surface leads to less target protein being adsorbed at a certain concentration compared to the 1% FBS samples. Less target on the surface results in smaller currents and the response is shifted towards higher concentrations.

To demonstrate the general applicability of the proposed sensing concept for the assaying of circulating biomarkers, 1% FBS samples spiked with cTnI as another common protein biomarker were interrogated using the proposed assay. Figure 3-13 shows a calibration curve as obtained by performing an amperometric dot blot assay on samples

of different concentrations of cTnI spiked into 1%FBS using the associated biotinylated antibodies for on-surface recognition of target protein within the film. It is evident that the signal obtained is increasing together with the concentration of target protein spiked into the original sample solution. These results demonstrate the applicability of the assay for cTnI detection.

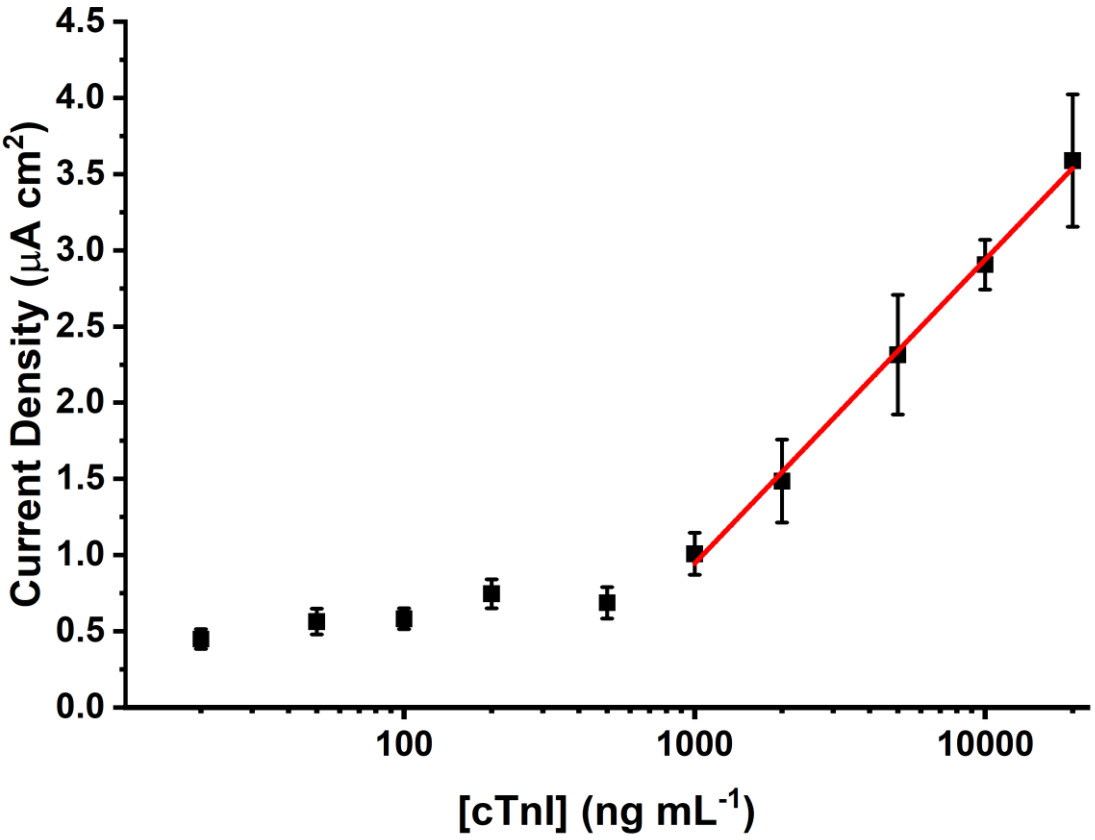


Figure 3-13 Dose response curve for amperometric dot blot assay on SPCE performed on samples of cTnI spiked in 1% FBS. The red line shows a linear fit (R^2 = 0.99) to the semi-logarithmic data with a slope of 0.38 ± 0.01 μA cm^{-2} log(ng mL^{-1})$^{-1}$ and an intercept at -5.0 ± 0.2 μA cm^{-2}. Error bars denote the standard deviation between three independent measurements.

However, it can be seen that rather than resembling the curve for CRP in 1% FBS, for the curve for cTnI in 1% FBS, the signal onset is shifted towards higher concentrations while the maximum attainable signal is reduced by about a third (to 3.6 ± 0.4 μA cm^{-2}). This

can potentially be attributed to the intrinsic adsorption properties of cTnI, but also the difference in molecular properties of cTnI and CRP. As discussed in more detail in 1.5, cTnI is a small protein of 209 amino acids with a mass of 24 kDa suspected to remain largely unordered (without a stable tertiary structure).[152] This lack of a tertiary structure would mean a more substantial adsorption of the whole peptide chain to the electrode surface, causing parts of the protein to be inaccessible for antibody binding. For these reasons, there will be less epitopes exposed to the solution phase for a protein film formed from exposure of the surface to a certain concentration of cTnI leading to a lower signal generation compared to that obtained for the CRP samples. As explained above, from the similar assay statistics of the assay performed for CRP spike in PBS and 1% FBS, it was hypothesised that the procedure used to create the protein film from the 1% FBS samples did not lead to a full monolayer coverage of protein on the electrode. Therefore, it was expected that a prolonged exposure time would lead to a higher protein coverage and in turn to a higher surface concentration of target protein accessible for antibody interaction. Because the results obtained for the calibration with cTnI were significantly shifted (towards higher concentration) compared to the CRP response, varying the exposure time was tested for cTnI spiked into 1% FBS to investigate its effects on the assay statistics for cTnI. Several incubation times were tested and 4 minutes of incubation seemed to show the largest improvement in signal generation compared to the standard 2 minutes of exposure. The two calibration curves for 2 and 4 minutes of exposure to the protein solution are depicted in Figure 3-14. The results show that a significantly increased signal is reached for this extended exposure time especially within the lower range of concentrations. While below 1000 ng mL^{-1} the signals associated with different concentration for the 2 minutes exposure are not

significantly distinguishable, the data for the 4 minutes exposure shows a clear trend of increasing signal with concentration. This trend can be fitted with a semi-log linear fit resulting in a sensitivity of 0.36 ± 0.02 µA cm^{-2} log(ng mL^{-2})$^{-1}$ and an LOD of 0.9 ± 0.2 ng mL^{-1}. This indicates the increase in sensitivity at lower concentrations achieved by the increase in exposure time.

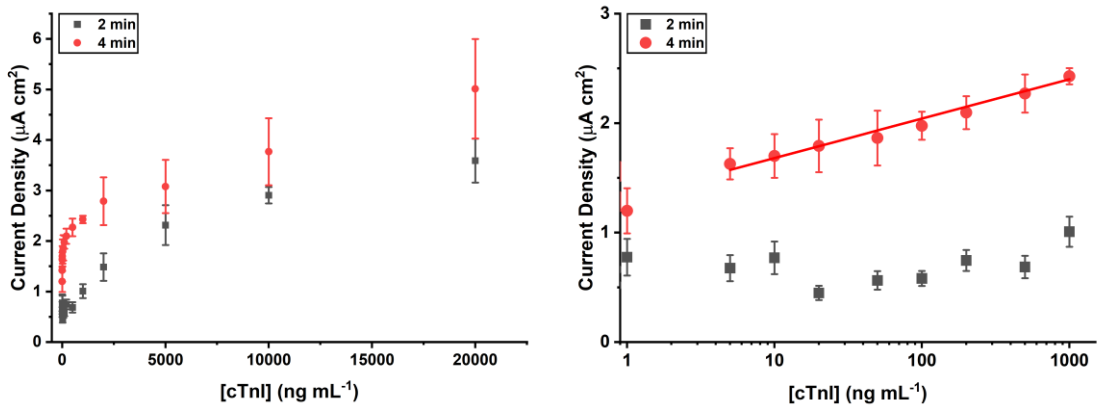


Figure 3-14 Left: Full calibration curves for cTnI spiked into 1%FBS for 2 and 4 min exposure to protein solution. Right: Enlarged region from left graph, for the lower range of concentrations of these two curves in semi-log format. A clear improvement in signal generated at lower target concentrations can be seen from the data when using the extended incubation time, although the errors for each measurement are significantly increased for the 4 min incubation, potentially cuased by the increase in interfering proteins on the surface. The red line shows a linear fit ($R^2 = 0.98$) to the semi-logarithmic data with a slope of 0.36 ± 0.02 µA cm^{-2} log(ng mL^{-1})$^{-1}$ and an intercept at 1.32 ± 0.05 µA cm^{-2}. Error bars denote standard deviation from three independent measurements.

The specificity of the response for cTnI was assessed by comparing the signal obtained from a mid-range concentration of target protein spiked into 1%FBS with the signals recorded from exposure to different interfering proteins (see Figure 3-15). It is evident from this data that the generated signal is indeed specific to the relevant target protein and the signals from interfering proteins (BSA, HSA, Fibrinogen, Myoglobin, all at a

concentration of 1 mg mL^{-1} resembling their abundance in 1% serum) remain consistently below 20% of the specific signal for 10 µg mL^{-1} cTnI spiked in 1% FBS. The background signal from interfering species obtained for the cTnI antibodies is slightly reduced compared to the signal obtained from CRP antibodies exposed to surfaces carrying non-target protein. This is potentially caused by a higher non-specific adsorption of the CRP antibodies when compared with the cTnI antibodies.

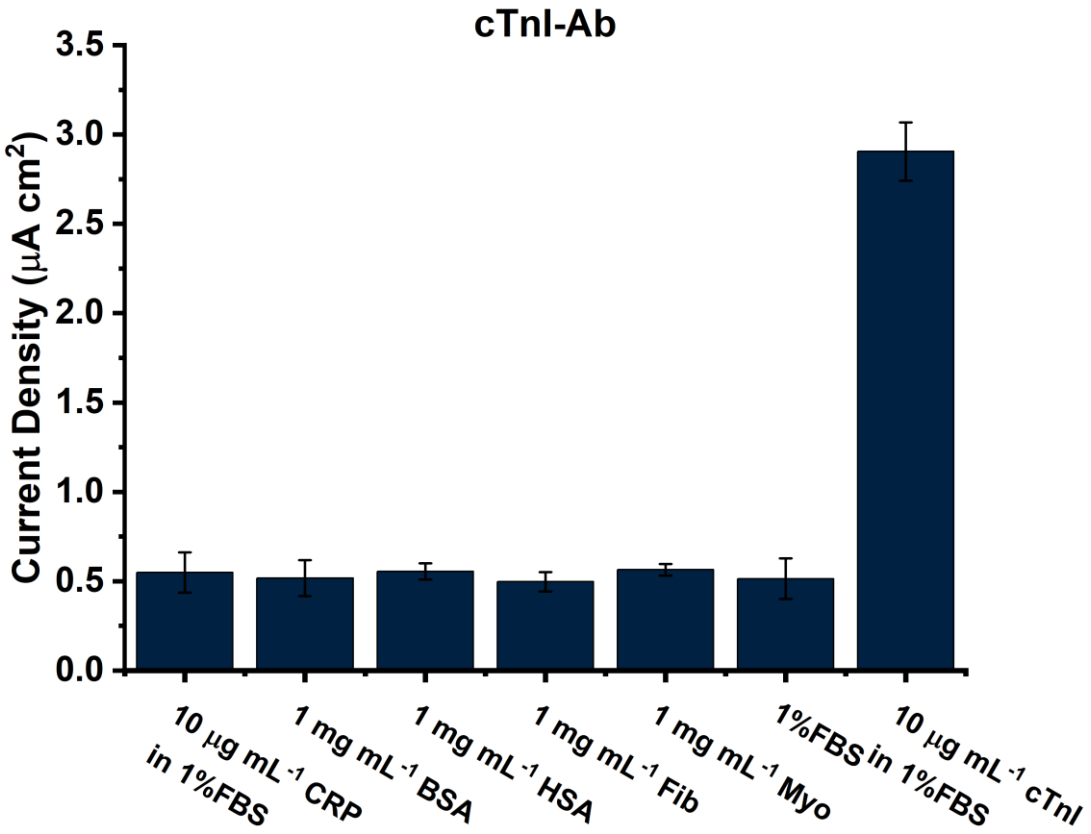


Figure 3-15 Specificity analysis for amperometric dot blot assay on SPCE arrays performed using cTnI-antibodies on samples of different interfering proteins or target protein cTnI spiked into 1% FBS. The signals from interfering proteins (common in serum) at concentrations of 1 mg mL^{-1} remain consistently below 20% of the specific signal for 10 µg mL^{-1} cTnI spiked in 1% FBS. Crossinteractions was also tested with 10 µg mL^{-1} CRP in 1% FBS, showing a similarly low response as the pure 1% FBS sample. Error bars denote the standard deviation between three independent measurements.

3.2.4 Microfluidic Integration of Assay

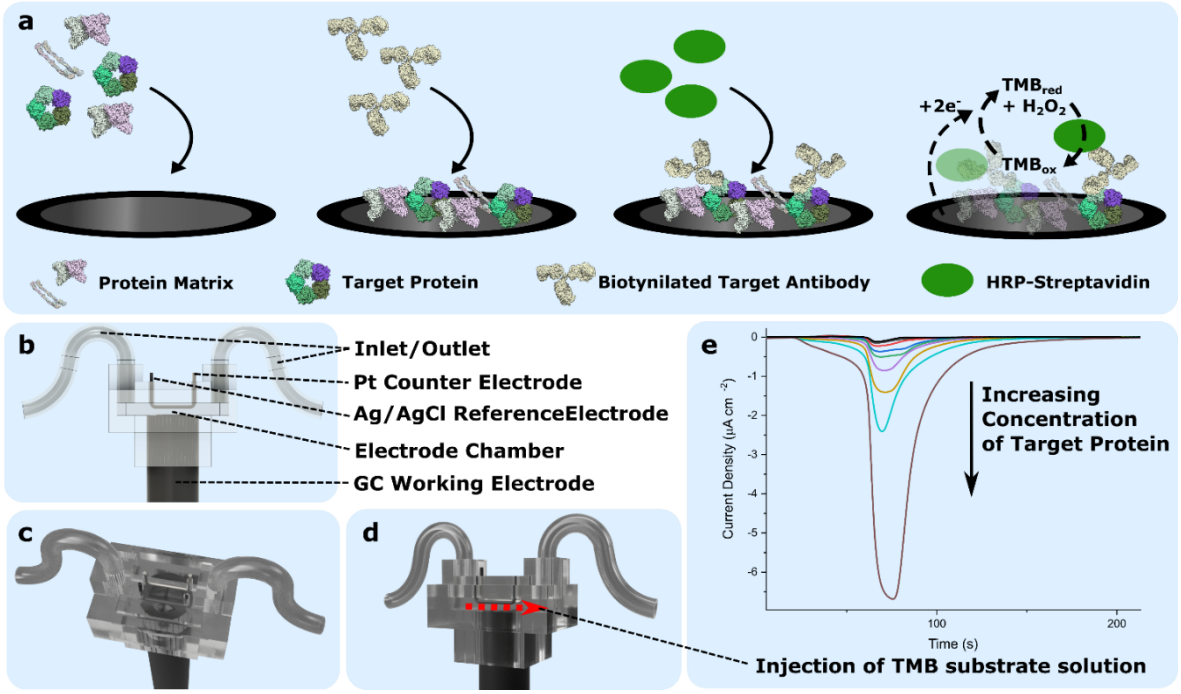


Figure 3-16 Schematic depiction of amperometric dot blot assay with microfluidic integration of the electrochemical measurement and resulting response curves.

The amperometric Dot blot assay in a static format as introduced above yielded results demonstrating the general principle is functioning. However, for the static format several potentials for improvement can be identified including the turn-around time, repeatability, assay handling as well as specificity and sensitivity. It has been suggested before, that the performance of HRP-TMB amplified assays can be improved by performing them under flow.[220] The flow cell standardises the electrode setup, as well as the substrate injection and increases the repeatability of the measurement. Moreover, performing the chronoamperometric measurement under flow omits the long equilibration time to reach a steady state bypassing issues like differences in the loss of HRP activity due to variabilities in the equilibration pathway (stemming from differences in the injection phase) and speeding up the whole measurement process.

Herein, it was therefore tested how the transfer of the amperometric dot blot assay as introduced earlier towards a microfluidic setup would improve the performance. Figure 3-16 depicts the general concept of the assay under flow, where the surface is prepared as before by exposure to the sample solution and then biotinylated antibodies and the HRP-Streptavidin conjugate, sequentially. The electrode is then mounted in a flow cell as illustrated that houses an electrode chamber containing a platinum counter electrode and a Nafion coated Ag|AgCl reference electrode. PBS is flown through the electrode chamber with a flowrate of 100 µL min^{-1} entering at an inlet and exiting through an outlet channel on opposite sides of the electrode chamber (see 2.5 for more detail). The chronoamperometric measurement is then performed under flow. After an initial equilibration time, a volume of 100 µL of the substrate solution is injected to the channel and results in a peak in the current density as illustrated in the lower right of Figure 3-16. The size of this peak is correlated with the initial concentration of target protein in the sample solution.

As a single measurement under flow can be performed within less than 250 s, the time requirement for the electrochemical measurement is sped up by a factor of 8 when compared to the 2000 s of time needed for a single measurement in the static format on the SPCE arrays. The total turnaround time of the assay is decreased by roughly one third (by ca. 25 min), where the total assay time is the sum of measurement time plus the incubation times of sample (2 min), antibodies (20 min) and HRP-conjugate (20 min). Moreover, the peaks recorded upon an injection can be integrated to obtain the total charge transferred within that injection to generate a more robust signal that is not influenced by the small differences in the peak shape, which can be caused by small differences of the electrode arrangement inside the microfluidic channel after changing

the working electrode. Further, the reliability of a measurement for a single electrode can be improved by performing multiple injections of the substrate solution in sequence and taking the average between the experimental values obtained from the repeated injections. An example curve with three such repeated measurements is shown in Figure 3-17. It can be seen that for every injection a spike occurs in the current density-time profile at the respective time of injection. As expected, these spikes obtained from one electrode with a protein film formed from exposure to one concentration of CRP spiked into 1%FBS are highly similar and repeatable. Each of the peaks starts with a small increase in reduction current caused by exchange of substrate solution and buffer and the associated charge redistribution at the electrode within the electrode chamber. This initial change in reduction current is followed by a steep increase. The TMB that has been oxidised at the HRP-modified electrode is quickly being reduced at the surface. Subsequently, the signal then decreases rapidly after reaching a maximum current density as the substrate solution is exchanged by the running buffer again. After every injection the background current can be seen to decrease back to a value close to 0 µA cm^{-2}.

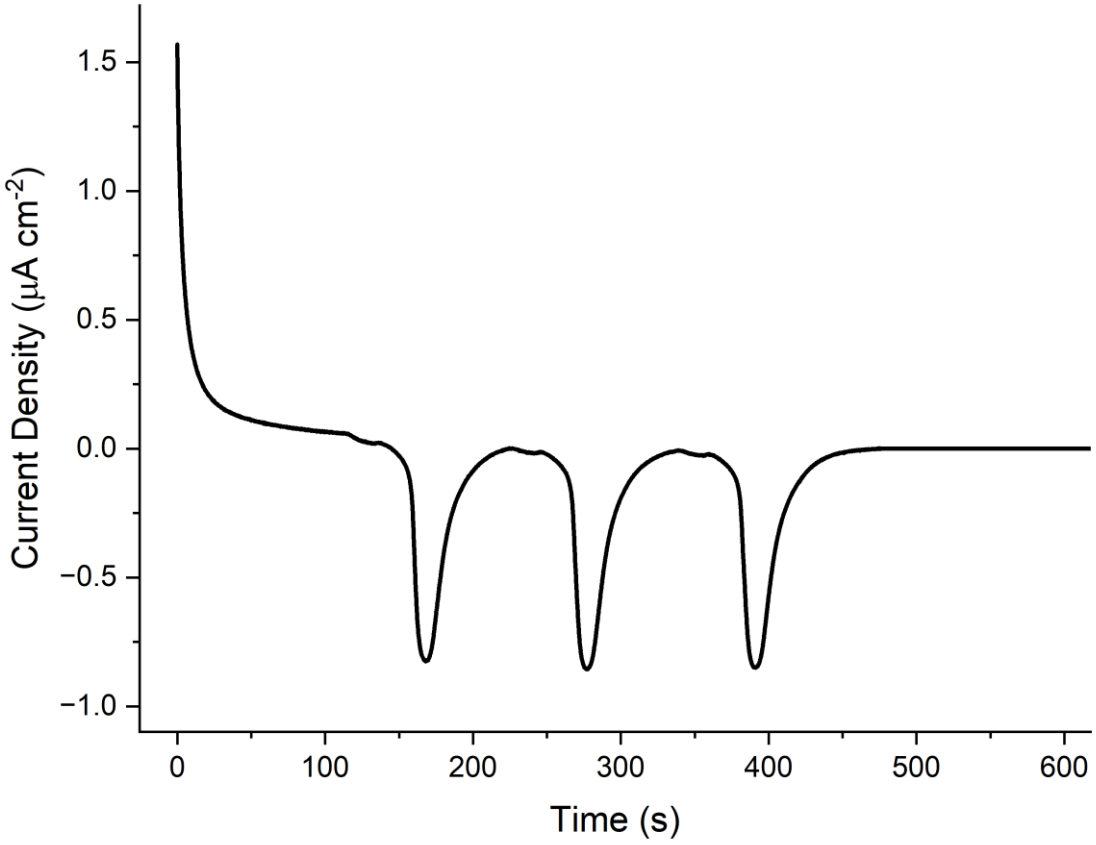


Figure 3-17 Representative curve for response from repeated injection of 100 µL of TMB substrate solution on electrode prepared by exposure to solution of 200 ng mL^{-1} CRP and subsequent assay steps.

When representative peaks recorded on electrodes, which were prepared as explained above by exposure to solutions with different concentrations of target protein spiked into the 1%FBS, are overlayed one obtains the plot shown in Figure 3-18. The injection in these curves was performed at 0 s and the initial lag can be explained by the extension of the tubing running from the injector to the electrode chamber. It can be seen that the curves align very well and the reduction current is reduced to its background level at a time of 200 s after the injection. A clear correlation of peak dimensions with concentration in the original sample solution is evident. The remaining current density

increase obtained for 1% FBS with no CRP present is caused by non-specific adsorption of antibodies and HRP-molecules to the protein film.

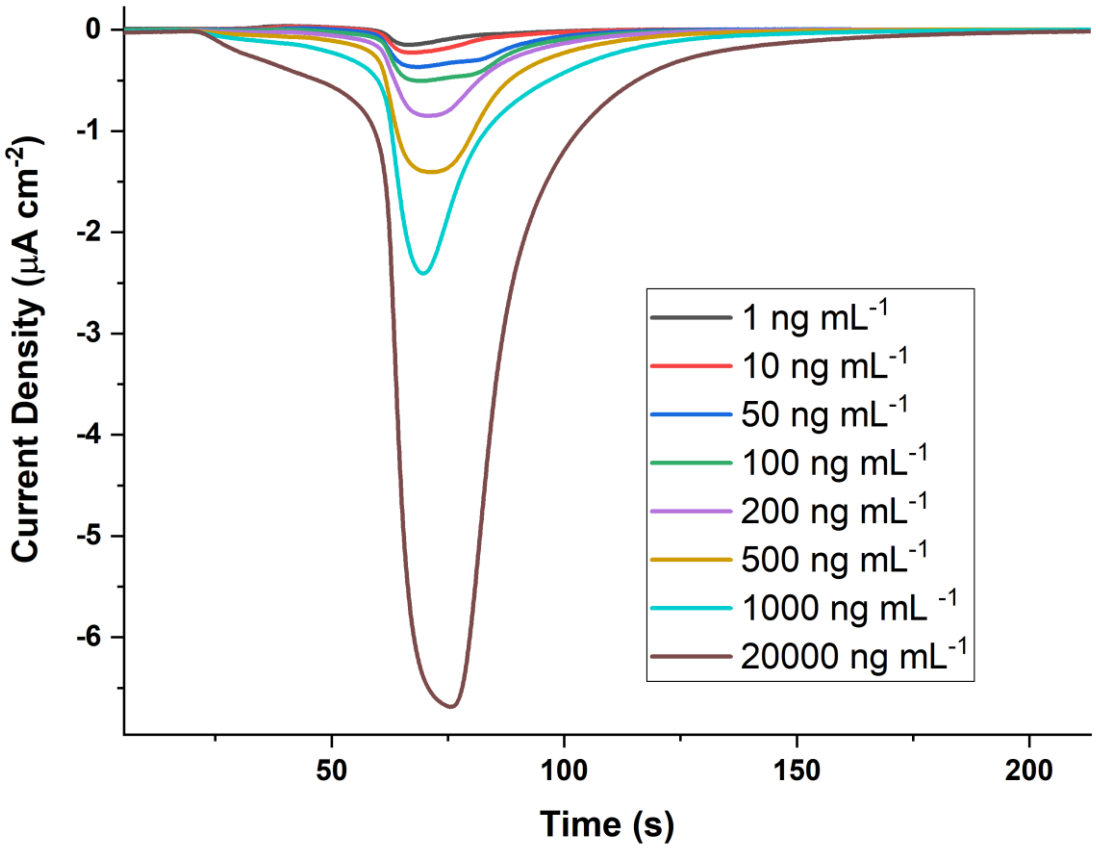


Figure 3-18 Representative response curves for microfluidically integrated amperometric dot blot for different concentrations of CRP spiked into 1% FBS. A time shift was applied so that the time of injection coincides for all shown curves.

When the current density spikes are integrated and averaged (3 repeated injections per electrode, 3 electrodes per concentration), the associated calibration curve shown in Figure 3-19 is obtained. The data can be seen to follow a Langmuir curve with a linear range spanning from 1 to 200 ng mL^{-1} covering the relevant clinical range for CRP. It can further be seen that the datapoints have a reduced error compared to the static format indicating the higher repeatability caused by the measures taken above enabled through the microfluidic integration. Interestingly, the reduction in signal that was obtained in

the static assay is not evident for the assay performed under flow for the investigated concentration range. This might be due to the different modes of measurement that are performed under static and microfluidic conditions. While for the static measurements the steady state current recorded is equivalent to the current density of TMB reduction at the electrode surface at which the inflow of oxidised TMB produced at the HRP molecules is a constant (and balancing the reduction), the microfluidic measurement records a current spike with dimensions that are correlated to the total number of oxidised TMB reduced at the electrode within a certain time of exposure of the surface carrying HRP molecules but not necessarily reaching a steady-state. The two modes of response (Langmuir-like or with a dropped plateau) seen across the different variants of the amperometric dot blot introduced here, will be discussed in the theoretical considerations following the next section (c.f. 3.2.6).

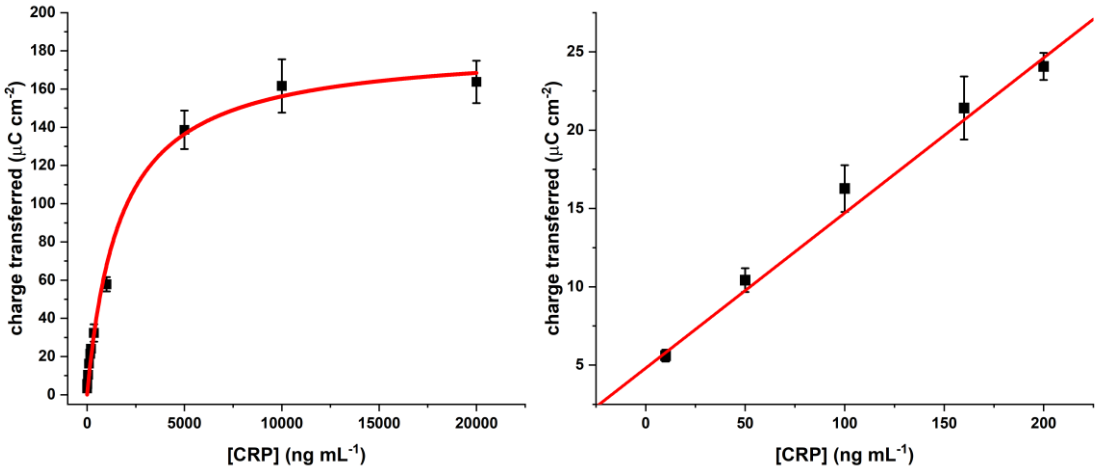


Figure 3-19 Left: Full calibration curve of micrfluidically integrated amperometric dot blot assay. The red lines corresponds to a Langmuir-Freundlich fit as a guide to the eye. Right: Linear range of calibration curve. The fit corresponds to a linear curve with an intercept of 4.8 ± 0.4 µC cm^{-2} and a slope of 99 ± 4 µC mL cm^{-2} pg^{-1} with a correlation coefficient R^2 = 0.99

Further, the specificity of the obtained response towards target protein was tested by evaluating the response for samples carrying interfering proteins (BSA, Fibrinogen, HSA, Myoglobin, all at concentrations of 1 mg mL^{-1}) similar to the experiments performed for the static assay. The results for this analysis are depicted in Figure 3-20 and show the high specificity that is achieved for the amperometric dot blot assay under flow. The signals attained from these interfering proteins were typically <5% of the specific signal to a medium clinically relevant CRP concentration (200 ng mL^{-1}), all spiked into 1% FBS. These results show that the specificity is improved significantly for the assay performed under flow compared to the static assay. This is potentially caused by the smaller rate of error that is apparent in the signal from the assay performed under flow leading to smaller statistical deviations and therefore a lower average background signal.

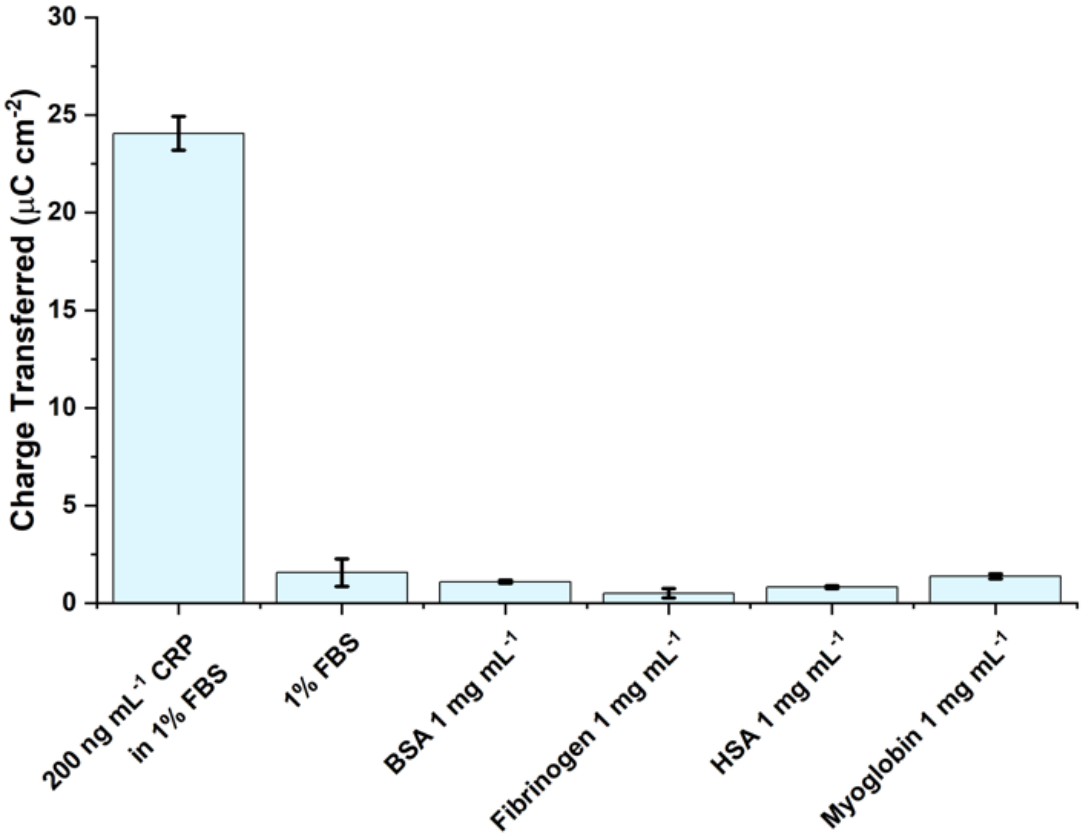


Figure 3-20 Specificity analysis of microfluidically integrated amperometric dot blot assay showing response to target and different interfering proteins spiked into 1%FBS sample. The interfering proteins are chosen for their high abundance in serum (BSA, HSA) and their known potential to interfer in diagnostic assays (Fibrinogen, Myoglobin).

For an assessment of the sensing performance of the amperometric dot blot assay under flow several samples of 1%FBS spiked with CRP in concentrations not included in the calibration curve were prepared to perform a spike recovery test. The spiked and associated recovered concentrations can be viewed in Table 3-1 together with the percentage recovery. This analysis shows a high accuracy in recovery with recovery percentages consistently lying in a range of 98 to 108 % of the original spiked concentration. All the observed concentrations lie in the window of concentrations relevant for clinical quantification of CRP serum levels.

Table 3-1 Spike recovery analysis on microfluidically integrated amperometric dot blot assay.

Spiked Concentration in 1% FBS [ng mL^{-1}]	Measured Concentration [ng mL^{-1}]	Percentage Recovery [%]
20	21	105
40	43	108
80	83	104
120	117	98

3.2.5 Transfer to Other Electrode Surfaces

The phenomenon of non-specific protein adsorption is a general one and applies to various surface geometries and structures. Therefore, it was expected that also the working principle of the amperometric dot blot assay, introduced and evaluated in the above, would proof generally applicable for different electrode surfaces. To examine this hypothesis, several electrode surfaces were tested for the use in an amperometric dot blot format under flow. Apart from the electrode and protein film preparation, the assay was performed in the same way as introduced above. The surfaces examined include clean polycrystalline gold electrodes and the same electrodes functionalised with a SAM of HT molecules as well as a 3-MPA SAM. For the latter carbodiimide coupling was employed for the protein film formation to include a surface that forms chemical bonds with the protein matrix. Although the SAM modified electrode means giving up the advantage of omitting the requirement for electrode modification, the idea here is to show that the dot blot concept proposed in this work remains generally transferrable to various electrode surfaces. A calibration curve for the plain gold surface can be seen in Figure 3-21. The signal was also compared to subsequent measurements for just 1%FBS to show the specificity of the signal while ruling out any accumulating

signal over time (cf. Figure 7-7). The dose response curve on gold clearly shows a performance comparable with that on the GCE surface and provides significant signals above an LOD of 10 ng mL^{-1}. As mentioned for the dose response curves shown earlier, again, the Langmuir fit performed, although sufficiently accurate, does not explain the curves behaviour to its full extent as for higher concentrations it lacks a clear plateau. This will be discussed in more detail in the theoretical considerations following this section (c.f. 3.2.6). Finally, dose response curves for the other surfaces mentioned are shown in the appendix (c.f. Figure 7-8).

As expected, apart from the surface carrying a hexanethiol SAM all surfaces can be seen to exhibit the hypothesised behaviour of a signal generation correlated with target concentration in the original complex sample. When looked at individually the hexanethiol SAM surface qualitatively shows this behaviour too, but the signal is significantly diminished for all concentrations so that its curve seems flat compared to the other surfaces. This is probably due to a blocking of electron transfer from oxidised TMB due to the dense coverage of the electrode by the SAM. Nonetheless, these results together demonstrate the general applicability of the assay principle to various surface morphologies and thus confirm the initial hypothesis of an electrochemical dot blot principle, which was to use the electrode surface itself independent of its material or modification as the substrate for target protein adsorption.

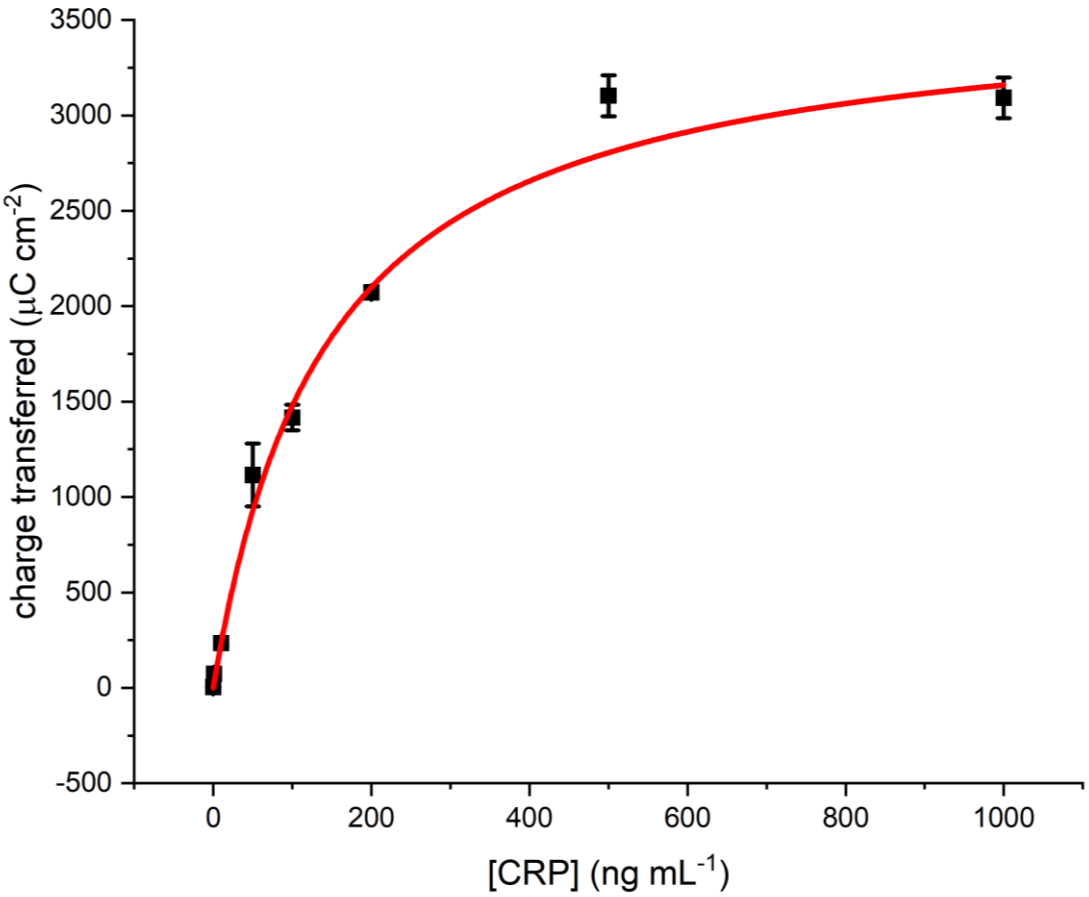


Figure 3-21 Calibration curve of microfluidically integrated amperometric dot blot assay on polycrystalline gold disk electrode. Performed for the indicated concentrations of CRP spiked into 1% FBS. The red line corresponds to a Langmuir fit with a plateau at 3616 ± 247 µC cm^{-2} and a half maximum concentration of 143 ± 20 ng mL^{-1}. Error bars denote the standard deviation between three independent measurements.

3.2.6 Theoretical Considerations for an Amperometrically Amplified Dot Blot Assay

As briefly highlighted above, the dose response curves obtained for the Amperometric Dot Blot work presented herein, do not entirely follow the Langmuir behaviour that is typically expected in sensing applications. On the one hand side, this can have multiple reasons, a discussion of which would go beyond the scope of this thesis. Among them is the insight that the Langmuir curve is just one of many estimations of the actual systems

behaviour.[221] On the other hand, the data presented show a fairly obvious disparity with the Langmuir curve, the dose response curves obtained show a behaviour which either indicates a retarded plateauing behaviour at very high target concentrations or a distinct decrease in signal after reaching a maximum response. To elucidate the origins of the observed behaviour, this paragraph provides some theoretical background into the anticipated signal in the context of the results on the amperometric dot blot format presented above.

For simplicity, the system is reduced to yield a most basic scenario. A fluid phase substrate solution comprising hydrogen peroxide and TMB is considered, within which hydrogen peroxide is present in a notably higher concentration compared to TMB ($H_2O_2 \gg TMB$). This fluid is in contact with an electrode featuring attached HRP molecules in close proximity. The physical dimensions are not further considered here. The system can then be characterized by the ensuing reaction scheme:

$$HRP + H_2O_2 \underset{k_{-1}}{\overset{k_1}{\rightleftharpoons}} \text{C-1} + H_2O$$

$$\text{C-1} + AH_2 \xrightarrow{k_2} \text{C-2} + AH \qquad \text{Eq. 8}$$

$$\text{C-2} + AH_2 \xrightarrow{k_3} HRP + AH + H_2O$$

Hereby, HRP, C-1 and C-2 describe the different oxidation states of the HRP molecule, while AH_2 stands for the fully reduced state of TMB. In addition to these chemical reactions, the diffusion of molecules and any external fluxes (e.g. in the case of a microfluidic integration) as well as the reduction of TMB at the electrode would have to be taken into account to describe the full system. However, as the timescale of the chronoamperometric measurement taken is always much greater than that of the diffusive processes involved, the role of diffusion becomes merely a factor of

proportionality when the focus lies on the overall calibration curve (i.e. final signal after a certain time vs concentration of target rather than a time dependent signal curve). Because the measured output current I_s is then proportional to the rate at which TMB is oxidised at the HRP (diffusion influences the associated proportionality constant, but does not qualitatively change this relation), the system can be described through the following differential equation:[222]

$$\frac{d}{dt}[TMB] = -c_{HRP}\frac{k_3[TMB][H_2O_2]}{\frac{k_3}{k_1}[TMB] + [H_2O_2]} \qquad \text{Eq. 9}$$

Hereby, c_{HRP} denotes the total surface concentration of HRP molecules, $[TMB]$ describes the concentration of TMB at a given time t, $[H_2O_2]$ the concentration of hydrogen peroxide at time t, k_3 and k_1 are the respective reaction rate constants from Eq. 8. Under the assumption that there is an excess of H_2O_2 compared to TMB (i.e. $[H_2O_2] \gg [TMB]$, Eq. 9 simplifies and can be rewritten for the concentration of oxidised TMB at time t, $[TMB_{ox}]$, with c_{TMB} describing the total concentration of TMB molecules in the system ($c_{TMB} = [TMB_{ox}] + [TMB]$) to obtain the following differential equation:

$$\frac{d}{dt}[TMB_{ox}] \approx c_{HRP} \cdot k_3(c_{TMB} - [TMB_{ox}]) \qquad \text{Eq. 10}$$

Eq. 10 can be solved, and using the initial condition of $[TMB_{ox}] = 0$ at $t = 0$ one obtains:

$$[TMB_{ox}] = c_{TMB}(1 - e^{-c_{HRP} \cdot k_3 \cdot t}) \qquad \text{Eq. 11}$$

$$[TMB] = c_{TMB} - [TMB_{ox}] = c_{TMB} \cdot e^{-c_{HRP} \cdot k_3 \cdot t}$$

To derive an expression for the measured output current I_m measured at time t_m, one can now take the derivative of Eq. 11 with regards to time and evaluate the expression at time t_m at which the measurement is taken:

$$I_m \propto \frac{d}{dt}[TMB_{ox}] = -c_{HRP} \cdot k_3 \cdot c_{TMB} \cdot e^{-c_{HRP} \cdot k_3 \cdot t_m} \qquad \text{Eq. 12}$$

Now, to fully describe the output signal as a function of the original target protein concentration one has to consider the following relation between the concentration of HRP on the surface and the target protein at the surface, where it is assumed that the interaction of protein with the surface follows a Langmuir adsorption isotherm to the first order,[94] and the interaction of target with the biotinylated antibody as well as that between antibody and Streptavidin-poly-HRP-conjugate reaches saturation and is therefore negligible. The accessible surface sites for adsorption of target proteins are denoted with $c_{surface}$, while the concentration of surface adsorbed analyte is $c_{adsorbed}$:

$$c_{HRP} \propto c_{adsorbed} = \frac{c_{surface} \cdot c_{analyte} \cdot K_a}{c_{analyte} \cdot K_a + 1} \qquad \text{Eq. 13}$$

Together with Eq. 12, this yields a relationship connecting the output current I_m with the analyte concentration $c_{analyte}$, where the two cumulative constants $C_0 = c_{surface} \cdot k_3 \cdot c_{TMB} > 0$ and $C_1 = c_{surface} \cdot k_3 \cdot t_m > 0$ were introduced for simplification:

$$I_m \propto -\frac{c_{surface} \cdot c_{analyte} \cdot K_a}{c_{analyte} \cdot K_a + 1} \cdot k_3 \cdot c_{TMB} \cdot e^{-\frac{c_{surface} \cdot c_{analyte} \cdot K_a}{c_{analyte} \cdot K_a + 1} \cdot k_3 \cdot t_m}$$

$$I_m \propto \frac{C_0}{1 + \frac{1}{K_a c_{analyte}}} \cdot \exp\left[-\frac{C_1}{1 + \frac{1}{K_a c_{analyte}}}\right] \quad \text{Eq. 14}$$

This expression shows a sharp increase for small values of $c_{analyte}$, reaches a maximum $I_m^{max} \propto \frac{C_0}{e \cdot C_1}$ at $c_{analyte}^{max} = \frac{1}{K_a(C_1 - 1)}$ for $C_1 > 1$ and approaches a horizontal asymptote when its limit regarding an increasing analyte concentration is evaluated according to the following:

$$\lim_{c_{analyte} \to \infty} I_m \propto C_0 e^{-C_1} \quad \text{Eq. 15}$$

While for $C_1 \leq 1$ the expression does not reach a maximum but instead monotonically increases and approaches the same limit for high concentrations of $c_{analyte}$. This result provides a theoretical framework that predicts two qualitatively distinct possible outcomes for any calibration curves measured via the amperometric dot blot assay associated with the two regimes of $C_1 > 1$ and $C_1 \leq 1$ (see Figure 3-22). For the first case a Langmuir-like increase in signal with ascending concentration is followed by a maximum signal after which the signal drops exponentially back to the mentioned asymptote, while in the second case the curve follows a Langmuir-like curve modulated by an exponential factor that is dependent on the analyte concentration leading to a stretched Langmuir curve. The transition between these two outcomes is smooth and again depends on the value of C_1, where for increasing values of this constant higher than one the maximum shifts towards lower concentrations and the drop in signal becomes more significant. This means depending on the value of C_1 the phenomenon of the signal drop will only become apparent above certain concentration. As C_1 is

modulated by the target surface concentration upon protein film formation $c_{surface}$. The surfaces of these two systems (GCE vs SPCE) are different and therefore can be assumed to also have different adsorption properties towards protein from the solution, which again results in a difference in the target surface concentration upon protein film formation $c_{surface}$. Especially, as the SPC electrodes are plasma cleaned before their application in the assay, their surface could be expected to have a higher carrying capacity due to the nature of plasma cleaned carbon.[223] An increase in the surface concentration of target again would correlate with an increase in C_1. Such a shift in C_1 might have resulted in a shift of the curve towards the regime that exhibits a maximum with a subsequent reduced plateau for the SPC electrodes. In any case, the theoretical framework derived here, can explain the two distinct shapes seen for the amperometric assay performed in a static format.

However, when the microfluidic format is taken into consideration, the above consideration must fail due to the mode of measurement whereby the current is not left for equilibration, but rather the instant rate of reduction of TMB_{ox} is recorded and then integrated over time. This means the substrate is constantly replenished through flow until it is replaced by the running buffer. For these reasons the theoretical consideration given above cannot be applied to the microfluidic format directly, but can still provide a rough estimate of the behaviour.

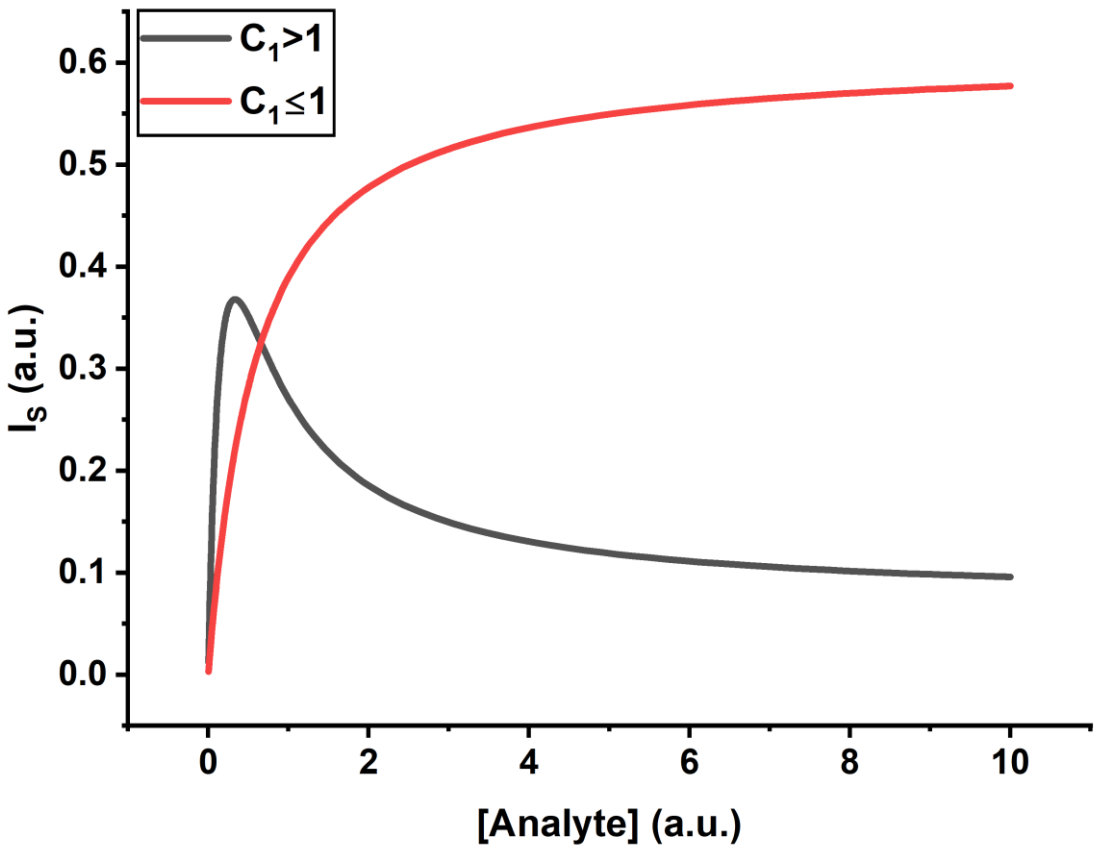


Figure 3-22 Theoretical calibration curves calculated for two distinct parameter sets that produce resulting curves in each of the two predicted regimes of response, the Langmuir-like regime (red curve) and the Hook-like regime (grey curve).

3.3 Conclusions and Future Work

Herein, the concept of an electrochemical dot blot assay for the quantification of protein biomarkers in the context of diagnostic settings was developed and tested. First, to gain an understanding of the underlying concept of protein adsorption at electrode surfaces, the adsorption of mixed protein solutions was observed via electrochemical and SPR based methodologies. From these results an exposure time for protein film formation was chosen based on the antagonistic needs for high target protein content within the surface film and a good electrochemical accessibility. It was further examined to use an

electroactive antibody conjugate for the electrochemical transduction. For this purpose, a conjugate of CRP antibody and Methylene Blue NHS ester was formed and found to yield specific signal generating capabilities. However, due to the inherently low signal for such a setup, an amperometrically amplified format based on the combination of biotinylated target antibodies and poly-HRP-Streptavidin conjugates together with a substrate solution containing H_2O_2 and TMB was chosen for any further experiments.

Based on these considerations, a sensing platform omitting any surface functionalisation of the sensing electrodes was established for the amperometrically amplified quantification of target protein from 1% diluted serum. This was achieved by utilising native adsorption of protein to clean, unmodified electrode surfaces directly for target recruitment from a complex sample. Due to this employment of unmodified electrodes the proposed assay is extremely facile and simple in implementation and the factor of stability of surface modification can be completely dismissed. The transfer of the assay to screen-printed-carbon electrodes demonstrated the versatility of the assay and showed improved assay statistics with an LOD of 16 ± 6 ng mL^{-1}. The assay was further confirmed to work for both two different target proteins (CRP, cTnI) and the assay statistics for the cTnI quantification were shown to be omptimisable by a change in incubation time for the protein film formation (LOD 0.9 ± 0.2 ng mL^{-1}). The microfluidic integration of the assay for the CRP quantification showcased the beneficial capabilities of such microfluidic setup for a further improvement of the assay statistics (LOD 2 ± 1 ng mL^{-1}) relative to the SPCE CRP assay. Moreover, the turnaround time was shown to be significantly reduced (by about 33%) and the assay handling facilitated due the omittance of manual steps during the injection of substrate solution. The signal in all these variations was shown to be specific to the target protein with low levels (<5% for

the microfluidic platform) of noise from interfering proteins. Finally, this was demonstrated for different electrode surfaces (polycrystalline gold, glassy carbon, MHA-SAM) to highlight the general applicability of the assay concept. Theoretical considerations for this sensing platform were performed and yielded results indicating two distinct regimes of target response based on the properties of the system at hand. These theoretically predicted regimes had been visible in the experimental results presented earlier.

As the presented results are demonstrating the basic functionality of the proposed concept and investigate the potential of the methodology, there remain several aspects open for further interrogation. As the fundamental principle is based on the adsorption of protein to electrode surfaces, this process could be a potential starting point for further optimisation. Additional electrode surfaces need to be investigated and the differences in their applicability for the assay compared. The interaction of electrode surfaces and specific target proteins could benefit from further elucidation. Although in the presented work it was focused on the simple case of native adsorption to yield advantages associated with the use of unmodified electrodes, future work could also interrogate different electrode modifications like NHS modified carbon for its potential in such an assay. The time of protein adsorption is potentially a target for optimisation for every target protein that is chosen for quantification. As the relative concentration seems to become more relevant at longer adsorption times, another potential project could look into the depletion of serum, i.e., the removal of the most abundant proteins, to change the relative concentration in favour of the target protein. Many more subjects remain open for further optimisation of the assay and it is meant to form a starting point for further exploration in future work.

Chapter 4

Faradaic Shotgun Tagging for the Voltammetric Quantification of Target Protein in Complex Media

4.1 Introduction

As discussed earlier in 1.1, novel electrochemical techniques satisfying the current requirements for decentralised, clinical POC testing are highly sought for. Traditional electrochemical biosensing methods can generally be categorized into labelled and label-free methodologies.[44] Where the former is relying on two subsequent recognition processes, while the latter is based on a single recognition event at the electrode surface. Both of these classes of electrochemical immunosensors are associated with their own advantages and limitations, which have been discussed in 1.2.2.

In an approach to combine the advantages of both these pathways, in this work it is proposed to use so called ensemble protein labelling in combination with a surface recognition event for the electrochemical quantification of protein biomarkers in complex samples. Although ensemble protein labelling, also known as shotgun tagging, has been applied in different contexts, it has not found application in electrochemical

diagnostics yet. The technique has traditionally found application in mass spectrometry (MS) quantification, where the technique involves derivatizing peptides with specific isotopic masses,[224] or isobaric mass tags.[225, 226] Over the past decade, a diverse range of MS applications employing such tagging strategies has been introduced to support the analysis of protein binding interactions.[227] However, it is important to note that MS methods remain costly, operationally demanding, unfit for decentralised applications and generally cannot be scaled easily.[228] Ensemble protein labelling using fluorescent or chemiluminescent probes has also been extensively applied in cell-based protein imaging.[229] Various bioconjugation strategies, such as aryl-diazonium,[230] azlactone,[231] vinyl sulfone,[232] and NHS-ester/isothiocyanate approaches, have been utilized for this purpose.[233] Among these, succinimidyl ester methods, which operate effectively under neutral pH conditions with readily available reagents, are widely prevalent.[225, 226, 234, 235] They target primary amine groups at the N termini of polypeptide chains or exposed lysine residues, which are known to be abundantly present in proteins in general.[236]

As discussed in 1.2.2, the traditional strategy for labelled electrochemical immunosensing of target protein within a complex sample involves the generation of a specific label, such as a labelled antibody derivative, in combination with a sandwich type second recognition event at an electrode for a sandwich type quantification. To overcome disadvantages associated with the generation of specific labels and the complexities involved in handling such assays, label-free methodologies have been introduced (see 1.2.2 for more detail). Aiming to omit the secondary recognition in original sandwich-type assays, the proposed electrochemical quantification of target protein from non-specifically (shotgun) tagged complex samples using a Faradaic label in combination with a specific capture at an electrode poses a novel strategy for protein

biosensing. The working principle is sketched in Figure 4-1. The proposed assay is based on the tagging of all proteins in a complex sample with the redox tag methylene blue-NHS ester in a first step (c.f. Figure 4-2). In a subsequent step, electrodes carrying antibodies as recognition elements are exposed to the solution of the tagged proteins to recruit tagged target proteins to the surface. After washing the electrode to remove non-specific protein, a DPV measurement is used to quantify the electrochemical tag at the surface and thereby the target protein concentration in the original sample. By employing ensemble labelling of all proteins in a complex sample, this strategy enables circumventing the potentially labour-intensive (and costly) construction and characterization of sandwich tags, such as redox-tagged antibodies, (see 1.2.2 for more detail) while simultaneously maintaining the advantageous properties of such approaches regarding signal generation. The proposed strategy therefore aims to pose a significant improvement compared to traditional labelled (i.e., sandwich) techniques. This improvement would be of similar degree as that of the already applied label-free approaches (single-step immunorecognition with no secondary labelling event), but the novel technique would provide a turn-on signal, which avoids limitations of the label-free techniques caused by drift and instabilities of the baseline signal (c.f. 1.2.2). Furthermore, due to its inherently non-specific labelling process, the proposed methodology is readily applicable for the simultaneous analysis of multiple protein targets from the same sample by employing multiple electrodes with different antibodies (see Figure 4-1).

This work aims to demonstrate the proof-of-concept for the proposed sensing mechanism in the design of a sensor capable of performing duplex biomarker analysis from the same sample solution. The nonspecific succinimidyl ester tagging of proteins

in serum prior to target capture and voltammetric quantification is introduced for the two crucial cardiovascular biomarkers C-reactive protein (CRP) and cardiac troponin I (cTnI) as model biomarkers (for more details see 1.5). For this purpose, the establishment of the target recruiting electrodes based on the commonly used physisorption of antibodies to electrodes is summarised. Then the experiments undertaken to confirm the applicability of the shotgun tagging approach for the quantification of proteins from complex samples are discussed. The principle and statistics of the assay in a static format are then presented. Subsequently, the integration of this method into a microfluidic mixing system, which significantly shortens assay durations and renders the assay applicable in a semi-automated setup, is demonstrated. Finally, the developed system is validated through its application in spike recovery analysis using serum samples spiked with the selected biomarkers, as well as through the analysis of real patient samples.

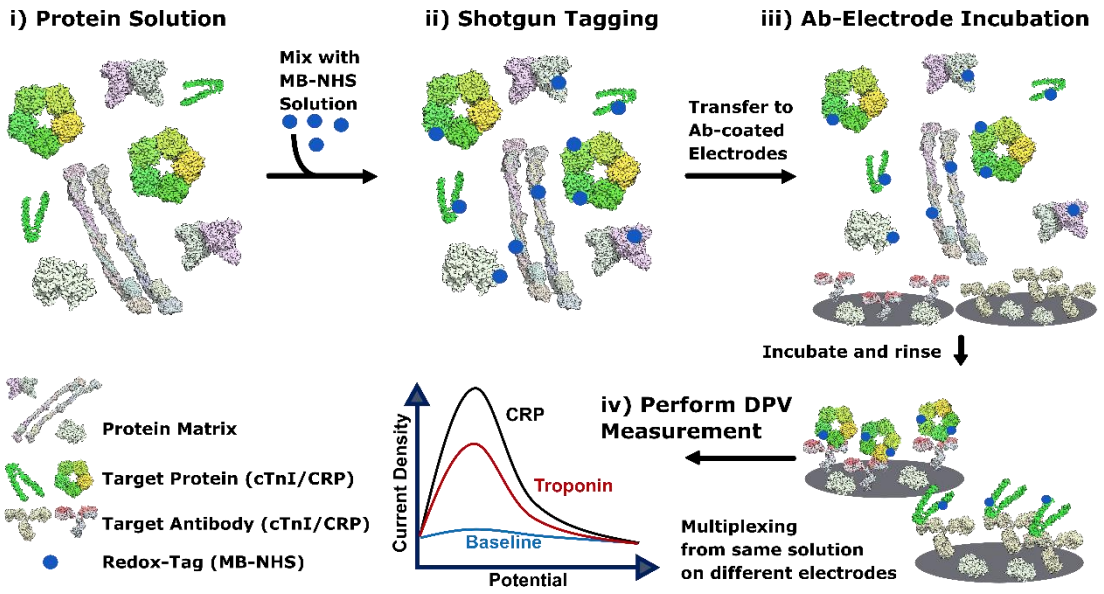


Figure 4-1 Schematic depiction of the experimental concept of the faradaic shotgun tagging for voltammetric protein quantification. i) The mixture of proteins from the sample to be analysed (including the target proteins and other interfering proteins) is

prepared. ii) The sample is mixed with the MB-NHS label for ensemble tagging of proteins. iii) The mixture is then incubated with the Ab-functionalised electrodes (multiple for multiple target proteins). iv) After a washing step (to remove any non-specific proteins from the electrodes) a DPV measurement reports on the target protein concentration in the original sample. Adapted from [237] according to CC license.

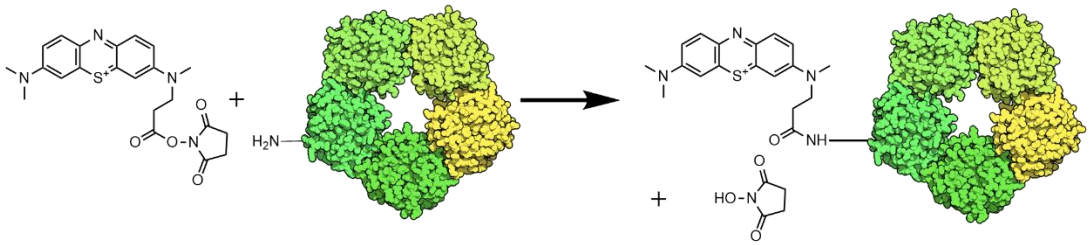


Figure 4-2 Schematic depiction of process for tagging of protein (CRP) with Methylene Blue NHS ester (MB-NHS) targeting the amine residues on the protein. For more detailed discussion of the coupling mechanism see 1.4.1. Adapted from [237] according to CC license.

4.2 Results and Discussion

4.2.1 Establishment of Assay Concept and Working Conditions

This section will summarise the establishment of the core assay conditions, while the main results will follow in sections 4.2.2 to 4.2.5. The core principle of the proposed assay requires the non-specific labelling with MB-NHS of proteins in a complex sample (see 2.4.2.1). This is done by mixing a buffered solution of proteins with a solution of the dye in DMSO. In a subsequent step antibody modified electrodes (c.f. 2.3.3) are incubated with the tagged protein mixture to recruit the target protein. After a washing step, the surface bound tag and thereby the target protein is quantified through a DPV measurement (c.f. 2.4.2.2). The electron transfer between the electrode and MB-NHS

bound at the surface causes a peak at around -0.4 V vs Ag|AgCl with a peak current correlated to the surface concentration of Methylene Blue.[238] Coating electrodes with antibodies as recognition elements through physisorption is a well-established protocol that has been shown to result in good surface coverage of antibodies.[239] In this work, the coating of GCEs with antibodies through physisorption was used to form responsive electrodes by incubating them with antibody solution overnight and subsequent blocking with BSA (see 2.3.3 for details). The successful modification was confirmed by EIS measurements showing the characteristic increase in charge transfer resistance after functionalisation (see appendix Figure 7-9) as well as specificity data shown later in this text.

A final concentration of 10 µg mL^{-1} of MB-NHS in DMSO was chosen according the manufacturer's protocol, yielding a final concentration of 19 µM, approximately five times higher than the estimated total serum protein concentration as detailed in 2.4.2.1. To validate the covalent attachment of MB-NHS to the proteins, an SDS-PAGE analysis was conducted (see 2.3.8 for experimental details), revealing the characteristic fluorescent signal emitted by MB-tagged proteins (see Figure 7-12). The successful covalent tagging of protein with the MB-NHS label was confirmed by performing an in-gel fluorescence experiment. Samples were prepared by labelling 1 mg mL^{-1} BSA in MES buffer according to the standard preparation as for the assay. Methylene blue is natively fluorescent and its presence can therefore be confirmed in fluorescence measurements. The labelled BSA shows fluorescence when illuminated in the gel, while the fluorescence is absent for the native BSA. In the case of non-specific attachment of the tag, the staining would be expected to be removed from the protein upon the gel electrophoresis. As the sensing platform relies on the quantification of target proteins

via the specific electrochemical response generated by the MB-NHS tag, before any other measurements it was confirmed that none of the proteins interrogated (target and interfering) exhibits a native electrochemical response in the range of potentials observed (see appendix Figure 7-10). This was done by interrogating native and MB-NHS tagged proteins (for experimental detail see 2.4.2.7.2). To maximize the achievable signal range, the optimal buffer conditions are determined by evaluating the Faradaic response (magnitude of peak current) to target proteins in relation to the buffer pH used for the protein dilution and MB-NHS tag concentration (see 2.4.2.7.1 for experimental detail). It was observed that the largest signal span was achieved using MES buffer at pH 6.0, in accordance with established succinimidyl ester coupling efficiencies.[240] For this analysis, the assay was performed using different pH buffers to dilute the protein solutions. The buffers used had pH values of 5.0, 6.0, 7.0 and 8.0 in Sodium Acetate, MES and Phosphate (pH 8.0, pH 9.0) buffers respectively. The results, shown in Figure 7-11 (appendix), demonstrate the change in response as function of CRP concentration at the studied pH values corresponding to each of the selected buffers. The coupling performed in 100 mM MES buffer at pH 6.0 showed the highest signal to noise ratio and a broader dynamic range. Therefore, these coupling conditions were applied for all further measurements.

To confirm the specificity of the electrochemical signal upon successful capture of MB-tagged proteins, a control experiment was conducted (see 2.4.2.7.3 for experimental detail). For this purpose, electrodes coated with 100 µg mL^{-1} BSA, representing an antibody-free interface, were exposed to different concentrations of common proteins labelled with MB-NHS ester as to the assay protocol. These proteins included 100 µg mL^{-1} BSA, 100 µg mL^{-1} HSA, 10 ng mL^{-1} CRP, 100 ng mL^{-1} CRP, 10 ng mL^{-1} cTnI, and 100 ng

mL^{-1} cTnI. The recorded electrochemical faradaic responses observed were consistent with the background noise levels (consistently less than 20% of the specific signal from 30 ng mL^{-1}), signifying low non-specific binding (see appendix Figure 7-13). This experimental outcome reaffirms the specificity of the faradaic signals detected on antibody-modified electrodes to the interaction of on-surface antibodies with the target species. Further, the specificity of the assay was evaluated by comparing the response upon exposure of antibody labelled surfaces to different interfering proteins and target protein CRP (c.f. 2.3.10.2 and 2.4.2.5 for experimental detail). The electrochemical measurements were performed on GC electrodes via DPV and the SPR experiments were conducted using gold chips (see appendix Figure 7-15), more in depth specificity analysis will be discussed in the following sections.

It was further concluded through SPR measurements that the labelling of target proteins exhibited no significant impact on the binding affinity of immobilized antibodies towards their respective target (see appendix Figure 7-14). The affinities of anti-CRP modified SPR chips toward native and MB-labelled CRP were investigated by exposing the chips to several concentrations of free CRP, or MB-Labelled CRP. The cumulative capture of CRP onto the SPR chip as measured by SPR was fitted using a 1:1 binding model to estimate the respective rate constants. The apparent dissociation constant (K_D) for native and MB-labelled CRP were calculated from the fitted curves. Statistical analysis of the results showed that, considering the measurement errors, there is no significant difference in the observed dissociation constants (K_D) between MB-labelled CRP (9.5×10^{-10} M) and free CRP (2.8×10^{-10} M). The values closely resemble those found through Langmuir–Freundlich fitting of the electrochemically resolved response, approximating 5.0 nM, serving as an estimation of the thermodynamic properties of the system.[221]

4.2.2 Static Assay for Single Target Protein

Using the conditions determined as explained in the previous section, assays were performed for diluted human serum spiked with a range of concentrations for the two target proteins CRP and cTnI separately. Under static conditions, each sample was incubated with MB-NHS for 30 minutes for the non-specific labelling process, followed by reaction termination through the addition of ethanolamine and hydroxylamine. Subsequently, the labelled samples were incubated with the electrodes, which were modified with antibodies in a previous step according to the protocol found in 2.3.3. This incubation step was set to a duration of 15 minutes before undergoing differential pulse voltammetry (DPV) sweeps in a 0.1 M aqueous KCl solution. The resulting voltammetric curves revealed robust correlations between the concentrations of CRP and cTnI, and their respective DPV peak currents at -0.4 V (see Figure 4-3). The response curves follow Langmuir isotherms and a semi-logarithmic region can be identified. The assay in this format achieved detection limits (LOD) of 1 pg mL^{-1} for CRP and 0.3 pg mL^{-1} for cTnI, with dynamic ranges spanning from 1 pg mL^{-1} to 100 ng mL^{-1} for CRP and from 0.6 pg mL^{-1} to 20 ng mL^{-1} for cTnI (Figure 4-3). Towards higher concentration the DPV signals reached saturation, indicating a plateau in the signal response as expected.

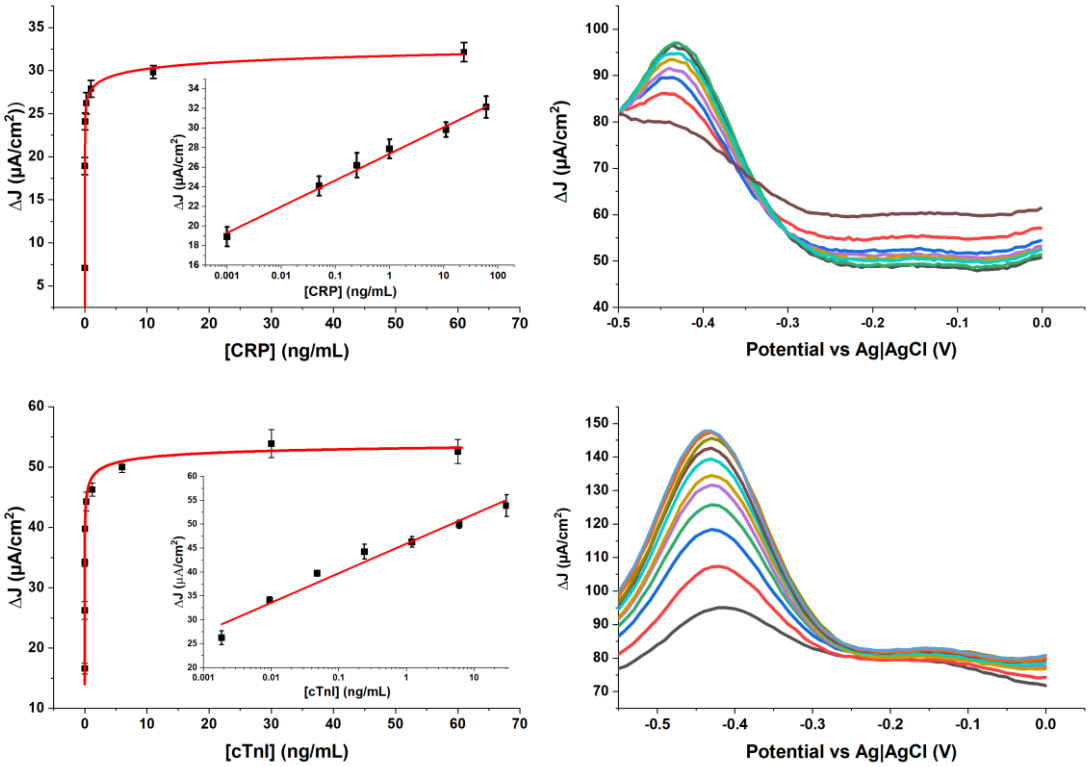


Figure 4-3 Langmuir–Freundlich fits of (upper) CRP spiked in 1% human serum in MES buffer and (lower) cTnI spiked in 1% human serum in MES buffer. Representative DPV peaks as function of (upper) increasing CRP connection on anti-CRP-decorated GCE sensors and (lower) cTnI at anti-cTnI sensors. The bottom DPV voltammograms are the background signals from incubation with unspiked 1% HS. Error bars represent standard deviations between three independent measurements at three different electrodes. Insets are associated linear semi-log correlation trends with correlation coefficients (R^2) of 0.99 and 0.97, respectively. Adapted from [237] according to CC license.

The robust differentiation between specific target proteins and non-specific binding was evaluated through the measurement of voltammetric responses when sensors were exposed to common proteins expressed in serum, namely human serum albumin (HSA), fibrinogen, and bovine serum albumin (BSA) was tested, each labelled with the MB tag. Additionally, the antibody cross-reactivity was investigated by assessing responses to elevated concentrations of CRP at anti-cTnI-modified electrodes, and conversely, high concentrations of cTnI at anti-CRP-modified electrodes. All findings consistently

indicated a high degree of specificity, (see Figure 4-4) corroborating analogous SPR analyses (Figure 7-15). The response (peak current density) to a variety of interfering species, is consistently <10% of the target-specific signal (30 ng mL^{-1} CRP) at anti-CRP interfaces and <20% at anti-cTnI interfaces (4.8 ng mL^{-1} cTnI) with all studied interferents, indicative of good specificity and low cross-reactivity. Furthermore, repeat exposure of anti-CRP- or anti-cTnI-modified electrodes to MB-labelled 1% FBS resulted in no discernible change in background signal, remaining at the background levels (see Figure 4-4, insets). This additional observation reinforces the conclusion that the faradaic DPV signal is predominantly dependent on the specific recruitment of target analytes, with minimal contribution from non-specific protein adsorption on the electrode surface.

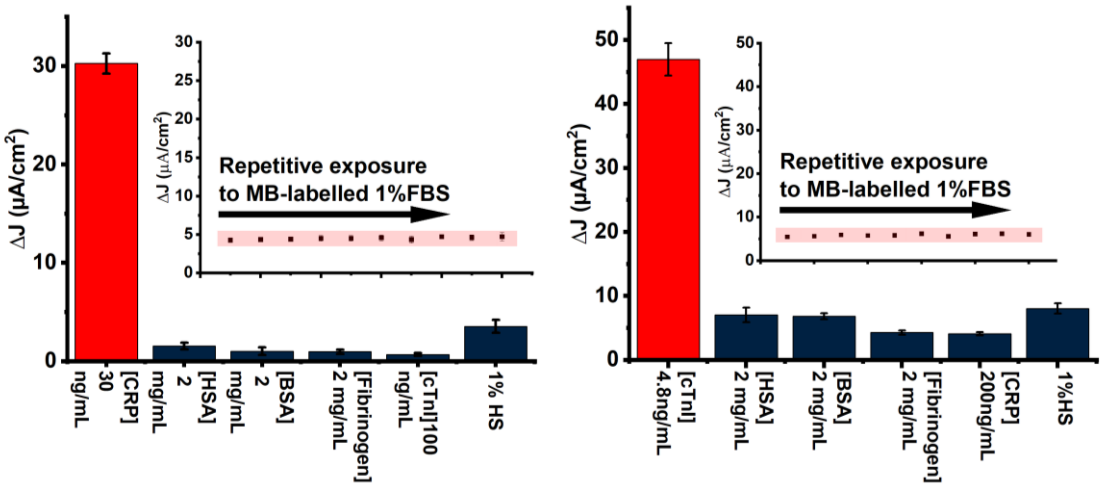


Figure 4-4 Electrochemical specificity analysis for (left) anti-CRP-modified electrodes and (right) anti-cTnI-modified electrodes in offline single protein analyses. The response (peak current density) to a variety of interfering (HSA, BSA, Fibrinogen, 1% HS) species is shown. Insets show the response of the anti-CRP-modified electrode and the anti-cTnI-modified electrode upon repetitive exposure to MB-labeled 1% FBS. Error bars represent the standard deviation between three independent measurements. Adapted from [237] according to CC license.

4.2.3 Static Assay for Multiple Target Proteins (Multiplexing)

As sketched in 4.1, the simultaneous detection and quantification (multiplexing) of multiple target proteins can be performed from the same solution by employing multiple electrodes coated with the associated antibodies. In an evaluation of offline multiplexing, mixtures of CRP and cTnI (spiked into 1% human serum) were examined using two electrodes, one functionalized with anti-CRP and the other with anti-cTnI in combination with the same labelling procedure as for the single assay. The ensuing responses (see Figure 4-5) closely resemble those obtained with individual protein spikes, underscoring the minimal levels of interface and antibody cross-reactivity.

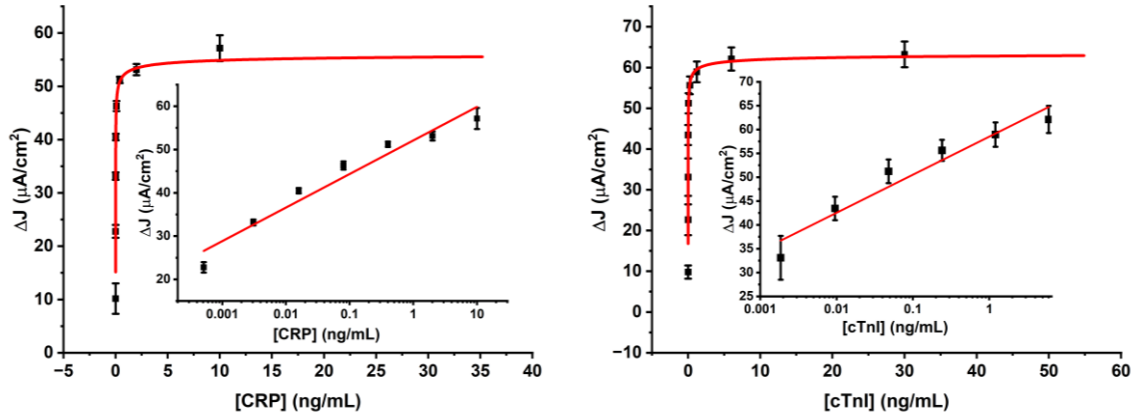


Figure 4-5 Langmuir–Freundlich fits from offline multiplexed protein assays as detected from mixed samples of both proteins at a CRP-responsive sensor (A) and a cTnI-responsive sensor in dilute serum (B). Respective LODs are 1.0 pg mL^{-1} for CRP and 0.6 pg mL^{-1} for cTnI. Insets depict associated linear semi-log correlation plots with correlation coefficients (R^2) of 0.95 and 0.94 for CRP and cTnI, respectively. Error bars represent standard deviations between three independent measurements performed on three different electrodes. Adapted from [237] according to CC license.

4.2.4 Microfluidic Integration of Assay

Subsequently, a microfluidic Y-shaped serpentine mixer was designed and employed to enhance the mixing of samples and reagents, as well as to reduce assay time within a sealed, low-volume chamber directly accessible via a syringe pump. Initial evaluations were conducted using a setup with an electrode chamber containing one working electrode for the quantification of single target proteins (refer to Figure 7-16 and Figure 7-17). Subsequently, the design of the microfluidic setup was extended to enable the simultaneous detection of both markers spiked into human serum in a multiplexed format using two working electrodes simultaneously. The integration of two sensor electrodes in-line allowed for the quantification of dual markers in a multiplexed fashion, all within a 15-minute timeframe (see Figure 4-6). The sample and the MB tag were introduced into their respective chambers through pipetting before being mixed in the serpentine channel by pumping at a flow rate of 20 µL min^{-1}. Subsequently, the mixture was incubated in the electrode chamber for 10 minutes, followed by a washing step consisting of running 0.1 M KCl solution at a flow rate of 100 µL min^{-1} for 60 seconds. Simultaneous differential pulse voltammetry (DPV) analysis was performed at both working electrodes (see 2.4.2.3 for experimental detail).

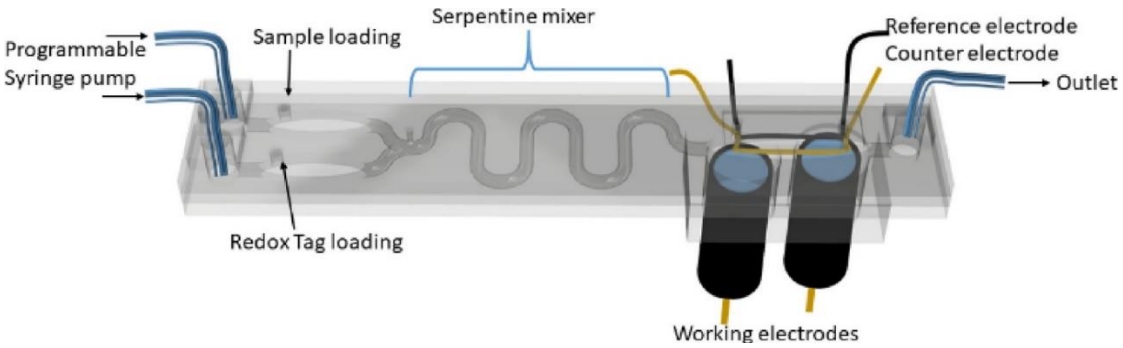


Figure 4-6 Schematic representation of the microfluidic chip used for sample handling and electrochemical detection. The chip houses an electrode compartment with two

working disc electrodes (6.4 mm outer diameter), a Nafion coated reference Ag/AgCl wire electrode and counter platinum wire electrode. A serpentine mixing channel designed to mix sample and reagent connects the electrode compartment to the respective loading chambers. The chambers are loaded with forty microliters of sample and reagent and then closed using adhesive tape. A syringe pump connected to the inlets is used to pump through the serpentine channel the fluids through the channel for 5 min, then 10 min of incubation and 1 min of washing follow. Adapted from [237] according to CC license.

The microfluidic integration further enhanced the assay specificity when compared to that observed in the static assay, as indicated by notably lower responses to interfering species (less than 10% for both anti-CRP- and anti-cTnI-modified electrodes; see Figure 7-18). This improved performance for the platform after microfluidic integration can be attributed to a facilitated mixing and washing processes that enable a more standardised performance.[241, 242]

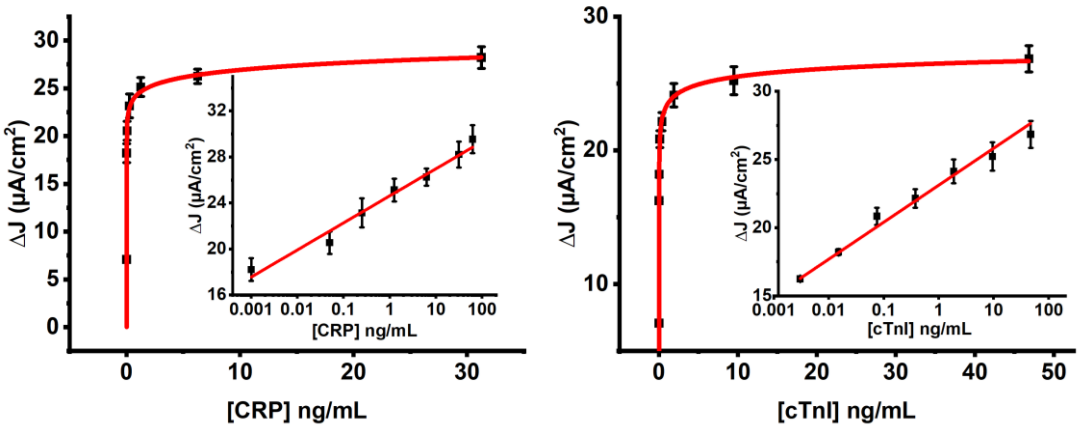


Figure 4-7 Representative Langmuir–Freundlich fits from online multiplexed assays for (A) CRP and (B) cTnI both spiked in 1% human serum in 0.1 M MES buffer. Insets represent the semi-logarithmic region of the curves fitted to a linear response function with correlation coefficients (R^2) of 0.978 for CRP and 0.993 for cTnI. Error bars represent standard deviations between three independent measurements on three different electrodes. Adapted from [237] according to CC license.

The online microfluidic protein configuration demonstrates high levels of assay reproducibility and accuracy, characterized by linear dose-response trends (refer to Figure 4-7 and Figure 7-19) spanning the ranges of 1.0–100 ng mL^{-1} for CRP and 3–62.5 ng mL^{-1} for cTnI. Standard deviations observed across three independent measurements on three distinct sensor electrodes for each protein target were consistently below 10%, indicative of highly commendable reproducibility.

4.2.5 Spike Recovery and Patient Sample Analysis

An assessment of the assay accuracy, conducted through spiked recovery experiments in serum, revealed a highly accurate diagnostic performance (see **Table 4-1** and **Table 4-2**). All calculated recoveries fell within the range of 90-110% of the originally added concentration. This indicates the precise measurement of the target proteins within the intricate matrix of diluted human serum, that contains a multitude of other interfering proteins (such as HSA).

Table 4-1: Spike recovery of CRP in 1% Human Serum. Adapted from [237] according to CC license.

Added CRP Conc. [pg/mL]	Recovered Conc. [pg/mL]	Percent Recovery
261	308	118%
661	664	100%
761	762	100%
1761	1626	92%

Table 4-2: Spike recovery of cTnI in 1% Human Serum. Adapted from [237] according to CC license.

Added cTnI Conc. [pg/mL]	Recovered Conc. [pg/mL]	Percent Recovery
110	118	107%

466	485	104%
1152	1095	95%
1728	1784	103%

To underscore the clinical utility of the proposed assay, randomized patient samples were subjected to analysis using the established quantification protocol, and the estimated concentrations of CRP and cTnI were compared to immunoassay results obtained from an Abbott Architect system (see Figure 4-8). The outcomes of both, CRP and cTnI, analyses exhibited strong correlations.

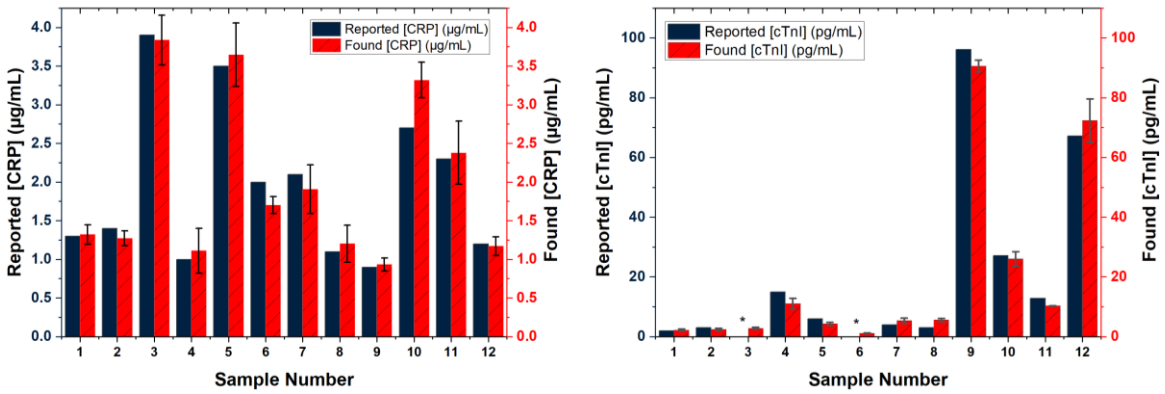


Figure 4-8 Results of CRP concentrations (A) and cTnI concentrations (B) estimated via the proposed shotgun tagging assay blind compared against a reference immunoassay for 12 patient samples (asterisks represent samples where cTnI levels were lower than the immunoassay LOD, i.e., <2 pg/mL). Error bars represent standard deviations from two independent measurements on two different electrodes. Adapted from [237] according to CC license.

The accurate and multiplexed detection of CRP and cTnI holds substantial potential to significantly enhance clinical diagnostics and monitoring, in the case of cTnI and CRP improvements therein yield the potential to reduce mortality rates and significantly improve treatment outcomes for cardiovascular disease (CVD).[12, 243, 244] The analytical

performance outlined above, featuring detection limits as low as 0.6 pg mL^{-1} in serum and dynamic ranges spanning over six orders of magnitude, compare favourably with recent electrochemical platforms designed for CRP and cTnI sensing.[12] Importantly, the proposed method requires a mere 25 µL of sample per assay and the entire analytical process can be completed within just 15 minutes, from sample dilution to readout. This is well below the recognized guidelines recommending an analysis within 1 hour of patient admission, a target that presents a substantial challenge to the applicability of currently available clinical methods.[245]

4.3 Conclusions and Future Work

Presented herein is a single-step assay of notably lower complexity compared to current state-of-the art sensor designs. It is proposed as an alternative for current labelled electrochemical immunosensor designs. By omitting the generation of a specific secondary label and the additional steps in handling associated with relying on a secondary recognition event, the novel methodology not only facilitates the assay applicability, but also enable improved efficiency for the simultaneous quantification of several biomarkers from the same sample solution. The assay is designed for the electrochemical detection of two prevalent cardiac biomarker proteins, CRP and cTnI, serving as representative target proteins. It offers a signal turn-on assay in a highly specific format, effectively amalgamating the advantages associated with both label-free and sandwich-type assays. Furthermore, this method can easily be applied to diverse target proteins within a given sample, thereby establishing it as a cost-effective and readily accessible means for the simultaneous quantification of multiple biomarkers. The reported assays deliver remarkable sensitivity, attaining detection

limits below 1 pg mL^{-1}, while at the same time dynamic ranges spanning over 5–6 orders of magnitude are achieved.

By incorporating this methodology into a semi-automated microfluidic format, a streamlined process requiring minimal user intervention was achieved. The resulting assay provides results within durations of less than 15 minutes. To highlight its clinical relevance, a blind patient sample recovery analysis was conducted. This analysis revealed a strong correlation with standard immunoassay results for both markers. Moreover, the proposed methodology offers universal applicability, maintains robust performance in complex biological samples, and entails a low cost (below US$ 5 per sample consumable cost, as compared to US$ 35 per sample for conventional ELISA).[246] The integration of microfluidics also presents the possibility of fully automated and highly scalable applications for point-of-care use, requiring minimal user training. As stated in 1.6, the study is meant to contribute to the expansion of electrochemical biosensing methodologies to stimulate the development of explorative designs catering the demand for future healthcare solutions. As such, much remains to be investigated and there is plenty of room for further work. Such future investigations, could aim to explore different surface designs. While within the presented work, the complexity of the recognition surface was consciously held simplistic due to the focus on the novel methodology, this also means much is to be gained from further optimisation of each of the involved steps. This is not limited to but could include the sensing (electrode) surface, the labelling process or the electrochemical quantification itself. Regarding the latter, further investigation could involve the amplification of the sensing process. One obvious example for this would be the combination of the presented work with the established redox cycling amplification[247], where MB is used as a mediator transferring

electrons to a redox shuttle (e.g., ferricyanide) in solutions reducing it. This has been shown to amplify the achievable signal for a certain number of MB molecules present on the electrode. In general, many options for further investigation of the proposed platform exist and could be explored in future.

Chapter 5

Electroactive Proteins as Low-Fouling and Transducing Building Blocks for Redox Capacitive Immunosensing of Target Protein

5.1 Introduction

As discussed in 1.2.5, reducing cost and complexities in sensing such as the need for dual recognition in typical sandwich assays is highly sought for and can be achieved through various means. As another approach towards this goal among electrochemical sensing methodologies, reagent-less methodologies have emerged as one of the most promising techniques due to their omittance of the need to spike the sample with any redox probe reducing the interference from such a solution probe, as well as the required end user intervention and cost.[248, 249] Redox Capacitance sensing has become a major field of interest within these reagent-less assays and its high sensitivity has been demonstrated using for example mixed self-assembled monolayers featuring ferrocenylated thiols,[250] thiolated peptide chains featuring a ferrocene moiety as redox active site,[251] Prussian Blue nanostructures,[252] as well as electroactive polymers.[58] One of the greatest

challenges for label-free biosensors in general is signal being generated from non-specific adsorption of protein in complex sample.[94] This challenge is commonly met by introducing low- or antifouling components into the sensing interfaces.[59] However, combining these properties in single components may greatly facilitate the formations of such sensing platforms. As discussed in 1.3.2, Proteins themselves have been extensively employed in biosensing for their anti-fouling properties.[112-114] However, so far such approaches have employed proteins solely for their anti-fouling properties while relying on pathways of transduction that are not exploiting the electroactive properties of protein itself.

As summarised in 1.4.2, the electroactive protein Azurin is well known for its ability to assemble onto self-assembled monolayers in an oriented and electrochemically accessible fashion as mentioned in the introduction.[134, 253] For its properties including its stability in physiological conditions and its hypothesised non-fouling nature as a protein (see 1.3.2) in combination with its electrochemical activity and the established mechanism of assembly onto an electrode, Azurin could be expected to yield potential as a building block for electrochemical protein sensing platforms. Therefore, in this work it is proposed to use the readily available electroactive protein Azurin from *P. aeruginosa* as a transducing and simultaneously anti-fouling building block for the formation of a biosensory surface for target protein immunosensing based on redox-capacitance. The redox centre would hereby act as a electrochemically accessible state on the surface in close proximity to a recognition element anchored next to or on the protein, which would render the surface electrochemically transducing similar to prior examples in literature as detailed in 1.2.2.

For this purpose, it is envisioned to explore SAM surfaces as a support for sensing platforms based on Azurin as an anti-fouling and transducing building block. Two molecules are used to create the SAMs herein, hexanethiol (HT) and mercapto-hexanoic acid (6-MHA). The HT SAM used was expected to produce a highly-ordered, hydrophobic surface for the oriented, irreversible adsorption of Azurin molecules in a later step as reported throughout literature. The 6-MHA film is expected to form a highly-ordered, hydrophilic surface structure with carboxyl end-groups available to solution access for the subsequent coupling of antibodies via carbodiimide chemistry. The mixed films were expected to yield surface structures with varying degrees of intermittent states between the two pure films. Such films would then expose hydrophobic alkyl groups to the solution phase for the adsorption of Azurin as well as hydrophilic carboxyl groups for the coupling of antibodies.

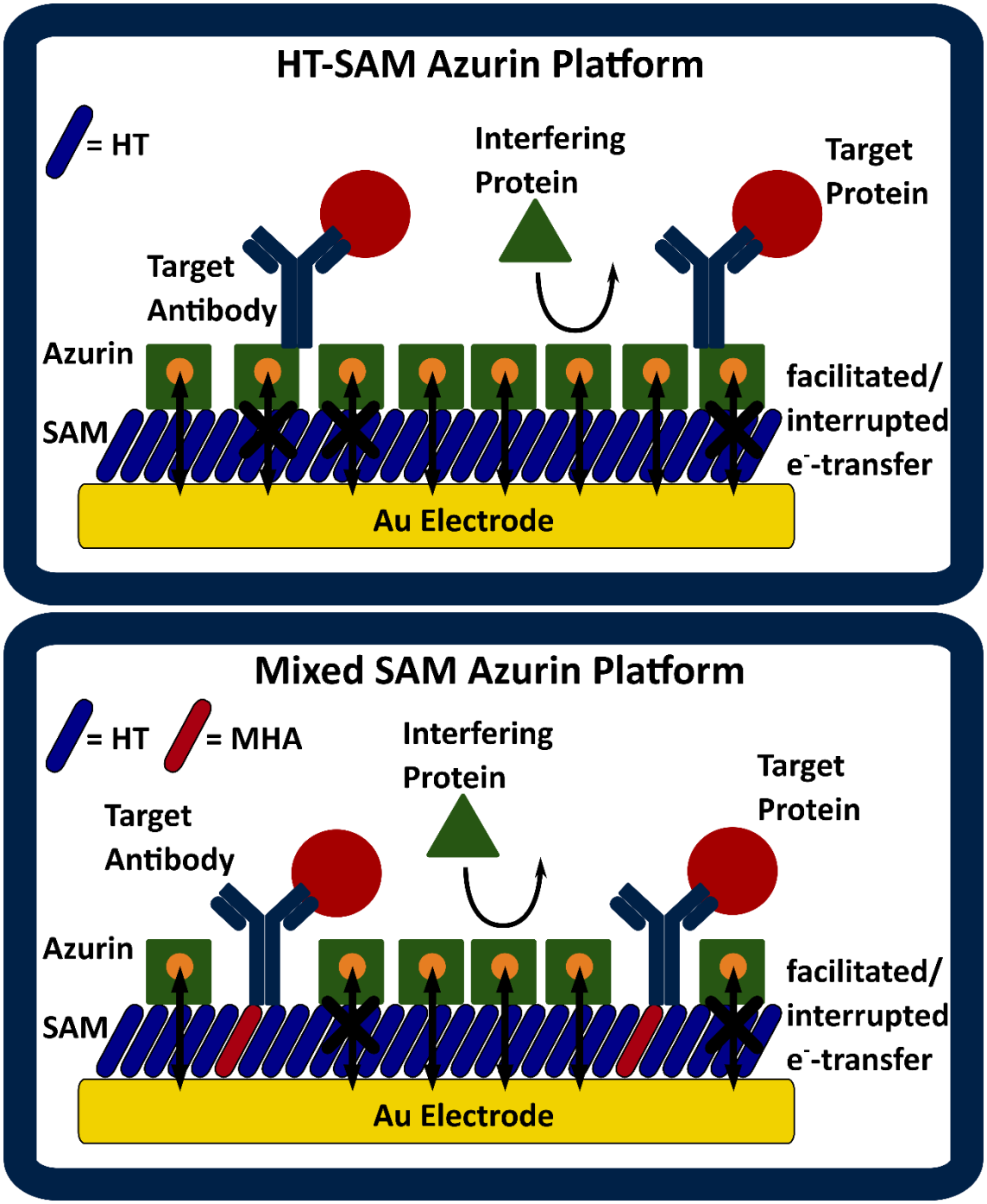


Figure 5-1 Schematic of the hypothesised redox capacitive biosensor platform utilising electroactive proteins as transducing and anti-fouling building blocks. The two proposed modes are based either on the physisorption of Azurin onto a pure HT SAM and the subsequent coupling of antibodies to the protein film (upper). Or the employment of a mixed SAM of HT and MHA, the coupling of antibodies to the carboxyl residues in MHA and the subsequent backfilling of the platform with Azurin (lower). The signal is

transduced by the change in redox accessibility caused by binding of antigen in proximity to the redox centre of the electroactive proteins.

5.2 Results and Discussion

To evaluate the feasibility of the proposed platform, first the assembly of self-assembled monolayers used later on as well as their characterisation on different gold surfaces are presented. Then a summary on the assembly of the electroactive proteins onto these surfaces and their further functionalisation with target antibodies is given together with their electrochemical properties and characteristics. Finally, the sensory performance of the so formed surfaces will be evaluated and the chapter will finish with a conclusion and an outlook on future prospects.

5.2.1 Self-Assembled-Monolayer Formation and Characterisation

Self-Assembled monolayers of hexanethiol (HT) and 6-mercaptohexanoic acid (6-MHA) as well as mixtures of different ratios (MHA:HT: 1:4, 1:49, 1:249) of these two constituents were produced on polycrystalline gold surfaces using a common procedure (c.f. 2.3).

The SAMs were formed by incubation of the gold surfaces in a dilute solution of the molecules in ethanol for 16 h. The surfaces were subsequently equilibrated in PBS buffer at room temperature for several hours. To characterise the SAMs formed on the polycrystalline gold electrodes surfaces, contact angle measurements, electrochemical stripping analysis, electrochemical impedance spectroscopy as well as surface plasmon resonance were applied. The results for the contact angle measurements are shown in Figure 7-22 and demonstrate a change in hydrophobicity accompanying the

functionalisation step of the gold surface. The contact angle of the freshly cleaned polycrystalline gold electrode surface was determined as 80 ± 3 ° in good agreement with literature.[254] The contact angles for the mixed SAM surfaces were determined to be 102 ± 1 °, 103 ± 1 °, 102 ± 2 °, 94 ± 1 ° and 34 ± 1 ° for the pure HT, 1:249 MHA:HT, 1:49 MHA:HT, 1:4 MHA:HT and pure MHA SAMs, respectively. The decreasing contact angle towards higher fractions of MHA in the solution of thiol-molecules is indicative of the higher ratio of COOH groups exposed to the liquid phase associated with the higher degree of MHA molecules incorporated into the film. However, it can be noted that at the lower ratios (1:249, 1:49 MHA:HT) the contact angle is largely dominated by the terminal methyl groups of the HT molecules hence no significant change in contact angle is measurable towards this end of the mixed films. These results are in line with previous results from literature on mixed SAMs of methyl and carboxyl terminated thiol molecules on gold.[255]

Reductive desorption analysis in aqueous 0.1M KOH solution was performed to confirm the actual Au-thiol bond formation of the SAMs as well as to estimate the molecular surface density of the films (see 2.3.1 for experimental detail). Example curves for such electrochemical stripping experiments are shown in Figure 7-23 and correspond well to the results of electrochemical desorption experiments for such films reported throughout literature.[256] It can be seen that the reductive desorption peak for the pure MHA SAM at -995±5 mV lies towards less cathodic potentials compared to the desorption peak of the pure HT-SAM at -1157±5 mV, whereas the peak of the mixed SAM is less well defined and lies in between those of the two pure SAMs. These results are in line with the expectations for the different reduction potentials resulting from the different headgroups and their water solubility.[257] More soluble compounds tend to

form less stable surface modifications. The peaks obtained through such measurements were integrated to estimate the number of molecules per area within the films formed from the charge transferred in the complete reductive desorption process.

The surface coverages as obtained from this analysis shown in Figure 7-24 demonstrate the formation of dense molecular layers in the films. The molecular coverages obtained are $3.4 \pm 0.4 \times 10^{-10}$ mol cm^{-2}, $3.8 \pm 0.8 \times 10^{-10}$ mol cm^{-2}, $7 \pm 2 \times 10^{-10}$ mol cm^{-2}, $7.7 \pm 0.4 \times 10^{-10}$ mol cm^{-2} and $7 \pm 1 \times 10^{-10}$ mol cm^{-2} for the pure HT, 1:249 MHA:HT, 1:49 MHA:HT, 1:4 MHA:HT and pure MHA SAMs, respectively. This is broadly in line with expectations for these types of monolayers.[256]

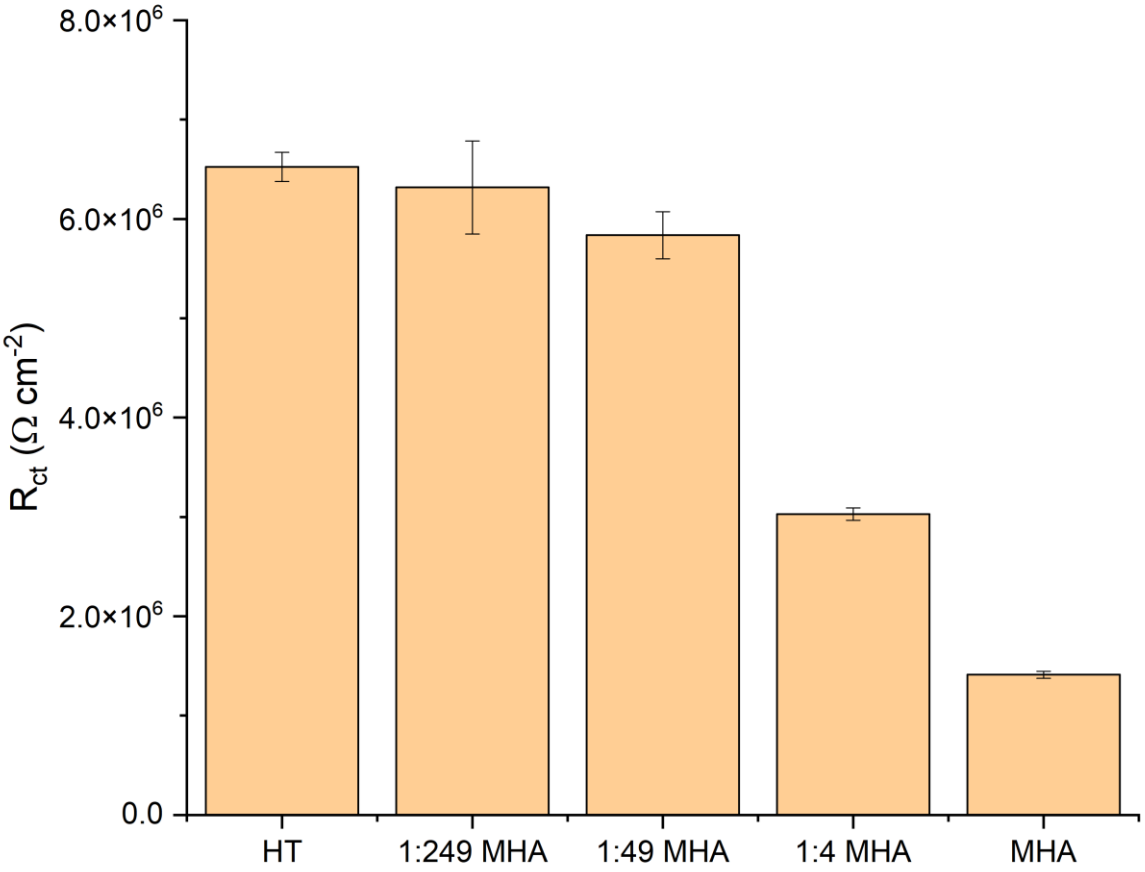


Figure 5-2 Charge transfer resistance as obtained from EIS analysis of different SAMs prepared on polycrystalline gold electrode surfaces. Error bars correspond to the standard deviation between three independent measurements.

To further establish a complete picture of the SAMs formed, electrochemical charge transfer resistance with ferrocyanide as the solution-phase redox probe were recorded using EIS. The corresponding results depicted in Figure 5-2 show charge transfer resistances of 6.5 ± 0.1 MΩ cm^{-2}, 6.3 ± 0.5 MΩ cm^{-2}, 5.8 ± 0.2 MΩ cm^{-2}, 3.0 ± 0.1 MΩ cm^{-2} and 1.41 ± 0.03 MΩ cm^{-2} for pure HT, 1:249 MHA:HT, 1:49 MHA:HT, 1:4 MHA:HT and pure MHA SAMs, respectively. These values are comparable to results from literature.[258] As expected, the different SAMs all pose an increase compared to the resistance recorded for a plain gold electrode of 4 ± 1 kΩ cm^{-2} indicating a dense insulating film being formed. However, from a pure HT SAM over the mixed surfaces to the pure MHA SAM the charge transfer resistance is gradually decreasing by 80% of the resistance for a pure HT SAM. Again, this indicates the successful integration of the carboxyl terminated molecules into the film at higher ratios of the MHA to the HT component. It has been reported in literature, that the charge transfer resistance can be seen to decrease with the incorporation of carboxyl termini into the SAM.[259]

To confirm the successful formation of the two pure SAMs of HT and MHA as well as the adsorption of Azurin onto the HT surface, XPS analysis was performed. For this, gold coated silicon platelets were used to form SAMs as mentioned in the methods section. The XPS elemental composition analysis revealed the samples to be composed of no other elements than Au, O, N, S, C, Na and I, where the iodine peak is attributed to a contamination of the vacuum chamber and Na (only in MHA-SAM) to a salt contamination (c.f. Figure 5-3 and Figure 7-20).

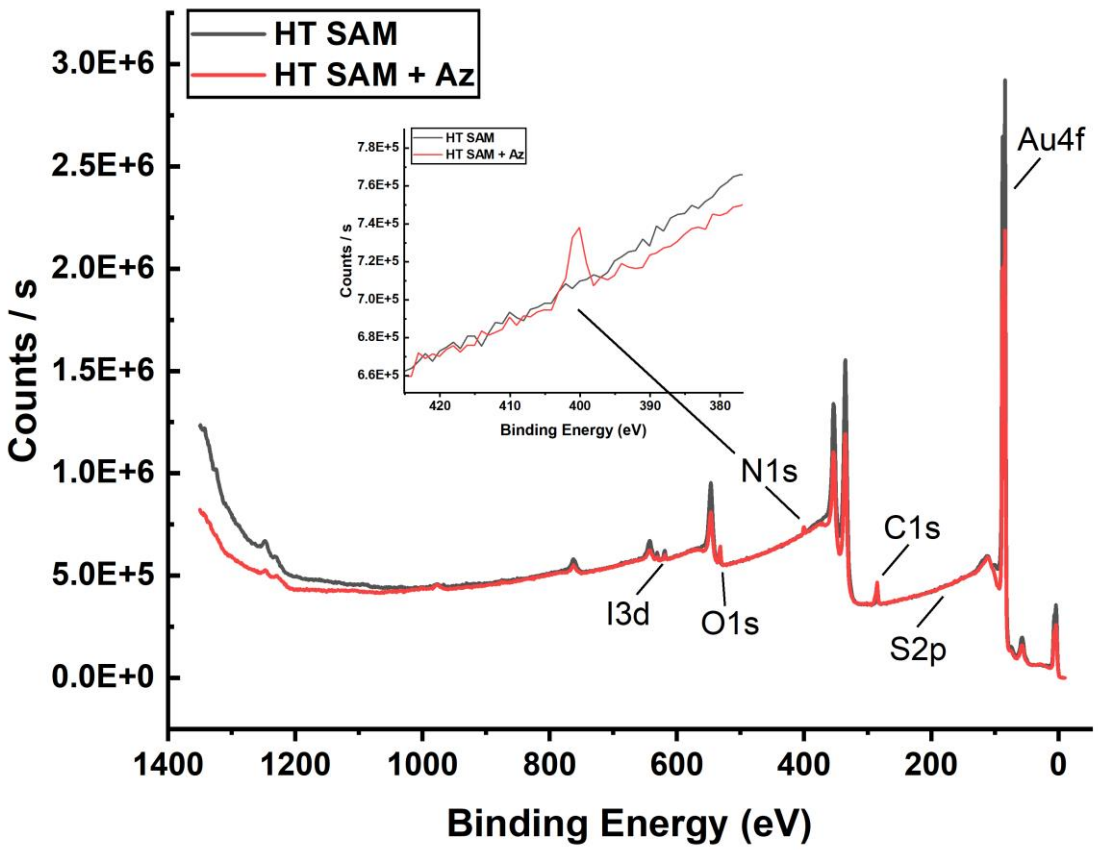


Figure 5-3 Low resolution survey XPS spectra of HT-SAM with and without Azurin adsorbed to it, indicating the appearance of a N1s peak due to the protein adsorption. All unassigned peaks arise from other orbitals of the same elements. Inset: Magnification of the N1s region.

The analysis of the higher resolution spectra of the peaks for O, N, S and C is shown in Figure 5-4. The plots show a comparative analysis of the peaks obtained on a gold surface, a gold surface carrying an HT SAM as well as one with Azurin adsorbed on such a SAM. The C1s region reveals two distinct chemical environments appearing for the gold and the HT-SAM that can be assigned to the C-C and C-X (X = O, S) bonds.[260-262] This is expected for the HT-SAM, while the peaks could be caused by contaminations on the gold surface. When Azurin is adsorbed to the surface a third peak associated to the O=C-O environment found in the protein appears in the C1s region indicating adsorption of the protein.[263] Similarly, the N1s region was observed and only for the surface featuring

the protein a peak becomes apparent, caused by the presence of amide bonds and nitrogen containing side chains such as lysine and histidine within the protein.[264] The O1s region showed small contributions most probably due to contaminants adsorbing to the gold surface, which become suppressed after the SAM formation, while contributions from oxygen containing amino acids within the protein lead to a rise after protein adsorption. The S2p region shows two peaks associated with the gold sulfur bond for the surfaces with SAM and with SAM and protein.[263] This confirms the formation of a chemisorbed SAM of HT on the gold surface.

The idea of generating different SAM surfaces that incorporate distinct ratios of HT vs MHA molecules is aiming to explore two different modes of the proposed Azurin based sensing platform (c.f. Figure 5-7 and Figure 5-15). One being based on a pure HT film that is used to generate a film of adsorbed Azurin onto which antibodies are coupled through the formation of carbodiimide bonds between carboxy groups on the Azurin molecules and amine groups on the antibodies. The second mode aims to use the carboxy groups in the mixed SAM to first couple antibodies to these residues in the SAM and in a second step introduce the electroactive protein through subsequent physisorption on the remaining surface (see Figure 5-5 for schematic illustration). The differences in availability of carboxyl termini for the various SAM surfaces investigated was further confirmed by recording SPR mass changes after the carbodiimide coupling of CRP antibodies revealing a correlation between the ratio of MHA molecules in the SAM solution and the mass of antibodies covalently coupled to the surface.

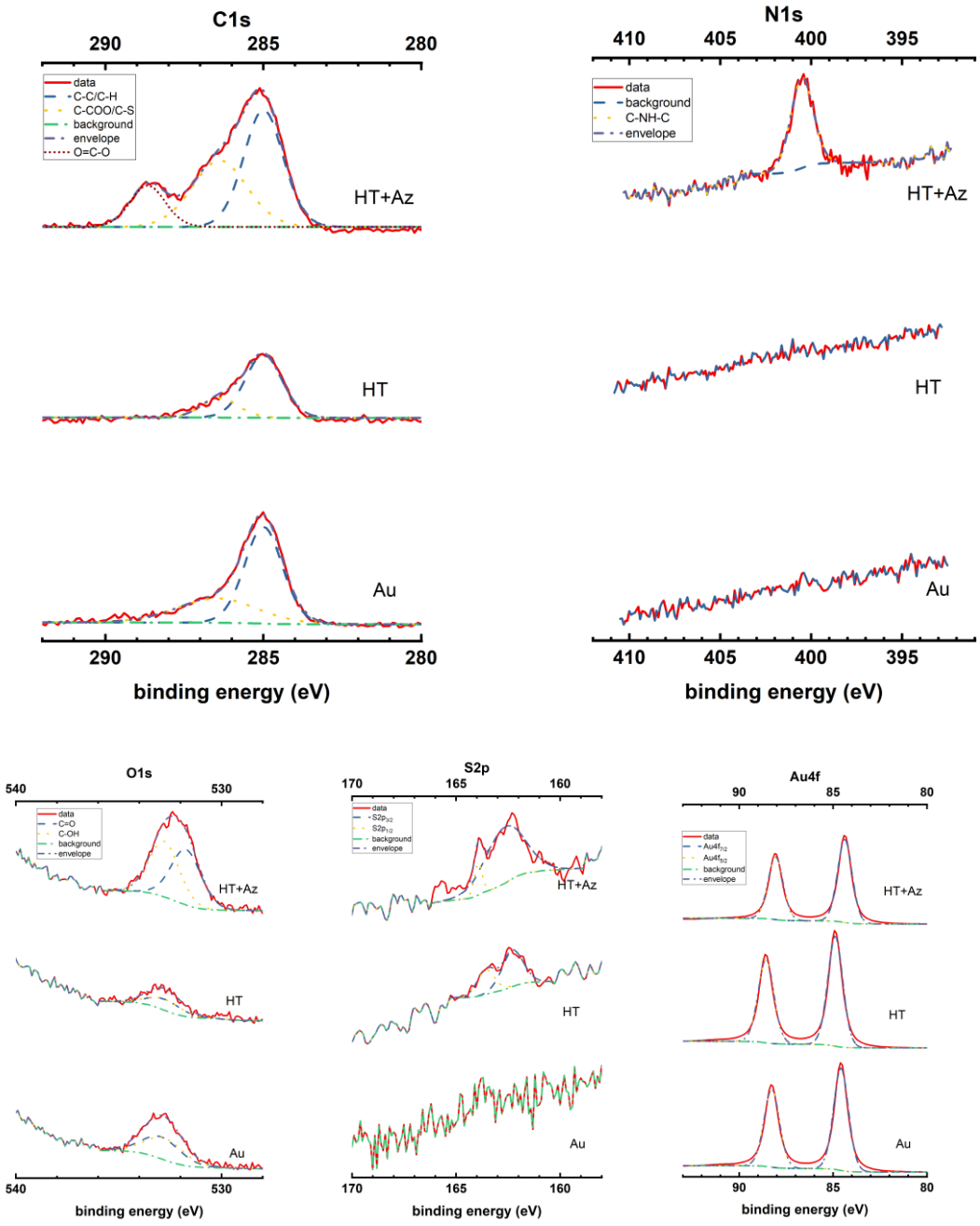


Figure 5-4 XPS analysis of gold surfaces with and without the formation of an HT SAM as well as the adsorption of Azurin on the SAM. As explained in more detail in the text, the C1s spectra show a peak (corresponding to O=C-O groups in the protein) appearing after the adsorption of Azurin to the surface. Similarly, a N1s peak becomes apparent after protein adsorption. The S2p spectra show the appearance of a peak associated with the gold thiol bond formation, while the Au4f and O1s spectra are shown for completeness.

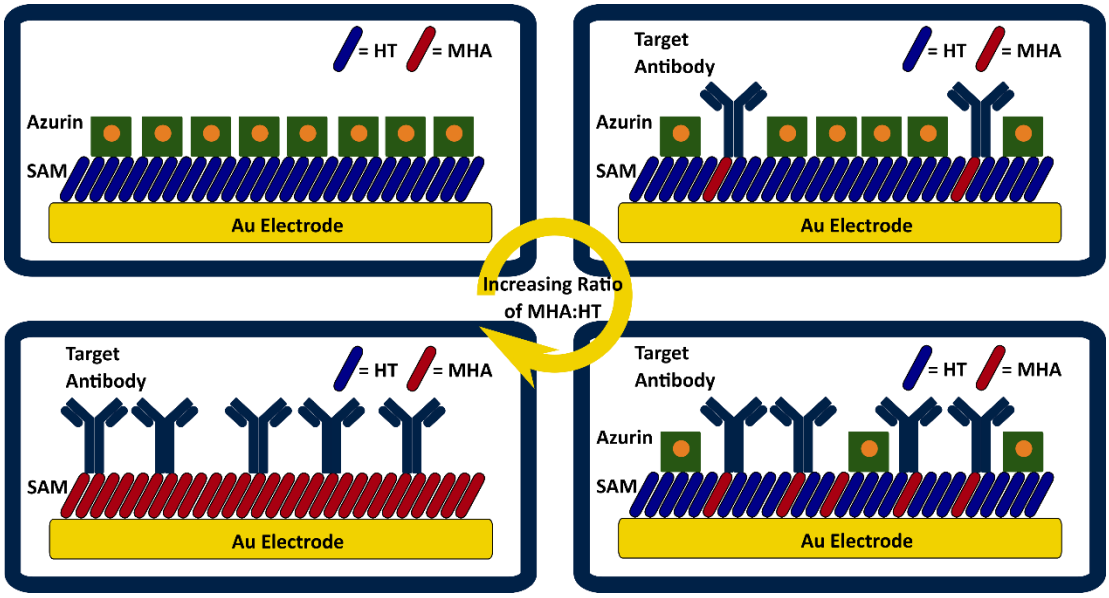


Figure 5-5 Schematic illustration of surfaces for Azurin based sensing platforms featuring SAMs with different ratios of MHA vs HT for the coupling of antibodies to carboxyl moieties in MHA and the adsorption of Azurin on the HT sites.

The associated results shown in Figure 5-6 reveal a mass added after the coupling procedure of 62 ± 3 ng cm^{-2}, 230 ± 3 ng cm^{-2} and 250 ± 3 ng cm^{-2} for the 1:249 MHA:HT, 1:49 MHA:HT and 1:4 MHA:HT surfaces corresponding to theoretical distances between two neighbouring antibodies on the surface of 22 nm, 12 nm and 10 nm, respectively. Whereas the antibody coverage for the 1:249 MHA:HT SAM remains far below the theoretical limit of 290 ng cm^{-2}, the SAMs with a higher ratio of MHA seem to level of just below this theoretical limit coverage calculated assuming the closest circle packing (c.f. 2.6.3). The clearly visible correlation between MHA and antibody coupling provides further evidence for the formation of the mixed SAMs as expected from the procedure and demonstrates that the utilisation of mixed SAMs allows for the tuning of spaces on the SAM available for the subsequent coupling of antibodies versus methyl groups exposed for the adsorption of Azurin. To test this hypothesis the incorporation of Azurin was tested on the different SAMs after antibody coupling by physisorption from a dilute

protein solution. The results obtained from these SPR experiments, depicted in Figure 5-6, show the masses adsorbed from such an injection are 56 ± 6 ng cm^{-2}, 13 ± 4 ng cm^{-2}, 9 ± 3 ng cm^{-2} and 0 ± 2 ng cm^{-2} on the pure HT, 1:249 MHA:HT, 1:49 MHA:HT and 1:4 MHA:HT SAMs, respectively.

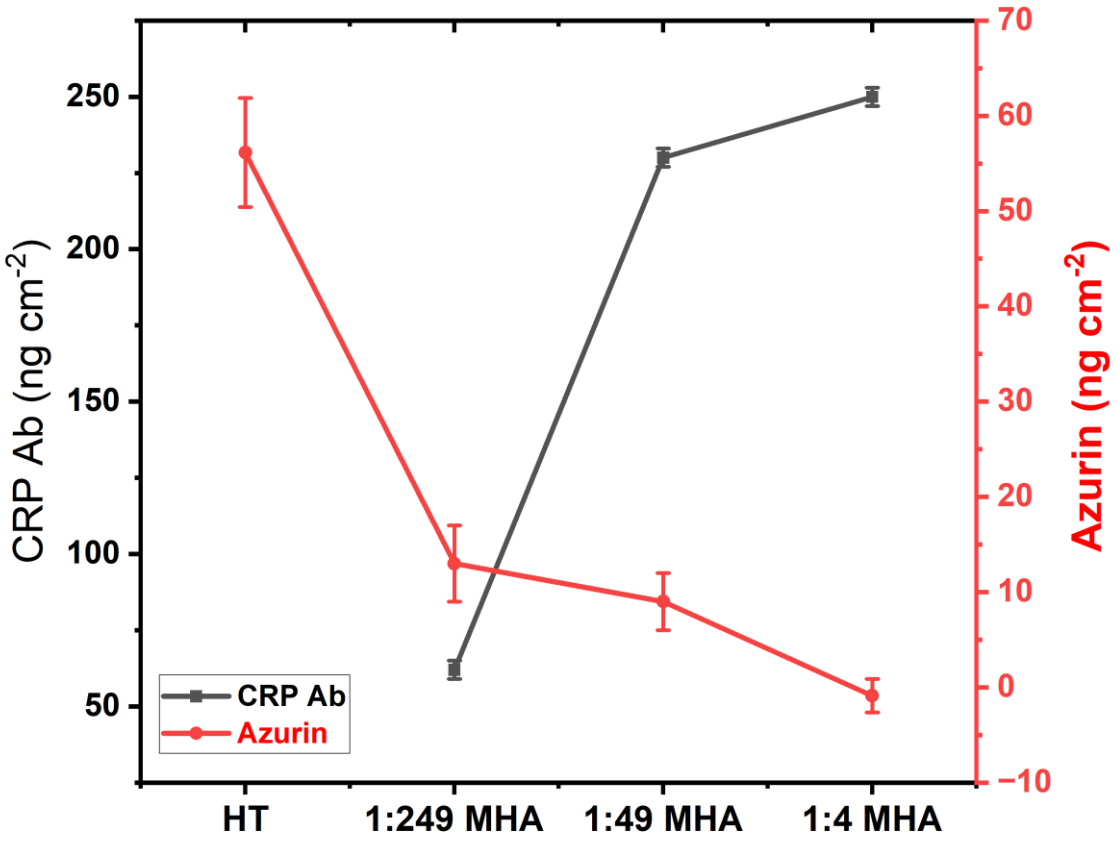


Figure 5-6 Mass added by coupling CRP-antibody and backfilling with Azurin as obtained by SPR measurements on different SAMs prepared on polycristalline gold surfaces on glass slides. The Azurin achieves a high loading on the pure HT SAM with no antibodies present as expected (left). This loading reduces with increasing antibody coverage on the SAMs with varying degrees of carboxy groups, while as hypothesised the antibody coverage can be seen to increase with the number of these carboxy residues.

Based on theoretical consideration (see 2.6.3), these numbers indicate a monolayer coverage for the HT SAM, while as expected the coverage decreases with an increasing surface concentration of antibodies coupled to the surface. This suggest there might be

an ideal ratio for the change of signal obtained in an electrochemical sensing setting. For further studies, it was chosen to work with two surfaces, one being the pure hexanthiol SAM for its maximised Azurin coverage and the other being the 1:49 MHA:HT SAM for its optimized coverage of Azurin together with antibodies compared to the other surfaces.

5.2.2 Protein Assembly and Electrochemical Addressability of Azurin on Hexanthiol SAM

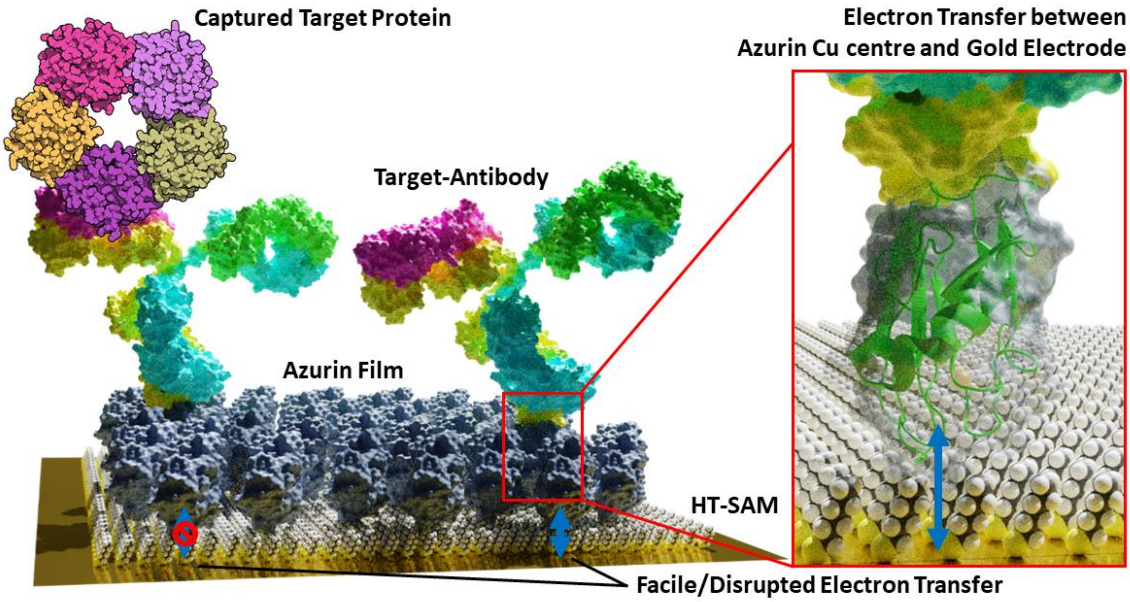


Figure 5-7 Schematic depiction of the hypothesised platform featuring Azurin physisorbed on a hexanethiol SAM with antibodies couples onto the protein layer for the redox capacitive sensing of target protein.

A schematic depiction of the hypothesised sensing platform featuring a high coverage protein layer of adsorbed Azurin on a hexanethiol SAM with antibodies chemically coupled to the Azurins is shown in Figure 5-7. Such surfaces can be formed by adsorbing the protein Azurin onto SAMs of hexanethiol on gold and the subsequent coupling of antibodies to the protein film. The sensing platform established in this way are expected to exhibit the anti-fouling properties native to proteins due their zwitterionic character

as introduced in 1.3.2, while simultaneously forming a stable electrochemically addressable sensing surface in physiological conditions.

First, to analyse the fouling and response behaviour of a platform formed like this, SPR measurements were performed. For this, gold coated quartz slides were coated with a SAM of hexanethiol and subsequently a film of Azurin was formed on these surfaces via physisorption (c.f. 2.3). To test the anti-fouling capabilities of such a surface, it was exposed to 1%FBS as a complex protein matrix. Figure 5-8 shows the SPR results for the mass of protein adsorbed on clean gold versus that on a surface of Azurin adsorbed on the HT-SAM from a complex sample of 1%FBS. The data shows a change of 165 ± 3 ng cm^{-2} on the gold surface versus 36 ± 6 ng cm^{-2} on the Azurin HT film indicating the antifouling capabilities of the Azurin film.

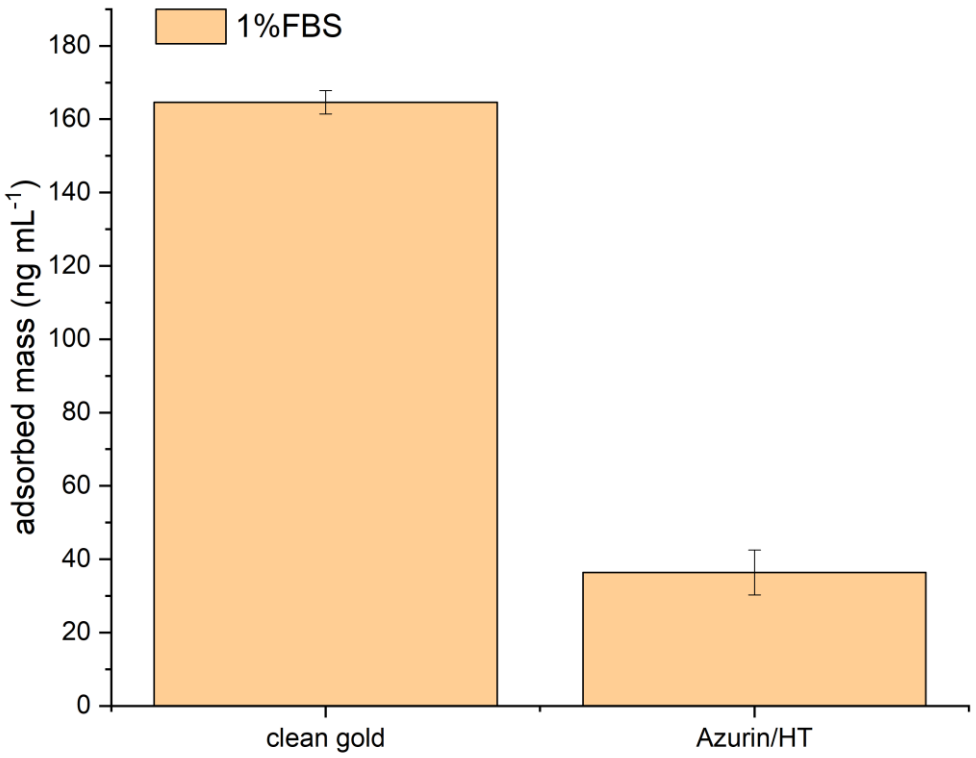


Figure 5-8 Adsorbed mass after injection of 1%FBS to a clean gold surface and the Azurin covered SAM on gold as obtained from SPR measurements. A clear reduction in non-specific adsorption from the protein mixture is apparent on the Azurin film, indicating the anti-fouling capabilities of the redox protein. Datapoints are averages of three independent measurements. Error bars represent standard deviation.

To further analyse the formation of the complete sensing platform including antibodies as the recognition elements, SPR measurements of the antibody coupling onto the Azurin HT film as well as specific and non-specific response of the so formed surface were performed (for details see 2.3.10.3). The data shown in Figure 5-9 show the change in the SPR signal occurring after the antibody coupling of 40 ± 4 RU. The surface shows a significant specific signal from exposure to 20 µg mL^{-1} CRP (signal change of 22 ± 4 RU) compared to the non-specific signal obtained upon injection of a complex sample of 1% HS (10 ± 6 RU). However, the change in signal is only significant for high concentrations of target protein.

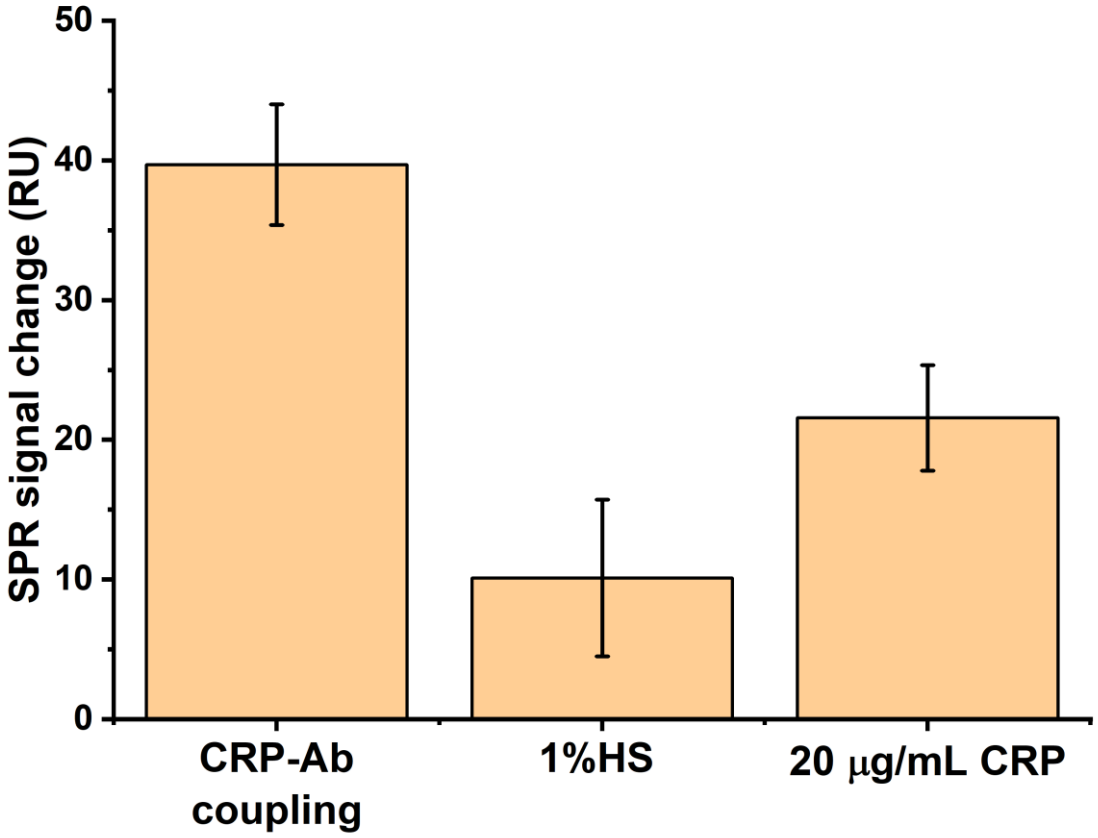


Figure 5-9 Change in SPR signal upon coupling of antibodies as well as subsequent exposures to 1%HS and the target protein CRP as obtained from SPR measurements. The higher change in signal from specific target indicates the functionality of the platform as a sensing surface. The datapoints are averages between three independent measurements and the error bars show the associated standard deviation.

To test the electrochemical addressability of the Azurin films, protein films were established as explained earlier on an HT SAM formed on polycrystalline gold electrodes by adsorption from an 8 µM solution in 10 mM Potassium Phosphate (KPh) buffer (c.f. 1.4.2) with conditions similar to established procedures for the immobilisation of Azurin on hexanethiol.[265] The so formed protein films were then tested electrochemically in 10mM KPh buffer. Cyclic voltammetry of the HT SAM before and after adsorption of Azurin can be seen in Figure 5-10. Whereas the voltammogram of the plain SAM shows a typical double layer charging behaviour, the voltammogram after the Azurin

adsorption shows a distinct pair of peaks with the anodic peak at 92 ± 3 mV and the cathodic peak at 62 ± 3 mV, respectively. This corresponds to a half-wave potential of 77 ± 6 mV and a peak separation of 30 ± 6 mV in agreement with previous results of Azurin films formed on alkanethiol SAMs.[134, 265-267] The peaks can further be integrated to find the amount of electrochemically accessible Azurin from the charge transferred in a full oxidation or reduction of the surface bound proteins. This yields coverages of 4 ± 1 pmol cm^{-2} corresponding to a mass of 56 ng cm^{-2}, which corresponds well with the coverage obtained from SPR analysis and is in line with previous reports observing the electrochemically addressable protein in such films.[268]

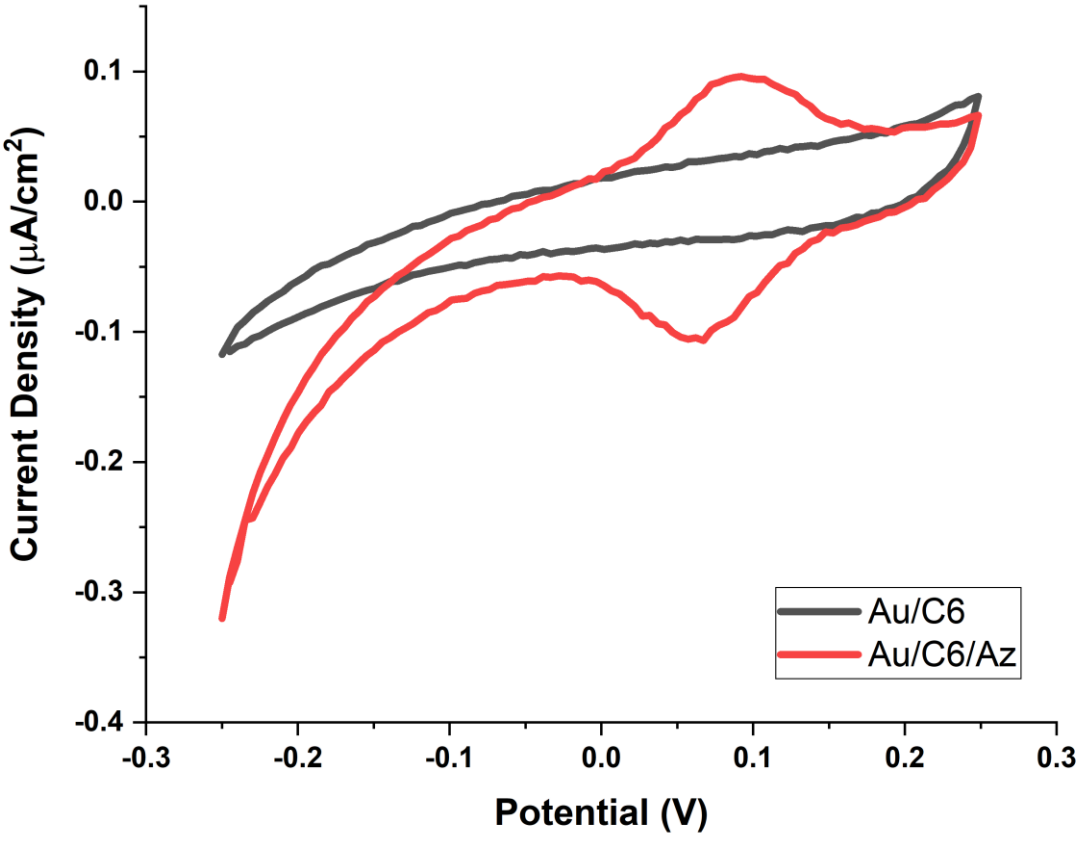


Figure 5-10 Representative cyclic voltammograms of hexanethiol SAM and the same SAM surface after adsorption of Azurin.

To test for Azurin being irreversibly adsorbed to the surface voltammograms for several scan rates were recorded to obtain the relation between the scan rate and the peak current for oxidation as well as reduction. The results shown in Figure 5-11 reveal a linear correspondence between the scan rate and the peak current indicating Azurin indeed being irreversibly adsorbed to the SAM.[134, 269] The linear relationship between the scan rate and the peak current is a well-known indicator of an electroactive species adsorbed to the electrode in contrast to a linear relationship between the square root of the scan rate and the peak-current characteristic for a diffusive electron exchange process.

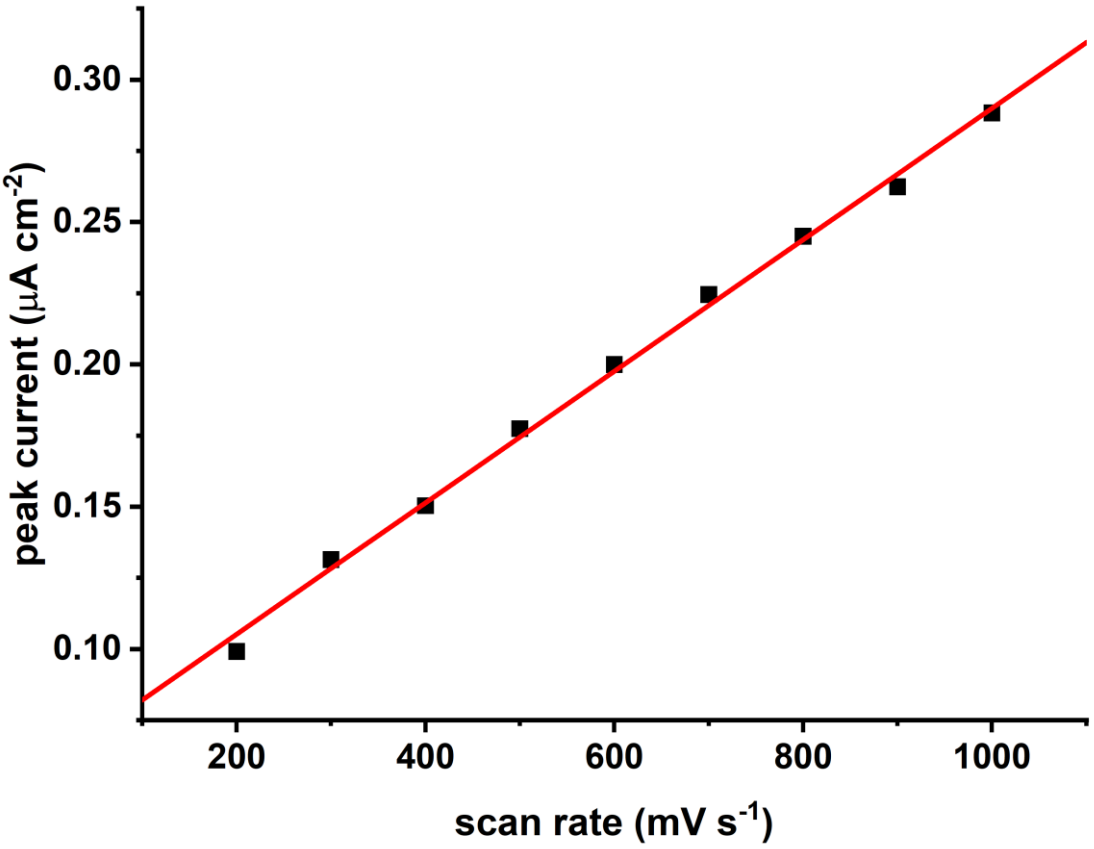


Figure 5-11 Peak currents versus scanrate recorded at hexanethiol SAMs with Azurin physisorbed to them. The characteristic linear relationship between the scanrate and the peak current is indicative of the irreversible adsorption of the electroactive protein

to the SAM surface. The red line corresponds to a linear fit with a correlation coefficient $R^2 = 0.997$

Because the surface concentration of the electrochemical accessible states provided by the protein are naturally lower than a typical electroactive SAM like a film of ferrocenethiols, capacitance spectroscopy was used as a highly sensitive method to get a more detailed image of the chargeable states created after the adsorption of Azurin to the SAM. As an equilibrium method it allows to measure the electrochemical properties of the platform at hand with very low disturbance to the system. Capacitance spectroscopic Nyquist plots as recorded for the HT-SAM before and after Azurin adsorption and after coupling of antibodies are shown in Figure 5-12. The curves recorded at the half-wave potential show an increase of redox capacitance as taken from the inflection point in the Nyquist plot from 1.61 ± 0.05 µF cm^{-2} for the HT-SAM to 3.56 ± 0.05 µF cm^{-2} for the SAM with adsorbed Azurin. This is broadly in line with previous results for a similar film featuring Azurin.[134] It can further be shown that this redox capacity created by the protein can be tuned in and out of by changing the potential (Figure 5-12). Hereby, the maximum redox capacitance is reached at a potential of 90 ± 5 mV coinciding with the half-wave potential as expected, while the capacitance returns to the normal double layer capacitance without the additionally chargeable redox state being accessible at potentials higher than 0.25 and lower than -0.1 V. The difference of capacitance in (90mV) and out (-100mV) of resonance with the Azurin redox centre is denoted as ΔC_r.

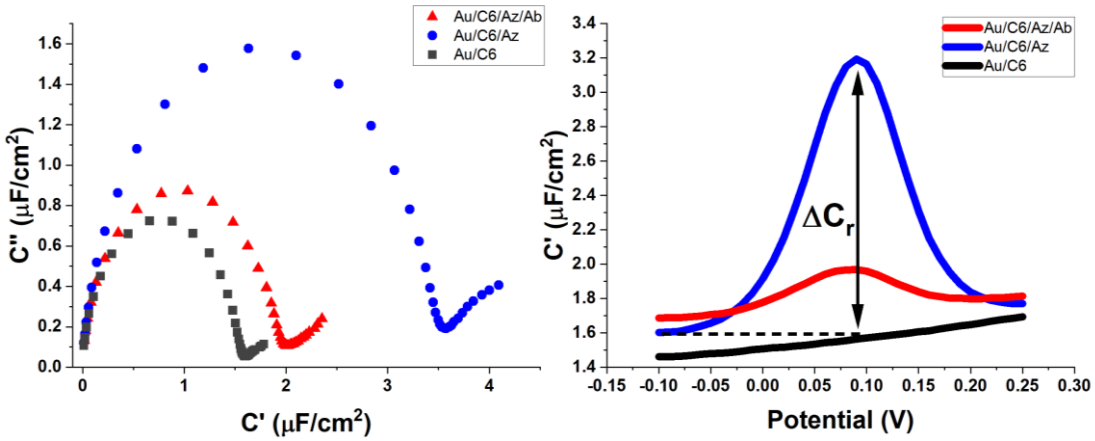


Figure 5-12 Representative Nyquist-type plots of electrochemical capacitance spectroscopy addressability recorded at a bias voltage of 90 mV (left) and the associated capacitance-potential scans recorded at a frequency of 100 Hz.

Antibodies are then coupled to this platform to create the desired interface for protein quantification. The carboxyl groups present in the Azurin film are targeted for carbodiimide coupling with the amine residues in the antibodies. The tethering of the antibodies performed via EDC/NHS coupling relates to a significant decrease in redox capacitance of 2.04 ± 0.05 µF cm^{-2} on average (c.f. Figure 5-12). This change in signal indicates a substantial change in electrochemical addressability of the Azurin layer caused by the immobilisation step. This hints towards the Azurin redox centre's responsivity towards molecular changes in its close proximity, which is supportive of the further hypothesised use of the platform in sensing applications. Together with the small change in adsorbed mass observed in the SPR experiments (as discussed above), this indicates the high sensitivity of the Azurin redox capacitance to such changes in the molecular environment. The platform functionalised this way, is now tested for its stability in a possible sensing scenario, i.e. by recurring incubation in blank sample (PBS), washing and subsequent electrochemical measurement, the signal is stable (standard

deviation of less than 10% of the base signal, c.f. Figure 5-13). To further examine the non-specific signal change attained through the interaction of a complex sample matrix with the surface, the surface was exposed to 1% FBS for 1 h before further ECS measurements. The results show that the surface exhibits a highly stable signal (not deviating from baseline within errors, c.f. Figure 5-13) even after such an extended exposure to complex sample.

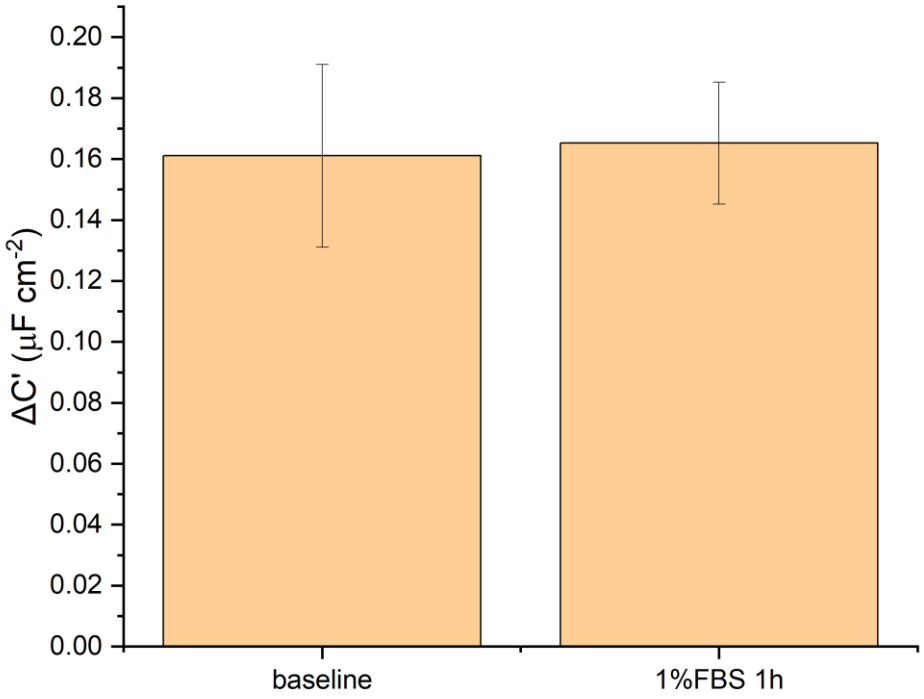


Figure 5-13 The difference in capacitance in and outside of potential window is plotted for a baseline and after a 1h incubation in 1%FBS. The data show a stable baseline and no significant change in signal upon exposure to the interfering proteins. Datapoints are averages of 3 measurements. Error bars denote the standard deviation.

When the specific signal is tested similarly by exposing the surface to different concentrations of the target analyte CRP and again recording the differential redox

capacitance the analysis (c. f. Figure 5-14) shows a similarly stable signal, however. This indicates the addressability of Azurin remains unchanged after the significant change found after antibody coupling either because the platform does not change in composition and structure upon exposure to neither specific nor non-specific protein or because the Azurin copper site remains its accessibility even when protein is binding or adsorbing to the surface.

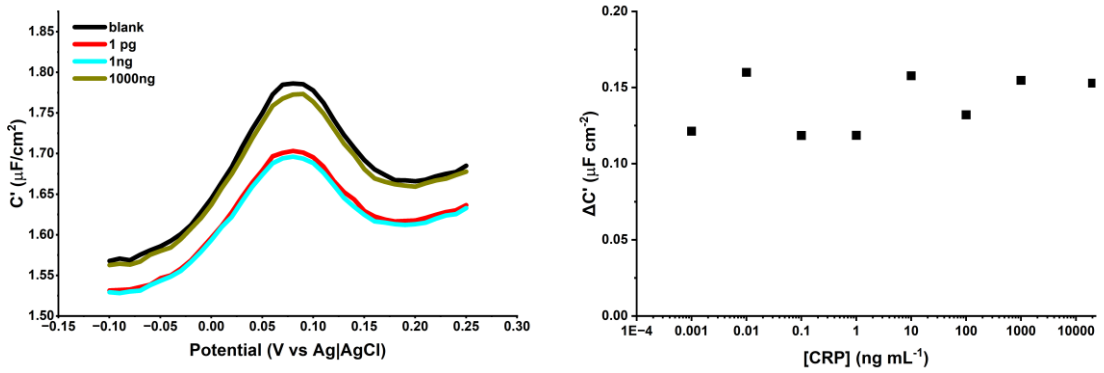


Figure 5-14 Left: Represantative curves of the Azurin platform with antibodies coupled to it exposed to various concentrations of antigen. Capacitance versus potential plotted for the sensing platform incubated in different concentrations of CRP. Right: The redox capacitance shift plotted versus the concentration of CRP antigen added in the incubation step. The redox capacitance shift was expected to decrease with increasing concentration. However, such a correlation could not be detected.

5.2.3 Assembly and Electrochemical Adressability of Azurin on Mixed SAM of 1:49 MHA:HT

As introduced in 5.1, a second mode of building a sensing platform featuring Azurin as an anti-fouling and transducing building block was investigated. This platform is based on the coupling of antibodies to carboxyl residues in a mixed SAM of hexanethiol and mercaptohexanoic acid and subsequent backfilling of the remaining surface with Azurin through physisorbtion(c.f. 5.2.1). A schematic depiction of the mixed SAM featuring

antibodies coupled to its carboxyl residues and Azurin adsorbed onto the methyl residues exposed on the surface not covered by the antibodies is imaged in Figure 5-15. As discussed earlier (c.f. 5.2.1) such a platform would potentially accommodate an optimal ratio of recognition sites (antibodies) to electrochemical accessible proteins surrounding these sites. Such a platform should accommodate a high number of antibodies while maintaining enough unfilled space surrounding them to be filled with Azurin in the backfilling step to yield maximum attainable signal for a concentration range of interest. Although an optimal ratio in this case is not trivial to find, herein the SAM of 1:49 MHA:HT was chosen for further examination because of the relatively high number of Azurin and antibodies it accommodates according to the SPR measurements discussed in 5.2.1.

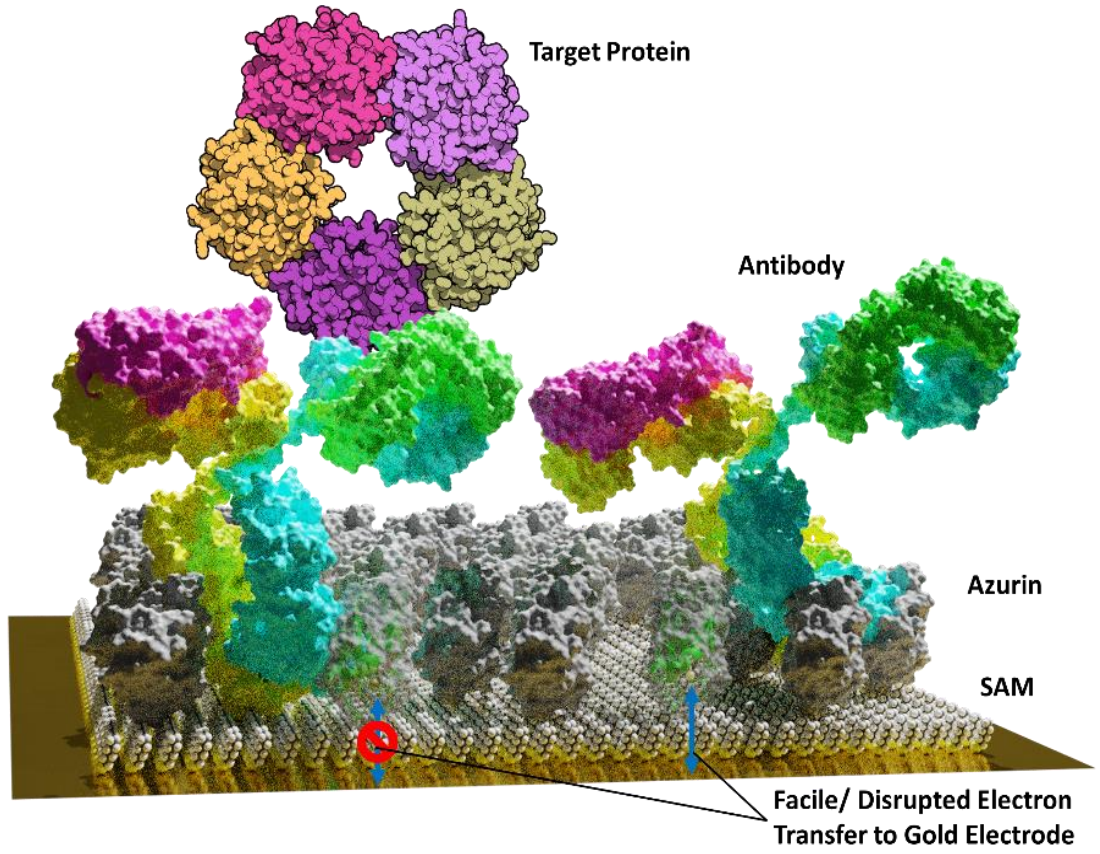


Figure 5-15 Schematic depiction of sensing platform featuring antibodies coupled to carboxyl residues in a mixed SAM of hexanethiol and mercaptohexanoic acid and backfilled with Azurin. The backfilling with electroactive proteins provides non-fouling and transducing capabilities to the platform. In contrast to a coupling of antibodies to an Azurin layer, the ratio of recognition events to transducer can be tuned via the constituents of the SAM.

To investigate the sensing capabilities of the proposed platform, the surface formed through coupling of antibodies to a mixed SAM (1:49 MHA:HT) and subsequent backfilling with Azurin, was examined in SPR measurements. These experiments reveal that the surface is indeed specifically capturing target protein as evident from the SPR signal obtained for 20 µg mL^{-1} of CRP versus that obtained from exposure to 1 mg mL^{-1} BSA as an interfering species (see Figure 5-16). A dose response curve is shown in Figure 7-27 and demonstrates a Langmuir-like sensing behaviour.



Figure 5-16 Adsorbed masses for an injection of BSA or target protein CRP on the backfilled sensing platform as obtained from SPR measurments. The significant difference in response indicates the surface capture to be specific to target protein. Datapoints are averages of three independent measurements, error bars denote the standard deviation.

To assess the electrochemical addressability of Azurin in such a film cyclic voltammetry was performed as described earlier. The comparison of example curves between the mixed SAM with antibodies coupled to it and the same surface after the adsorption of the redox molecule can be seen in Figure 5-17. This reveals a pair of distinct peaks appearing after the incorporation of Azurin at 117 ± 5 mV and 42 ± 5 mV for oxidation and reduction, respectively. These results correspond to a half-wave potential of 80 ± 10 mV in good agreement with literature results and the results from a pure HT SAM

featuring Azurin as discussed earlier. The peak separation of 75 ± 10 mV is significantly higher than that of Azurin on the pure HT SAM but within the range of expectation.[130] Again, the peaks can be integrated to yield the surface coverage of electrochemically addressable Azurin. The average coverage found for the observed surfaces was calculated to be 2.4 ± 0.4 pmol cm^{-2}. This corresponds to 34 ± 6 ng cm^{-2} broadly in line with the results obtained in the SPR measurements discussed above.

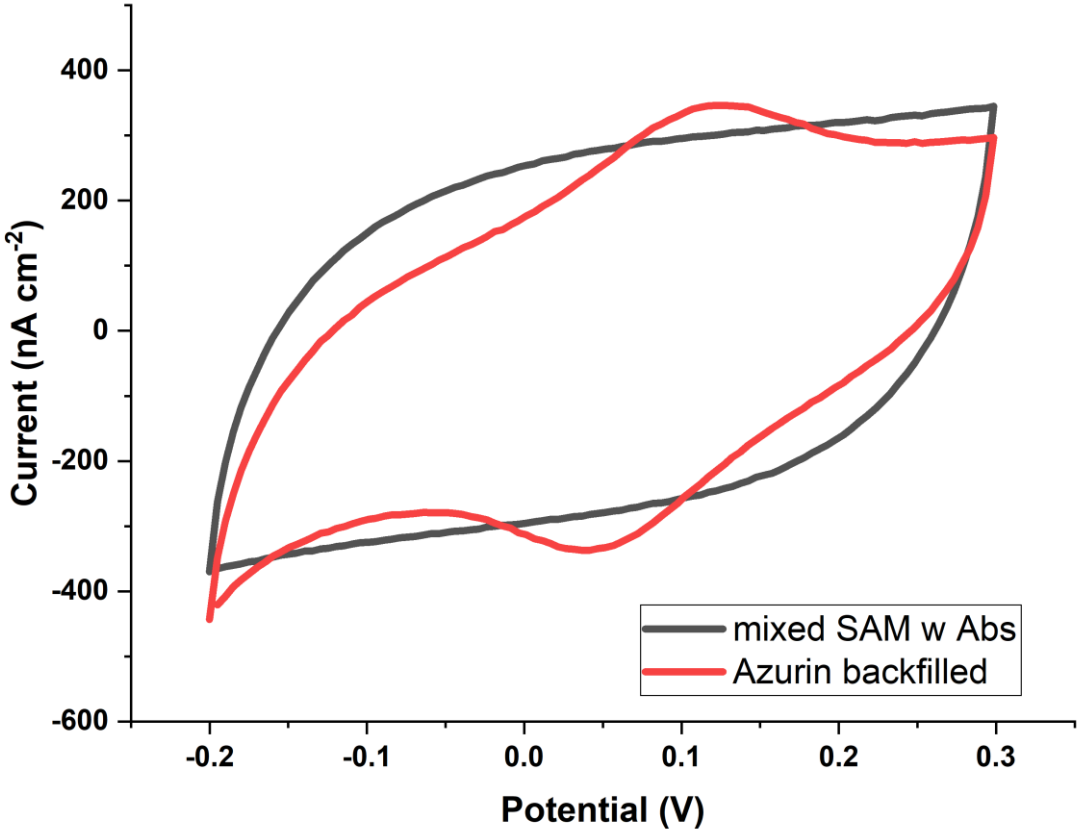


Figure 5-17 Cyclic voltammograms as obtained from a mixed SAM of 1:49 MHA:HT with antibodies coupled to it before and after Azurin backfilling. This shows the electrochemical adressability is present even when Azurin is physisorbed to the mixed SAM already featuring antibodies indicating the oriented adsorption of the electrochemical protein on the remaining hexanethiol covered surface surrounding the recognition elements. CVs were recorded in PBS using a scanrate of 100 mV s^{-1}.

Similarly, the resonance caused by the incorporation of Azurin into the film can be detected in electrochemical capacitance spectroscopic measurements (see representative curve in Figure 5-18). As can be seen, the electrochemical accessibility of Azurin spans the same potentials as seen earlier for the pure hexanethiol SAM (-0.1 to 0.25 mV) and has a maximum at 90 ± 5 mV with 2.14 ± 0.02 µF cm^{-2} corresponding to a redox capacitance ΔC_r of 0.43 ± 0.04 µF cm^{-2}.

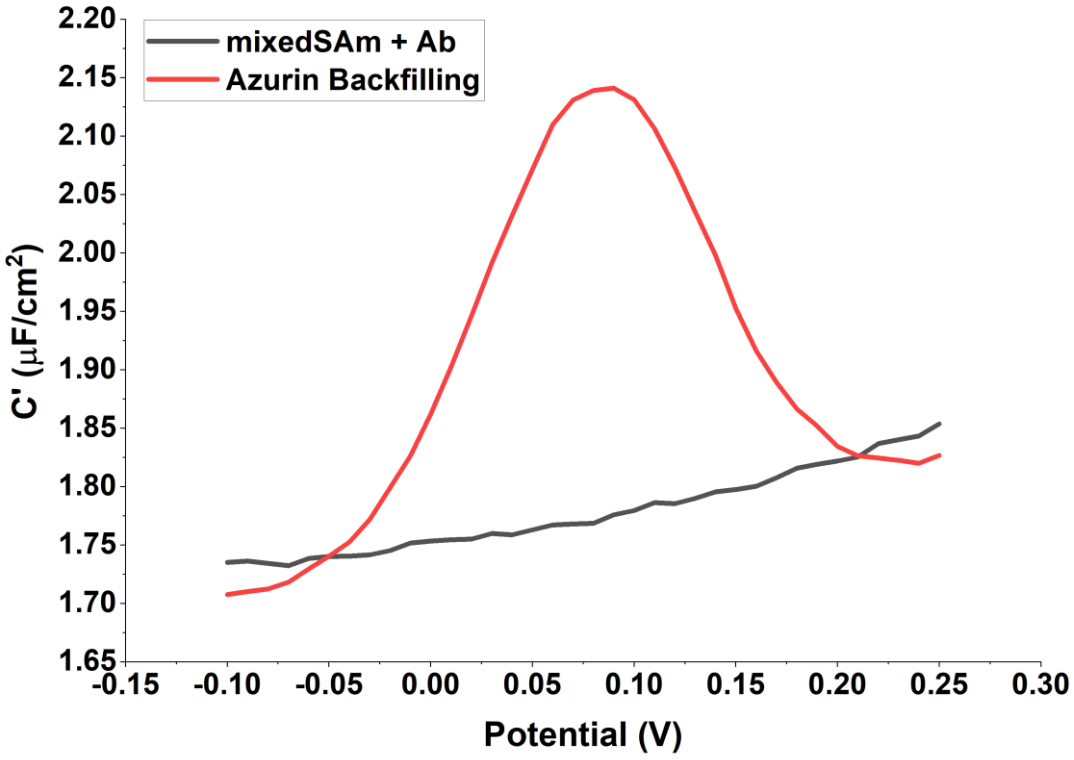


Figure 5-18 Representative capacitance versus potential plot as obtained from a mixed SAM of 1:49 MHA:HT with antibodies coupled to it before and after Azurin backfilling. In contrast to the platform obtained through antibody coupling onto the Azurin layer, the configuration presented here (antibodies coupled to the surface, then backfilled with Azurin), the electrochemical signal is not diminished through the integration of recognition elements.

When this baseline redox capacitance is measured for repeated blank incubations a baseline capacitance can be determined shown in Figure 5-19. Further, the signal

changes for incubation of 100 ng mL^{-1} and 10 µg mL^{-1} target protein as well as 1% FBS as a complex sample without target protein were recorded. It can be seen that similarly to the pure HT-SAM the signal changes are not significant and do not allow for a reliable detection let alone quantification of CRP.

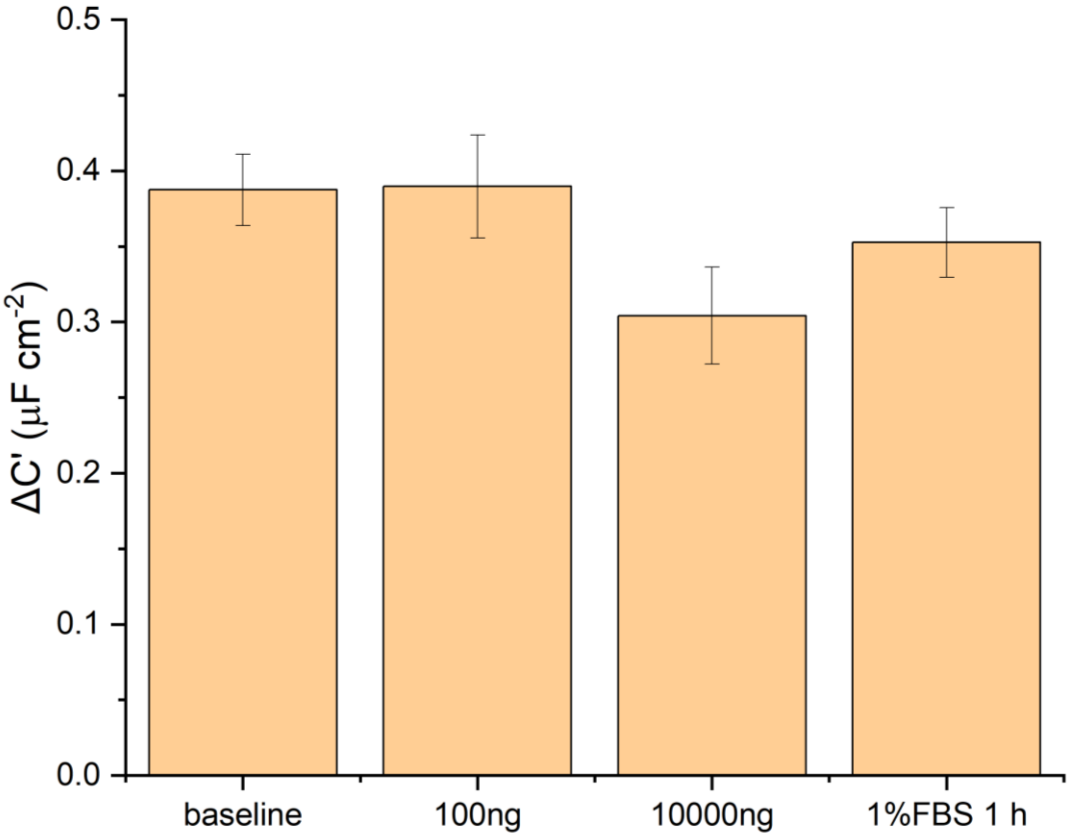


Figure 5-19 Redox capacitance signal measured for Azurin backfilled sensing platform (1:49 MHA:HT with antibodies) to different stimuli. Small changes in signal are apparent after an incubation with a solution of 10 µg mL^{-1} target concentration, while for lower concentrations no significant change could be detected. The change in signal to non-specific protein (1%FBS) for an extended time is less evident indicating a specific response, but of relatively low sensitivity as a response only manifests at relatively high target concentrations.

5.3 Conclusions and Future Work

In this work, it was tested to use Azurin as a low fouling and transducing building block for the formation of a sensor to quantify target protein CRP. For this purpose, different SAM surfaces featuring mixtures of HT and MHA molecules were formed and characterized to demonstrate their formation as expected from previous literature results. After establishing surfaces with the expected properties, these surfaces exposing different ratios of methyl and carboxyl groups were utilised for the formation of protein films. The mixed films were shown to exhibit tunable incorporation of antibodies via EDC/NHS coupling corresponding to the surface exposure of carboxyl groups. Similarly, the adsorption of Azurin on such films showed an indirect proportionality to the antibodies bound on the surface, which again was expected. The idea behind the use of these different surfaces was to test two different modes of a potential sensing platform. The first mode is based on a monolayer of Azurin as a transducing and antifouling building block adsorbed onto a pure HT SAM, which is then functionalised with recognition elements by the coupling of antibodies onto the protein film via carbodiimide bond formation between carboxyl groups on the Azurin and amine residues on the antibodies. This mode is hypothesized to maximise both the Azurin and antibody coverage. A second mode of establishment focuses on the use of the mixed SAMs to first integrate antibodies to the surfaces and then backfill the remaining surface with Azurin as the transducing and anti-fouling building block. The ratio of antibodies to Azurin then becomes tunable by the ratio of carboxyl to methyl residues in the SAM (MHA to HT molecules). This second mode was hypothesized to decrease the distance between the epitope binding site on the antibody and the transducing copper centre of

Azurin, while also providing the possibility to choose a ratio of transducer to recognition element. Due to the results found regarding antibody and Azurin incorporation in these mixed films, the subsequent investigations regarding the utilization of such surfaces for the electrochemical specific quantification of target protein were focused on the pure HT SAM with Azurin adsorbed and antibodies coupled onto the protein film and the 1:49 MHA:HT SAM with antibodies coupled to the surface carboxyl groups and Azurin subsequently adsorbed on the remaining surface. The analysis of electrochemical accessibility of Azurin in these films showed results as expected from previous literature reports and exhibited low-fouling capabilities as hypothesized. In SPR measurements the surfaces showed specific receptive behavior towards target protein, the mixed SAM more so than the pure HT SAM. The electrochemical signal changes upon target exposure, however, remained marginal and did not indicate the expected ability to detect or quantify target protein electrochemically via the observed platforms. This was the case for both platforms, although the mixed SAM (1:49 MHA:HT) seems to show more promising results for a specific electrochemical response at high concentrations. The reasons for this unresponsive behaviour could be versatile and could not be further examined within this work. However, one potential reason that seems rather significant involves the inherent properties of electrochemical proteins. Evolved to facilitate the electron transfer with other molecules, their design is often thought to be able to shield the redox centre from the surrounding solvent to reduce the reorganisation energy needed for a change in the charging state of the redox centre. As mentioned in 1.2.2, the redox capacitive transduction of recognition events is not yet entirely understood in its molecular mechanisms, but a hypothesised cause of the change in redox capacitance is the change in solvent access triggered by binding events close to the redox site, which

in turn change the accessibility of the chargeable states due to hindered counter ion reorganisation. Although clear conclusions are not possible without further elucidation of both the mechanism of the redox capacitive sensing mode as well as the electrochemical unresponsiveness of the proposed Azurin surface, these considerations regarding the solvent shielding provide a valid hypothesis for a potential cause of the latter. This hypothesis could be a starting point for future work investigating the mechanisms of the failure of the redox capacitive based sensing for the proposed platform. A future study could investigate proteins like BSA that were tagged electrochemically to understand the potential of these conjugates as anti-fouling and transducing building blocks in similar assays, while simultaneously elucidating the influence of the redox centre being buried inside or tagged outside the protein. Other work could focus on different proteins with similar properties to Azurin, such as the cytochromes with their heme group being known to engage in electrochemical charge transfer with electrodes coated with carboxyl terminated thiols.

Chapter 6

Conclusions and Outlook

In addressing the pressing need for innovative electrochemical methods for protein biomarker quantification, this thesis set out to explore unconventional techniques with a focus on scalability and simplicity. Recognizing the challenges faced by current biosensing methodologies, the goal was to offer new perspectives in the field of point-of-care testing (POCT). The posed challenges range from sensitivity and specificity to design complexity, robustness, stability, ease of handling, time requirements, and multiplexing capabilities.

The thesis prioritized the development of methodologies that consider practical constraints and aim for pragmatic solutions with clinical practice in mind. Three distinct concepts were explored, each based on the formation of a protein film on the sensing electrode.

The developed electrochemical dot blot assay showcases a novel approach for protein biomarker quantification in diagnostic settings. The employment of unmodified electrodes, specifically in a microfluidic setup, demonstrated simplicity, stability, and good assay statistics. The assay successfully quantified two target proteins (CRP, cTnI) with low limits of detection, and its applicability across different electrode surfaces was confirmed. Future work could delve into optimizing protein adsorption processes,

exploring additional electrode surfaces, and investigating modifications like NHS-modified carbon. Further improvements may involve depleting serum to enhance the relative concentration of target proteins.

The presented single-step assay utilising Faradaic shotgun tagging of complex samples represents a marked departure from current electrochemical immunosensor designs. Its efficiency lies in the omission of a specific secondary label, streamlining the assay process. The method successfully quantified cardiac biomarkers CRP and cTnI with high sensitivity and a broad dynamic range. Integration into a microfluidic format reduced assay time, making it potentially suitable for point-of-care applications. Future investigations could explore different surface designs, further optimise each step of the assay, and consider amplification techniques like redox cycling. The low cost and potential for fully automated applications make this method a promising avenue for future healthcare solutions.

The Azurin-based sensor, designed for low fouling and transduction, presented challenges in achieving the expected electrochemical response for CRP quantification. While the chosen SAM surfaces demonstrated tuneable incorporation of antibodies and Azurin and the SPR measurements showed promising results regarding non-fouling and specific sensing capabilities, the electrochemical signal changes upon target exposure were marginal. The unresponsiveness may be attributed to the solvent shielding effect on the redox centre of Azurin. Future work could explore proteins like BSA for their potential in similar assays, investigating the influence of the location of redox centre.

Understanding the mechanisms of redox capacitive sensing and addressing the limitations of the proposed platform are critical for advancing this approach.

While this work may not present fully mature, market-ready biosensors, it introduces concepts meant to stimulate further exploration, adaptation, optimization, and potential combination with established technologies. The emphasis on scalability, practicality, and a departure from traditional methodologies positions these concepts as valuable contributions to the evolving landscape of electrochemical immunosensing. The presented concepts may hopefully feed into the important endeavours made throughout scientific research around the globe that seek disruptive solutions and advancements in biosensing technologies to solve challenges in future healthcare.

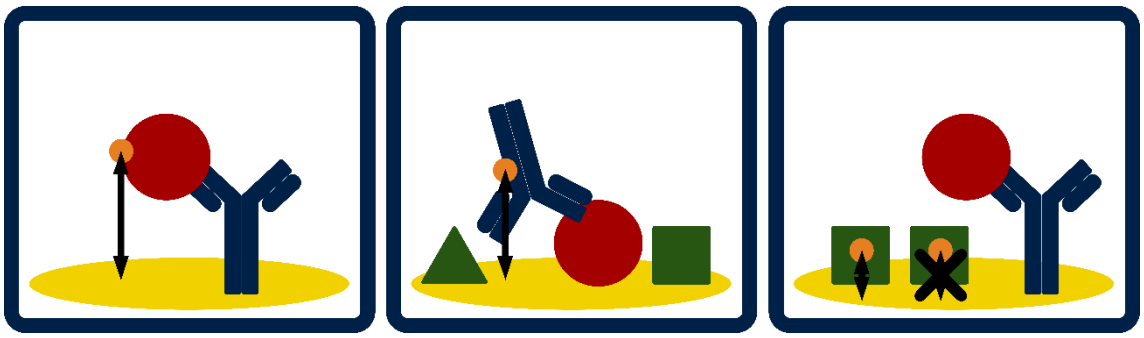


Figure 6-1 Schematic depiction of envisioned assays as presented within this work. From left to right: The faradaic shotgun tagging for protein quantification from complex sample, the electrochemical dot blot assay on unmodified electrode surfaces, the utilisation of electroactive protein as a non-fouling and transducing unit in redox capacitive sensing.

Chapter 7

Appendix

7.1 Appendix Chapter 3

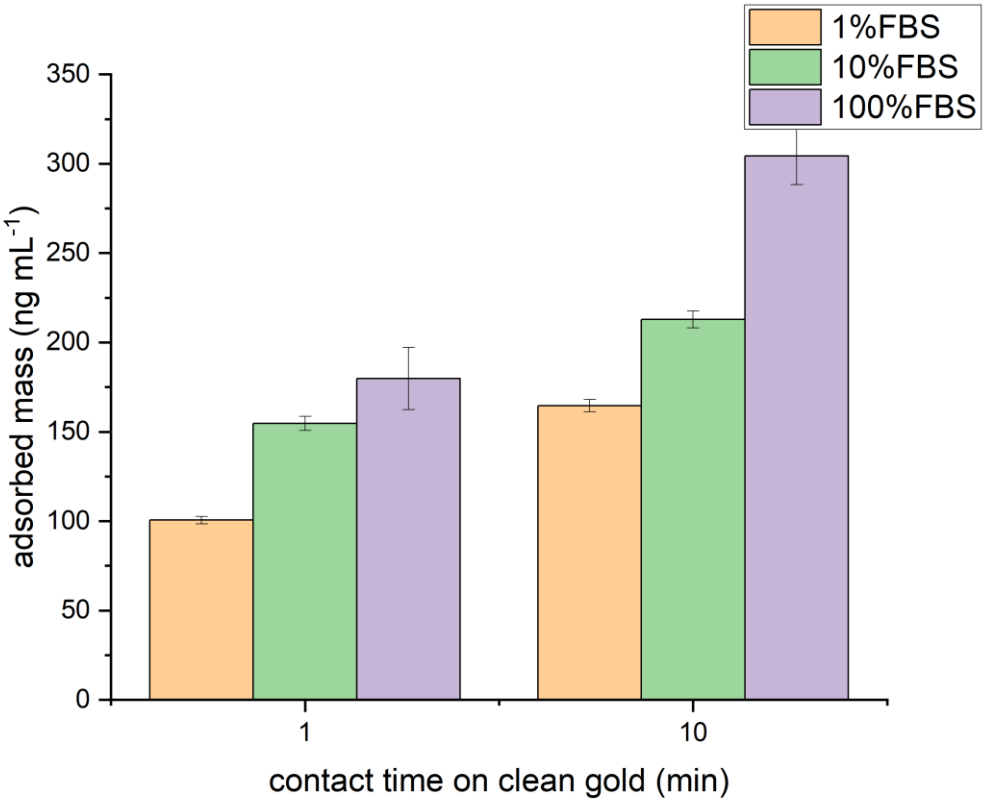


Figure 7-1 Mass adsorbed at clean gold surface after 1 min and 10 min exposure to 1%, 10% and 100% FBS, recorded via SPR measurements. Error bars denote standard deviation between three independent measurements.

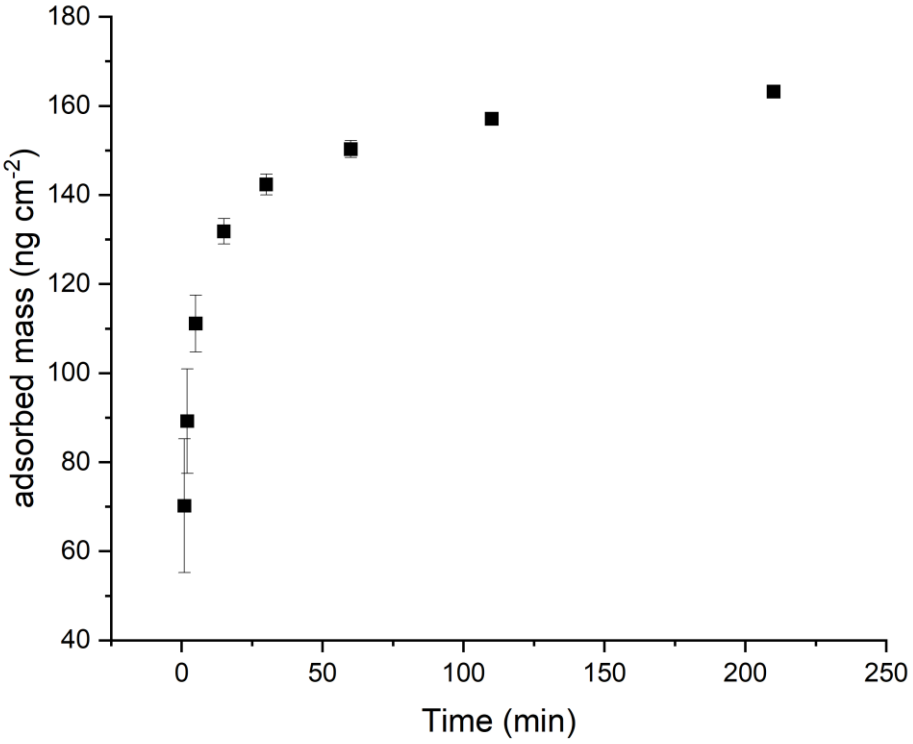


Figure 7-2 SPR measurement of 1%FBS adsorption versus accumulative exposure time. Error bars denote standard deviation between three independent measurements.

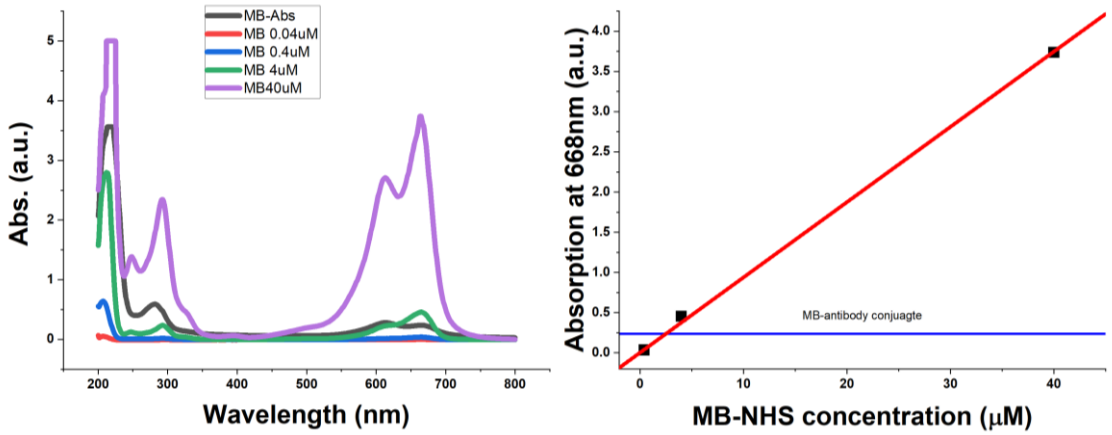


Figure 7-3 Left: UV-Vis absorbance curves recorded for different concentrations of MB-NHS and the MB-antibody conjugate in water. Right: Calibration curve and MB-Ab conjugate intensities used for estimation of conjugation efficiency. 668 nm (one of the typical double maxima observed for methylene blue),[270], while the antibody concentration is inferred from the lysine peak.[271]

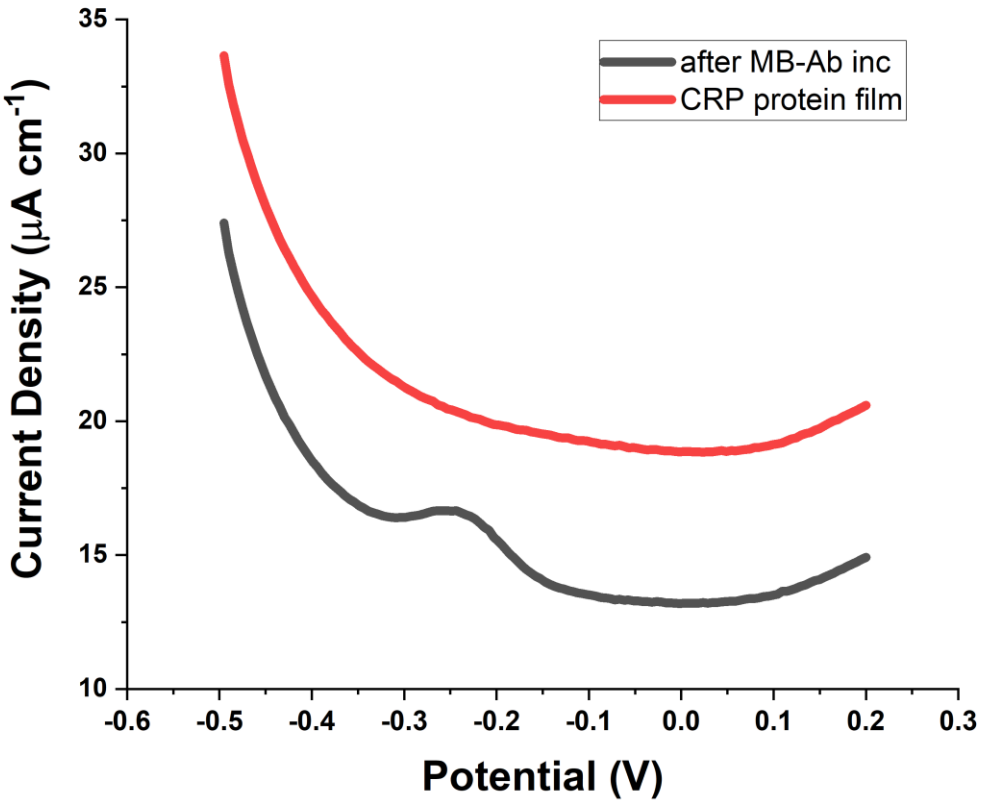


Figure 7-4 SWV curves of GCE coated with CRP protein before and after exposure to MB-Ab conjugate. While the curve recorded after the protein film formation does not show any peaks, after the incubation with antibody conjugates a peak emerges at the potential of -243 ± 5 mV in the expected range for a methylene blue derivative.[272]

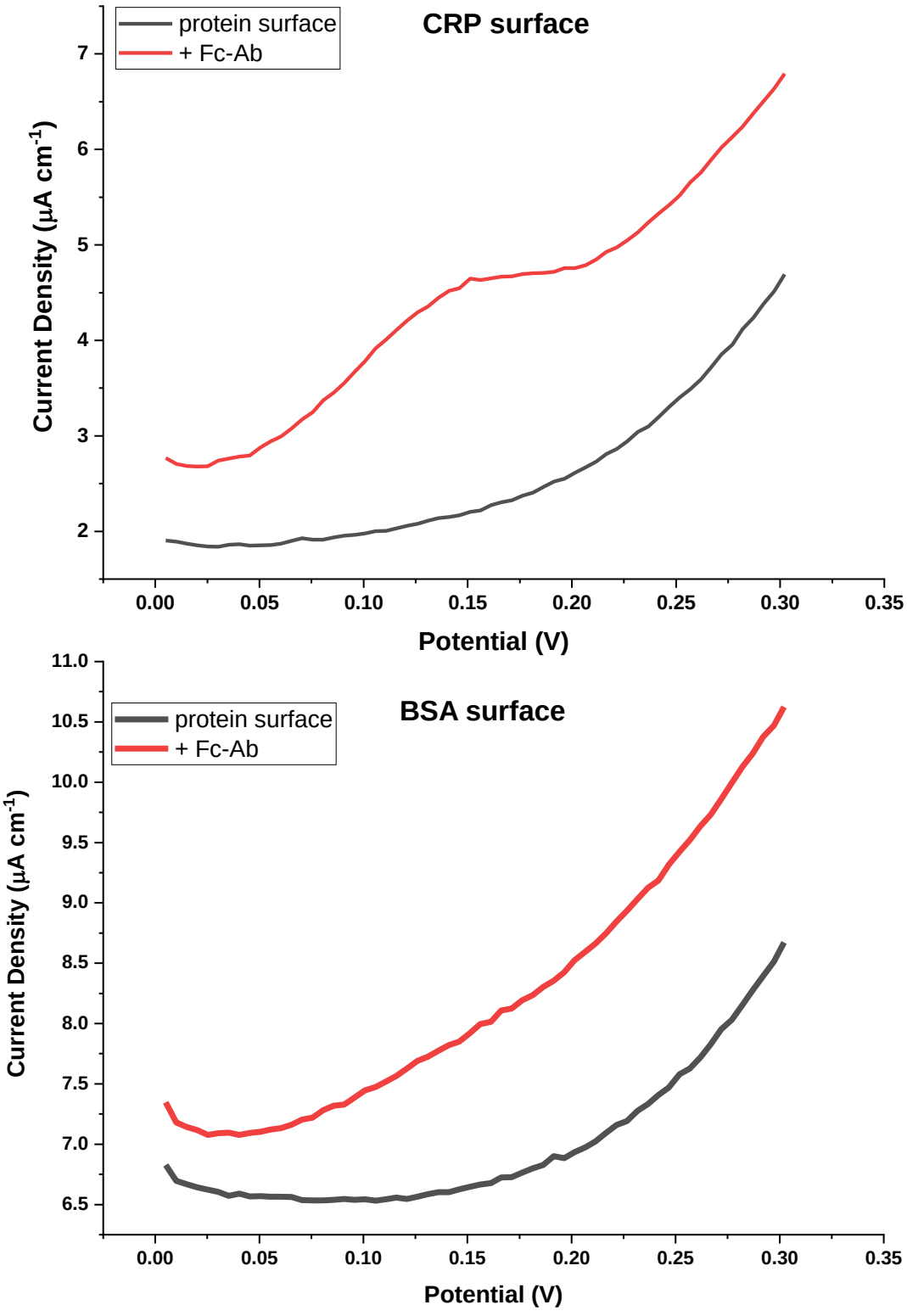


Figure 7-5 Electrochemical SWV analysis of ferrocene-antibody conjugates for the detection of electrode adsorbed target protein. Conjugates were exposed to an electrode that was coated with CRP (upper), BSA (lower) and after washing of non-

specifically adsorbed molecules, SWV measurement was carried out. The peak appearing for the CRP while not for the BSA surface indicates the specific binding of antibody conjugates to the CRP adsorbed on the electrode.

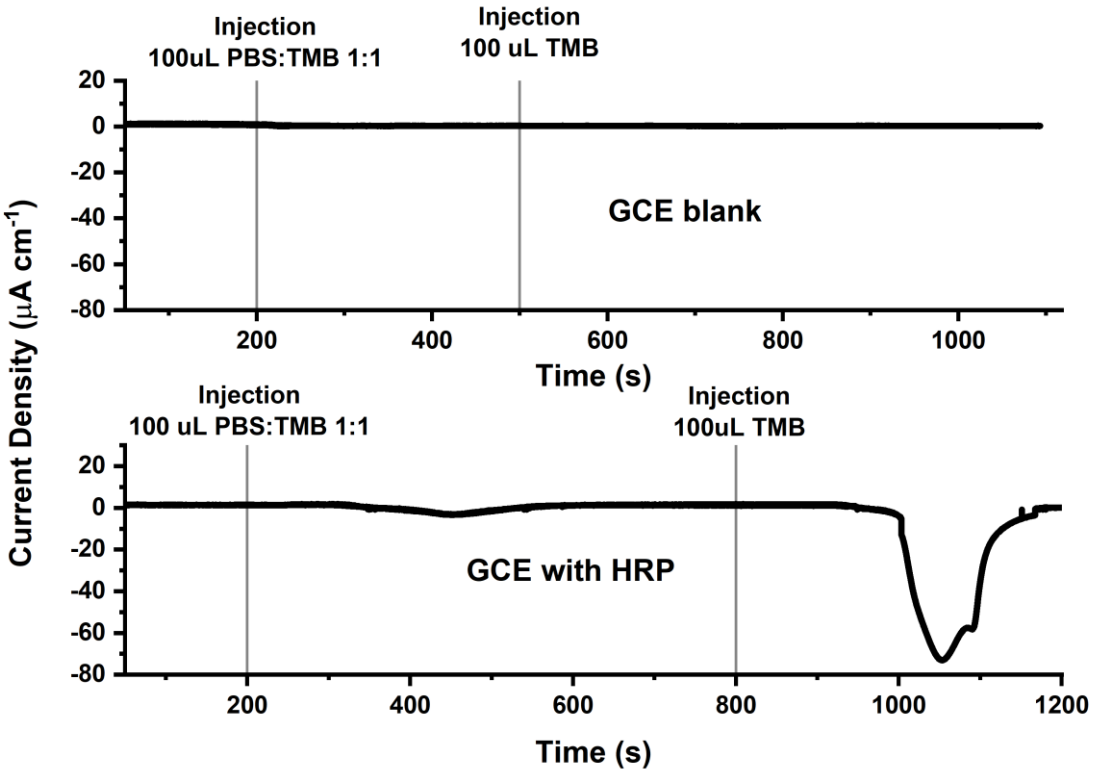


Figure 7-6 Control experiment for TMB substrate solution injection to microfluidic Dot Blot setup with GCE that was either freshly cleaned (upper) or coated with HRP (lower). The absence of any significant response in the cleaned (blank) GCE versus a significant response for both the concentrations of substrate injection on the HRP coated GCE indicate the current response stemming from the presence of HRP molecules on the surface of the electrode.

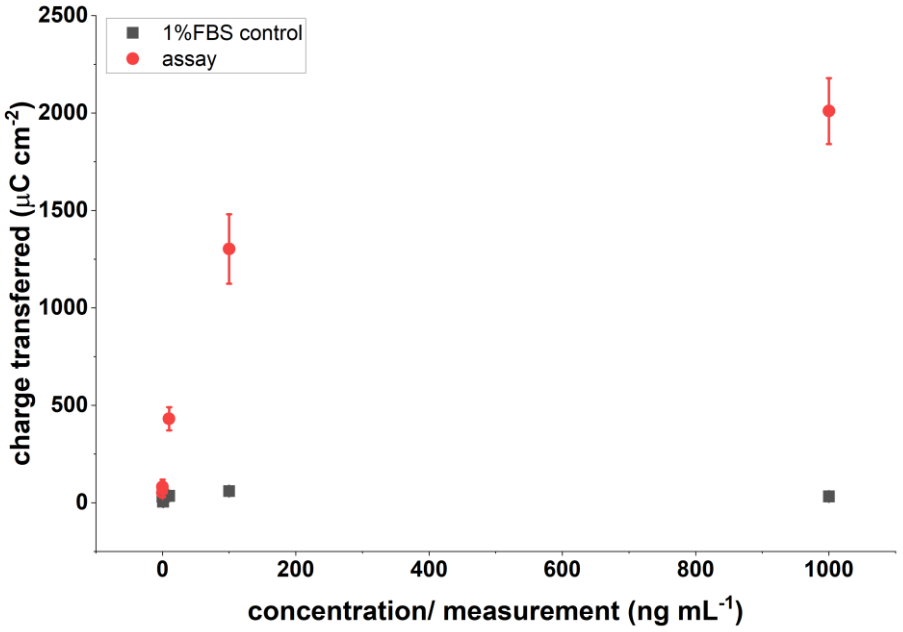


Figure 7-7 Calibration curve of microfluidically integrated amperometric dot blot assay on polycrystalline gold disk electrode with (red circles) and without (grey squares) target protein in 1% FBS.

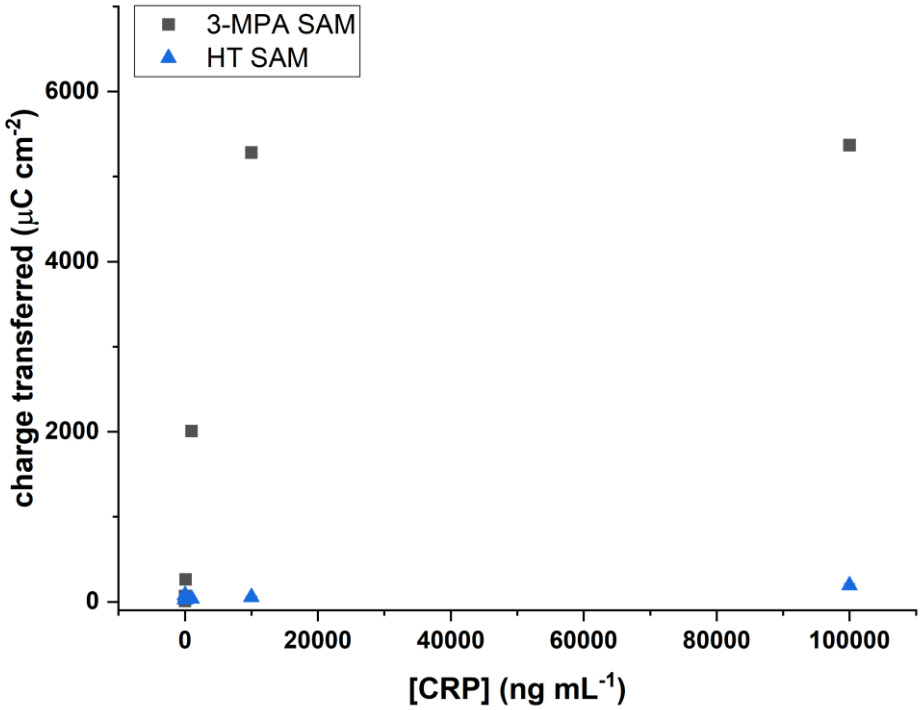


Figure 7-8 Amperometric Dot Blot performed on 3-MPA-SAM and HT-SAM prepared on gold. EDC/NHS mediated carbodiimide coupling was utilised to form a protein film on

the 3-MPA SAM, while the samples were physisorbed on the HT-SAM modified electrodes.

7.2 Appendix Chapter 4

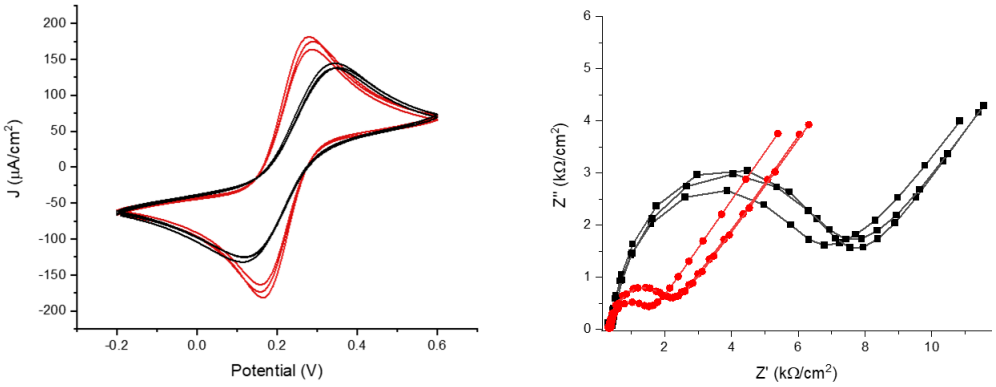


Figure 7-9 : Electrochemical investigation of glassy carbon electrodes before (red circles) and after (black squares) physisorption of CRP antibodies for 18h. Measurements were performed in 5mM [Fe(CN)6]4-/3-. Left: cyclic voltammograms recorded with scan rate of 100mV/s against Ag|AgCl reference electrode. Right: EIS measurements recorded at potential of 0.215V within a frequency range of 0.1 to 100kHz. Adapted from [237] according to CC license.

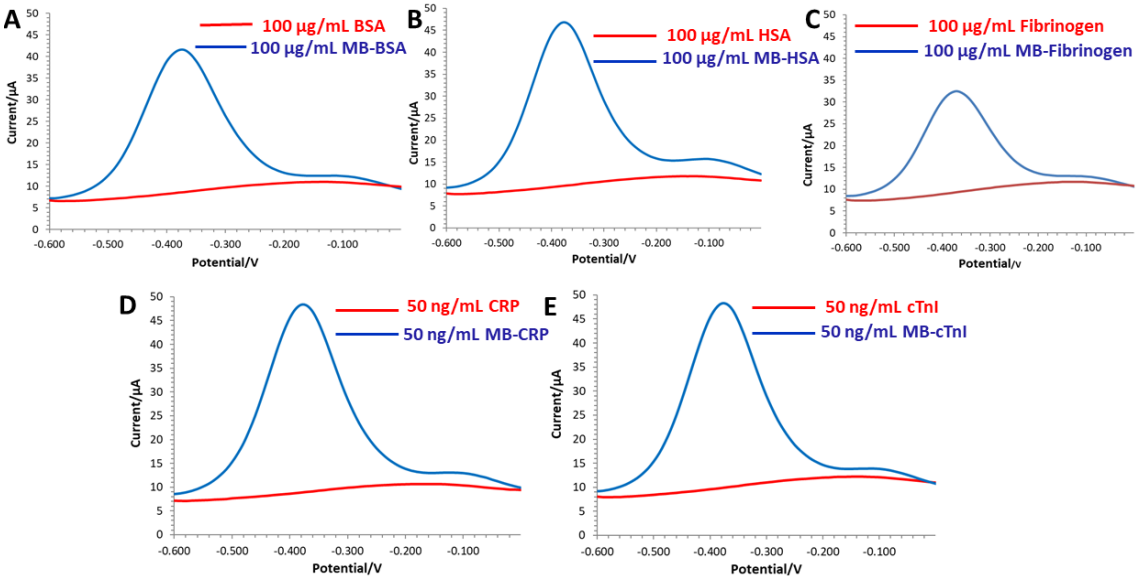


Figure 7-10 Electrochemical interrogation of proteins adsorbed on bare unmodified GCE electrodes. Electrodes were exposed to the native proteins or MB-Tagged proteins for 15 min, washed and subsequently the DPV signals were recorded. DPVs for (A) BSA and MB-BSA, (B) HSA and MB-HSA, (C) Fibrinogen and MB-Fibrinogen, (D) CRP and MB-CRP, and (E) cTnI and MB-cTnI showed that none of the observed proteins exhibited any intrinsic electrochemical response and all are succesfully labelled with MB after incubation with MB-NHS. Adapted from [237] according to CC license.

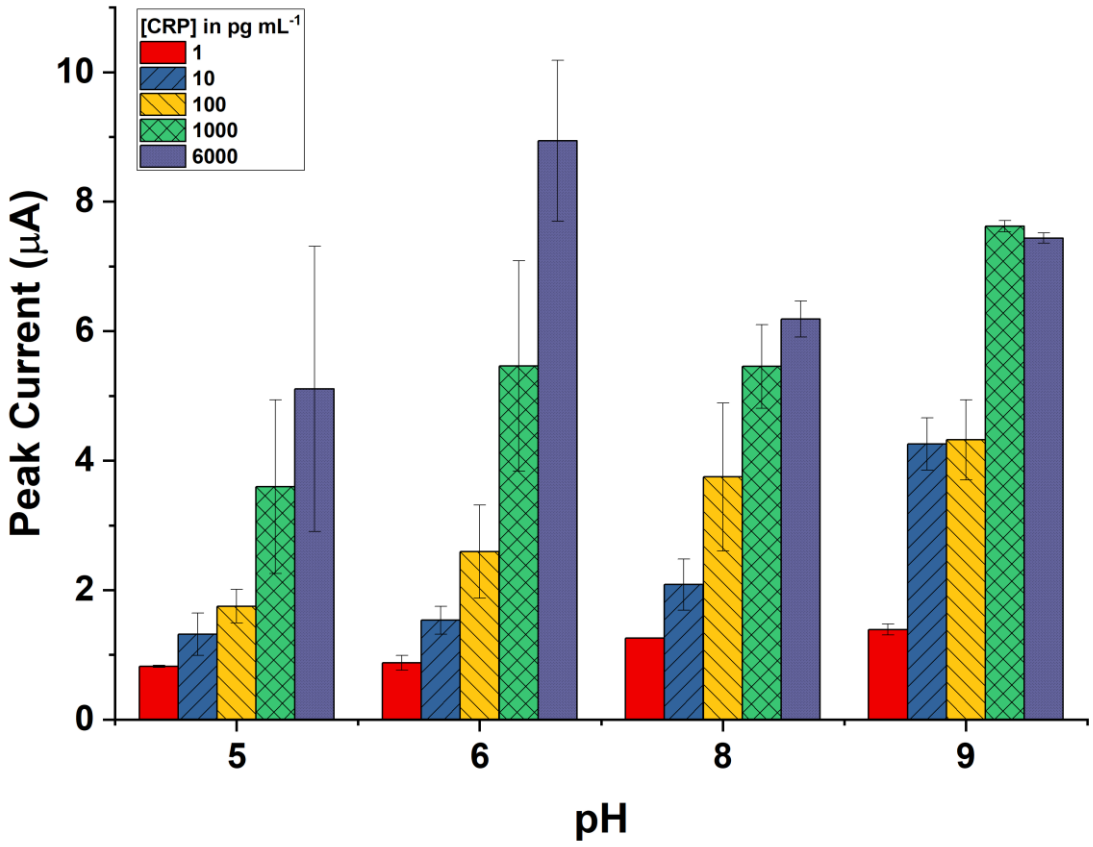


Figure 7-11 Optimization assay performance regarding labelling with MB-NHS performed under different pH conditions. The average response over two independent measurements with increasing CRP concentration is shown for protein solutions buffered at the indicated pH values. Buffers used were 100 mM Acetate buffer at pH 5.0, 100mM MES buffer at pH 6.0 and 100mM potassium phosphate buffer at pH 8.0 and pH 9.0.

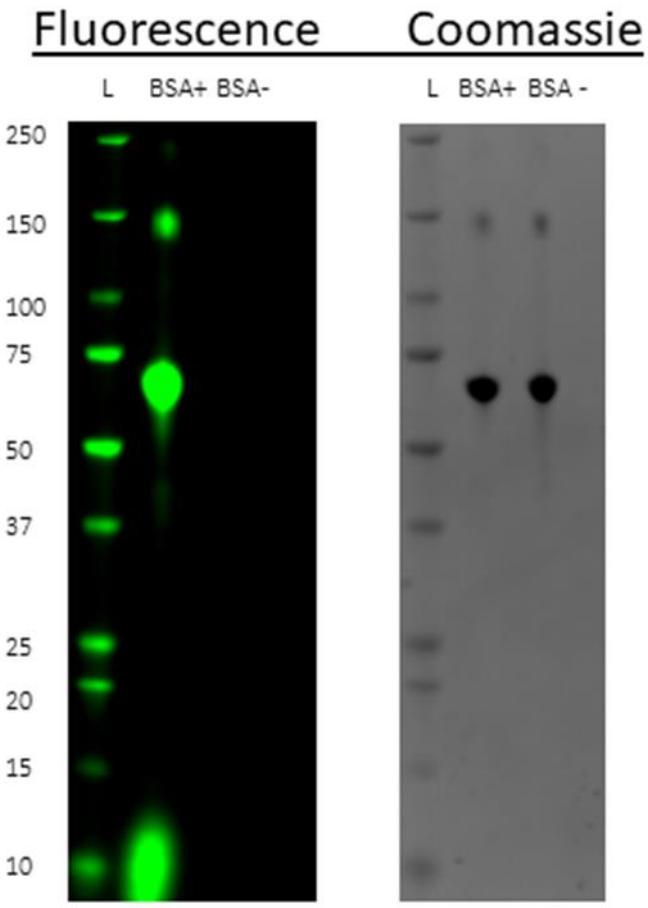


Figure 7-12 In-gel fluorescence and Coomassie images as obtained from performing gel electrophoresis of native and MB-labelled BSA protein. Both images show the same gel with in-gel fluorescence and Coomassie stain including a fragment ladder, the labelled BSA and the native BSA from left to right, respectively. Adapted from [237] according to CC license.

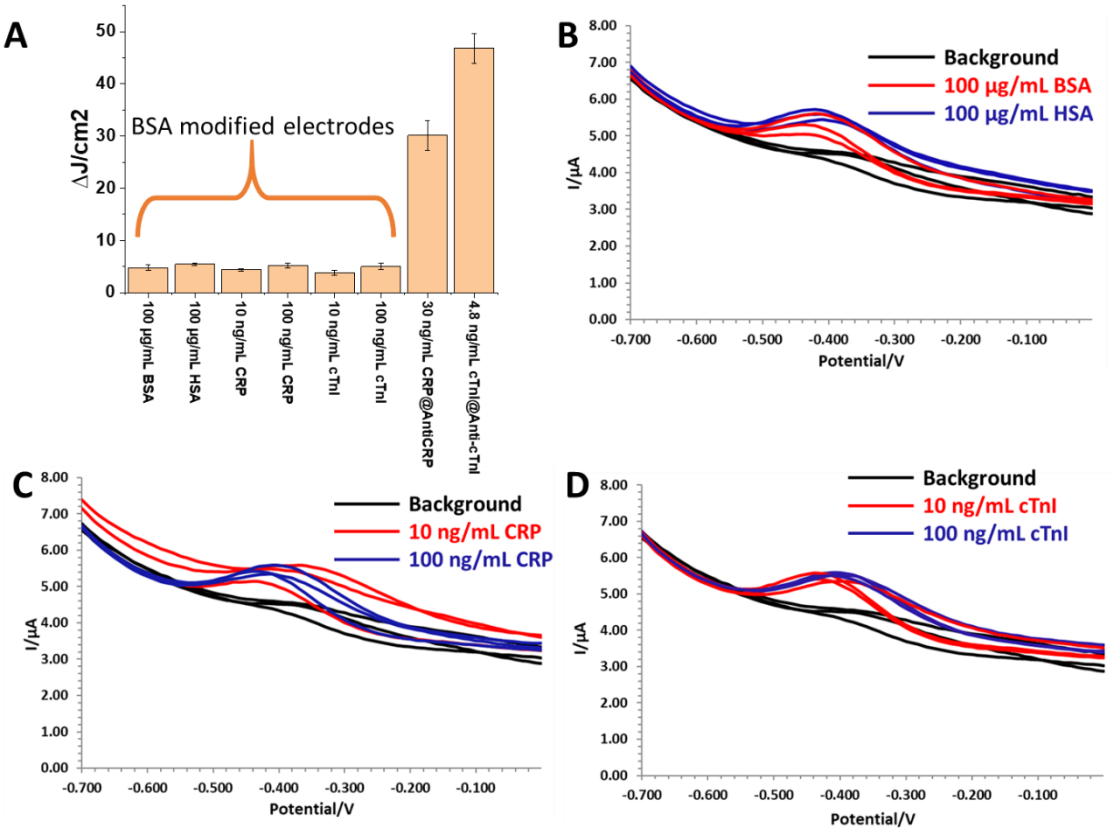


Figure 7-13 Comparison of specific and non-specific response MB-labelled proteins exposed to BSA modified electrodes and anti-body modified electrodes. (A) Electrochemical response obtained from BSA modified electrodes exposed to 100 µg mL^{-1} BSA, 100 µg mL^{-1} HSA, 10 ng mL^{-1} CRP, 100 ng mL^{-1} CRP, 10 ng mL^{-1} cTnI, and 100 ng mL^{-1} cTnI as compared to the specific response of anti-CRP modified electrode exposed to 30 ng mL^{-1} CRP and anti-cTnI modified electrode exposed to 4.8 ng mL^{-1} cTnI. Raw unprocessed voltammograms of BSA electrodes against (B) 100 µg mL^{-1} BSA and 100 µg mL^{-1} HSA; (C) 10 ng mL^{-1} CRP, 100 ng mL^{-1} CRP; and (D) 10 ng mL^{-1} cTnI, and 100 ng mL^{-1} cTnI. Adapted from [237] according to CC license.

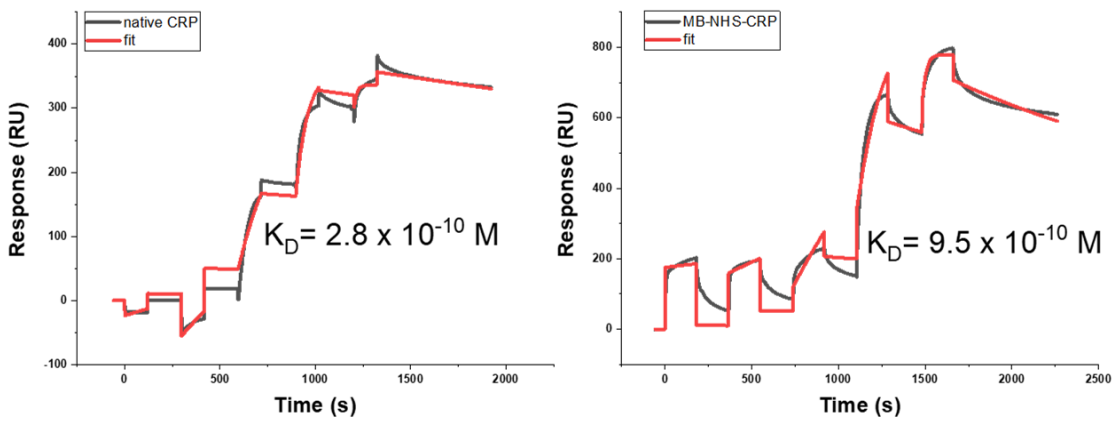


Figure 7-14 SPR measurements of the affinity of the native CRP (left) and the MB-tagged CRP (right) as obtained on a gold surface modified by CRP antibody physisorption. The black lines show the recorded data, the red lines denote the associated 1:1 Binding fits performed with the BicaoreX100 Evaluation Software. Adapted from [237] according to CC license.

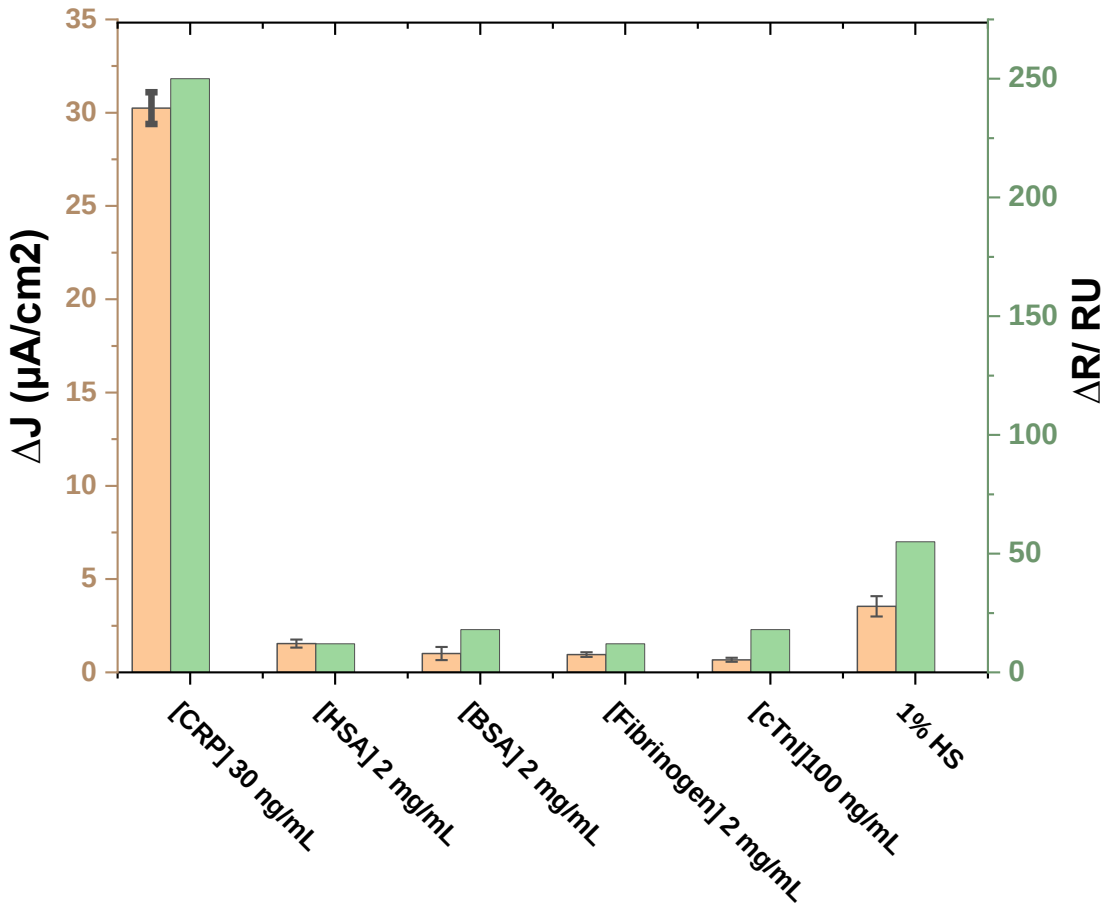


Figure 7-15 Specificity measured via SPR (right axis, green) and DPV (left axis, orange) on GC electrodes and gold SPR chips modified with physiosorbed anti-CR, respectively. Data represents changes in signal upon exposure of the interface to 30 ng mL^{-1} CRP, 2 mg mL^{-1} human serum albumin, 2 mg mL^{-1} bovine serum albumin, 2 mg mL^{-1} fibrinogen, 100 ng mL^{-1} cTnI, and 1% human serum. All measurements were performed in MES buffer. The concentrations used represent estimates for protein content of 10 to 100 times diluted human serum. Adapted from [237] according to CC license.

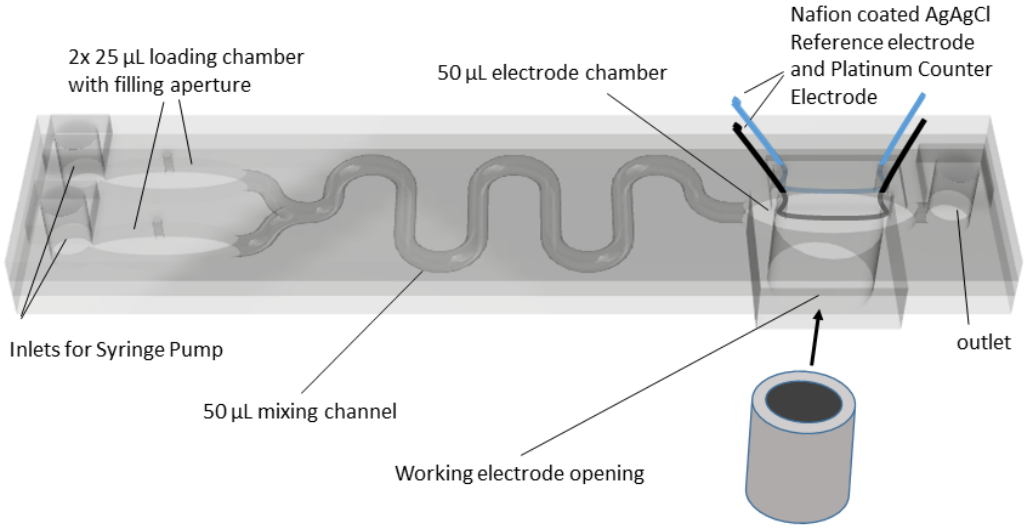


Figure 7-16 Schematic representation for the design of the microfluidic chip utilised for sample handling and electrochemical detection. An electrode compartment with reference Ag/AgCl and counter platinum electrodes is connected to a serpentine channel for mixing of mix sample and labelling reagent pumped from their respective loading chambers. Through injection holes on the top of these chambers, 25 µL of sample and reagent are injected into each compartment, respectively. The holes are then closed using Kapton tape. Flexible tubing connects a programmable syringe pump to the channels. Adapted from [237] according to CC license.

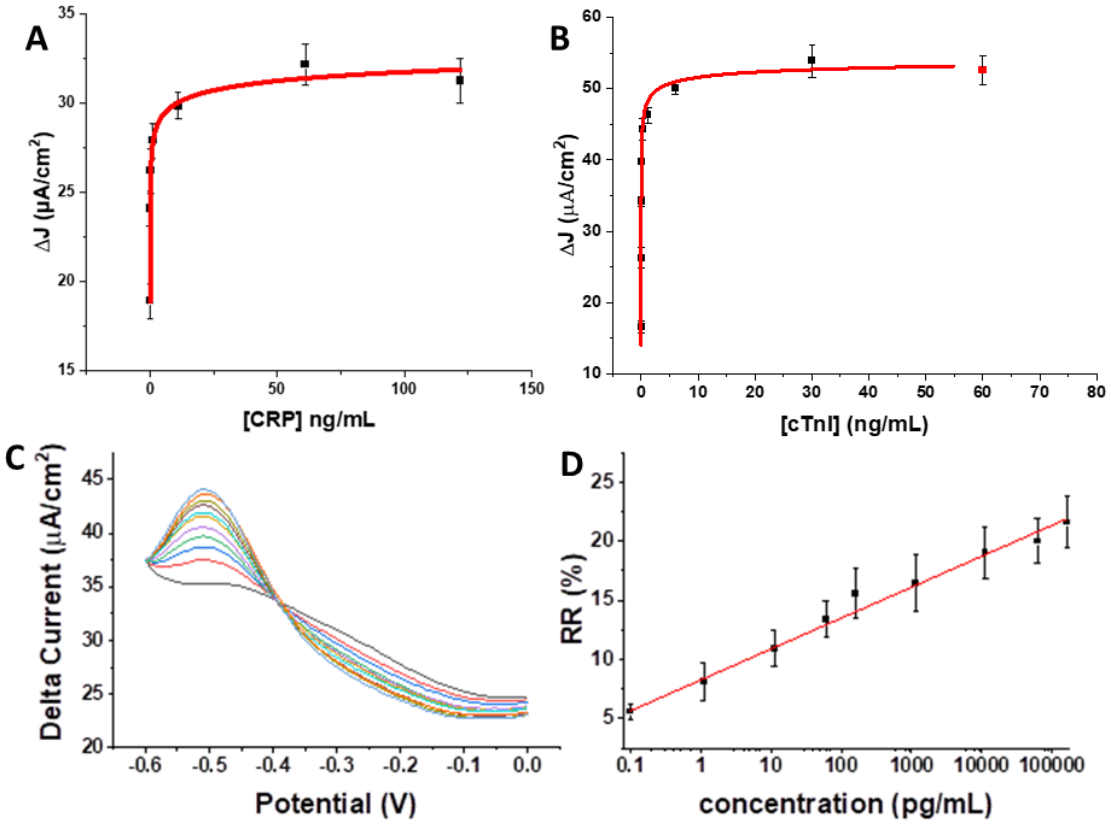


Figure 7-17 Representative extended calibration of singleplex assay in microfluidic configuration of (A) CRP and (B) cTnI showing a response curve fitted to a Langmuir-Freundlich function. (C) Background corrected sample DPV curves as function of increasing concentrations of CRP spiked into 1% HS via the microfluidic cell. (D) Calibration curve plotted as relative response vs CRP concentration in 1% HS (R^2= 0.992). Data points are the average of three independent measurements on 3 different electrodes with error bars representing standard deviation. Adapted from [237] according to CC license.

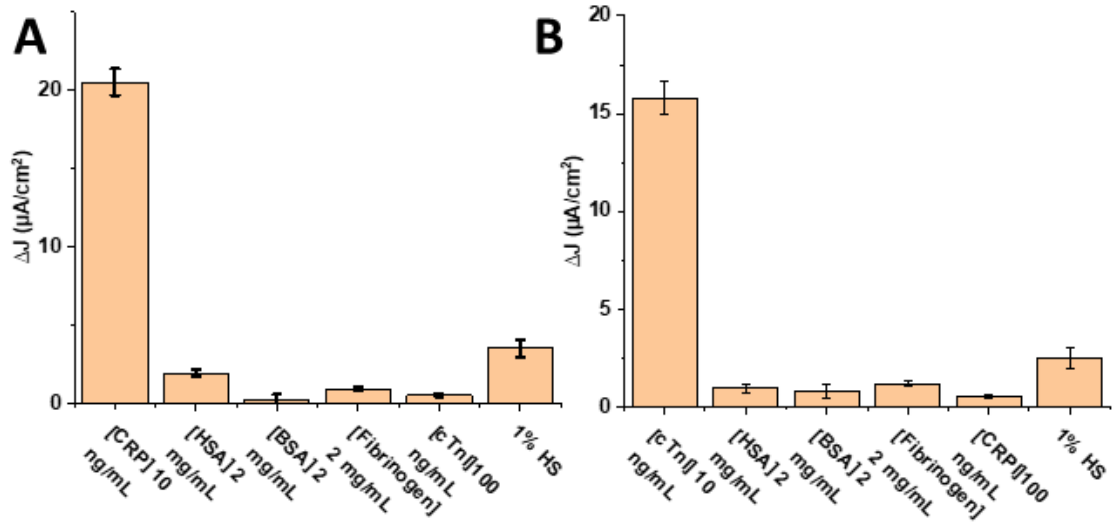


Figure 7-18 Study of electrochemical specificity for (A) Anti-CRP modified electrodes and (B) Anti-cTnI modified electrode for the online microfluidic multiplexed configuration of the assay. The response to the investigated interfering species was between 5-15% of the target-specific signal indicating a good specificity and low cross-reactivity towards other proteins. Error bars represent the standard deviation from two independent measurements. Adapted from [237] according to CC license.

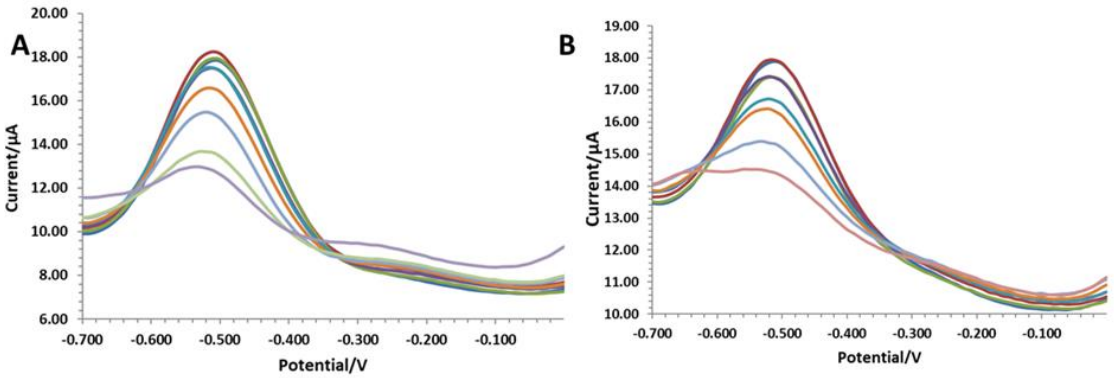


Figure 7-19 Representative DPV curves for the multiplexed on-line assay in microfluidic configuration. DPV curves on CRP-antibody modified GC electrode exposed to increasing CRP concentration (A) and cTnI-antibody modified GC electrode exposed to increasing cTnI concentration. Adapted from [237] according to CC license.

7.3 Appendix Chapter 5

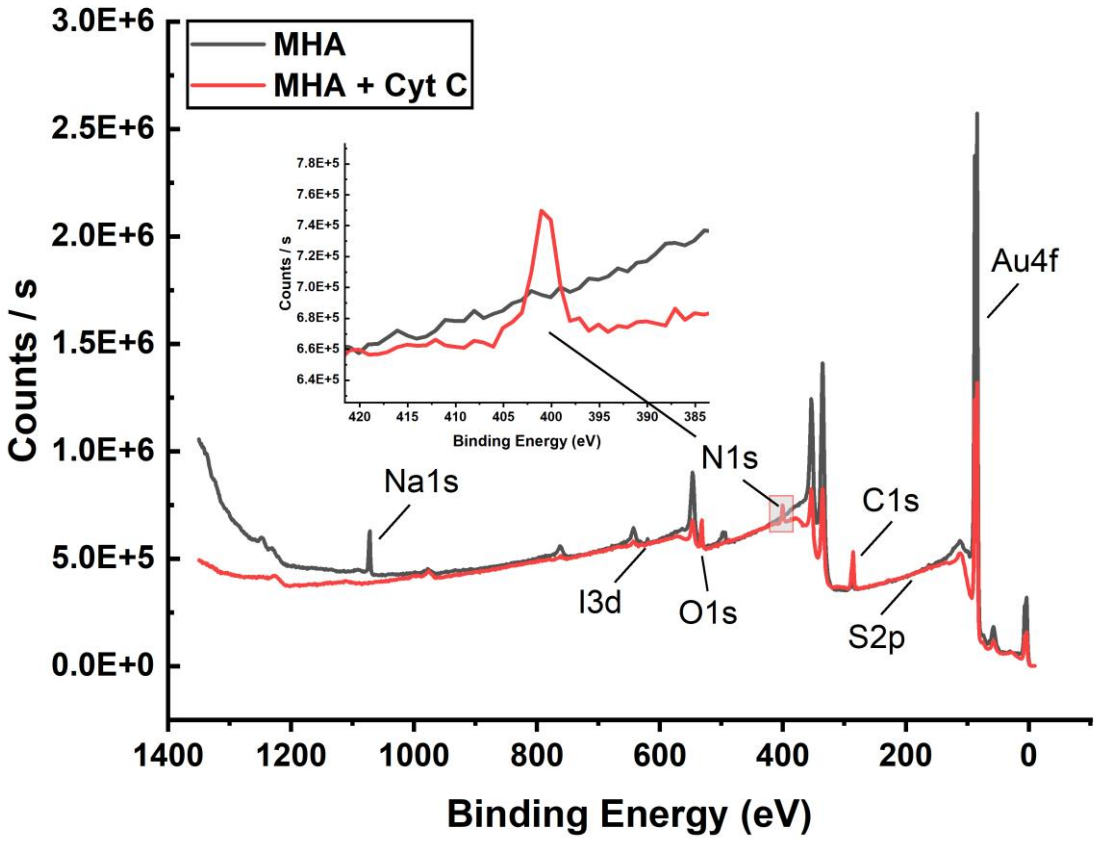


Figure 7-20 Low resolution survey XPS spectra of MHA-SAM with and without Cytochrome C adsorbed to it, indicating the appearance of a N1s peak due to the protein adsorption. All unassigned peaks arise from other orbitals of the same elements. Inset: Magnification of the N1s region.

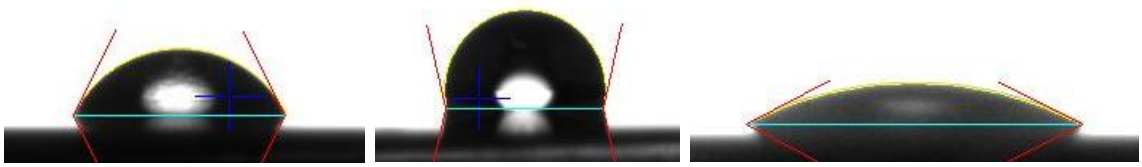


Figure 7-21 Exemplary images of contact angle measurements of Au screen printed electrodes with different surface modifications using the software FTA32. Surface modification from left to right: plain Au, Hexanethiol, Azurin on Hexanethiol.

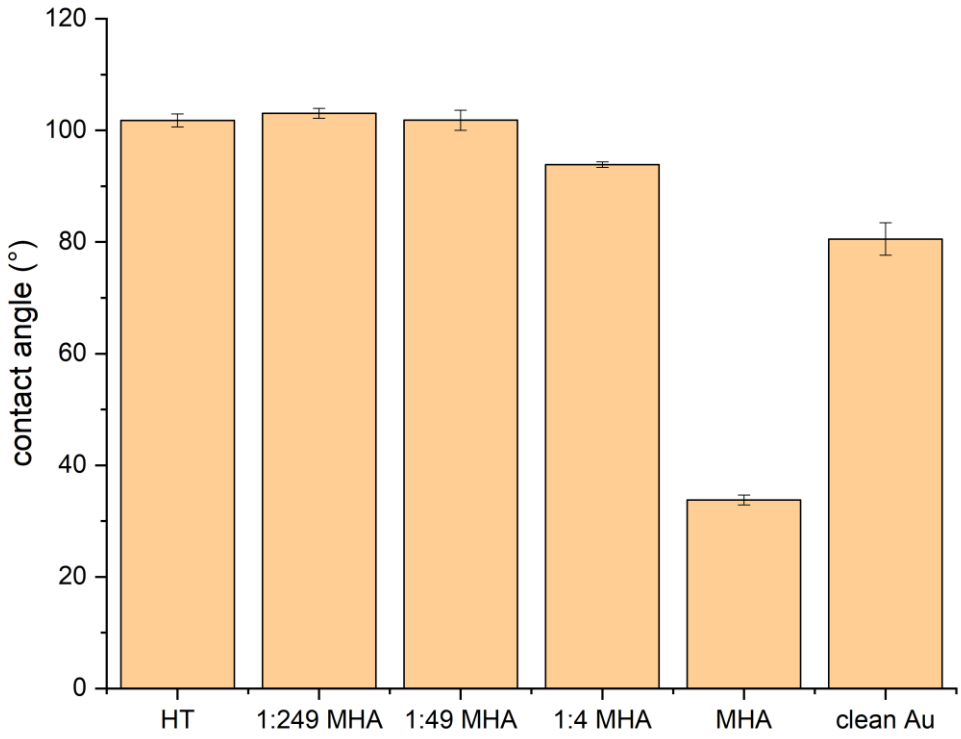


Figure 7-22 Water contact angle of different SAMs prepared on polycristalline gold electrode surfaces.

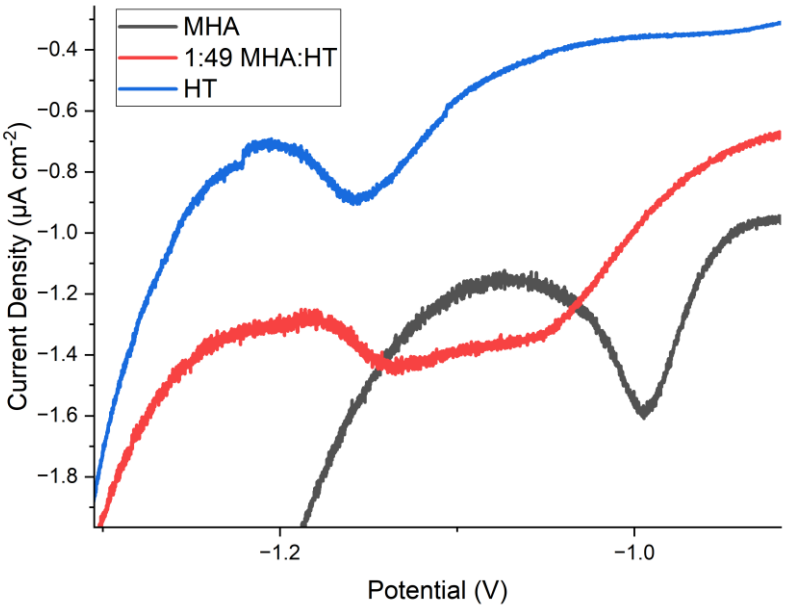


Figure 7-23 Electrochemical Stripping Analysis of different SAMs prepared on polycrystalline gold electrode surfaces.

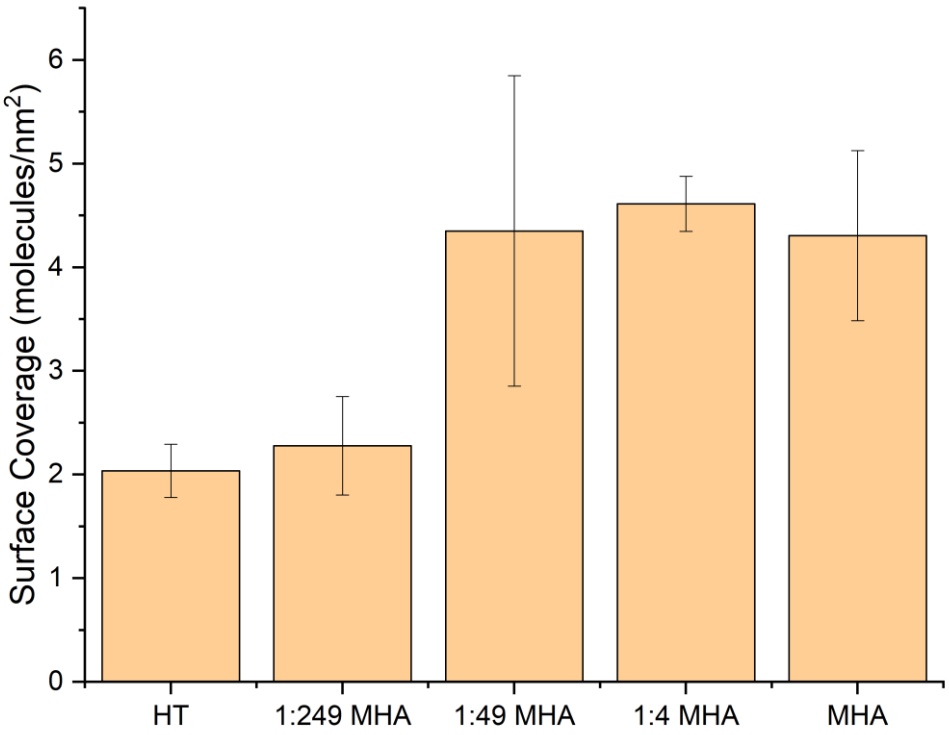


Figure 7-24 Molecular surface coverages for the mixed SAMs on polycrystalline gold as calculated from electrochemical stripping voltammetry.

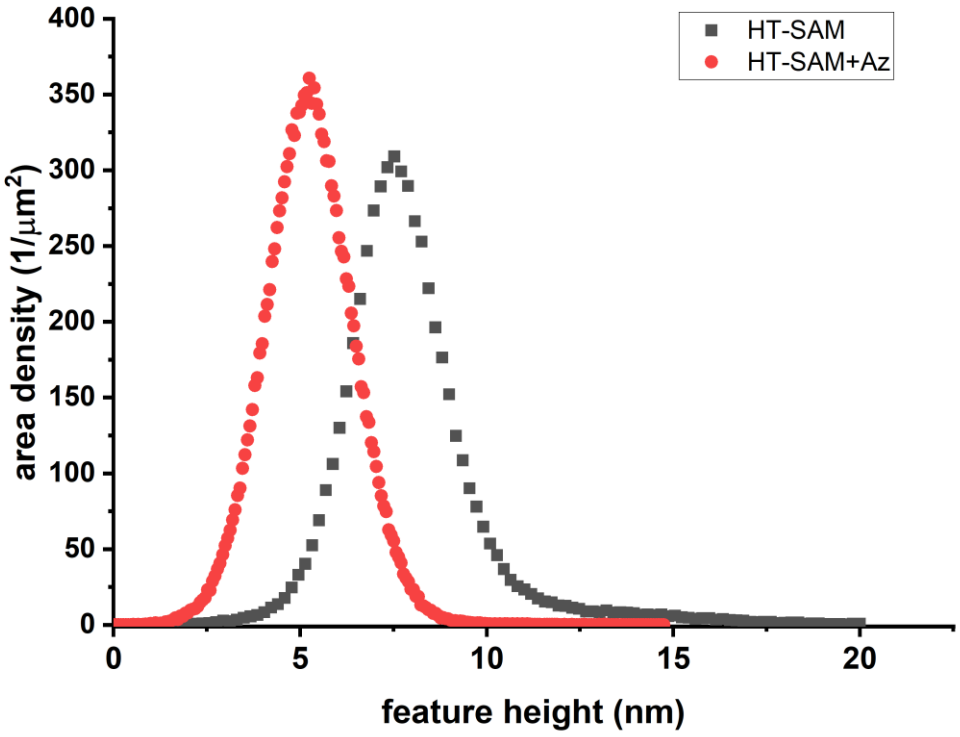


Figure 7-25 AFM height measurement of Azurin physisorbed on HT-SAM.

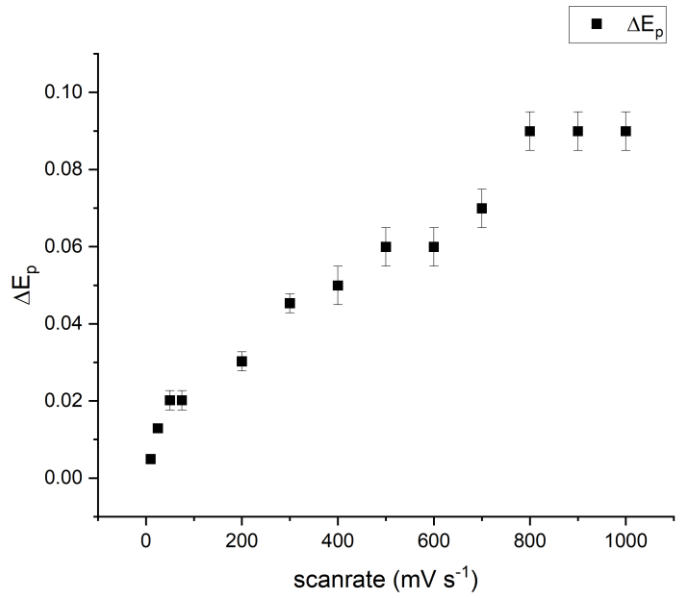


Figure 7-26 Peak seperation plotted versus scanrate as recorded on hexanethiol SAMs with adsorbed Azurin.

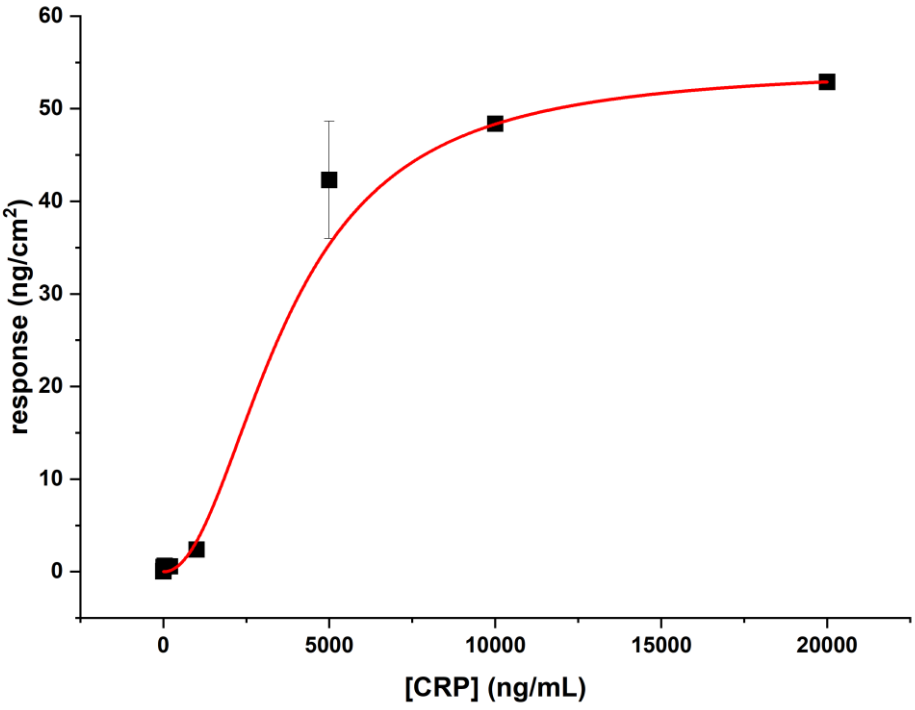


Figure 7-27 SPR dose response curve of mixed SAM (1:49 MHA:HT) with antibodies coupled via EDC/NHS and backfilled with Azurin.

References

1. Whitford, D., *Proteins: structure and function*. John Wiley & Sons: 2013.

2. Finkelstein, A. V.; Ptitsyn, O., *Protein physics: a course of lectures*. Elsevier: 2016.

3. Zhao, X.; Lin, C.-W.; Wang, J.; Oh, D. H., Advances in rapid detection methods for foodborne pathogens. *J. Microbiol. Biotechnol.* **2014,** *24* (3), 297-312.

4. Zaguri, M.; Kandel, S.; Rinehart, S. A.; Torsekar, V. R.; Hawlena, D., Protein quantification in ecological studies: a literature review and empirical comparisons of standard methodologies. *Methods in Ecology and Evolution* **2021,** *12* (7), 1240-1251.

5. Geyer, P. E.; Holdt, L. M.; Teupser, D.; Mann, M., Revisiting biomarker discovery by plasma proteomics. *Molecular systems biology* **2017,** *13* (9), 942.

6. Borrebaeck, C. A., Precision diagnostics: moving towards protein biomarker signatures of clinical utility in cancer. *Nature Reviews Cancer* **2017,** *17* (3), 199-204.

7. Jayan, H.; Pu, H.; Sun, D.-W., Recent development in rapid detection techniques for microorganism activities in food matrices using bio-recognition: A review. *Trends in Food Science & Technology* **2020,** *95*, 233-246.

8. Balayan, S.; Chauhan, N.; Rosario, W.; Jain, U., Biosensor development for C-reactive protein detection: A review. *Applied Surface Science Advances* **2022,** *12*, 100343.

9. Luppa, P. B.; Müller, C.; Schlichtiger, A.; Schlebusch, H., Point-of-care testing (POCT): Current techniques and future perspectives. *TrAC, Trends Anal. Chem.* **2011,** *30* (6), 887-898.

10. Gnoth, C.; Johnson, S., Strips of hope: accuracy of home pregnancy tests and new developments. *Geburtshilfe und Frauenheilkunde* **2014,** *74* (07), 661-669.

11. Peto, T.; Affron, D.; Afrough, B.; Agasu, A.; Ainsworth, M.; Allanson, A.; Allen, K.; Allen, C.; Archer, L.; Ashbridge, N., COVID-19: Rapid antigen detection for SARS-CoV-2 by lateral flow assay: A national systematic evaluation of sensitivity and specificity for mass-testing. *EClinicalMedicine* **2021,** *36*, 100924.

12. Szunerits, S.; Mishyn, V.; Grabowska, I.; Boukherroub, R., Electrochemical cardiovascular platforms: Current state of the art and beyond. *Biosens. Bioelectron.* **2019,** *131*, 287-298.

13. Gubala, V.; Harris, L. F.; Ricco, A. J.; Tan, M. X.; Williams, D. E., Point of care diagnostics: status and future. *Anal. Chem.* **2012,** *84* (2), 487-515.

14. Nayak, S.; Blumenfeld, N. R.; Laksanasopin, T.; Sia, S. K., Point-of-care diagnostics: recent developments in a connected age. *Anal. Chem.* **2017,** *89* (1), 102-123.

15. Chadha, U.; Bhardwaj, P.; Agarwal, R.; Rawat, P.; Agarwal, R.; Gupta, I.; Panjwani, M.; Singh, S.; Ahuja, C.; Selvaraj, S. K., Recent progress and growth in biosensors technology: A critical review. *Journal of Industrial and Engineering Chemistry* **2022,** *109*, 21-51.

16. Fraden, J., *Handbook of modern sensors : physics, designs, and applications*. Fourth ed.; Springer Verlag: New York, 2010.

17. Bhalla, N.; Jolly, P.; Formisano, N.; Estrela, P., Introduction to biosensors, 2016.

18. Danzer, K., Selectivity and specificity in analytical chemistry. General considerations and attempt of a definition and quantification. *Fresenius' journal of analytical chemistry* **2001,** *369*, 397-402.

19. Reznik, Y., *Handbook of diabetes technology*. Springer: Cham, 2019.

20. Sela-Culang, I.; Kunik, V.; Ofran, Y., The structural basis of antibody-antigen recognition. *Frontiers in immunology* **2013,** *4*, 302.

21. Deng, B.; Lin, Y.; Wang, C.; Li, F.; Wang, Z.; Zhang, H.; Li, X.-F.; Le, X. C., Aptamer binding assays for proteins: the thrombin example—a review. *Anal. Chim. Acta* **2014,** *837*, 1-15.

22. Wilson, I. A.; Stanfield, R. L., Antibody-antigen interactions. *Current opinion in structural biology* **1993,** *3* (1), 113-118.

23. Wang, X.; Walt, D. R., Simultaneous detection of small molecules, proteins and microRNAs using single molecule arrays. *Chemical Science* **2020,** *11* (30), 7896-7903.

24. Lagrand, W. K.; Visser, C. A.; Hermens, W. T.; Niessen, H. W.; Verheugt, F. W.; Wolbink, G.-J.; Hack, C. E., C-reactive protein as a cardiovascular risk factor: more than an epiphenomenon? *Circulation* **1999,** *100* (1), 96-102.

25. Scholler, N.; Urban, N., CA125 in ovarian cancer. **2007**.

26. Wettersten, N.; Maisel, A., Role of cardiac troponin levels in acute heart failure. *Cardiac failure review* **2015,** *1* (2), 102.

27. Banerjee, S., Empowering clinical diagnostics with mass spectrometry. *ACS omega* **2020,** *5* (5), 2041-2048.

28. Vékey, K.; Telekes, A.; Vertes, A., *Medical applications of mass spectrometry*. Elsevier: 2011.

29. Bollella, P.; Katz, E., Biosensors—Recent advances and future challenges. *Sensors* **2020,** *20* (22), 6645.

30. Arshavsky-Graham, S.; Heuer, C.; Jiang, X.; Segal, E., Aptasensors versus immunosensors—Which will prevail? *Engineering in Life Sciences* **2022,** *22* (3-4), 319-333.

31. Murphy, A. C.; Wechsler, M. E.; Peppas, N. A., Recent advancements in biosensing approaches for screening and diagnostic applications. *Current Opinion in Biomedical Engineering* **2021,** *19*, 100318.

32. Wu, D.; Milutinovic, M. D.; Walt, D. R., Single molecule array (Simoa) assay with optimal antibody pairs for cytokine detection in human serum samples. *Analyst* **2015,** *140* (18), 6277-6282.

33. Chowdhury, F.; Williams, A.; Johnson, P., Validation and comparison of two multiplex technologies, Luminex® and Mesoscale Discovery, for human cytokine profiling. *Journal of immunological methods* **2009,** *340* (1), 55-64.

34. Vashist, S. K.; Luong, J. H., *Handbook of immunoassay technologies: approaches, performances, and applications*. Academic Press: 2018.

35. Cohen, L.; Walt, D. R., Single-molecule arrays for protein and nucleic acid analysis. *Annual Review of Analytical Chemistry* **2017,** *10*, 345-363.

36. Hui, Y.; Huang, Z.; Alahi, M. E. E.; Nag, A.; Feng, S.; Mukhopadhyay, S. C., Recent advancements in electrochemical biosensors for monitoring the water quality. *Biosensors* **2022,** *12* (7), 551.

37. Farghaly, O. A.; Hameed, R. A.; Abu-Nawwas, A.-A. H., Analytical application using modern electrochemical techniques. *Int. J. Electrochem. Sci* **2014,** *9* (1), 3287-3318.

38. Vigneshvar, S.; Sudhakumari, C.; Senthilkumaran, B.; Prakash, H., Recent advances in biosensor technology for potential applications–an overview. *Frontiers in bioengineering and biotechnology* **2016,** *4*, 11.

39. Blair, E. O.; Corrigan, D. K., A review of microfabricated electrochemical biosensors for DNA detection. *Biosens. Bioelectron.* **2019,** *134*, 57-67.

40. Stefano, J. S.; Orzari, L. O.; Silva-Neto, H. A.; de Ataíde, V. N.; Mendes, L. F.; Coltro, W. K. T.; Paixão, T. R. L. C.; Janegitz, B. C., Different approaches for fabrication of low-cost electrochemical sensors. *Current Opinion in Electrochemistry* **2022,** *32*, 100893.

41. Khanmohammadi, A.; Aghaie, A.; Vahedi, E.; Qazvini, A.; Ghanei, M.; Afkhami, A.; Hajian, A.; Bagheri, H., Electrochemical biosensors for the detection of lung cancer biomarkers: A review. *Talanta* **2020,** *206*, 120251.

42. Pastucha, M.; Farka, Z.; Lacina, K.; Mikušová, Z.; Skládal, P., Magnetic nanoparticles for smart electrochemical immunoassays: a review on recent developments. *Microchimica Acta* **2019,** *186*, 1-26.

43. Felix, F. S.; Angnes, L., Electrochemical immunosensors–a powerful tool for analytical applications. *Biosens. Bioelectron.* **2018,** *102*, 470-478.

44. Sharafeldin, M.; Davis, J. J., Point of Care Sensors for Infectious Pathogens. *Anal. Chem.* **2020**.

45. Li, H.; Li, S.; Xia, F., Electrochemical Sandwich Assays for Protein Detection. *Biosensors Based on Sandwich Assays* **2018**, 47-68.

46. Chikkaveeraiah, B. V.; Mani, V.; Patel, V.; Gutkind, J. S.; Rusling, J. F., Microfluidic electrochemical immunoarray for ultrasensitive detection of two cancer biomarker proteins in serum. *Biosens. Bioelectron.* **2011,** *26* (11), 4477-4483.

47. Rahn, K. L.; Peramune, U.; Zhang, T.; Anand, R. K., Label-Free Electrochemical Methods for Disease Detection. *Annual Review of Analytical Chemistry* **2023,** *16*, 49-69.

48. Singh, A.; Sharma, A.; Ahmed, A.; Sundramoorthy, A. K.; Furukawa, H.; Arya, S.; Khosla, A., Recent advances in electrochemical biosensors: Applications, challenges, and future scope. *Biosensors* **2021,** *11* (9), 336.

49. Zhong, H.; Zhao, C.; Chen, J.; Chen, M.; Luo, T.; Tang, W.; Liu, J., Electrochemical immunosensor with surface-confined probe for sensitive and reagentless detection of breast cancer biomarker. *RSC Advances* **2020,** *10* (38), 22291-22296.

50. Fernandes, F. C.; Goes, M. S.; Davis, J. J.; Bueno, P. R., Label free redox capacitive biosensing. *Biosens. Bioelectron.* **2013,** *50*, 437-40.

51. Yang, H.; Xu, Y.; Hou, Q.; Xu, Q.; Ding, C., Magnetic antifouling material based ratiometric electrochemical biosensor for the accurate detection of CEA in clinical serum. *Biosens. Bioelectron.* **2022,** *208*, 114216.

52. Luo, X.; Davis, J. J., Electrical biosensors and the label free detection of protein disease biomarkers. *Chem. Soc. Rev.* **2013,** *42* (13), 5944-5962.

53. Bueno, P. R.; Bedatty Fernandes, F. C.; Davis, J. J., Quantum capacitance as a reagentless molecular sensing element. *Nanoscale* **2017,** *9* (40), 15362-15370.

54. Filik, H.; Avan, A. A., Nanostructures for nonlabeled and labeled electrochemical immunosensors: Simultaneous electrochemical detection of cancer markers: A review. *Talanta* **2019,** *205*, 120153.

55. Cho, I.-H.; Lee, J.; Kim, J.; Kang, M.-s.; Paik, J. K.; Ku, S.; Cho, H.-M.; Irudayaraj, J.; Kim, D.-H., Current technologies of electrochemical immunosensors: Perspective on signal amplification. *Sensors* **2018,** *18* (1), 207.

56. de Eguilaz, M. R.; Cumba, L. R.; Forster, R. J., Electrochemical detection of viruses and antibodies: A mini review. *Electrochem. Commun.* **2020,** *116*, 106762.

57. Kanyong, P.; Patil, A. V.; Davis, J. J., Functional Molecular Interfaces for Impedance-Based Diagnostics. *Annu Rev Anal Chem (Palo Alto Calif)* **2020,** *13* (1), 183-200.

58. Baradoke, A.; Hein, R.; Li, X.; Davis, J. J., Reagentless redox capacitive assaying of CRP at a polyaniline interface. *Anal. Chem.* **2020**.

59. Jiang, C.; Wang, G.; Hein, R.; Liu, N.; Luo, X.; Davis, J. J., Antifouling Strategies for Selective In Vitro and In Vivo Sensing. *Chem Rev* **2020**.

60. Ronkainen, N. J.; Halsall, H. B.; Heineman, W. R., Electrochemical biosensors. *Chem. Soc. Rev.* **2010,** *39* (5), 1747-1763.

61. Bollella, P.; Gorton, L., Enzyme based amperometric biosensors. *Current opinion in Electrochemistry* **2018,** *10*, 157-173.

62. Police Patil, A. V.; Chuang, Y.-S.; Li, C.; Wu, C.-C., Recent advances in electrochemical immunosensors with nanomaterial assistance for signal amplification. *Biosensors* **2023,** *13* (1), 125.

63. Scholz, F., Voltammetric techniques of analysis: the essentials. *ChemTexts* **2015,** *1* (4), 17.

64. Gulaboski, R., The future of voltammetry. *Macedonian Journal of Chemistry and Chemical Engineering* **2022,** *41* (2), 1-12.

65. Purohit, B.; Vernekar, P. R.; Shetti, N. P.; Chandra, P., Biosensor nanoengineering: Design, operation, and implementation for biomolecular analysis. *Sensors International* **2020,** *1*, 100040.

66. Magar, H. S.; Hassan, R. Y.; Mulchandani, A., Electrochemical impedance spectroscopy (EIS): Principles, construction, and biosensing applications. *Sensors* **2021,** *21* (19), 6578.

67. Wang, S.; Zhang, J.; Gharbi, O.; Vivier, V.; Gao, M.; Orazem, M. E., Electrochemical impedance spectroscopy. *Nature Reviews Methods Primers* **2021,** *1* (1), 41.

68. Bertok, T.; Lorencova, L.; Chocholova, E.; Jane, E.; Vikartovska, A.; Kasak, P.; Tkac, J., Electrochemical impedance spectroscopy based biosensors: Mechanistic principles, analytical examples and challenges towards commercialization for assays of protein cancer biomarkers. *ChemElectroChem* **2019,** *6* (4), 989-1003.

69. Van Haeverbeke, M.; Stock, M.; De Baets, B., Equivalent electrical circuits and their use across electrochemical impedance spectroscopy application domains. *Ieee Access* **2022,** *10*, 51363-51379.

70. Harrington, D. A.; Van Den Driessche, P., Mechanism and equivalent circuits in electrochemical impedance spectroscopy. *Electrochim. Acta* **2011,** *56* (23), 8005-8013.

71. Kokkinos, C.; Economou, A.; Prodromidis, M. I., Electrochemical immunosensors: Critical survey of different architectures and transduction strategies. *TrAC, Trends Anal. Chem.* **2016,** *79*, 88-105.

72. Bueno, P. R.; Davis, J. J., Charge transport and energy storage at the molecular scale: from nanoelectronics to electrochemical sensing. *Chem. Soc. Rev.* **2020,** *49* (21), 7505-7515.

73. Ricci, F.; Adornetto, G.; Palleschi, G., A review of experimental aspects of electrochemical immunosensors. *Electrochim. Acta* **2012,** *84*, 74-83.

74. Mahmudunnabi, R. G.; Farhana, F. Z.; Kashaninejad, N.; Firoz, S. H.; Shim, Y.-B.; Shiddiky, M. J., Nanozyme-based electrochemical biosensors for disease biomarker detection. *Analyst* **2020,** *145* (13), 4398-4420.

75. Mohan, J. M.; Amreen, K.; Javed, A.; Dubey, S. K.; Goel, S., Emerging trends in miniaturized and microfluidic electrochemical sensing platforms. *Current Opinion in Electrochemistry* **2022,** *33*, 100930.

76. Rackus, D. G.; Shamsi, M. H.; Wheeler, A. R., Electrochemistry, biosensors and microfluidics: a convergence of fields. *Chem. Soc. Rev.* **2015,** *44* (15), 5320-5340.

77. Noviana, E.; McCord, C. P.; Clark, K. M.; Jang, I.; Henry, C. S., Electrochemical paper-based devices: Sensing approaches and progress toward practical applications. *Lab on a Chip* **2020,** *20* (1), 9-34.

78. da Silva, E. N. T.; Ferreira, V. S.; Lucca, B. G., Rapid and inexpensive method for the simple fabrication of PDMS-based electrochemical sensors for detection in microfluidic devices. *Electrophoresis* **2019,** *40* (9), 1322-1330.

79. Ambrosi, A.; Bonanni, A., How 3D printing can boost advances in analytical and bioanalytical chemistry. *Microchimica Acta* **2021,** *188*, 1-17.

80. Taleat, Z.; Khoshroo, A.; Mazloum-Ardakani, M., Screen-printed electrodes for biosensing: A review (2008–2013). *Microchimica Acta* **2014,** *181*, 865-891.

81. Hayat, A.; Marty, J. L., Disposable screen printed electrochemical sensors: Tools for environmental monitoring. *Sensors* **2014,** *14* (6), 10432-10453.

82. da Silva, E. T.; Souto, D. E.; Barragan, J. T.; de F. Giarola, J.; de Moraes, A. C.; Kubota, L. T., Electrochemical biosensors in point-of-care devices: recent advances and future trends. *ChemElectroChem* **2017,** *4* (4), 778-794.

83. Gooding, J. J., Fundamental Science Still Needed to Drive Sensing Forward. ACS Publications: 2021; Vol. 6, pp 4267-4268.

84. Yáñez-Sedeño, P.; Campuzano, S.; Pingarrón, J. M., Multiplexed electrochemical immunosensors for clinical biomarkers. *Sensors* **2017,** *17* (5), 965.

85. Gooding, J. J., Sensors and the Surface Chemistry Conundrum. ACS Publications: 2023; Vol. 8, pp 1-2.

86. Lim, S. A.; Ahmed, M. U., Electrochemical immunosensors and their recent nanomaterial-based signal amplification strategies: A review. *RSC advances* **2016,** *6* (30), 24995-25014.

87. Plutarch, *Assays and Micellanies*. The Project Gutenberg: 2009.

88. Institute, W. H. O., *The History and Prevention of Fouling*. United States department of the Navy, Bureau of Ships: 1952.

89. Schultz, M. P.; Bendick, J.; Holm, E.; Hertel, W., Economic impact of biofouling on a naval surface ship. *Biofouling* **2011,** *27* (1), 87-98.

90. AlSawaftah, N.; Abuwatfa, W.; Darwish, N.; Husseini, G., A comprehensive review on membrane fouling: Mathematical modelling, prediction, diagnosis, and mitigation. *Water* **2021,** *13* (9), 1327.

91. Gooding, J. J., What Is a "Real Sample"? ACS Publications: 2018; Vol. 3, pp 1609-1609.

92. Downard, A. J.; Roddick, A. D., Protein adsorption at glassy carbon electrodes: The effect of covalently bound surface groups. *Electroanalysis* **1995,** *7* (4), 376-378.

93. Moulton, S.; Barisci, J.; Bath, A.; Stella, R.; Wallace, G., Investigation of protein adsorption and electrochemical behavior at a gold electrode. *J. Colloid Interface Sci.* **2003,** *261* (2), 312-319.

94. Rabe, M.; Verdes, D.; Seeger, S., Understanding protein adsorption phenomena at solid surfaces. *Adv. Colloid Interface Sci.* **2011,** *162* (1-2), 87-106.

95. Frutiger, A.; Tanno, A.; Hwu, S.; Tiefenauer, R. F.; Voros, J.; Nakatsuka, N., Nonspecific binding—fundamental concepts and consequences for biosensing applications. *Chem. Rev.* **2021,** *121* (13), 8095-8160.

96. Norde, W. In *Driving forces for protein adsorption at solid surfaces*, Macromolecular Symposia, Wiley Online Library: 1996; pp 5-18.

97. Lee, J., *Adsorption and Transport of Colloids at Interface and in Bulk*. Louisiana State University and Agricultural & Mechanical College: 2021.

98. Bharti, B.; Meissner, J.; Klapp, S. H.; Findenegg, G. H., Bridging interactions of proteins with silica nanoparticles: The influence of pH, ionic strength and protein concentration. *Soft Matter* **2014,** *10* (5), 718-728.

99. Marichal, L.; Degrouard, J.; Gatin, A.; Raffray, N.; Aude, J.-C.; Boulard, Y.; Combet, S.; Cousin, F.; Hourdez, S.; Mary, J., The Importance of Protein Size in Protein-Nanoparticle Interactions: From Protein Corona to Colloidal Self-Assembly. *Langmuir* **2020**.

100. Liu, N.; Xu, Z.; Morrin, A.; Luo, X., Low fouling strategies for electrochemical biosensors targeting disease biomarkers. *Analytical Methods* **2019,** *11* (6), 702-711.

101. Sanko, V.; Kuralay, F., Label-Free Electrochemical Biosensor Platforms for Cancer Diagnosis: Recent Achievements and Challenges. *Biosensors* **2023,** *13* (3), 333.

102. Silva, S. M.; Li, M.; Mendes, A. X.; Moulton, S. E., Reagentless protein-based electrochemical biosensors. *Analyst* **2023,** *148* (9), 1930-1938.

103. Russo, M. J.; Han, M.; Desroches, P. E.; Manasa, C. S.; Dennaoui, J.; Quigley, A. F.; Kapsa, R. M.; Moulton, S. E.; Guijt, R. M.; Greene, G. W., Antifouling strategies for electrochemical biosensing: mechanisms and performance toward point of care based diagnostic applications. *ACS sensors* **2021,** *6* (4), 1482-1507.

104. Lin, P.-H.; Li, B.-R., Antifouling strategies in advanced electrochemical sensors and biosensors. *Analyst* **2020,** *145* (4), 1110-1120.

105. Li, Q.; Wen, C.; Yang, J.; Zhou, X.; Zhu, Y.; Zheng, J.; Cheng, G.; Bai, J.; Xu, T.; Ji, J., Zwitterionic biomaterials. *Chem. Rev.* **2022,** *122* (23), 17073-17154.

106. Vogt Jr, R. V.; Phillips, D. L.; Henderson, L. O.; Whitfield, W.; Spierto, F. W., Quantitative differences among various proteins as blocking agents for ELISA microtiter plates. *Journal of immunological methods* **1987,** *101* (1), 43-50.

107. Wang, R.; Zhou, X.; Zhu, X.; Yang, C.; Liu, L.; Shi, H., Isoelectric bovine serum albumin: robust blocking agent for enhanced performance in optical-fiber based DNA sensing. *ACS sensors* **2017,** *2* (2), 257-262.

108. Tang, Z.; Fu, Y.; Ma, Z., Bovine serum albumin as an effective sensitivity enhancer for peptide-based amperometric biosensor for ultrasensitive detection of prostate specific antigen. *Biosens. Bioelectron.* **2017,** *94*, 394-399.

109. Lin, Y.; Liu, K.; Wang, C.; Li, L.; Liu, Y., Electrochemical immunosensor for detection of epidermal growth factor reaching lower detection limit: Toward oxidized glutathione as a more efficient blocking reagent for the antibody functionalized silver nanoparticles and antigen interaction. *Anal. Chem.* **2015,** *87* (16), 8047-8051.

110. Mojsoska, B.; Larsen, S.; Olsen, D. A.; Madsen, J. S.; Brandslund, I.; Alatraktchi, F. A. a., Rapid SARS-CoV-2 detection using electrochemical immunosensor. *Sensors* **2021,** *21* (2), 390.

111. Baldo, B. A.; Tovey, E. R.; Ford, S. A., Comparison of different blocking agents and nitrocellulose in the solid phase detection of proteins by labelled antisera and protein A. *J. Biochem. Bioph. Methods* **1986,** *12* (5-6), 271-279.

112. Park, J. H.; Jackman, J. A.; Ferhan, A. R.; Ma, G. J.; Yoon, B. K.; Cho, N. J., Temperature-Induced Denaturation of BSA Protein Molecules for Improved Surface Passivation Coatings. *ACS Appl Mater Interfaces* **2018,** *10* (38), 32047-32057.

113. Ma, C.; Wu, B.; Zhang, G., Protein-protein resistance investigated by quartz crystal microbalance. *Colloids Surf B Biointerfaces* **2013,** *104*, 5-10.

114. Pillai, S.; Arpanaei, A.; Meyer, R. L.; Birkedal, V.; Gram, L.; Besenbacher, F.; Kingshott, P., Preventing protein adsorption from a range of surfaces using an aqueous fish protein extract. *Biomacromolecules* **2009,** *10* (10), 2759-2766.

115. Bernbom, N.; Jørgensen, R. L.; Ng, Y. Y.; Meyer, R. L.; Kingshott, P.; Vejborg, R. M.; Klemm, P.; Besenbacher, F.; Gram, L., Bacterial adhesion to stainless steel is reduced by aqueous fish extract coatings. *Biofilms* **2006,** *3* (1), 25-36.

116. Liebana, S.; Drago, G. A., Bioconjugation and stabilisation of biomolecules in biosensors. *Essays Biochem* **2016,** *60* (1), 59-68.

117. Leva-Bueno, J.; Peyman, S. A.; Millner, P., A review on impedimetric immunosensors for pathogen and biomarker detection. *Medical microbiology and immunology* **2020,** *209* (3), 343-362.

118. Suni, I. I., Substrate materials for biomolecular immobilization within electrochemical biosensors. *Biosensors* **2021,** *11* (7), 239.

119. Yüce, M.; Kurt, H., How to make nanobiosensors: surface modification and characterisation of nanomaterials for biosensing applications. *RSC advances* **2017,** *7* (78), 49386-49403.

120. Grabarek, Z., & Gergely, J., Zero-length crosslinking procedure with the use of active esters. *Anal. Biochem.* **1990,** *185* (1), 131-135.

121. Ulman, A., Formation and structure of self-assembled monolayers. *Chem. Rev.* **1996,** *96* (4), 1533-1554.

122. Yan, X.; Tang, J.; Tanner, D.; Ulstrup, J.; Xiao, X., Direct electrochemical enzyme electron transfer on electrodes modified by self-assembled molecular monolayers. *Catalysts* **2020,** *10* (12), 1458.

123. Vericat, C.; Vela, M.; Benitez, G.; Carro, P.; Salvarezza, R., Self-assembled monolayers of thiols and dithiols on gold: new challenges for a well-known system. *Chem. Soc. Rev.* **2010,** *39* (5), 1805-1834.

124. Calam, T. T.; Hasdemir, E., Comparative characterizations of self-assembled monolayers of 1, 6-hexanedithiol and 1-hexanethiol formed on polycrystalline gold electrode. *Comptes rendus de l'Académie bulgare des Sciences* **2019,** *72* (3).

125. Noh, J.; Konno, K.; Ito, E.; Hara, M., Growth processes and control of two-dimensional structure of carboxylic acid-terminated self-assembled monolayers on Au (111). *Japanese journal of applied physics* **2005,** *44* (2R), 1052.

126. Kim, S.; Yoo, H., Self-assembled monolayers: Versatile uses in electronic devices from gate dielectrics, dopants, and biosensing linkers. *Micromachines* **2021,** *12* (5), 565.

127. Gaigalas, A. K., & Niaura, G., Measurement of electron transfer rates between adsorbed azurin and a gold electrode modified with a hexanethiol layer. *Journal of colloid and interface science.* **1997,** *193* (1), 60-70.

128. ARVIDSSON, R. H., NORDLING, M., & LUNDBERG, L. G. , The azurin gene from Pseudomonas aeruginosa: cloning and characterization. *European journal of biochemistry,* **1989,** *179* (1), 195-200.

129. van de KAMP, M., SILVESTRINI, M. C., BRUNORI, M., Van BEEUMEN, J., HALI, F. C., & CANTERS, G. W. , Involvement of the hydrophobic patch of azurin in the electron-transfer reactions with cytochrome c551 and nitrite reductase. European journal of biochemistry. **1990,** *194* (1), 109-118.

130. Chi, Q.; Zhang, J.; Andersen, J. E.; Ulstrup, J., Ordered assembly and controlled electron transfer of the blue copper protein azurin at gold (111) single-crystal substrates. *The Journal of Physical Chemistry B* **2001,** *105* (20), 4669-4679.

131. Chi, Q.; Farver, O.; Ulstrup, J., Long-range protein electron transfer observed at the single-molecule level: In situ mapping of redox-gated tunneling resonance. *Proceedings of the National Academy of Sciences* **2005,** *102* (45), 16203-16208.

132. Zhang, J.; Chi, Q.; Kuznetsov, A.; Hansen, A. G.; Wackerbarth, H.; Christensen, H. E. M.; Andersen, J. E. T.; Ulstrup, J., Electronic properties of functional biomolecules at metal/aqueous solution interfaces. ACS Publications: 2002; Vol. 106, pp 1131-1152.

133. Yokoyama, K.; Leigh, B. S.; Sheng, Y.; Niki, K.; Nakamura, N.; Ohno, H.; Winkler, J. R.; Gray, H. B.; Richards, J. H., Electron tunneling through Pseudomonas aeruginosa azurins on SAM gold electrodes. *Inorg. Chim. Acta* **2008,** *361* (4), 1095-1099.

134. Bueno, P. R.; Mizzon, G.; Davis, J. J., Capacitance spectroscopy: a versatile approach to resolving the redox density of states and kinetics in redox-active self-assembled monolayers. *J. Phys. Chem. B* **2012,** *116* (30), 8822-9.

135. Cardoso, R.; Nasir, K., Primary prevention of cardiovascular disease: 2019 and beyond. *Nature Reviews Cardiology* **2019,** *16* (7), 387-388.

136. Zhou, F.; Lu, M.; Wang, W.; Bian, Z.-P.; Zhang, J.-R.; Zhu, J.-J., Electrochemical Immunosensor for Simultaneous Detection of Dual Cardiac Markers Based on a Poly(Dimethylsiloxane)-Gold Nanoparticles Composite Microfluidic Chip: A Proof of Principle. *Clin. Chem.* **2010,** *56* (11), 1701-1707.

137. Zhang, N.; Ma, Z.-Y.; Ruan, Y.-F.; Zhao, W.-W.; Xu, J.-J.; Chen, H.-Y., Simultaneous photoelectrochemical immunoassay of dual cardiac markers using specific

enzyme tags: a proof of principle for multiplexed bioanalysis. *Analytical chemistry* **2016,** *88* (4), 1990-1994.

138. Radha Shanmugam, N.; Muthukumar, S.; Chaudhry, S.; Anguiano, J.; Prasad, S., Ultrasensitive nanostructure sensor arrays on flexible substrates for multiplexed and simultaneous electrochemical detection of a panel of cardiac biomarkers. *Biosensors and Bioelectronics* **2017,** *89*, 764-772.

139. Boonkaew, S.; Jang, I.; Noviana, E.; Siangproh, W.; Chailapakul, O.; Henry, C. S., Electrochemical paper-based analytical device for multiplexed, point-of-care detection of cardiovascular disease biomarkers. *Sensors and Actuators B: Chemical* **2021,** *330*, 129336.

140. Black, S.; Kushner, I.; Samols, D., C-reactive protein. *J. Biol. Chem.* **2004,** *279* (47), 48487-48490.

141. Sproston, N. R.; Ashworth, J. J., Role of C-reactive protein at sites of inflammation and infection. *Frontiers in immunology* **2018,** *9*, 754.

142. Shrivastava, A. K.; Singh, H. V.; Raizada, A.; Singh, S. K., C-reactive protein, inflammation and coronary heart disease. *The Egyptian Heart Journal* **2015,** *67* (2), 89-97.

143. Kotru, S.; Klimuntowski, M.; Ridha, H.; Uddin, Z.; Askhar, A. A.; Singh, G.; Howlader, M. M., Electrochemical sensing: A prognostic tool in the fight against COVID-19. *TrAC, Trends Anal. Chem.* **2021,** *136*, 116198.

144. Začiragić, A.; Huskić, J.; Hadžović-Džuvo, A.; Valjevac, A.; Avdagić, N.; Mulabegović, N., Serum C-reactive protein concentration and measures of adiposity in patients with type 2 diabetes mellitus. *Bosnian journal of basic medical sciences* **2007,** *7* (4), 322.

145. Vanhaverbeke, M.; Veltman, D.; Pattyn, N.; De Crem, N.; Gillijns, H.; Cornelissen, V.; Janssens, S.; Sinnaeve, P. R., C-reactive protein during and after myocardial infarction in relation to cardiac injury and left ventricular function at follow-up. *Clinical Cardiology* **2018,** *41* (9), 1201-1206.

146. Pepys, M. B.; Hirschfield, G. M., C-reactive protein: a critical update. *The Journal of clinical investigation* **2003,** *111* (12), 1805-1812.

147. Kamath, D. Y.; Xavier, D.; Sigamani, A.; Pais, P., High sensitivity C-reactive protein (hsCRP) & cardiovascular disease: an Indian perspective. *The Indian journal of medical research* **2015,** *142* (3), 261.

148. Greenland, P.; Alpert, J. S.; Beller, G. A.; Benjamin, E. J.; Budoff, M. J.; Fayad, Z. A.; Foster, E.; Hlatky, M. A.; Hodgson, J. M.; Kushner, F. G., 2010 ACCF/AHA guideline for assessment of cardiovascular risk in asymptomatic adults: a report of the American College of Cardiology Foundation/American Heart Association task force on practice guidelines developed in collaboration with the American Society of Echocardiography, American Society of Nuclear Cardiology, Society of Atherosclerosis Imaging and Prevention, Society for Cardiovascular Angiography and Interventions, Society of Cardiovascular Computed Tomography, and Society for Cardiovascular Magnetic Resonance. *Journal of the American College of Cardiology* **2010,** *56* (25), e50-e103.

149. Ouyang, M.; Tu, D.; Tong, L.; Sarwar, M.; Bhimaraj, A.; Li, C.; Coté, G. L.; Di Carlo, D., A review of biosensor technologies for blood biomarkers toward monitoring cardiovascular diseases at the point of care. *Biosens. Bioelectron.* **2020**, 112621.

150. Maynard, S.; Menown, I.; Adgey, A., Troponin T or troponin I as cardiac markers in ischaemic heart disease. BMJ Publishing Group Ltd: 2000.

151. Park, K. C.; Gaze, D. C.; Collinson, P. O.; Marber, M. S., Cardiac troponins: from myocardial infarction to chronic disease. *Cardiovascular research* **2017,** *113* (14), 1708-1718.

152. Katrukha, I., Human cardiac troponin complex. Structure and functions. *Biochemistry (Moscow)* **2013,** *78*, 1447-1465.

153. Hickman, P. E.; Abhayaratna, W. P.; Potter, J. M.; Koerbin, G., Age-related differences in hs-cTnI concentration in healthy adults. *Clin. Biochem.* **2019,** *69*, 26-29.

154. Welsh, P.; Preiss, D.; Hayward, C.; Shah, A. S.; McAllister, D.; Briggs, A.; Boachie, C.; McConnachie, A.; Padmanabhan, S.; Welsh, C., Cardiac troponin T and troponin I in the general population: comparing and contrasting their genetic determinants and associations with outcomes. *Circulation* **2019,** *139* (24), 2754-2764.

155. Fathil, M.; Arshad, M. M.; Gopinath, S. C.; Hashim, U.; Adzhri, R.; Ayub, R.; Ruslinda, A.; Nuzaihan, M.; Azman, A.; Zaki, M., Diagnostics on acute myocardial infarction: Cardiac troponin biomarkers. *Biosensors and Bioelectronics* **2015,** *70*, 209-220.

156. Menzel, A.; Samouda, H.; Dohet, F.; Loap, S.; Ellulu, M. S.; Bohn, T., Common and novel markers for measuring inflammation and oxidative stress ex vivo in research and clinical practice—which to use regarding disease outcomes? *Antioxidants* **2021,** *10* (3), 414.

157. Clerico, A.; Zaninotto, M.; Aimo, A.; Dittadi, R.; Carraro, P.; Rampoldi, E.; Correale, M.; Vignati, G.; Fortunato, A.; Trenti10, T., High-sensitivity Point of Care Testing (POCT) methods for Cardiac Troponins: analytical features and clinical relevance. *biochimica clinica* **2023**, 1.

158. Roberts, W. L., CDC/AHA workshop on markers of inflammation and cardiovascular disease: application to clinical and public health practice: laboratory tests available to assess inflammation—performance and standardization: a background paper. *Circulation* **2004,** *110* (25), e572-e576.

159. Ridker, P. M., Clinical application of C-reactive protein for cardiovascular disease detection and prevention. *Circulation* **2003,** *107* (3), 363-369.

160. Abdellaoui, A.; Al-Khaffaf, H., C-reactive protein (CRP) as a marker in peripheral vascular disease. *European journal of vascular and endovascular surgery* **2007,** *34* (1), 18-22.

161. Cummins, B.; Auckland, M. L.; Cummins, P., Cardiac-specific troponin-l radioimmunoassay in the diagnosis of acute myocardial infarction. *American heart journal* **1987,** *113* (6), 1333-1344.

162. Katus, H. A.; Looser, S.; Hallermayer, K.; Remppis, A.; Scheffold, T.; Borgya, A.; Essig, U.; Geuss, U., Development and in vitro characterization of a new immunoassay of cardiac troponin T. *Clinical chemistry* **1992,** *38* (3), 386-393.

163. Hermsen, D.; Apple, F.; Garcia-Beltran, L.; Jaffe, A.; Karon, B.; Lewandrowski, E.; Mühlbacher, A.; Müller, R.; Ordonez, J.; Pagani, F., Results from a multicenter evaluation of the 4th generation Elecsys Troponin T assay. *Clinical laboratory* **2007,** *53* (1-2), 1-9.

164. Fraser, C. G., Optimal analytical performance for point of care testing. *Clinica chimica acta* **2001,** *307* (1-2), 37-43.

165. Gaze, D. C., Rapid cardiovascular diagnostics. *Proof and Concepts in Rapid Diagnostic Tests and Technologies* **2016**, 17-33.

166. Leigh, J. A.; Alvarez, M.; Rodriguez, C. J., Ethnic minorities and coronary heart disease: an update and future directions. *Current atherosclerosis reports* **2016,** *18*, 1-10.

167. Dhara, K.; Mahapatra, D. R., Review on electrochemical sensing strategies for C-reactive protein and cardiac troponin I detection. *Microchem. J.* **2020,** *156*, 104857-104857.

168. Johnson, A.; Song, Q.; Ko Ferrigno, P.; Bueno, P. R.; Davis, J. J., Sensitive affimer and antibody based impedimetric label-free assays for C-reactive protein. *Anal. Chem.* **2012,** *84* (15), 6553-6560.

169. Kanyong, P.; Davis, J. J., Homogeneous functional self-assembled monolayers: Faradaic impedance baseline signal drift suppression for high-sensitivity immunosensing of C-reactive protein. *J. Electroanal. Chem.* **2020,** *856*.

170. Adesina, A.; Adeniyi, O.; Mashazi, P., Online regeneration of a piezoelectric and impedimetric immunosensor for the detection of C-reactive protein on the oriented antibody gold surface. *Analytical Methods* **2023,** *15* (9), 1157-1167.

171. Boonkaew, S.; Chaiyo, S.; Jampasa, S.; Rengpipat, S.; Siangproh, W.; Chailapakul, O., An origami paper-based electrochemical immunoassay for the C-reactive protein using a screen-printed carbon electrode modified with graphene and gold nanoparticles. *Microchimica Acta* **2019,** *186*, 1-10.

172. Resende, L. O.; De Castro, A. C. H.; Andrade, A. O.; Madurro, J. M.; Brito-Madurro, A. G., Immunosensor for electrodetection of the C-reactive protein in serum. *J. Solid State Electrochem.* **2018,** *22*, 1365-1372.

173. Ribeiro, S. H.; Alves, L. M.; Flauzino, J. M.; Moço, A. C.; Segatto, M. S.; Silva, J. P.; Borges, L. F.; Madurro, J. M.; Madurro, A. G., Reusable Immunosensor for Detection of C-reactive Protein in Human Serum. *Electroanalysis* **2020,** *32* (10), 2316-2322.

174. Dong, S.; Zhang, D.; Cui, H.; Huang, T., ZnO/porous carbon composite from a mixed-ligand MOF for ultrasensitive electrochemical immunosensing of C-reactive protein. *Sensors and Actuators B: chemical* **2019,** *284*, 354-361.

175. Kanyong, P.; Catli, C.; Davis, J. J., Ultrasensitive Impedimetric Immunosensor for the Detection of C-Reactive Protein in Blood at Surface-Initiated-Reversible Addition-Fragmentation Chain Transfer Generated Poly(2-hydroxyethyl methacrylate) Brushes. *Anal. Chem.* **2020,** *92* (7), 4707-4710.

176. Lehr, J.; Fernandes, F. C. B.; Bueno, P. R.; Davis, J. J., Label-free capacitive diagnostics: exploiting local redox probe state occupancy. *Anal. Chem.* **2014,** *86* (5), 2559-2564.

177. Bakirhan, N. K.; Ozcelikay, G.; Ozkan, S. A., Recent progress on the sensitive detection of cardiovascular disease markers by electrochemical-based biosensors. *J. Pharm. Biomed. Anal.* **2018,** *159*, 406-424.

178. Mizzon, G. Bioelectrochemistry by fluorescent cyclic voltammetry. Oxford University, UK, 2012.

179. Harrington, B. e. a. *Inkscape*, 2004-2005.

180. Community, B. O. *Blender - a 3D modelling and rendering package*, Stichting Blender Foundation: Amsterdam, 2018.

181. Tarini, M.; Cignoni, P., QuteMol. **2006**.

182. Tkac, J.; Davis, J. J., An optimised electrode pre-treatment for SAM formation on polycrystalline gold. *J. Electroanal. Chem.* **2008,** *621* (1), 117-120.

183. Pace, C. N.; Vajdos, F.; Fee, L.; Grimsley, G.; Gray, T., How to measure and predict the molar absorption coefficient of a protein. *Protein Sci.* **1995,** *4* (11), 2411-2423.

184. Whang, T.-J.; Huang, H.-Y.; Hsieh, M.-T.; Chen, J.-J., Laser-induced silver nanoparticles on titanium oxide for photocatalytic degradation of methylene blue. *International journal of molecular sciences* **2009,** *10* (11), 4707-4718.

185. Bu, S.; Wang, K.; Li, Z.; Wang, C.; Hao, Z.; Liu, W.; Wan, J., An electrochemical biosensor based on methylene blue-loaded nanocomposites as signal-amplifying tags to detect pathogenic bacteria. *Analyst* **2020,** *145* (12), 4328-4334.

186. Pheeney, C. G.; Barton, J. K., DNA electrochemistry with tethered methylene blue. *Langmuir* **2012,** *28* (17), 7063-7070.

187. Ju, H.; Zhou, J.; Cai, C.; Chen, H., The electrochemical behavior of methylene blue at a microcylinder carbon fiber electrode. *Electroanalysis* **1995,** *7* (12), 1165-1170.

188. Oesch, U., & Janata, J. , Electrochemical study of gold electrodes with anodic oxide films—I. Formation and reduction behaviour of anodic oxides on gold. *Electrochim. Acta* **1983,** *28* (9), 1237-1246.

189. Redón, P.; Shahzad, A.; Iqbal, T.; Wijns, W., Benefits of Home-Based Solutions for Diagnosis and Treatment of Acute Coronary Syndromes on Health Care Costs: A Systematic Review. *Sensors* **2020,** *20* (17), 5006.

190. Bloom, J. R., Early detection of cancer. Psychologic and social dimensions. *Cancer* **1994,** *74* (S4), 1464-1473.

191. Van Luijt, P.; Heijnsdijk, E.; de Koning, H., Cost-effectiveness of the Norwegian breast cancer screening program. *International journal of cancer* **2017,** *140* (4), 833-840.

192. Rasmussen, J.; Langerman, H., Alzheimer's disease–why we need early diagnosis. *Degenerative neurological and neuromuscular disease* **2019**, 123-130.

193. Rahimi, H.; Salehiabar, M.; Barsbay, M.; Ghaffarlou, M.; Kavetskyy, T.; Sharafi, A.; Davaran, S.; Chauhan, S. C.; Danafar, H.; Kaboli, S., CRISPR systems for COVID-19 diagnosis. *ACS sensors* **2021,** *6* (4), 1430-1445.

194. Gu, C.; Xie, L.; Li, B.; Zhang, L.; Li, F.; Wang, W.; Su, J.; Xu, Z., Quantification of Tumor Abnormal Proteins in the Diagnosis and Postoperative Prognostic Evaluation of Gastric Cancer. *Clinical Medicine Insights: Oncology* **2022,** *16*, 11795549221104440.

195. Scherl, A., Clinical protein mass spectrometry. *Methods* **2015,** *81*, 3-14.

196. Kanyong, P.; Patil, A. V.; Davis, J. J., Functional Molecular Interfaces for Impedance-Based Diagnostics. *Annual Review of Analytical Chemistry* **2020,** *13* (1), 183-200.

197. Liu, J.; Lu, W.; Zhang, L.; Yang, J.; Yao, Z.-P.; He, Y.; Li, Y., Integrated hand-held electrochemical sensor for multicomponent detection in urine. *Biosens. Bioelectron.* **2021,** *193*, 113534.

198. Pohanka, M., Electrochemical Hand-Held Biosensors for Biological Warfare Agents Assay. *Int. J. Electrochem. Sci* **2022,** *17* (220961), 2.

199. Andryukov, B. G.; Besednova, N. N.; Romashko, R. V.; Zaporozhets, T. S.; Efimov, T. A., Label-free biosensors for laboratory-based diagnostics of infections: Current achievements and new trends. *Biosensors* **2020,** *10* (2), 11.

200. Khristunova, E.; Dorozhko, E.; Korotkova, E.; Kratochvil, B.; Vyskocil, V.; Barek, J., Label-free electrochemical biosensors for the determination of Flaviviruses: Dengue, Zika, and Japanese Encephalitis. *Sensors* **2020,** *20* (16), 4600.

201. Florea, A.; Melinte, G.; Simon, I.; Cristea, C., Electrochemical biosensors as potential diagnostic devices for autoimmune diseases. *Biosensors* **2019,** *9* (1), 38.

202. Baradoke, A.; Hein, R.; Li, X.; Davis, J. J., Reagentless Redox Capacitive Assaying of C-Reactive Protein at a Polyaniline Interface. *Anal. Chem.* **2020,** *92* (5), 3508-3511.

203. Lichtenberg, J. Y.; Ling, Y.; Kim, S., Non-specific adsorption reduction methods in biosensing. *Sensors* **2019,** *19* (11), 2488.

204. Xu, L.-C.; Bauer, J. W.; Siedlecki, C. A., Proteins, platelets, and blood coagulation at biomaterial interfaces. *Colloids and Surfaces B: Biointerfaces* **2014,** *124*, 49-68.

205. Sandhyarani, N., Surface modification methods for electrochemical biosensors. In *Electrochemical Biosensors*, Elsevier: 2019; pp 45-75.

206. Trilling, A. K.; Beekwilder, J.; Zuilhof, H., Antibody orientation on biosensor surfaces: a minireview. *Analyst* **2013,** *138* (6), 1619-1627.

207. Citartan, M., Aptamers as the powerhouse of dot blot assays. *Talanta* **2021,** *232*, 122436.

208. Wang, C.; Liu, D.; Wang, Z., Gold nanoparticle based dot-blot immunoassay for sensitively detecting Alzheimer's disease related β-amyloid peptide. *Chem. Commun.* **2012,** *48* (67), 8392-8394.

209. Surti, P. V.; Kim, M. W.; Kailasa, S. K.; Mungray, A. K.; Park, J. P.; Park, T. J., Progress on dot-blot assay as a promising analytical tool: Detection from molecules to cells. *TrAC, Trends Anal. Chem.* **2022**, 116736.

210. Pividori, M.; Merkoçi, A.; Alegret, S., Classical dot–blot format implemented as an amperometric hybridisation genosensor. *Biosens. Bioelectron.* **2001,** *16* (9-12), 1133-1142.

211. Szűcs, J.; Gyurcsányi, R. E., Towards protein assays on paper platforms with potentiometric detection. *Electroanalysis* **2012,** *24* (1), 146-152.

212. Chikkaveeraiah, B. V.; Bhirde, A. A.; Morgan, N. Y.; Eden, H. S.; Chen, X., Electrochemical immunosensors for detection of cancer protein biomarkers. *ACS nano* **2012,** *6* (8), 6546-6561.

213. Zhu, G.; Lee, H. J., Electrochemical sandwich-type biosensors for α− 1 antitrypsin with carbon nanotubes and alkaline phosphatase labeled antibody-silver nanoparticles. *Biosens. Bioelectron.* **2017,** *89*, 959-963.

214. Hosseini Ghalehno, M.; Mirzaei, M.; Torkzadeh-Mahani, M., Electrochemical aptasensor for tumor necrosis factor α using aptamer–antibody sandwich structure and cobalt hexacyanoferrate for signal amplification. *Journal of the Iranian Chemical Society* **2019,** *16* (8), 1783-1791.

215. Elgrishi, N.; Rountree, K. J.; McCarthy, B. D.; Rountree, E. S.; Eisenhart, T. T.; Dempsey, J. L., A Practical Beginner's Guide to Cyclic Voltammetry. *J. Chem. Educ.* **2017,** *95* (2), 197-206.

216. Moo, J. G. S.; Veksha, A.; Oh, W.-D.; Giannis, A.; Udayanga, W. C.; Lin, S.-X.; Ge, L.; Lisak, G., Plastic derived carbon nanotubes for electrocatalytic oxygen reduction reaction: Effects of plastic feedstock and synthesis temperature. *Electrochem. Commun.* **2019,** *101*, 11-18.

217. Wright, A. K.; Thompson, M., Hydrodynamic structure of bovine serum albumin determined by transient electric birefringence. *Biophys. J.* **1975,** *15* (2), 137-141.

218. Leeman, M.; Choi, J.; Hansson, S.; Storm, M. U.; Nilsson, L., Proteins and antibodies in serum, plasma, and whole blood—size characterization using asymmetrical flow field-flow fractionation (AF4). *Analytical and bioanalytical chemistry* **2018,** *410*, 4867-4873.

219. Dundas, C. M.; Demonte, D.; Park, S., Streptavidin–biotin technology: improvements and innovations in chemical and biological applications. *Appl. Microbiol. Biotechnol.* **2013,** *97*, 9343-9353.

220. Fanjul-Bolado, P.; González-García, M. B.; Costa-García, A., Amperometric detection in TMB/HRP-based assays. *Analytical and Bioanalytical chemistry* **2005,** *382* (2), 297-302.

221. Latour, R. A., The Langmuir isotherm: a commonly applied but misleading approach for the analysis of protein adsorption behavior. *Journal of biomedical materials research part A* **2015,** *103* (3), 949-958.

222. Marquez, L. A.; Dunford, H. B., Mechanism of the oxidation of 3, 5, 3 ‘, 5 ‘-tetramethylbenzidine by myeloperoxidase determined by transient-and steady-state kinetics. *Biochemistry* **1997,** *36* (31), 9349-9355.

223. Wang, S.; Chang, K.; Yuan, C.-J., Enhancement of electrochemical properties of screen-printed carbon electrodes by oxygen plasma treatment. *Electrochim. Acta* **2009,** *54* (21), 4937-4943.

224. Ong, S.-E.; Mann, M., Mass spectrometry–based proteomics turns quantitative. *Nature chemical biology* **2005,** *1* (5), 252-262.

225. Rauniyar, N.; Yates III, J. R., Isobaric labeling-based relative quantification in shotgun proteomics. *Journal of proteome research* **2014,** *13* (12), 5293-5309.

226. Bantscheff, M.; Lemeer, S.; Savitski, M. M.; Kuster, B., Quantitative mass spectrometry in proteomics: critical review update from 2007 to the present. *Anal Bioanal Chem* **2012,** *404* (4), 939-65.

227. Mendoza, V. L.; Vachet, R. W., Probing protein structure by amino acid-specific covalent labeling and mass spectrometry. *Mass Spectrom. Rev.* **2009,** *28* (5), 785-815.

228. Nair, H.; Clark, W., Mass Spectrometry for the Clinical Laboratory. Elsevier Science. **2017**.

229. Schneider, A. F. L.; Hackenberger, C. P. R., Fluorescent labelling in living cells. *Curr. Opin. Biotechnol.* **2017,** *48*, 61-68.

230. Sengupta, S.; Chandrasekaran, S., Modifications of amino acids using arenediazonium salts. *Organic & Biomolecular Chemistry* **2019,** *17* (36), 8308-8329.

231. Bénard, A.; Forcher, G.; Le Bohec, M.; Montembault, V.; Pascual, S.; Fontaine, L., Azlactone-based heterobifunctional linkers with orthogonal clickable groups: efficient tools for bioconjugation with complete atom economy. *Organic & Biomolecular Chemistry* **2018,** *16* (39), 7124-7128.

232. Söveges, B.; Imre, T.; Szende, T.; Póti, Á. L.; Cserép, G. B.; Hegedűs, T.; Kele, P.; Németh, K., A systematic study of protein labeling by fluorogenic probes using cysteine targeting vinyl sulfone-cyclooctyne tags. *Organic & Biomolecular Chemistry* **2016,** *14* (25), 6071-6078.

233. Koniev, O.; Wagner, A., Developments and recent advancements in the field of endogenous amino acid selective bond forming reactions for bioconjugation. *Chem. Soc. Rev.* **2015,** *44* (15), 5495-5551.

234. Kalkhof, S.; Sinz, A., Chances and pitfalls of chemical cross-linking with amine-reactive N-hydroxysuccinimide esters. *Analytical and bioanalytical chemistry* **2008,** *392*, 305-312.

235. Wiese, S.; Reidegeld, K. A.; Meyer, H. E.; Warscheid, B., Protein labeling by iTRAQ: a new tool for quantitative mass spectrometry in proteome research. *Proteomics* **2007,** *7* (3), 340-350.

236. Ward, C. C.; Kleinman, J. I.; Nomura, D. K., NHS-esters as versatile reactivity-based probes for mapping proteome-wide ligandable hotspots. *ACS chemical biology* **2017,** *12* (6), 1478-1483.

237. Sharafeldin, M.; Fleschhut, F.; James, T.; Davis, J. J., A quantification of target protein biomarkers in complex media by faradaic shotgun tagging. *Analytical Chemistry* **2022,** *94* (5), 2375-2382.

238. García-González, R.; Costa-García, A.; Fernández-Abedul, M. T., Methylene blue covalently attached to single stranded DNA as electroactive label for potential bioassays. *Sensors and Actuators B: Chemical* **2014,** *191*, 784-790.

239. Sarcina, L.; Scandurra, C.; Di Franco, C.; Caputo, M.; Catacchio, M.; Bollella, P.; Scamarcio, G.; Macchia, E.; Torsi, L., A stable physisorbed layer of packed capture antibodies for high-performance sensing applications. *Journal of Materials Chemistry C* **2023**.

240. Wickramathilaka, M. P.; Tao, B. Y., Characterization of covalent crosslinking strategies for synthesizing DNA-based bioconjugates. *Journal of biological engineering* **2019,** *13* (1), 1-10.

241. Ng, A. H.; Uddayasankar, U.; Wheeler, A. R., Immunoassays in microfluidic systems. *Analytical and bioanalytical chemistry* **2010,** *397*, 991-1007.

242. Lion, N.; Reymond, F.; Girault, H. H.; Rossier, J. S., Why the move to microfluidics for protein analysis? *Curr. Opin. Biotechnol.* **2004,** *15* (1), 31-37.

243. Roth, G. A.; Johnson, C.; Abajobir, A.; Abd-Allah, F.; Abera, S. F.; Abyu, G.; Ahmed, M.; Aksut, B.; Alam, T.; Alam, K., Global, regional, and national burden of cardiovascular diseases for 10 causes, 1990 to 2015. *Journal of the American College of Cardiology* **2017,** *70* (1), 1-25.

244. Adams, J.; Apple, F., New blood tests for detecting heart disease. *Circulation* **2004,** *109* (3), e12-e14.

245. Apple, F. S.; Wu, A. H.; Sandoval, Y.; Sexter, A.; Love, S. A.; Myers, G.; Schulz, K.; Duh, S.-H.; Christenson, R. H., Sex-specific 99th percentile upper reference limits for high sensitivity cardiac troponin assays derived using a universal sample bank. *Clin. Chem.* **2020,** *66* (3), 434-444.

246. Dalvie, M. A.; Sinanovic, E.; London, L.; Cairncross, E.; Solomon, A.; Adam, H., Cost analysis of ELISA, solid-phase extraction, and solid-phase microextraction for the monitoring of pesticides in water. *Environ. Res.* **2005,** *98* (1), 143-150.

247. Boon, E. M.; Ceres, D. M.; Drummond, T. G.; Hill, M. G.; Barton, J. K., Mutation detection by electrocatalysis at DNA-modified electrodes. *Nat. Biotechnol.* **2000,** *18* (10), 1096-1100.

248. Wang, C.; Zhao, Q., A reagentless electrochemical sensor for aflatoxin B1 with sensitive signal-on responses using aptamer with methylene blue label at specific internal thymine. *Biosens. Bioelectron.* **2020,** *167*, 112478.

249. Bedatty Fernandes, F. C.; Patil, A. V.; Bueno, P. R.; Davis, J. J., Optimized Diagnostic Assays Based on Redox Tagged Bioreceptive Interfaces. *Anal. Chem.* **2015,** *87* (24), 12137-44.

250. Santos, A.; Bueno, P. R.; Davis, J. J., A dual marker label free electrochemical assay for Flavivirus dengue diagnosis. *Biosens. Bioelectron.* **2018,** *100*, 519-525.

251. Piccoli, J.; Hein, R.; El-Sagheer, A. H.; Brown, T.; Cilli, E. M.; Bueno, P. R.; Davis, J. J., Redox Capacitive Assaying of C-Reactive Protein at a Peptide Supported Aptamer Interface. *Anal. Chem.* **2018,** *90* (5), 3005-3008.

252. Santos, L. K.; Mendonça, P. D.; Assis, L. K.; Prudêncio, C. R.; Guedes, M. I. F.; Marques, E. T.; Dutra, R. F., A Redox-Probe-Free Immunosensor Based on Electrocatalytic Prussian Blue Nanostructured Film One-Step-Prepared for Zika Virus Diagnosis. *Biosensors* **2022,** *12* (8), 623.

253. de Groot, M. T.; Evers, T. H.; Merkx, M.; Koper, M. T., Electron Transfer and Ligand Binding to Cytochrome c 'Immobilized on Self-Assembled Monolayers. *Langmuir* **2007,** *23* (2), 729-736.

254. Rafiee, J.; Mi, X.; Gullapalli, H.; Thomas, A. V.; Yavari, F.; Shi, Y.; Ajayan, P. M.; Koratkar, N. A., Wetting transparency of graphene. *Nature materials* **2012,** *11* (3), 217-222.

255. Arima, Y.; Iwata, H., Effect of wettability and surface functional groups on protein adsorption and cell adhesion using well-defined mixed self-assembled monolayers. *Biomaterials* **2007,** *28* (20), 3074-3082.

256. Widrig, C. A.; Chung, C.; Porter, M. D., The electrochemical desorption of n-alkanethiol monolayers from polycrystalline Au and Ag electrodes. *Journal of electroanalytical chemistry and interfacial electrochemistry* **1991,** *310* (1-2), 335-359.

257. Kemnade, N.; Chen, Y.; Muglali, M. I.; Erbe, A., Electrochemical reductive desorption of alkyl self-assembled monolayers studied in situ by spectroscopic ellipsometry: evidence for formation of a low refractive index region after desorption. *Physical Chemistry Chemical Physics* **2014,** *16* (32), 17081-17090.

258. Xu, Q.; Evetts, S.; Hu, M.; Talbot, K.; Wade-Martins, R.; Davis, J. J., An impedimetric assay of α-synuclein autoantibodies in early stage Parkinson's disease. *RSC Adv.* **2014,** *4* (102), 58773-58777.

259. Kim, K.; Kwak, J., Faradaic impedance titration of pure 3-mercaptopropionic acid and ethanethiol mixed monolayers on gold. *J. Electroanal. Chem.* **2001,** *512* (1-2), 83-91.

260. López, G. P.; Castner, D. G.; Ratner, B. D., XPS O 1s binding energies for polymers containing hydroxyl, ether, ketone and ester groups. *Surf. Interface Anal.* **1991,** *17* (5), 267-272.

261. Ciampi, S.; Böcking, T.; Kilian, K. A.; James, M.; Harper, J. B.; Gooding, J. J., Functionalization of acetylene-terminated monolayers on Si (100) surfaces: a click chemistry approach. *Langmuir* **2007,** *23* (18), 9320-9329.

262. Zorn, G.; Liu, L.-H.; Árnadóttir, L.; Wang, H.; Gamble, L. J.; Castner, D. G.; Yan, M., X-ray photoelectron spectroscopy investigation of the nitrogen species in photoactive perfluorophenylazide-modified surfaces. *The Journal of Physical Chemistry C* **2014,** *118* (1), 376-383.

263. Techane, S. D.; Gamble, L. J.; Castner, D. G., Multitechnique characterization of self-assembled carboxylic acid-terminated alkanethiol monolayers on nanoparticle and flat gold surfaces. *The Journal of Physical Chemistry C* **2011,** *115* (19), 9432-9441.

264. Song, S.; Clark, R. A.; Bowden, E. F.; Tarlov, M. J., Characterization of cytochrome c/alkanethiolate structures prepared by self-assembly on gold. *The Journal of Physical Chemistry* **1993,** *97* (24), 6564-6572.

265. Salverda, J. M.; Patil, A. V.; Mizzon, G.; Kuznetsova, S.; Zauner, G.; Akkilic, N.; Canters, G. W.; Davis, J. J.; Heering, H. A.; Aartsma, T. J., Fluorescent cyclic voltammetry of immobilized azurin: direct observation of thermodynamic and kinetic heterogeneity. *Angew. Chem. Int. Ed. Engl.* **2010,** *49* (33), 5776-9.

266. Fristrup, P., Grubb, M., Zhang, J., Christensen, H. E. M., Hansen, A. M., & Ulstrup, J. , Voltammetry of native and recombinant Pseudomonas aeruginosa azurin on

polycrystalline Au-and single-crystal Au (111)-surfaces modified by decanethiol monolayers. *J. Electroanal. Chem.* **2001,** *511* (1-2), 128-133.

267. Chi, Q.; Zhang, J.; Jensen, P. S.; Christensen, H. E.; Ulstrup, J., Long-range interfacial electron transfer of metalloproteins based on molecular wiring assemblies. *Faraday Discuss.* **2006,** *131*, 181-195.

268. Fleming, B. D., Praporski, S., Bond, A. M., & Martin, L. L., Electrochemical quartz crystal microbalance study of azurin adsorption onto an alkanethiol self-assembled monolayer on gold. *Langmuir* **2008,** *24* (1), 323-327.

269. Bard, A. J.; Faulkner, L. R.; White, H. S., *Electrochemical methods: fundamentals and applications*. John Wiley & Sons: 2022.

270. Fernandez-Perez, A.; Marban, G., Visible light spectroscopic analysis of methylene blue in water; what comes after dimer? *ACS omega* **2020,** *5* (46), 29801-29815.

271. Stoscheck, C. M., [6] Quantitation of protein. In *Methods Enzymol.*, Elsevier: 1990; Vol. 182, pp 50-68.

272. Won, B. Y.; Shin, S.; Baek, S.; Jung, Y. L.; Li, T.; Shin, S. C.; Cho, D.-Y.; Lee, S. B.; Park, H. G., Investigation of the signaling mechanism and verification of the performance of an electrochemical real-time PCR system based on the interaction of methylene blue with DNA. *Analyst* **2011,** *136* (8), 1573-1579.